UC Riverside
UC Riverside Electronic Theses and Dissertations

Title

A Multi-Scale Analysis of Post-Wildfire Sediment Cascades in Mountainous Southern California, USA

Permalink

https://escholarship.org/uc/item/4951v3r0

Author

Guilinger, James Joseph

Publication Date

2021

Copyright Information

Peer reviewed|Thesis/dissertation

UNIVERSITY OF CALIFORNIA

RIVERSIDE

A Multi-Scale Analysis of Post-Wildfire Sediment Cascades in Mountainous Southern California, USA

A Dissertation submitted in partial satisfaction
of the requirements for the degree of

Doctor of Philosophy

in

Environmental Sciences

by

James Joseph Guilinger

September 2021

Dissertation Committee:

      Dr. Andrew B. Gray, Chairperson
      Dr. Nicolas C. Barth
      Dr. Hoori Ajami
      Dr. Francis K. Rengers

The Dissertation of James Joseph Guilinger is approved:

_____

_____

_____

Committee Chairperson

University of California, Riverside

Copyright Acknowledgements

Chapter 2 of this dissertation is a reprint of a publication, Guilinger et al. 2020, *from Journal of Geophysical Research: Earth Surface*, coauthored by Andrew B. Gray, Nicolas C. Barth, and Brandon T. Fong. Chapter 3 of this dissertation is a manuscript in preparation for submission to *Nature Geoscience* in Fall 2021 coauthored by Andrew B. Gray and Nicolas C. Barth. Chapter 4 of this dissertation is a manuscript in preparation for submission to *Environmental Science and Technology* currently being coauthored in Fall 2021 by Andrew Gray, Nic Barth, Chris Stranksy, John Rudolph, Rebekah Guill, Garth Engelhorn, and Melissa Varela.

Dedication

To my best friend and wife Kylie Ziona Guilinger, whose deep love and companionship made all this work possible.

ABSTRACT OF THE DISSERTATION

A Multi-Scale Analysis of Post-Wildfire Sediment Cascades in Mountainous Southern California, USA

by

James Joseph Guilinger

Doctor of Philosophy, Department of Environmental Sciences
University of California, Riverside, September 2021
Dr. Andrew B. Gray, Chairperson

Wildfire is a major disturbance in vegetated mountainous regions worldwide. When intense fire burns through steep landscapes, it increases the likelihood of destructive sediment-laden floods and debris flows by increasing the amount of runoff and sediment available to erode. Despite increased work in documenting and modeling postfire erosion, there is still uncertainty regarding the amount of sediment produced and delivered to downstream communities following fire and how these processes may be impacted by greater watershed reburning rates as fire frequency increases. In this dissertation, we sought to answer the following questions organized by chapter. Chapter 2: How do sediment supplies evolve in response to repeat rainfall events? Chapter 3: Do sediment supplies in channels depend on previous fire-flood cycles? Chapter 4: What is the impact of fire-associated runoff from steep, severely burned watersheds on lake systems? Using spatiotemporally nested scales of remote sensing analysis and hydrometeorological monitoring, we show that time-dependent sediment availability is an important factor in controlling sediment yields from low-order burned catchments (Chapter 2), that inter-fire accumulations are important sediment supplies and time since previous probable fire-flood cycles could be a useful indicator of channel sediment availability (Chapter 3), and that postfire runoff delivery to downstream freshwater areas by fire is a very important component nutrient and sediment budgets over long timescales (Chapter 4). This research ultimately shows that sediment supplies in headwater channels can become limited by previous fire-flood cycles, with implications for the amount of

headwater sediment yields both at the storm cycle scale (Chapter 2), over the scale of subsequent

reburn and fire-flood cycles (Chapter 3), and the delivery of sediments and other sediment-

associated constituents to downstream waterbodies (Chapter 4). This work advances a more

detailed understanding of postfire erosional cycles and highlights additional legacy controls on

postfire sediment cascades across many time (1 month-100 year) and space (1 ha to 10 km^2)

scales.

Table of Contents

List of Figures

List of Tables

Chapter 1. Introduction

"Beyond the interior valleys—some fifty thousand feet away and a vertical mile above you—are the summits … so clearly visible in the dry blue sky that just below their ridgelines you can almost count the boulders that are bunched there like grapes…the muzzle-loader is charged. For a full-scale flat-out debris flow to burst forth from the mountains, the final requirement is a special-intensity storm."

-John McPhee, *Los Angeles Against the Mountains* (1988)

One of California's most sought-after traits is its largely stable dry weather and diversity in topography, vegetation, and microclimates. However, McPhee's words above describe a hazard that undoubtedly exists against this literal and metaphorical backdrop: large slugs of sediment that come down those mountains all at once. This hazard that has existed for millennia, but we must now contend with it given the urbanization exists along steep mountain ranges with >2,000 meters of relief from summit to sea that is among some of the steepest in North America. This hazard is exacerbated by an intense wildfire regime (and rapidly intensifying with climate change) and highly erodible rock and soil thrust up along the margin of two major tectonic plates grinding past one another. Ultimately, this dissertation is a narrative about this interplay of fire, earth, and water.

1.0 Wildfire Ecology and Trends Within Southern California

Wildfire on planet Earth has existed since at least the Ordivician (~440 million years before present) (e.g., Bowman et al., 2011; Lu et al., 2021). Wildfire plays a key role in ecosystem functioning of many biomes (Keeley & Pausas, 2019), including shrublands and conifer systems of southern California where this study is focused (e.g., Keeley & Fotheringham,

2001). In particular, chaparral is a fire-adapted community that maintains its biodiversity through primarily stand-replacing fire occurring on return intervals of 30-80 years (Minnich, 1983; Keeley and Fotheringham, 2001). Chaparral systems of southern California are thought of as ignition-limited systems (Keeley and Fotheringham, 2001) and recent studies have shown that fire frequency is most correlated with human ignitions and by extension, human population (Syphard & Keeley, 2020). Additionally, a factor unique to southern California chaparral systems is the presence of foehn (or "Santa Ana") winds which are very dry downslope winds that can cause extremely rapid and intense fire spread (Keeley and Fotheringham, 2001). Wind-driven fires in southern California appear to dominate much of total burn area in this region both prior to Euro-American colonization (Mensing et al., 1999) and in the modern 21st-century urbanization of the region (Keeley & Fotheringham, 2001). Studies have shown that fire suppression has not been effective at controlling fire in these systems. This is primarily driven by a few factors: (1) wind-driven fires during extreme fire weather which dominate total burn area are nearly impossible to control and burn through stands regardless of their age (Keeley & Fotheringham, 2001; Keeley & Syphard, 2019). (2) The vast majority of fire ignitions are human-caused, thus any gains made in suppressing fires during less extreme fire weather are likely cancelled out by subsidies in human-driven ignitions (Keeley & Syphard, 2019). Instead, the major problem is the increasing impact of these fires due to expansion and greater population of the wildland-urban interface (Keeley and Syphard, 2019; Radeloff et al., 2018). An extension of this hazard is postfire runoff impacts, which can present risks to those within and downstream of burn scars for months to years following fire (Shakesby and Doerr, 2006). I outline the impacts of wildfire on hydro-geomorphic processes in the section below.

1.1 Wildfire Impacts on Hydrology and Upland Sediment Cascades

Infiltration, the process by which precipitation enters the subsurface, is a key process in the hydrologic cycle. Wildfire drastically alters hydrologic responses through reduction in soil infiltration capacity (e.g., Ebel et al., 2012; McGuire et al., 2018; Nyman et al., 2014), increased net precipitation (R. a. Shakesby & Doerr, 2006) and decreased evapotranspiration (e.g., Atchley et al., 2018; Kinoshita & Hogue, 2015) through the loss of canopy and ground cover. Unburned forested and shrubland catchments generally have high infiltration capacities (e.g., Moody et al., 2016) with a propensity to produce runoff through subsurface stormflow or saturation excess overland flow during prolonged and sustained rainfall periods (Fig 3) (Mirus & Loague, 2013). Forested catchments and shrublands burned by fire undergo a suite of disturbances that generally act to lower the sorptivity and saturated hydraulic conductivity of their soils, One of the most well-reported effects is increased soil-water repellency, which is primarily caused by the precipitation of hydrophobic compounds on the ash or burned duff layer - mineral soil interface (e.g., DeBano, 1981; Ebel & Martin, 2017; Shakesby & Doerr, 2006). Additionally, other impacts to soil surface properties include: the clogging of pores with ash and other burned organics (Bodí et al., 2014), soil sealing from unabated rainfall impact energy (Larsen et al., 2009), and hyper-dry conditions present at the soil surface following fire that markedly decrease sorptivity, especially when combined with soil-water repellency (Ebel et al., 2012).

Wildfire drastically increases the amount of sediment available for erosion, either through the release of sediment built up behind low-growing vegetation (Lamb et al., 2011) or through the destruction of surface soil cohesion through radiant heat imparted by the fire itself (Nyman et al., 2013). This increase in material available for entrainment and greater runoff generation make wildfire a particularly effective agent for increasing sediment transport. Below is an outline describing these processes, which together represent various parts of the postfire sediment

3

cascade (or sum of all sediment transfer processes). These are also schematically represented in Figure 1.1.

1.1.1. Soil erosion: Just at it can be conceptualized for hydrological conceptual models, soils in burn settings can be thought of as a two-layer system with loose ash/organic layer overlying primarily mineral soil with reduced cohesion. The degree of litter consumption and depth of the low-cohesion layer into the mineral soil is generally a function of near-ground burn intensity, with severe fire producing extremely loose ash and a cohesionless layer extending up to a decimeter into the soil profile (Parsons et al., 2010; Shakesby & Doerr, 2006). Immediately following fire, this ash/organic layer is susceptible to wind erosion (Sankey et al., 2009) and in some cases may be significantly depleted prior to the first post-fire storm if significant wind events take place. During runoff generation and routing immediately following fire, this material is easily entrained by overland flow that commonly coalesces into rills which may be topographically steered into gully systems in convergent terrain. Additionally, it has been shown that on long planar hillslopes with minimal convergence, dendritic rill networks may span their full length, such as in the burned hillslopes in the Santa Ynez Mountains that eroded during the 2018 Montecito, CA debris flows (Alessio et al., 2021). Additionally, raindrop impacts (aka – rainsplash) on barren slopes have been shown to be significant component of sediment flux and acts in concert with flow-driven processes to route material to rill networks (McGuire et al., 2016; Staley et al., 2014).

1.1.2. Instability-driven dry weather erosion: In steep landscapes above or near the angle of repose (usually set by the internal angle of friction of soils around ~30-35 degrees, (Lamb et al., 2011), materials are near their stability threshold, therefore significant components of downslope movement can happen during dry weather through rockfall and dry ravel,

the avalanching of loose material downslope following random perturbations such as wind and animal trampling (e.g., DiBiase et al., 2017). Distributed sources for dry ravel constitute small sediment dams behind vegetation, which are catastrophically released during and immediately following wildfire. This cycle of dry ravel pulse following fire is well-documented in the Transverse Ranges of southern California (e.g., Florsheim et al., 1991, 2016; Lamb et al., 2011) and is shown to be an important entrainment source of debris flows during subsequent runoff events (Prancevic et al., 2014; DiBiase and Lamb, 2020).

1.1.3. Shallow landslides: Wildfire commonly kills a significant amount of vegetation, resulting in the loss of soil root cohesion. This results in decreased shear strength and an increase in the prevalence of shallow landslides when soils become saturated during long, intense storm events. However, this process usually does not occur until a few years following the fire, following the partial recovery of soil infiltration and sufficient time for root decay to occur (Rengers et al., 2020; Terwilliger and Waldron, 1991).

1.1.4. Post-fire debris flows: In the presence of intense rainfall, such as precipitation that is orographically-enhanced in mountainous terrain, the combination of increased sediment availability and runoff amplification can lead to *runoff-generated debris flows* (Cannon et al. , 2003; Kean et al., 2011; Schmidt et al., 2011; Staley et al., 2014). Debris flows are highly energetic non-Newtonian fluids composed of approximately equal volumes of sediment and water, making them very effective at running out long distances and entraining more material along their flow paths (Iverson, 1997). Runoff-generated debris flows can form from the progressive entrainment of material upstream. These differ from debris flows that occur outside **recently** burned areas, which are usually created from

rainfall-triggered slope failures that can be traced easily back to their source (e.g., Tillery & Rengers, 2019; Montgomery & Dietrich, 1994).

1.1.5. **Channel erosion:** Runoff amplified from hillslopes and flows that have transitioned into debris flows can end up carving new channels (also referred to as gullies) in previously unchannelized valleys and mobilize material on the beds of preexisting channels and entrain material via bank erosion. The age of these deposits may be as young as the fire itself (as in the dry ravel example above [Lamb et al., 2011]) or they may be composed of material pre-dating the fire that has been delivered from upstream or locally from the hillslope (Cannon et al., 2001) or a mixture of both.

1.1.6. **Downstream deposition:** In higher-order channels where slopes decrease and channels become less confined, debris and sediment entrained in the uplands can be deposited within the channel, or along a floodplain if one exists, significantly altering landforms and the ecological function of these landscapes (Brogan et al., 2019; Chin et al., 2019). Following hydrologic recovery of upstream contributing areas and a concomitant decrease in sediment supply, this material will be reworked by more sediment-starved flows (e.g., Moody, 2017), potentially elevating sediment flux for many years to decades following fire. In the case of very large sediment pulses, channel incision may result in the abandonment and stabilization of this material, forming a river terrace (Pierce & Meyer, 2008). Large debris flows created during very intense rainfall can traverse through channel networks and deposit on slopes in alluvial fans (e.g., Kean et al., 2019; Santi et al., 2008).

Erosive processes outlined above act to supply sediment to overland flow simultaneously during runoff events, making it difficult to derive a complete process-based understanding of post-fire erosion. The relative contribution of each depends on a variety of factors including: the

magnitude of the storm event and the total amount of sediment available in different process domains, which is a function of prior storm history that may act to deplete sediment and the degree of vegetation regrowth that acts to stabilize sediment sources. **These complicated and transient dynamics highlight the need for more detailed observations of runoff and sediment transport in wildfire-affected landscapes across many temporal and spatial scales to further our mechanistic understanding of this chain of processes.**

1.2. Research Aims of Chapters 2-4

This dissertation is ordered by the spatial (and by extension temporal) scale of inquiry (Fig 1B). In Chapter 2, we are interested in understanding the relative contributions of net erosion on hillslopes from shallower erosional processes such as inter-rill and rill erosion versus more incisional erosion in colluvial hollows and channels and how this might evolve from storm-to-storm. In Chapter 3, we expand out from this scale to explore similar processes across headwater channel networks with the goal of understanding sediment availability in colluvial hollows and valley bottoms. In Chapter 4, we explore the whole sediment cascade from source-to-sink and consider its impacts on a freshwater system downstream. These results are summarized and placed in the context of the field in Chapter 5.
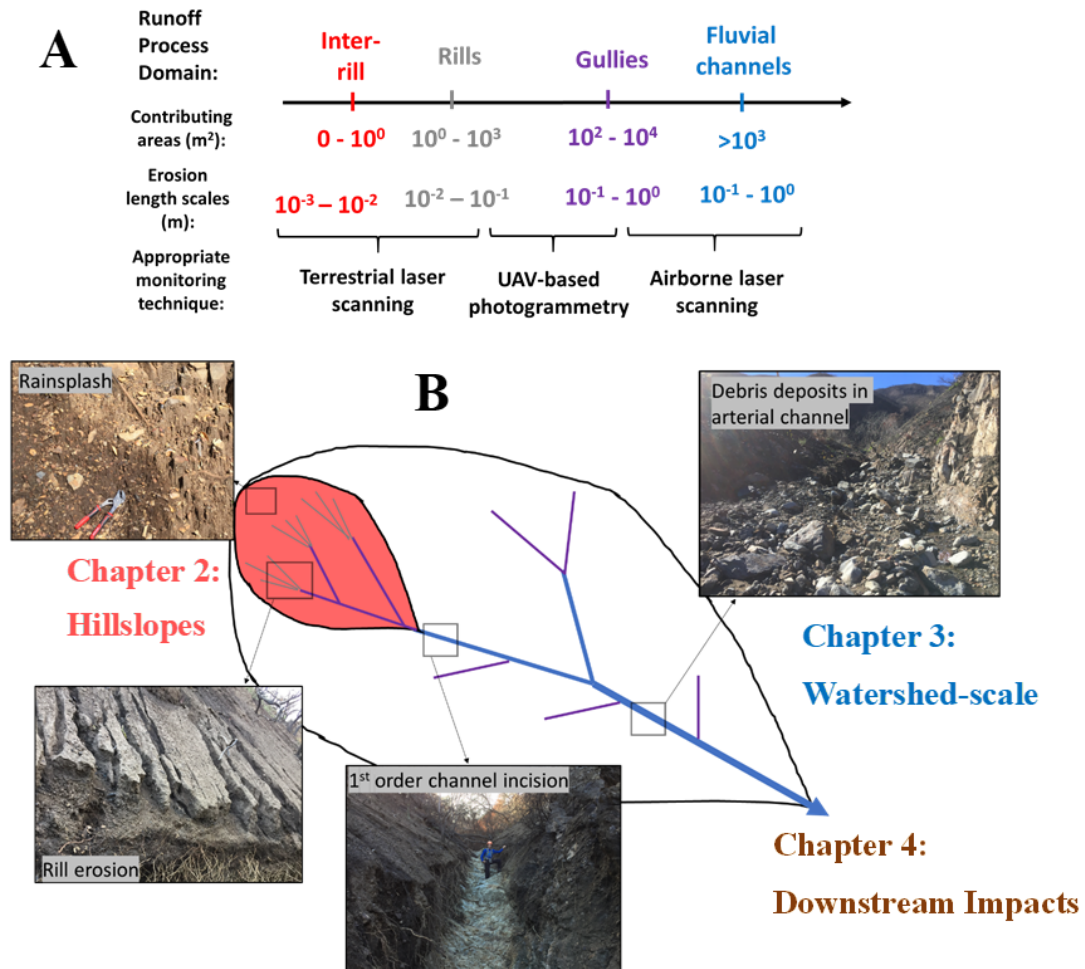
Figure 1.1. Schematic representation of scales and processes represented in this dissertation. **A.** Surface change detection across scales is used widely in all chapters and this shows plot shows the types of remote sensing applied. **B.** A non-exhaustive watershed schematic showing relevant process domains of the postfire sediment cascade and their relevant scale. Studies in this dissertation are placed in the approximate spatial scale of these domains.

Chapter 1 References

Alessio, P., Dunne, T., & Morell, K. D. (2021). Post-wildfire Generation of Debris-flow Slurry by Rill Erosion on Colluvial Hillslopes. *ESSOAR Pre-Print Archive*

Atchley, A. L., Kinoshita, A. M., Lopez, S. R., Trader, L., & Middleton, R. (2018). Simulating Surface and Subsurface Water Balance Changes Due to Burn Severity. *Vadose Zone Journal*, *17*(1), 0. https://doi.org/10.2136/vzj2018.05.0099

Barnhart, T. B., & Crosby, B. T. (2013). Comparing two methods of surface change detection on an evolving thermokarst using high-temporal-frequency terrestrial laser scanning, Selawik River, Alaska. *Remote Sensing*, *5*(6), 2813–2837. https://doi.org/10.3390/rs5062813

Benavides-Solorio, J., & MacDonald, L. H. (2001). Post-fire runoff and erosion from simulated rainfall on small plots, Colorado Front Range. *Hydrological Processes*, *15*(15), 2931–2952. https://doi.org/10.1002/hyp.383

Bodí, M. B., Martin, D. A., Balfour, V. N., Santín, C., Doerr, S. H., Pereira, P., Cerdà, A., & Mataix-Solera, J. (2014). Wildland fire ash: Production, composition and eco-hydro-geomorphic effects. *Earth-Science Reviews*, *130*, 103–127. https://doi.org/10.1016/j.earscirev.2013.12.007

Bowman, D. M. J. S., Balch, J., Artaxo, P., Bond, W. J., Cochrane, M. A., D'Antonio, C. M., Defries, R., Johnston, F. H., Keeley, J. E., Krawchuk, M. A., Kull, C. A., Mack, M., Moritz, M. A., Pyne, S., Roos, C. I., Scott, A. C., Sodhi, N. S., & Swetnam, T. W. (2011). The human dimension of fire regimes on Earth. *Journal of Biogeography*, *38*(12), 2223–2236. https://doi.org/10.1111/j.1365-2699.2011.02595.x

Brogan, D. J., Nelson, P. A., & MacDonald, L. H. (2019). Spatial and temporal patterns of sediment storage and erosion following a wildfire and extreme flood. *Earth Surface Dynamics*, *7*(2), 563–590. https://doi.org/10.5194/esurf-7-563-2019

Campos, I., Vale, C., Abrantes, N., Keizer, J. J., & Pereira, P. (2015). Effects of wildfire on mercury mobilisation in eucalypt and pine forests. *Catena*, *131*, 149–159. https://doi.org/10.1016/j.catena.2015.02.024

Cannon, S. H., Kirkham, R. M., & Parise, M. (2001). Wildfire-related debris-flow initiation processes, Storm King Mountain, Colorado. *Geomorphology*, *39*(3–4), 171–188. https://doi.org/10.1016/S0169-555X(00)00108-2

Cannon, Susan H., Boldt, E. M., Laber, J. L., Kean, J. W., & Staley, D. M. (2011). Rainfall intensity-duration thresholds for postfire debris-flow emergency-response planning. *Natural Hazards*, *59*(1), 209–236. https://doi.org/10.1007/s11069-011-9747-2

Cannon, Susan H., Gartner, J. E., Rupert, M. G., Michael, J. A., Rea, A. H., & Parrett, C. (2010). Predicting the probability and volume of postwildfire debris flows in the intermountain western United States. *Bulletin of the Geological Society of America*, *122*(1–2), 127–144. https://doi.org/10.1130/B26459.1

Cannon, Susan H., Gartner, J. E., Wilson, R. C., Bowers, J. C., & Laber, J. L. (2008). Storm rainfall conditions for floods and debris flows from recently burned areas in southwestern Colorado and southern California. *Geomorphology*, *96*(3–4), 250–269. https://doi.org/10.1016/j.geomorph.2007.03.019

Cattau, M. E., Wessman, C., Mahood, A., & Balch, J. K. (2020). Anthropogenic and lightning-started fires are becoming larger and more frequent over a longer season length in the U.S.A. *Global Ecology and Biogeography*, *29*(4), 668–681. https://doi.org/10.1111/geb.13058

Chin, A., Solverson, A. P., O'Dowd, A. P., Florsheim, J. L., Kinoshita, A. M., Nourbakhshbeidokhti, S., Sellers, S. M., Tyner, L., & Gidley, R. (2019). Interacting geomorphic and ecological response of step-pool streams after wildfire. *Bulletin of the Geological Society of America*, *131*(9–10), 1480–1500. https://doi.org/10.1130/B35049.1

Collins, B. D., Oakley, N. S., Perkins, J. P., East, A. E., Corbett, S. C., & Hatchett, B. J. (2020). Linking Mesoscale Meteorology With Extreme Landscape Response: Effects of Narrow Cold Frontal Rainbands (NCFR). *Journal of Geophysical Research: Earth Surface*, *125*(10), 1–19. https://doi.org/10.1029/2020JF005675

Coombs, J. S., & Melack, J. M. (2013). Initial impacts of a wildfire on hydrology and suspended sediment and nutrient export in California chaparral watersheds. *Hydrological Processes*, *27*(26), 3842–3851. https://doi.org/10.1002/hyp.9508

Cox, R. D., Preston, K. L., Johnson, R. F., Minnich, R. A., & Allen, E. B. (2014). Influence of landscape-scale variables on vegetation conversion to exotic annual grassland in southern California, USA. *Global Ecology and Conservation*, *2*, 190–203. https://doi.org/10.1016/j.gecco.2014.09.008

Crozier, M. J. (1999). Prediction of rainfall-triggered landslides: A test of the antecedent water status model. *Earth Surface Processes and Landforms*, *24*(9), 825–833. https://doi.org/10.1002/(SICI)1096-9837(199908)24:9<825::AID-ESP14>3.0.CO;2-M

Dibiase, R. A., Heimsath, A. M., & Whipple, K. X. (2012). Hillslope response to tectonic forcing in threshold landscapes. *Earth Surface Processes and Landforms*, *37*(8), 855–865. https://doi.org/10.1002/esp.3205

Dibiase, R. A., & Lamb, M. P. (2013). Vegetation and wildfire controls on sediment yield in bedrock landscapes. *Geophysical Research Letters*, *40*(6), 1093–1097. https://doi.org/10.1002/grl.50277

DiBiase, R. A., & Lamb, M. P. (2020). Dry sediment loading of headwater channels fuels post-wildfire debris flows in bedrock landscapes. *Geology*, *48*(2), 189–193. https://doi.org/10.1130/G46847.1

DiBiase, R. A., Whipple, K. X., Heimsath, A. M., & Ouimet, W. B. (2010). Landscape form and millennial erosion rates in the San Gabriel Mountains, CA. *Earth and Planetary Science Letters*, *289*(1–2), 134–144. https://doi.org/10.1016/j.epsl.2009.10.036

Donato, D. C., Fontaine, J. B., Campbell, J. L., Robinson, W. D., Kauffman, J. B., & Law, B. E. (2006). Post-wildfire logging hinders regeneration and increases fire risk. *Science*, *311*(5759), 352. https://doi.org/10.1126/science.1122855

Ebel, B. A., & Martin, D. A. (2017). Meta-analysis of field-saturated hydraulic conductivity recovery following wildland fire: Applications for hydrologic model parameterization and resilience assessment. *Hydrological Processes*, *31*(21), 3682–3696. https://doi.org/10.1002/hyp.11288

Ebel, B. A., & Moody, J. A. (2020). Parameter estimation for multiple post-wildfire hydrologic models. *Hydrological Processes*, *34*(21), 4049–4066. https://doi.org/10.1002/hyp.13865

Ebel, B. A., Moody, J. A., & Martin, D. A. (2012). Hydrologic conditions controlling runoff generation immediately after wildfire. *Water Resources Research*, *48*(3), 1–13. https://doi.org/10.1029/2011WR011470

Ellett, N. G., Pierce, J. L., & Glenn, N. F. (2019). Partitioned by process: Measuring post-fire debris-flow and rill erosion with Structure from Motion photogrammetry. *Earth Surface Processes and Landforms*, *44*(15), 3128–3146. https://doi.org/10.1002/esp.4728

Florsheim, J. L., Pellerin, B. a., Oh, N. H., Ohara, N., Bachand, P. a M., Bachand, S. M., Bergamaschi, B. a., Hernes, P. J., & Kavvas, M. L. (2011). From deposition to erosion: Spatial and temporal variability of sediment sources, storage, and transport in a small agricultural watershed. *Geomorphology*, *132*(3–4), 272–286. https://doi.org/10.1016/j.geomorph.2011.04.037

Florsheim, Joan L, & Gaffney, K. (2013). *Thresholds of stability in incised " Anthropocene " landscapes. October*. https://doi.org/10.1016/j.ancene.2013.10.006

Furbish, D. J., Roering, J. J., Doane, T. H., Roth, D. L., Williams, S. G. W., & Abbott, A. M. (2021). Rarefied particle motions on hillslopes - Part 1: Theory. *Earth Surface Dynamics*, *9*(3), 539–576. https://doi.org/10.5194/esurf-9-539-2021

Gabet, E. J. (2003). Sediment transport by dry ravel. *Journal of Geophysical Research: Solid Earth*, *108*(B1), 1–8. https://doi.org/10.1029/2001JB001686

Gabet, E. J., & Dunne, T. (2002). Landslides on coastal sage-scrub and grassland hillslopes in a severe El Niño winter: The effects of vegetation conversion on sediment delivery. *Bulletin of the Geological Society of America*, *114*(8), 983–990. https://doi.org/10.1130/0016-7606(2002)114<0983:LOCSSA>2.0.CO;2

Gao, P. (2013). Rill and Gully Development Processes. *Treatise on Geomorphology*, *7*, 122–131. https://doi.org/10.1016/j.physc.2009.10.149

Gartner, J. E., Cannon, S. H., & Santi, P. M. (2014). Empirical models for predicting volumes of sediment deposited by debris flows and sediment-laden floods in the transverse ranges of southern California. *Engineering Geology*, *176*, 45–56. https://doi.org/10.1016/j.enggeo.2014.04.008

Guilinger, J. J., Gray, A. B., Barth, N. C., & Fong, B. T. (2020). The Evolution of Sediment Sources Over a Sequence of Postfire Sediment-Laden Flows Revealed Through Repeat High-Resolution Change Detection. *Journal of Geophysical Research: Earth Surface*, *125*(10), 1–23. https://doi.org/10.1029/2020JF005527

Hungr, O., McDougall, S., & Bovis, M. (2007). Entrainment of material by debris flows. *Debris-Flow Hazards and Related Phenomena*, 135–158. https://doi.org/10.1007/3-540-27129-5_7

Hunsinger, G. B., Mitra, S., Warrick, J. A., & Alexander, C. R. (2008). Oceanic loading of wildfire-derived organic compounds from a small mountainous river. *Journal of Geophysical Research: Biogeosciences*, *113*(2), 1–14. https://doi.org/10.1029/2007JG000476

Iverson, R. M. (1997). of Debris. *American Geophysical Union*, *97*, 245–296.

Jackson, M., & Roering, J. J. (2009). Post-fire geomorphic response in steep, forested landscapes: Oregon Coast Range, USA. *Quaternary Science Reviews*, *28*(11–12), 1131–1146. https://doi.org/10.1016/j.quascirev.2008.05.003

Kampf, S. K., Brogan, D. J., Schmeer, S., MacDonald, L. H., & Nelson, P. A. (2016). How do geomorphic effects of rainfall vary with storm type and spatial scale in a post-fire landscape? *Geomorphology*, *273*, 39–51. https://doi.org/10.1016/j.geomorph.2016.08.001

Kean, J. W., Staley, D. M., Lancaster, J. T., Rengers, F. K., Swanson, B. J., Coe, J. A., Hernandez, J. L., Sigman, A. J., Allstadt, K. E., & Lindsay, D. N. (2019). Inundation, flow dynamics, and damage in the 9 January 2018 Montecito debris-flow event, California, USA: Opportunities and challenges for post-wildfire risk assessment. *Geosphere*, *15*(4), 1140–1163. https://doi.org/10.1130/GES02048.1

Kean, Jason W., & Staley, D. M. (2021). Forecasting the Frequency and Magnitude of Postfire Debris Flows Across Southern California. *Earth's Future*, *9*(3). https://doi.org/10.1029/2020EF001735

Kean, Jason W., Staley, D. M., & Cannon, S. H. (2011). In situ measurements of post-fire debris flows in southern California: Comparisons of the timing and magnitude of 24 debris-flow events with rainfall and soil moisture conditions. *Journal of Geophysical Research: Earth Surface*, *116*(4), 1–21. https://doi.org/10.1029/2011JF002005

Kean, Jason W., Staley, D. M., Leeper, R. J., Schmidt, K. M., & Gartner, J. E. (2012). A low-cost method to measure the timing of postfire flash floods and debris flows relative to rainfall. *Water Resources Research*, *48*(5), 1–8. https://doi.org/10.1029/2011WR011460

Keeley, J. E., & Fotheringham, C. J. (2001). Historic fire regime in southern California shrublands. *Conservation Biology*, *15*(6), 1536–1548. https://doi.org/10.1046/j.1523-1739.2001.00097.x

Keeley, J. E., Franklin, J., & Antonio, C. D. (2011). *The Landscape Ecology of Fire | Donald McKenzie | Springer*. 193–221. https://doi.org/10.1007/978-94-007-0301-8

Keeley, J. E., & Pausas, J. G. (2019). Distinguishing disturbance from perturbations in fire-prone ecosystems. *International Journal of Wildland Fire*, *28*(4), 282–287. https://doi.org/10.1071/WF18203

Keeley, J. E., & Syphard, A. D. (2019). Twenty-first century California, USA, wildfires: fuel-dominated vs. wind-dominated fires. *Fire Ecology*, *15*(1). https://doi.org/10.1186/s42408-019-0041-0

Kinoshita, A. M., & Hogue, T. S. (2015). Increased dry season water yield in burned watersheds in Southern California. *Environmental Research Letters*, *10*(1). https://doi.org/10.1088/1748-9326/10/1/014003

Kirby, M. E., Poulsen, C. J., Lund, S. P., Patterson, W. P., Reidy, L., & Hammond, D. E. (2004). Late Holocene lake level dynamics inferred from magnetic susceptibility and stable oxygen isotope data: Lake Elsinore, southern California (USA). *Journal of Paleolimnology*, *31*(3), 275–293. https://doi.org/10.1023/B:JOPL.0000021710.39800.f6

Lague, D., Brodu, N., Leroux, J., Rennes, G., Rennes, U., & Beaulieu, C. De. (n.d.). *Accurate 3D comparison of complex topography with terrestrial laser scanner : application to the Rangitikei canyon (N-Z). February 2013*, 1–28.

Lamb, M. P., Scheingross, J. S., Amidon, W. H., Swanson, E., & Limaye, A. (2011). A model for fire-induced sediment yield by dry ravel in steep landscapes. *Journal of Geophysical Research: Earth Surface*, *116*(3), 1–13. https://doi.org/10.1029/2010JF001878

Larsen, I. J., MacDonald, L. H., Brown, E., Rough, D., Welsh, M. J., Pietraszek, J. H., Libohova, Z., de Dios Benavides-Solorio, J., & Schaffrath, K. (2009). Causes of Post-Fire Runoff and Erosion: Water Repellency, Cover, or Soil Sealing? *Soil Science Society of America Journal*, *73*(4), 1393. https://doi.org/10.2136/sssaj2007.0432

Lavé, J., & Burbank, D. W. (2004). Denudation processes and rates in the Transverse Ranges, southern California: Erosional response of a transitional landscape to external and anthropogenic forcing. *Journal of Geophysical Research*, *109*(F1), F01006. https://doi.org/10.1029/2003JF000023

Liu, T., McGuire, L. A., Wei, H., Rengers, F. K., Gupta, H., Ji, L., & Goodrich, D. C. (2021). The timing and magnitude of changes to Hortonian overland flow at the watershed scale during the post-fire recovery process. *Hydrological Processes*, *35*(5), 1–18. https://doi.org/10.1002/hyp.14208

Lu, M., Ikejiri, T., & Lu, Y. H. (2021). A synthesis of the Devonian wildfire record: Implications for paleogeography, fossil flora, and paleoclimate. *Palaeogeography, Palaeoclimatology, Palaeoecology*, *571*(February), 110321. https://doi.org/10.1016/j.palaeo.2021.110321

MacDonald, L. H., & Larsen, I. J. (2009). Runoff and Erosion from Wildfires and Roads: Effects and Mitigation, ch 9. *Land Restoration to Combat Desertification: Innovative Approaches, Quality Control and Project Evaluation , Dissmeyer 2000*, 145–167.

Martinez, D., & Anderson, M. A. (2013). Methane production and ebullition in a shallow, artificially aerated, eutrophic temperate lake (Lake Elsinore, CA). *Science of the Total Environment*, *454–455*, 457–465. https://doi.org/10.1016/j.scitotenv.2013.03.040

McCoy, S. W., Kean, J. W., Coe, J. A., Staley, D. M., Wasklewicz, T. A., & Tucker, G. E. (2010). Evolution of a natural debris flow: In situ measurements of flow dynamics, video imagery, and terrestrial laser scanning. *Geology*, *38*(8), 735–738. https://doi.org/10.1130/G30928.1

McGuire, L. A., Kean, J. W., Staley, D. M., Rengers, F. K., & Wasklewicz, T. A. (2016). Constraining the relative importance of raindrop- and flow-driven sediment transport mechanisms in postwildfire environments and implications for recovery time scales. *Journal of Geophysical Research: Earth Surface*, *121*(11), 2211–2237. https://doi.org/10.1002/2016JF003867

McGuire, L. A., Rengers, F. K., Kean, J. W., & Staley, D. M. (2017). Debris flow initiation by runoff in a recently burned basin: Is grain-by-grain sediment bulking or en masse failure to blame? *Geophysical Research Letters*, *44*(14), 7310–7319. https://doi.org/10.1002/2017GL074243

McGuire, L. A., Rengers, F. K., Kean, J. W., Staley, D. M., & Mirus, B. B. (2018). Incorporating spatially heterogeneous infiltration capacity into hydrologic models with applications for simulating post-wildfire debris flow initiation. *Hydrological Processes*, *32*(9), 1173–1187. https://doi.org/10.1002/hyp.11458

McPhee, J. (1988). The control of nature: Los Angeles against the mountains. New Yorker Magazine, Incorporated.

Mensing, S. A., Michaelsen, J., & Byrne, R. (1999). *142-1999-A 560-year record of Santa Ana fires reconstructed from charcoal deposited in the Santa Barbara Basin.pdf*. *305*, 295–305.

Miller, M. E., MacDonald, L. H., Robichaud, P. R., & Elliot, W. J. (2011). Predicting post-fire hillslope erosion in forest lands of the western United States. *International Journal of Wildland Fire*, *20*(8), 982–999. https://doi.org/10.1071/WF09142

Minnich, R. A. (1983). Fire Mosaics in Southern California and Northern Baja California. In *Science* (Vol. 219, Issue 4590, pp. 1287–1294). https://doi.org/10.1126/science.219.4590.1287

Mirus, B. B., & Loague, K. (2013). How runoff begins (and ends): Characterizing hydrologic response at the catchment scale. *Water Resources Research*, *49*(5), 2987–3006. https://doi.org/10.1002/wrcr.20218

Montgomery, D. R., & Dietrich, W. E. (1994). A physically based model for the topographical control on shallow landsliding. *Water Resources Research*, *30*(4), 1153–1171. https://doi.org/10.1029/93WR02979

Montgomery, D. R., Schmidt, K. M., Greenberg, H. M., & Dietrich, W. E. (2000). Forest clearing and regional landsliding. *Geology*, *28*(4), 311–314. https://doi.org/10.1130/0091-7613(2000)28<311:FCARL>2.0.CO;2

Moody, J. A. (2017). Residence times and alluvial architecture of a sediment superslug in response to different flow regimes. *Geomorphology*, *294*(April), 40–57. https://doi.org/10.1016/j.geomorph.2017.04.012

Moody, J. A., & Ebel, B. A. (2014). Infiltration and runoff generation processes in fire-affected soils. *Hydrological Processes*, *28*(9), 3432–3453. https://doi.org/10.1002/hyp.9857

Moody, J. A., Ebel, B. A., Nyman, P., Martin, D. A., Stoof, C., & Mckinley, R. (2016). Relations between soil hydraulic properties and burn severity. *International Journal of Wildland Fire*, *25*(3), 279–293. https://doi.org/10.1071/WF14062

Moody, J. A., & Martin, D. A. (2001). Initial hydrologic and geomorphic response following a wildfire in the Colorado front range. *Earth Surface Processes and Landforms*, *26*(10), 1049–1070. https://doi.org/10.1002/esp.253

Moody, J. A., & Martin, D. A. (2009). Synthesis of sediment yields after wildland fire in different rainfall regimes in the western United States. *International Journal of Wildland Fire*, *18*(1), 96–115. https://doi.org/10.1071/WF07162

Moody, J. A., & Martin, R. G. (2015). Measurements of the initiation of post-wildfire runoff during rainstorms using in situ overland flow detectors. *Earth Surface Processes and Landforms*, *40*(8), 1043–1056. https://doi.org/10.1002/esp.3704

Moody, J. A., Shakesby, R. A., Robichaud, P. R., Cannon, S. H., & Martin, D. A. (2013). Current research issues related to post-wildfire runoff and erosion processes. *Earth-Science Reviews*, *122*, 10–37. https://doi.org/10.1016/j.earscirev.2013.03.004

Murphy, B. P., Czuba, J. A., & Belmont, P. (2019). Post-wildfire sediment cascades: A modeling framework linking debris flow generation and network-scale sediment routing. *Earth Surface Processes and Landforms*, *44*(11), 2126–2140. https://doi.org/10.1002/esp.4635

Murphy, B. P., Yocom, L. L., & Belmont, P. (2018). Beyond the 1984 Perspective: Narrow Focus on Modern Wildfire Trends Underestimates Future Risks to Water Security. *Earth's Future*, *6*(11), 1492–1497. https://doi.org/10.1029/2018EF001006

Murphy, S. F., McCleskey, R. B., Martin, D. A., Holloway, J. A. M., & Writer, J. H. (2020). Wildfire-driven changes in hydrology mobilize arsenic and metals from legacy mine waste. *Science of the Total Environment*, *743*, 140635. https://doi.org/10.1016/j.scitotenv.2020.140635

Neely, A. B., & DiBiase, R. A. (2020). Drainage Area, Bedrock Fracture Spacing, and Weathering Controls on Landscape-Scale Patterns in Surface Sediment Grain Size. *Journal of Geophysical Research: Earth Surface*, *125*(10), 1–22. https://doi.org/10.1029/2020JF005560

Neris, J., Santin, C., Lew, R., Robichaud, P. R., Elliot, W. J., Lewis, S. A., Sheridan, G., Rohlfs, A. M., Ollivier, Q., Oliveira, L., & Doerr, S. H. (2021). Designing tools to predict and mitigate impacts on water quality following the Australian 2019/2020 wildfires: Insights from Sydney's largest water supply catchment. *Integrated Environmental Assessment and Management*, *00*(00), 1–11. https://doi.org/10.1002/ieam.4406

Nyman, P., Sheridan, G. J., Moody, J. A., Smith, H. G., Noske, P. J., & Lane, P. N. J. (2013). Sediment availability on burned hillslopes. *Journal of Geophysical Research: Earth Surface*, *118*(4), 2451–2467. https://doi.org/10.1002/jgrf.20152

Nyman, P., Sheridan, G. J., Smith, H. G., & Lane, P. N. J. (2014). Modeling the effects of surface storage, macropore flow and water repellency on infiltration after wildfire. *Journal of Hydrology*, *513*, 301–313. https://doi.org/10.1016/j.jhydrol.2014.02.044

Odigie, K. O., & Flegal, A. R. (2011). Pyrogenic remobilization of historic industrial lead depositions. *Environmental Science and Technology*, *45*(15), 6290–6295. https://doi.org/10.1021/es200944w

Odigie, K. O., Khanis, E., Hibdon, S. A., Jana, P., Araneda, A., Urrutia, R., & Flegal, A. R. (2016). Remobilization of trace elements by forest fire in Patagonia, Chile. *Regional Environmental Change*, *16*(4), 1089–1096. https://doi.org/10.1007/s10113-015-0825-y

Orem, C. A., & Pelletier, J. D. (2015). Quantifying the time scale of elevated geomorphic response following wildfires using multi-temporal LiDAR data: An example from the Las Conchas fire, Jemez Mountains, New Mexico. *Geomorphology*, *232*, 224–238. https://doi.org/10.1016/j.geomorph.2015.01.006

Overpeck, J. T., & Udall, B. (2020). Climate change and the aridification of North America. *Proceedings of the National Academy of Sciences of the United States of America*, *117*(22), 11856–11858. https://doi.org/10.1073/pnas.2006323117

Palucis, M. C., Ulizio, T. P., & Lamb, M. P. (2021). Debris flow initiation from ravel-filled channel bed failure following wildfire in a bedrock landscape with limited sediment supply. *GSA Bulletin*, 1–18. https://doi.org/10.1130/b35822.1

Parsons, A., Robichaud, P. R., Lewis, S. A., Napper, C., & Clark, J. T. (2010). Field guide for mapping post-fire soil burn severity. *USDA Forest Service - General Technical Report RMRS-GTR*, *243*, 1–49. https://doi.org/10.2737/RMRS-GTR-243

Passalacqua, P., Belmont, P., Staley, D. M., Simley, J. D., Arrowsmith, J. R., Bode, C. A., Crosby, C., Delong, S. B., Glenn, N. F., Kelly, S. A., Lague, D., Sangireddy, H., Schaffrath, K., Tarboton, D. G., Wasklewicz, T., & Wheaton, J. M. (2015). Earth-Science Reviews Analyzing high resolution topography for advancing the understanding of mass and energy transfer through landscapes : A review. *Earth Science Reviews*, *148*, 174–193. https://doi.org/10.1016/j.earscirev.2015.05.012

Pelletier, J. D., & Orem, C. A. (2014). How do sediment yields from post-wildfire debris-laden flows depend on terrain slope, soil burn severity class, and drainage basin area? Insights from airborne-LiDAR change detection. *Earth Surface Processes and Landforms*, *39*(13), 1822–1832. https://doi.org/10.1002/esp.3570

Pierce, J. L., Meyer, G. a, & Jull, a J. T. (2004). Fire-induced erosion and millennial- scale climate change in northern ponderosa pine forests. *Nature*, *432*(November), 87–90. https://doi.org/10.1038/nature03028.Published

Pierce, J. M. G. (2008). Long-term fire history from alluvial fan sediments: the role of drought and climate. *International Journal of Wildland Fire; 2008*, *17*(1), 84–95.

Poon, P. K., & Kinoshita, A. M. (2018). Spatial and temporal evapotranspiration trends after wildfire in semi-arid landscapes. *Journal of Hydrology*, *559*, 71–83. https://doi.org/10.1016/j.jhydrol.2018.02.023

Radeloff, V. C., Helmers, D. P., Kramer, H. A., Mockrin, M. H., Alexandre, P. M., Bar-Massada, A., Butsic, V., Hawbaker, T. J., Martinuzzi, S., Syphard, A. D., & Stewart, S. I. (2018). Rapid growth of the US wildland-urban interface raises wildfire risk. *Proceedings of the National Academy of Sciences*, *115*(13), 3314–3319. https://doi.org/10.1073/pnas.1718850115

Ralph, F. M., & Dettinger, M. D. (2011). Storms, floods, and the science of atmospheric rivers. *Eos*, *92*(32), 265–266. https://doi.org/10.1029/2011EO320001

Raymond, C. A., McGuire, L. A., Youberg, A. M., Staley, D. M., & Kean, J. W. (2020). Thresholds for post-wildfire debris flows: Insights from the Pinal Fire, Arizona, USA. *Earth Surface Processes and Landforms*, *45*(6), 1349–1360. https://doi.org/10.1002/esp.4805

Reneau, S. L. (2007). *Sediment delivery after a wildfi re*. *2*, 151–154. https://doi.org/10.1130/G23288A.1

Rengers, F. K., McGuire, L. A., Kean, J. W., Staley, D. M., Dobre, M., Robichaud, P. R., & Swetnam, T. (2021). Movement of Sediment Through a Burned Landscape: Sediment Volume Observations and Model Comparisons in the San Gabriel Mountains, California, USA. *Journal of Geophysical Research: Earth Surface*, *126*(7), 1–25. https://doi.org/10.1029/2020jf006053

Rengers, Francis K., McGuire, L. A., Oakley, N. S., Kean, J. W., Staley, D. M., & Tang, H. (2020). Landslides after wildfire: initiation, magnitude, and mobility. *Landslides*, *17*(11), 2631–2641. https://doi.org/10.1007/s10346-020-01506-3

Rickson, R. J. (2010). Fire Effects on Soils and Restoration Strategies. Edited by A. Cerda and P. R. Robichaud. Enfield, NH, USA: Science Publishers (2009), pp. 589, £85.00. ISBN 978-1-57808-526-2. *Experimental Agriculture*, *46*(02), 260. https://doi.org/10.1017/S0014479709990913

Riley, K., Pierce, J., & Meyer, G. A. (2015). Vegetative and climatic controls on Holocene wildfire and erosion recorded in alluvial fans of the Middle Fork Salmon River, Idaho. *Holocene*, *25*(5), 857–871. https://doi.org/10.1177/0959683615571423

Robinne, F. N., Hallema, D. W., Bladon, K. D., Flannigan, M. D., Boisramé, G., Bréthaut, C. M., Doerr, S. H., Di Baldassarre, G., Gallagher, L. A., Hohner, A. K., Khan, S. J., Kinoshita, A. M., Mordecai, R., Nunes, J. P., Nyman, P., Santín, C., Sheridan, G., Stoof, C. R., Thompson, M. P., … Wei, Y. (2021). Scientists' warning on extreme wildfire risks to water supply. *Hydrological Processes*, *35*(5), 0–3. https://doi.org/10.1002/hyp.14086

Roth, D. L., Doane, T. H., Roering, J. J., Furbish, D. J., & Zettler-Mann, A. (2020). Particle motion on burned and vegetated hillslopes. *Proceedings of the National Academy of Sciences of the United States of America*, *117*(41), 25335–25343. https://doi.org/10.1073/pnas.1922495117

Sankey, J. B., Germino, M. J., & Glenn, N. F. (2009). Aeolian sediment transport following wildfire in sagebrush steppe. *Journal of Arid Environments*, *73*(10), 912–919. https://doi.org/10.1016/j.jaridenv.2009.03.016

Sankey, Joel B., Kreitler, J., Hawbaker, T. J., McVay, J. L., Miller, M. E., Mueller, E. R., Vaillant, N. M., Lowe, S. E., & Sankey, T. T. (2017). Climate, wildfire, and erosion ensemble foretells more sediment in western USA watersheds. *Geophysical Research Letters*, *44*(17), 8884–8892. https://doi.org/10.1002/2017GL073979

Santi, P. M., deWolfe, V. G., Higgins, J. D., Cannon, S. H., & Gartner, J. E. (2008). Sources of debris flow material in burned areas. *Geomorphology*, *96*(3–4), 310–321. https://doi.org/10.1016/j.geomorph.2007.02.022

Santi, P. M., & MacAulay, B. (2019). Rainfall intensity limitation and sediment supply independence of post-wildfire debris flows in the western U.S. *Debris-Flow Hazards Mitigation: Mechanics, Monitoring, Modeling, and Assessment - Proceedings of the 7th International Conference on Debris-Flow Hazards Mitigation*, *2005*, 539–547.

Schmidt, K. M., Roering, J. J., Stock, J. D., Dietrich, W. E., Montgomery, D. R., & Schaub, T. (2001). The variability of root cohesion as an influence on shallow landslide susceptibility in the Oregon Coast Range. *Canadian Geotechnical Journal*, *38*(5), 995–1024. https://doi.org/10.1139/cgj-38-5-995

Schmidt, Kevin M., Hanshaw, M. N., Howle, J. F., Kean, J. W., Staley, D. M., Stock, J. D., & Bawden, G. W. (2011). Hydrologic Conditions and Terrestrial Laser Scanning of Post-fire Debris Flows in the San Gabriel Mountains, CA, U.S.A. *Debris-Flow Hazards Mitigation, Mechanics, Prediction, and Assessment*, 583–593. https://doi.org/10.4408/IJEGE.2011-03.B-064

Schwanghart, W., & Kuhn, N. J. (2010). TopoToolbox: A set of Matlab functions for topographic analysis. *Environmental Modelling and Software*, *25*(6), 770–781. https://doi.org/10.1016/j.envsoft.2009.12.002

Shakesby, R. a., & Doerr, S. H. (2006). Wildfire as a hydrological and geomorphological agent. *Earth-Science Reviews*, *74*(3–4), 269–307. https://doi.org/10.1016/j.earscirev.2005.10.006

Shakesby, R. A., & Doerr, S. H. (2006). *Wildfire as a hydrological and geomorphological agent*. *74*, 269–307. https://doi.org/10.1016/j.earscirev.2005.10.006

Sklar, L. S., Riebe, C. S., Marshall, J. A., Genetti, J., Leclere, S., Lukens, C. L., & Merces, V. (2017). The problem of predicting the size distribution of sediment supplied by hillslopes to rivers. *Geomorphology*, *277*, 31–49. https://doi.org/10.1016/j.geomorph.2016.05.005

Staley, D. M., Kean, J. W., & Rengers, F. K. (2020). The recurrence interval of post-fire debris-flow generating rainfall in the southwestern United States. *Geomorphology*, *370*, 107392. https://doi.org/10.1016/j.geomorph.2020.107392

Staley, D. M., Negri, J. A., Kean, J. W., Laber, J. L., Tillery, A. C., & Youberg, A. M. (2017). Prediction of spatially explicit rainfall intensity–duration thresholds for post-fire debris-flow generation in the western United States. *Geomorphology*, *278*, 149–162. https://doi.org/10.1016/j.geomorph.2016.10.019

Staley, D. M., Wasklewicz, T. A., & Kean, J. W. (2014a). Characterizing the primary material sources and dominant erosional processes for post-fire debris-flow initiation in a headwater basin using multi-temporal terrestrial laser scanning data. *Geomorphology*, *214*, 324–338. https://doi.org/10.1016/j.geomorph.2014.02.015

Staley, D. M., Wasklewicz, T. A., & Kean, J. W. (2014b). Characterizing the primary material sources and dominant erosional processes for post-fire debris-flow initiation in a headwater basin using multi-temporal terrestrial laser scanning data. *Geomorphology*, *214*, 324–338. https://doi.org/10.1016/j.geomorph.2014.02.015

Steeplands, C., California, S., Wohlgemuth, P. M., & Hubbert, K. R. (2008). *The Effects of Fire on Soil Hydrologic Properties and Sediment Fluxes in*. 115–122.

Stein, E. D., Brown, J. S., Hogue, T. S., Burke, M. P., & Kinoshita, A. (2012). Stormwater contaminant loading following southern California wildfires. *Environmental Toxicology and Chemistry*, *31*(11), 2625–2638. https://doi.org/10.1002/etc.1994

Swain, D. L., Langenbrunner, B., Neelin, J. D., & Hall, A. (2018). Increasing precipitation volatility in twenty-first-century California. *Nature Climate Change*, *8*(5), 427–433. https://doi.org/10.1038/s41558-018-0140-y

Syphard, A. D., & Keeley, J. E. (2015). Location, timing and extent of wildfire vary by cause of ignition. *International Journal of Wildland Fire*, *24*(1), 37–47. https://doi.org/10.1071/WF14024

Syphard, A. D., & Keeley, J. E. (2020). Mapping fire regime ecoregions in California. *International Journal of Wildland Fire*, *29*(7), 595–601. https://doi.org/10.1071/WF19136

Terwilliger, V. J., & Waldron, L. J. (1991). Effects of root reinforcement on soil-slip patterns in the Transverse Ranges of southern California. *Geological Society of America Bulletin*, *103*(6), 775–785. https://doi.org/10.1130/0016-7606(1991)103<0775:EORROS>2.3.CO;2

Thomas, M. A., Rengers, F. K., Kean, J. W., McGuire, L. A., Staley, D. M., Barnhart, K. R., & Ebel, B. A. (2021). Postwildfire Soil-Hydraulic Recovery and the Persistence of Debris Flow Hazards. *Journal of Geophysical Research: Earth Surface*, *126*(6), 1–25. https://doi.org/10.1029/2021JF006091

Thompson, J. R., Spies, T. A., & Ganio, L. M. (2007). Reburn severity in managed and unmanaged vegetation in a large wildfire. *Proceedings of the National Academy of Sciences of the United States of America*, *104*(25), 10743–10748. https://doi.org/10.1073/pnas.0700229104

Warrick, J. A., Hatten, J. A., Pasternack, G. B., Gray, A. B., Goni, M. A., & Wheatcroft, R. A. (2012). The effects of wildfire on the sediment yield of a coastal California watershed. *Bulletin of the Geological Society of America*, *124*(7–8), 1130–1146. https://doi.org/10.1130/B30451.1

Warrick, Jonathan A., Melack, J. M., & Goodridge, B. M. (2015). Sediment yields from small, steep coastal watersheds of California. *Journal of Hydrology: Regional Studies*, *4*, 516–534. https://doi.org/10.1016/j.ejrh.2015.08.004

Wester, T., Wasklewicz, T., & Staley, D. (2014). Functional and structural connectivity within a recently burned drainage basin. *Geomorphology*, *206*, 362–373. https://doi.org/10.1016/j.geomorph.2013.10.011

Westerling, A. L., Hidalgo, H. G., Cayan, D. R., & Swetnam, T. W. (2006). Warming and earlier spring increase Western U.S. forest wildfire activity. *Science*, *313*(5789), 940–943. https://doi.org/10.1126/science.1128834

Wheaton, J. M., Brasington, J., Darby, S. E., & Sear, D. A. (2010). Accounting for uncertainty in DEMs from repeat topographic surveys: Improved sediment budgets. *Earth Surface Processes and Landforms*, *35*(2), 136–156. https://doi.org/10.1002/esp.1886

Wheaton, J. M., Brasington, J., Darby, S. E., Sear, D. A., Sciences, W., & Hill, O. M. (2010). *Accounting for uncertainty in DEMs from repeat topographic surveys : improved sediment budgets*. *156*(December 2009), 136–156. https://doi.org/10.1002/esp.1886

Wilder, B. A., Lancaster, J. T., Cafferata, P. H., Coe, D. B. R., Swanson, B. J., Lindsay, D. N., Short, W. R., & Kinoshita, A. M. (2021). An analytical solution for rapidly predicting post-fire peak streamflow for small watersheds in southern California. *Hydrological Processes*, *35*(1), 1–14. https://doi.org/10.1002/hyp.13976

Williams, A. P., Abatzoglou, J. T., Gershunov, A., Guzman-Morales, J., Bishop, D. A., Balch, J. K., & Lettenmaier, D. P. (2019). Observed Impacts of Anthropogenic Climate Change on Wildfire in California. *Earth's Future*, *7*(8), 892–910. https://doi.org/10.1029/2019EF001210

Williams, A. P., Abatzoglou, J. T., Gershunov, A., Guzman-Morales, J., Bishop, D. A., Balch, J. K., & Lettenmaier, D. P. (2019). Observed impacts of anthropogenic climate change on wildfire in California. *Earth's Future*, 2019EF001210. https://doi.org/10.1029/2019EF001210

Wilson, C., Kampf, S. K., Ryan, S., Covino, T., MacDonald, L. H., & Gleason, H. (2021). Connectivity of post-fire runoff and sediment from nested hillslopes and watersheds. *Hydrological Processes*, *35*(1), 1–17. https://doi.org/10.1002/hyp.13975

Chapter 2. The evolution of sediment sources over a sequence of post-fire sediment-laden flows revealed through repeat high-resolution change detection

Key Points

- Repeat change detection was employed to explore the evolution of post-fire sediment sources over a series of storms following wildfire

- Headwater channel erosion decreased significantly over time, increasing the importance of shallow hillslope sources later in the season

- Event-scale sediment fluxes decreased over the season, which was driven by declining channel sediment supply

2.1. Abstract

Post-fire debris flows are particularly complex to study because they do not form discrete initiation locations and commonly involve multiple simultaneously operating erosional processes. Although recent work has begun to elucidate a more mechanistic understanding of post-fire debris flows, there is still a paucity of detailed sediment budgets characterizing these events. In this study, we seek to understand how post-fire sediment sources and erosional processes change over multiple storm cycles. To do this, we performed repeat high-resolution change detection in a headwater catchment burned by the 2018 Holy Fire in the Santa Ana Mountains, California, USA. This included terrestrial laser scanning in a zero-order catchment (0.95 ha) and unmanned aerial vehicle structure-from-motion of a headwater channel network (up to 6.5 ha). During the initial storm events that produced runoff-generated debris flows, we found that the evacuation of dry ravel and pre-fire colluvium accounted for half of the eroded material. These initial flows also acted to clear out much of the material stored within downstream headwater channel networks. In

21

subsequent storm events of equal or greater rainfall intensity, total erosion from the study site was subdued and the relative importance of shallow hillslope erosion from inter-rill and rill erosion was increased, as has been noted in similar studies in the region. Overall, this suggests that channel sediment supplies may be more rapidly depleted than hillslope sources, which may drive a trend of decreasing sediment fluxes over time from burned headwater catchments subject to repeated runoff events.

2.2. Introduction

Wildfire is an effective disturbance agent in many mountainous catchments across the world (e.g., Moody & Martin, 2009). In the first few years following fire, large increases in surface flow partitioning, especially infiltration-excess overland flow, contribute to elevated peak discharge (Atchley et al., 2018; Kinoshita & Hogue, 2015; Moody & Martin, 2001) and sediment yields (e.g., Swanson, 1981; Wagenbrenner & Robichaud, 2014; Warrick et al., 2012; 2015; Wohlgemuth & Hubbert, 2008). Fuel buildup from modern fire suppression (Murphy et al., 2018) and the lengthening of fire seasons in a warming climate are leading to enhanced fire activity in the western US (Westerling et al., 2006; Williams et al., 2019). The societal consequence of wildfire enhancement is exacerbated by the expansion of human development into the wildland-urban interface, where the threat of fire and post-fire hazards increase the risk to lives, infrastructure, and water resources in these communities (Murphy et al., 2018; Radeloff et al., 2018; Sankey et al., 2017). Increasing fire activity in a changing climate highlights the need to further understand its role in altering surface processes and the short-term hazards they engender (Sankey et al., 2017).

Wildfire tends to alter the hydrologic functioning of watersheds by amplifying runoff generation through the reduction of infiltration capacity. Causes for this reduction include: the

22

formation or enhancement of soil water repellency at the mineral soil surface (e.g., DeBano, 1981; Doerr et al., 2006; Hubbert et al., 2006; Shakesby & Doerr, 2006), clogging of pores through ash and other organics (Onda et al., 2008), soils reaching a hyper-dry state following fire (Moody & Ebel, 2012a), and the formation of structural seals caused by unabated raindrop impacts where little surface cover exists following fire (Larsen et al., 2009; Singer & Le Bissonnais, 1998). Additionally, wildfire markedly increases the amount non-cohesive sediment available for entrainment by amplified runoff. This can be caused by the reduction of soil aggregate stability on the hillslopes (Nyman et al., 2013) and the production of easily erodible ash layers (Gabet & Sternberg, 2008). In steep settings such as those considered in this study, wildfire can greatly amplify the amount of dry ravel being introduced to the channel network (e.g., DiBiase & Lamb, 2020; Florsheim et al., 1991; Gabet et al., 2003; Lamb et al., 2011).

This increase in erodible material and overland flow production results in extensive erosion in response to moderately intense rainfall through rill, rainsplash, and sheetflow processes on hillslopes (e.g., Rengers et al., 2016; Shakesby & Doerr, 2006; Wohlgemuth & Hubbert, 2008) and increased channel scour within and downstream of a burn scar (e.g., Moody & Martin, 2001; Santi et al., 2008). In response to high intensity rainfall, even without significant total rainfall depths and return intervals as low as one to two years, runoff can rapidly erode into soil and sediment to a point where it transitions into a runoff-generated debris flow that is capable of transporting large boulders and scouring into bedrock (e.g., Cannon et al. 2001, 2005; Cannon & Gartner, 2005; Kean et al., 2011, 2013; Staley et al., 2017). These runoff-generated debris flows differ from those generated by landslides, which are triggered by decreased shear strength through soil saturation from longer duration storms (Montgomery & Dietrich, 1994). Runoff-generated debris flows convey large pulses of sediment to downstream fluvial networks (e.g., Murphy et al., 2019; Nyman et al., 2020) and can run out kilometers onto alluvial fans where they

can destroy built infrastructure and threaten lives when exceptionally intense rainfall occurs over steep, severely burned watersheds (e.g., 2018 Montecito Debris Flows documented in Kean et al., 2019).

The exact processes responsible for transitioning runoff into debris flows are less well-understood than those from landslides because it is difficult to pinpoint precise locations where post-fire debris flows begin. Different mechanisms that have been proposed and observed include: 'firehose effects' in bedrock and alpine settings (Larsen et al., 2006; McCoy et al., 2010), rapid channel bed failure (e.g., Gregoretti & Fontana, 2008; Prancevic et al., 2014; Kean et al., 2013; McGuire et al., 2017), and the progressive bulking of flows through hillslope erosion and channel scour (e.g., Cannon et al., 2001; Gabet & Sternberg, 2008; Santi et al., 2008, 2013). Recent work coupling high resolution change detection and hydrologic monitoring show that hillslope sediment sources may be an important factor in many debris flow events (e.g., Staley et al., 2014; Rengers & McGuire, 2018). However, numerical modeling coupled with high resolution change detection reveal that the best predictor of debris flow initiation appears to be from channel bed failure following the exceedance of hydrodynamic thresholds (McGuire et al., 2016, 2017; Tang et al., 2019). There has been a great deal of recent progress in our understanding of post-fire debris flows and sediment-laden runoff, but the logistical hurdles involved with quickly obtaining data in rapidly-evolving post-fire settings has resulted in a paucity of direct observations and detailed measurements of post-wildfire debris flows (e.g., Schmidt et al., 2011; Staley et al., 2014) and other forms of post-fire runoff (e.g., Rengers et al., 2016; DeLong et al., 2018). These measurements are necessary to expand our knowledge of the mechanistic controls on post-fire erosional responses considering the significant natural variability that exists in fire-disturbed landscapes (Moody et al., 2013). Although inferred from previous studies (e.g., Kean et al., 2011; Wells & Wade, 1987), the role of decreasing sediment

availability can now be explored more fully with the use of high resolution change detection techniques such as terrestrial laser scanning (herein referred to as TLS) (e.g., Schmidt et al., 2011; Staley et al., 2014) and unmanned aerial vehicle Structure-from-Motion (herein referred to as SfM) (Ellett et al., 2019). TLS methods are able to resolve surface changes down to less than a centimeter such as those associated with widespread hillslope erosion on burned hillslopes (e.g., DeLong et al., 2018; Staley et al., 2014) and UAV-based SfM is able to resolve changes on the order of a decimeter (e.g., Barnhart et al., 2019; Ellett et al., 2019) that would be associated with the erosion of large rills, gullies, and channels.

In this study, we seek to understand the evolution of sediment sources in a steep headwater catchment over multiple storm cycles in a wet season immediately following wildfire. In light of the differences in rainfall and runoff erosion processes on hillslopes (e.g., inter-rill erosion and rill formation) versus channels (gully formation and channel scour), we hypothesize that the evolution of sediment availability will differ between these two process domains and that this will depend on the magnitude of previous storm cycles. We also seek to understand the degree to which a recently burned source headwater catchment tends towards a supply-limited state over effective storm sequences. In order to achieve these goals we utilize repeat topographic measurements over multiple storm cycles using UAV-based SfM at drainage areas up to 6.5 ha including headwater fluvial channels and terrestrial laser scanning (TLS) of a nested 0.95 ha convergent zero-order basin in a catchment in the Santa Ana Mountains burned by the 2018 Holy Fire near Lake Elsinore, California, U.S.A. Using these high-resolution datasets, we apportion sediment flux during these storm sequences to different channelized and hillslope morphological units. Additionally, we use hydrologic monitoring to track the magnitude of rainfall and runoff generation during this change detection campaign.

2.3. Study Site

This study was conducted in a small headwater catchment (monitored region for TLS = 0.95 ha and SfM = 6.5 ha), Leach Canyon (catchment area = 380 ha), in the northern Santa Ana Mountains of southern California (Figure 2.1). Leach Canyon was completely burned (> 95%) by the 2018 Holy Fire, which was ignited by arson in a coastal-draining valley (Trabuco Canyon in Orange County) and spread north and east over the high Santa Ana Mountains, burning through ~9,400 ha of very steep (> 30 degrees) chaparral-dominated terrain of the Cleveland National Forest (CALFire, 2019). There was particular concern for post-fire hazards to the foothill-bounding communities of Lake Elsinore and southern Corona, where steep drainages were partially or fully burned, resulting in high probabilities (60-80%) of debris flows in response to ~2-year short-duration high intensity (15 minute intensity = 24 mm hr^{-1}) rainfall (USGS, 2018; Schwartz & Stempniewicz, 2018). The last time Leach Canyon experienced a fire burning most of its area was during the 1954 Jameson Fire (CALFire, 2019).

Leach Canyon is in a hot dry-summer Mediterranean climate regime and receives an average of 481 mm of precipitation annually, primarily as rainfall between October and April (PRISM Climate Group, 2019). Precipitation in southern California is extremely variable, with a large portion of this rainfall delivered as narrow (only ~100s of km wide) moisture-laden bands emanating from the tropical Pacific referred to as atmospheric rivers (Dettinger et al., 2011). This meteorological phenomenon was an important factor for a few large storms during this study.

The underlying lithology of Leach Canyon is the Jurassic Bedford Canyon Formation, highly-deformed argillites and quartzites, interrupted by small intrusive bodies of granodiorite associated with the Cretaceous Peninsular Range Batholith (Morton & Miller, 2006). The northern Santa Ana mountains are asymmetrical, with a more gently-dipping southwest

escarpment interrupted by the Cristianitos and Mission Viejo faults (Taylor et al., 2006) and steeper northeast drainages along the margin of the active right-lateral Elsinore Fault System (Morton & Miller, 2006). Fluvial and marine terrace dating on the western side of the range indicate uplift rates of the northern Santa Ana Mountains on the order of 0.3-0.6 mm/yr (Taylor et al., 2006).

Within our 0.95 and 6.5 ha subbasins, much of the landscape is soil-mantled by very gravelly (~20-60% by mass) silt loam to silty clay. Though wind stripped away a significant portion of the lightest ash, there was still residual combusted duff layers across much of the mineral soil. Using quick qualitative tests of water droplet penetration while walking in the field, we noted soil repellency at the upper interfaces of mineral soil in many locations. The vegetation community at our site is chaparral shrubland, with standing skeletal biomass primarily composed of manzanita and chamise (especially on north-facing slopes). There were also some 'islands' of unburned riparian vegetation throughout the Holy Fire burn scar, with some of these patches present in our field area that acted to occlude measurements of topography along some portions of the channel network. Soil burn severity was primarily classified as moderate-to-high using burn area reflectance classification, though some areas of denser biomass consumption were classified into high severity (Schwartz & Stempniewicz, 2018). These values appear to be reasonable based on field observations and before-and-after orthoimagery comparisons. Owing to hillslope gradients at or above the angle of repose (> 32 degrees), thick post-fire ravel deposits comprised of primarily sand-sized fractions ranging from 0.1 to > 1 m depth were draped over pre-fire channel and colluvial fill throughout our study basin.
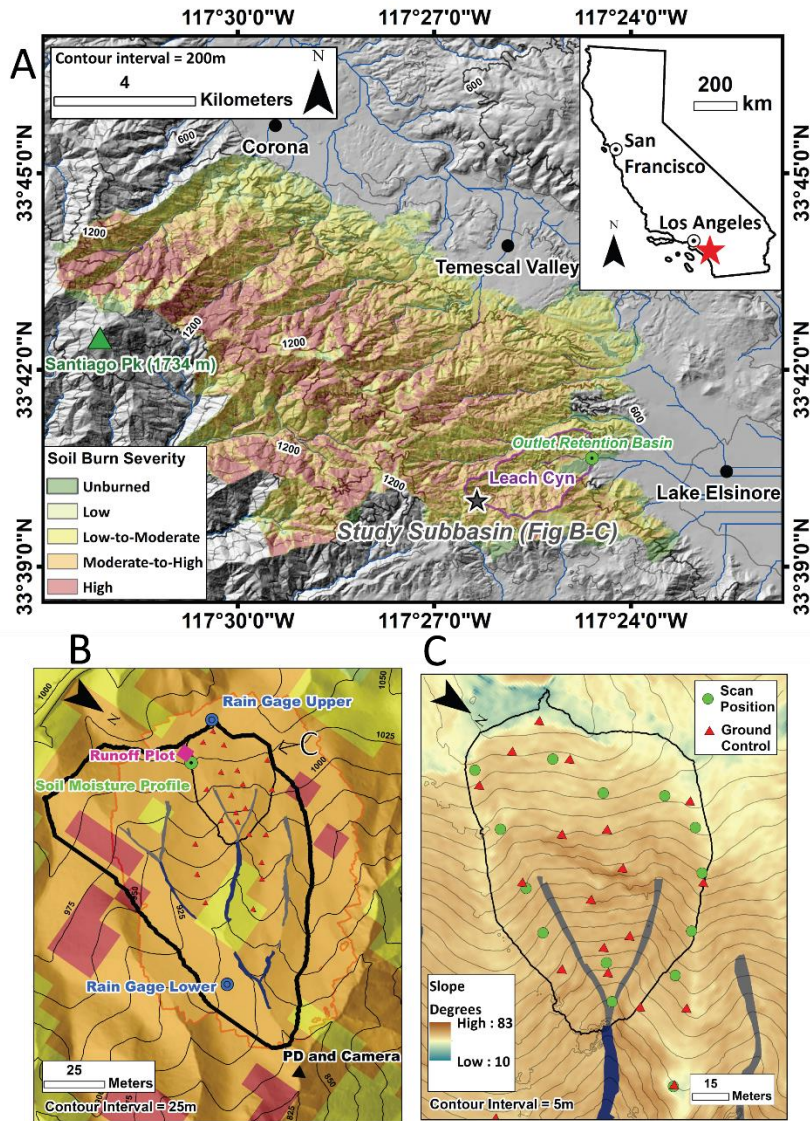
Figure 2.1. A. Shaded relief location map showing Holy Fire burn severity basemap, location of monitoring subcatchment (grey star), retention basin at outlet of Leach Canyon, and adjacent municipalities. Showing streamlines with drainage areas greater than 1 km2. B. Zoomed in map of 6.5 ha catchment flown with UAV and nested 0.95 ha zero-order catchment with USGS-derived airborne lidar hillshade and burn severity base layer. Red markers are ground control points and transparent red outline shows extent of UAV mapping. Locations of hydrologic monitoring equipment also shown (PD = pressure transducer). Blue polygons are fluvial channel valley bottoms and grey polygons are colluvial hollows with UAV-SfM coverage. C. Close-up of zero-order catchment with shaded slope basemap showing terrestrial laser scanner positions (green circles) and ground control points (red triangles). Same SfM outlines are all shown as polygons.

2.4. Methods

2.4.1. Ground Control Network

A network of 23 distributed permanent ground control points were established in the 0.95 and 6.5 ha study areas (Figure 2.1B-C). These consisted of half-inch diameter rebar monuments that were either driven into rock outcrops or deep into regolith with dimpled ends. These dimples were registered into a local cartesian XYZ system using a GeoMax Zoom80 robotic total station and prism (shorter range (< 3500 m) accuracy = 1 mm) from one base station that had a full viewshed of the area. Permanent CNC-machined cylindrical PVC reflectors (height and diameter = 10 cm) (Figure A1) were affixed to 16 monuments in the TLS area, and tennis balls were affixed to the remaining seven monuments outside the TLS area for use in georeferencing SfM images. Though in many cases UAV-SfM registration is done through survey markers affixed directly the ground (i.e. not above-ground), we found that UAV-SfM coregistration was possible through our technique of shared TLS and UAV-SfM points, which we describe below. Our approach of fixed control was done primarily to prevent land surface disturbance that is inevitable during repeated target setup in steep, loose topography that would bias measurements of surface change as well as put additional risk on field crews. Additionally, permanent ground control has the added benefit of reducing error associated with reoccupation of new points by surveying. We later reoccupied three points within the grid with static GNSS surveys in March 2020 in order to place results into a geodetic coordinate system, but all change detection analyses were performed in the local grid in order to make sure additional error was not introduced from GNSS occupation.

2.4.2. Terrestrial Laser Scanning

In the zero-order 0.95 ha catchment, four distinct TLS survey epochs took place (Table 2.1), each consisting of 13-15 scan positions (Figure 2.1C) using a Riegl VZ-400 scanner. The initial survey occurred two months after the fire following Forest Service permit approval and ground control establishment, but before any major runoff-producing storms (Table 2.1, Figure 2.2A). Given the potential dangers of surveying in steep, saturated hillslopes prone to rockfall, the remaining three surveys took place following major storm periods where the time between storms exceeded 48 hours and roads were deemed passable. Due to difficulty in mapping the full subcatchment, surveys were split into two days. Surveys were stitched together in RiSCAN PRO software using a minimum of three ground control points per stitch and further refined to ~5mm root mean square error (scanner accuracy) through the use iterative-closest point techniques between survey scenes. This process reduces the problem of misalignment that arises from the use of tiepoints alone, which in the case of cylindrical reflectors used in the study may be more significant than reflector discs that display their geometric center directly to the laser scanner. Since ground control was fixed between all monuments, error was minimized by co-registering scans belonging to the same surface differencing with the common control network following methods of Rengers et al. (2016). For example, for digital elevation model (DEM) of difference #1 (DoD1), October was subtracted from December, so these two scan surveys were co-registered under a single project. A deviation gate filter was then applied to remove mixed pulse returns that produced spurious points. Point clouds were then exported to CloudCompare version 2.10.2 (2019) where the plugin CANUPO (Brodu & Lague, 2012) was used to classify vegetation and low ground points to remove standing biomass. Any additional noise in the remaining ground cloud was removed. Finally, an octree-based resampling technique in CloudCompare was used to thin the cloud to the average gravity center of each cell by a fact, reducing ground point totals from ~180-

200 million points to ~80-100 million points. This was done to reduce the computational costs associated with post-processing the data and lessen the bias of oversampling closer to scan positions. Despite occupying more than a dozen scan locations, occlusion was a factor in our field site due to the complex and rugged nature of our 0.95 ha subcatchment, resulting in non-trivial data gaps that were not used for change detection. This occlusion significantly affected two deeply incised gullies in the zero-order basin, which was filled in with SfM data as we describe in the next sections.

2.4.3. UAV-based Structure-from-Motion

The process of UAV-SfM uses near-ground (10s-100s of meters) high-resolution oblique and nadir-view images with significant overlap to photogrammetrically reconstruct topographic surfaces and orthoimagery (e.g., Fonstad et al., 2013; James et al., 2017; Westoby et al., 2012). Using an autonomous flight plan with "terrain follow" provided by the Map Pilot app (Maps Made Easy, 2018), we performed seven flights with a DJI Mavic Pro (camera resolution = 12.35 megapixels) at 50 m above ground over a 6.5 ha area encompassing and surrounding the TLS scan zone (Figure 1.1B), four of which were spaced over the same storm cycles as the TLS epochs (Figure 1.2A and Table 1.1). Construction of registered dense point clouds and orthoimagery were performed using Agisoft Metashape Pro (2019). After correcting for rolling shutter from our DJI camera in Metashape, we followed USGS National Unmanned Aircraft Systems Project Office (2017) protocol for iterative error reduction and bundle adjustments in the following order: reduction of image geometry errors, reduction of pixel matching errors, and the minimization of reprojection residuals following the integration of our local XYZ ground control points (Figure 1B-C) (also see Barnhart et al., 2019 for further descriptions of this process). In this process, image projections for all photographs stayed well above the suggested minimum of 100. Our ground control network error was on the order 2-4 centimeters. For validation points, we

added three points from stable TLS-based landmarks (corners of rock surfaces) and left out some

monumented points during registration, with slightly higher errors on the order of 5-6

centimeters, largely consistent with other UAV-SfM studies of similar scope (e.g., Barnhart et al.,

2019; Ellett et al., 2019). Using a systematic error detection and correction toolbox introduced by

James et al. (2020) we also found that there was no detectable systematic 'doming' error that can

be common in SfM acquired with UAVs (see Figure A2). We also used a combination of

CANUPO (Brodu & Lague, 2012) and manual segmentation in CloudCompare to remove

vegetation points and low-ground noise in the SfM point clouds.

2.4.4. DEM of Difference and Uncertainty Analysis

In very high resolution topographic studies there is a tradeoff between errors caused by small grid

sizes estimated from sparse point coverage (low point densities) and surface representation errors

from larger grid sizes that may drown out smaller features such as rills (Passalacqua et al., 2015).

Any areas inside the watershed that had poor point coverage from occlusion or were significantly

affected by ingress/egress of field crews were removed by masking, allowing us to analyze 73%

of the watershed in DEMs from October, December, and January. As mentioned previously, low-

lying vegetation occluded non-trivial portions (regrowth shown in Figure A3) of the watershed

during the last scan in April 2019, resulting in an analysis of only about half of the watershed

area. Point clouds were rasterized into DEMs in MATLAB using triangular irregular network

(TIN) meshes (e.g., Staley et al., 2014) with the same cell size and spatial extent to ensure that all

cells were orthogonal and concurrent (Wheaton et al., 2010). We determined the optimal cell size

of the DEM to be 7.5 cm to ensure adequate reconstruction of small features like rills while

maintaining high enough point density per pixel (Appendix A, Figure A4).

For the first two change difference periods, surface differences were calculated with the DEM of

difference (DoD) method, whereby surface changes are calculated via the subtraction of an old

surface from a new surface, with negative values indicating surface lowering (erosion) and positive values indicating surface raising (deposition), which can be multiplied by cell size to obtain a volumetric change (Lane et al., 2003). TLS differencing encompassed a majority of the 0.95 ha hillslope site (referred to hereafter as the zero-order catchment) and SfM differencing was done in colluvial hollows in two adjacent headwater catchments (Figure 2.3) and in downstream valley bottoms where channelized erosion was expected to exceed the larger limit of detection of this method relative to TLS.

Since the same positions were reoccupied using fixed benchmarks (tiepoints and ICP-registration on conservative surfaces) for all timesteps, we empirically estimated the range of positional uncertainties using the root mean square error (RMSE) of conservative validation surfaces that we did not use for multitemporal alignment. This consisted of outcrops, large boulders, and the base of large trees (Figure A5). RMSE was determined for all three dimensions (x,y,z) and propagated to values of σ_h using Equation 1 for sixteen conservative surfaces distributed throughout the watershed per DoD (Table A1), with values ranging between 0.002-0.011 m.

$$RMSE = \sqrt{\frac{\sum_{i=1}^{n}(S_1-S_2)^2}{n}} \qquad (1)$$

Where S_1 and S_2 are the conservative point cloud surfaces from survey 1 (before) and survey 2 (after) of a differencing interval and n is the number of points used for a given surface. We also screened for potential systematic offsets by evaluating the signed average differences in all directions, with practically all values falling below scanner accuracy (0.005 m), ruling out systematic offsets as a significant error term (Tables A1 for TLS, Tables A2-3 for SfM). RMSE was determined for all three dimensions (x,y,z) as:

$$RMSE_{xyz} = \sqrt{RMSE_x^2 + RMSE_y^2 + RMSE_z^2} \qquad (2)$$

Where $RMSE_x$, $RMSE_y$, and $RMSE_z$ are surface differences propagated in all three dimensions. Components of this error involve a combination of uncertainty locating the centroids of tie points, tie point instability, slight changes in conservative surfaces used for alignment/validation (i.e., fire spalling of surfaces), and instrumental accuracy.

Because TLS provides a wealth of information on the complexity of modeled scenes, we elected to estimate difference uncertainty in a distributed manner using a Fuzzy Inference System (FIS) in the Geomorphic Change Detection Software package for ArcGIS 10.6 (Wheaton et al., 2010). For TLS, we defined our range of uncertainty using variability in $RMSE_{xyz}$, which ranged from 0.002-0.011 for all surveys. DoD uncertainties were determined using this equation:

$$\sigma_{DoD} = \sqrt{{\sigma_{before}}^2 + {\sigma_{after}}^2} \qquad (3)$$

Where σ_{before} and σ_{after} are uncertainty terms for surveys bracketing the period of change and σ_{DoD} is the propagated uncertainty. Uncertainties for σ_{before} and σ_{after} are determined through a convolution of local roughness, slope, and point density using a fuzzy logic rule classification that is bounded by the stable surface $RMSE_{xyz}$ values determined above (further details in Appendix A in Supplementary Information, Wheaton et al., 2010). Following Brasington et al. (2003) and Lane et al. (2003), limits of detection in the z-difference were derived using the 95% confidence interval below using the following:

$$LOD_{95\%} = 1.96 \times \sigma_{DoD} \qquad (4)$$

Where $LOD_{95\%}$ is the limit of detection for the 95% confidence interval and σ_{DoD} is the propagated error from before and after surveys for the change detection period. Spatially distributed $LOD_{95\%}$ ranged from 0.006 to 0.02 m for TLS (Figure 2.3, Table S1), similar to those reported in other post-fire studies (e.g., DeLong et al., 2018; Nourbakhshbeidokhti et al. 2019;

Orem & Pelletier, 2015; Staley et al., 2014). Further details on the methods used for spatially distributed uncertainty are outlined in the associated supplemental documents (Appendix A). We describe error analysis for SfM below, in which we use the same error propagation and limit of detection framework to determine significant change in DoDs.

2.4.5. TLS-to-SfM and SfM-to-SfM Alignments

In order to reduce relative error in our SfM point clouds and calculate further independent checks on spatial uncertainty of our SfM dataset, we used iterative closest point alignments in CloudCompare between our ground-only SfM and TLS point clouds acquired during the same epoch. This generally resulted in $RMSE_{xyz}$ between coeval clouds ranging from 0.02-0.03 (Table A2), with minimized systematic offsets, therefore we used 0.03 m as our error term for TLS-coaligned SfM grids. Following coalignment, we clipped out regions within colluvial hollows where channelized scour occluded ground and stitched together the TLS and SfM clouds into a single cloud (Figure A6-7). Further downstream and in surrounding colluvial hollows (herein referred to as SfM valley bottoms), we took a similar approach and performed iterative closest point registration on successive point clouds that were clipped out of valley bottoms, beginning with the 18 October 2018 SfM cloud, and determined (Table A3) that RMSE was 0.03 to 0.04m, slightly greater than within the TLS scan zones. Using the same error propagation technique above, we utilized uniform RMSE values of 0.03m ($LOD_{95\%}$ = 0.08 m for successive SfM measurements in DoD2 and $LOD_{95\%}$ = 0.06 m for TLS measurements compared to SfM measurements in colluvial axes in DoD1 - see Figure 2.3) for the SfM tied to TLS and 0.04 m ($LOD_{95\%}$ = 0.11 m) for surface differences in the SfM valley bottoms.

2.4.6. Delineation of Morphologic Units

High-resolution topography allows for the detection of centimeter-scale landforms and changes to these forms, which facilitates inquiry into the underlying physical processes shaping them

(Dietrich et al., 2003; Passalacqua et al., 2015; Staley et al., 2014). To understand the relative importance of processes and their associated morphologic domains, we used landscape morphometrics and slope-area domains to define and extract landscapes to partition surface changes into their respective morphologic units. We define three hillslope forms with differing process-domains: gullies, rills, and inter-rill zones. Additionally, we define the drainage area where fluvial channels begin. Gullies are generated by runoff-induced downcutting, forming continuous channels with cross-sections generally greater than 930 cm^2 (the 'square foot criterion' of Hauge, 1977 and Poesen et al., 2011). Rills, also formed by narrow concentrated incision, have support areas smaller than that of gullies with depths ranging from 0.05-0.3m and up to ~0.3 m wide (Gao, 2013). Here, we define inter-rill zones as hillslope zones (whether convergent, divergent or planar) without any definable, continuous centimeter-scale channelization that are subjected to processes such as rainsplash and sheetwash. We note that some hillslopes may be subject to little or no rill erosion, but in the context of significant rill formation on our burned hillslopes we refer to points on the hillslope without rills as inter-rill domains, an approach used in Rengers and McGuire (2018).

To delineate these features, we developed a flow accumulation raster (d-infinity of Tarboton, 1997) of both our 0.95 ha and 6.5 ha catchments. We developed slope-area plots in order to determine the slope-area roll over point where fluvial processes are dominant (see Figure A8), where it can be seen that a nearly flat slope transitions to a concave-up slope profile near the outlet of our watershed (at drainage areas >0.2 ha) (e.g., Montgomery & Foufoula-Georgiou, 1993; Staley et al., 2014). Using a combination of visual appearance of steep-sided banks and flow accumulation, two gullies were selected at the convergence of the primary rill networks located at the upslope end of two colluvial hollows (Figure 2.4A-B, blue polygons). Next, we extracted rill networks using an approach outlined by Rengers and McGuire (2018), we applied a

36

Gaussian filter (standard deviation = 5) to our DEMs and differenced them from our original

DEM, in which negative values represent localized depressions. Finally, a raster conditional was

applied where any depression cells with drainage area ≥ 1 m^2 and two centimeters of erosion were

classified as incipient rills in DoD1. These rills were carried over to DoD2 since they assumed to

be in existence during the start of erosional processes and the same analysis was performed to

delineate new rill formation (Figure 2.4B).

2.4.7. Hydrologic Monitoring

Because of this study's focus on storm event sequence in a headwater catchment, it was important

to continuously monitor local precipitation and runoff. We installed two rain calibrated 0.2 mm

tipping-bucket rain gages (Onset HOBO RG3-M), one located at a lower ridgeline (898 m

elevation) and one located at the top of the watershed (1045 m elevation) (Figure 2.1B). The

lower rain gage experienced a malfunction, but little difference in rainfall was found between

gages for the storms with monitoring overlap, so we elected to use the continuous record of the

upper-most gage. Rainfall intensities were derived from this data using the backward differencing

approach (Kean et al., 2011) for the following durations (I_D): 15-minute rainfall intensity (I_{15}) and

2-minute rainfall intensity (I_2). I_{15} generally corresponds to response times for burned catchments

of a similar size (0.01-1 km^2) to those measured in this study (Kean et al., 2011). We derived I_2 to

focus on rainfall-runoff dynamics at a small plot scale (0.2 m^2) using instrumentation described

below. Soil volumetric water content sensors (Campbell Scientific CS616) were installed in depth

profiles (5, 15, 30 cm) that were established on a north-facing shoulder slopes adjacent to the

upper rain gage. In order to detect hillslope runoff production during storm events, we installed a

~ 50 cm diameter circular runoff plot following the design of Moody and Ebel (2012b) to identify

storms that produced runoff near the upper drainage divide (pictured in Figure A9). We

calculated 2-minute runoff values (Q_2, mm hr^{-1}) by dividing discharge (mm^3/hr) from each bucket

tip of a repurposed Onset HOBO RG3-M 0.2-mm tipping bucket rain gage by the bounded plot area (mm^2). By converting to runoff values, we can facilitate the comparison of these values through a plot-scale runoff coefficient through the division of summed runoff by summed rainfall from the nearby tipping bucket gage. Finally, a Solinst Levelogger pressure transducer was installed further downslope in a hole drilled into bedrock channel (drainage area = 17 ha) to analyze the timing and peak pressure head (H_p) of sediment-laden flows as an integrated expression of watershed response (Kean et al., 2012). If significant rain was forecasted, the transducer was manually triggered to record at a 10-second frequency along with a barometric sensor (Solinst Barologger) tied to a tree adjacent to the channel in order to remove atmospheric pressure fluctuation from the pressure head time series. In addition to the pressure transducer, we also had timelapse photography taken from a GoPro camera in an enclosure pointed upstream at the transducer that was active for a large storm event on 14 February 2019 (see Supplementary Video 1). Located at the mouth of Leach Canyon (drainage area = 380 ha) is a flood and debris control basin, built and managed by Riverside County Flood Control and Water Conservation District, which provided timelapse videos contemporaneous with our measurements of sediment flux.

Table 2.1. Remote sensing data collection schedule. Note that data acquisition within a single day was not possible due to time limitations but all datasets acquired within a survey epoch bracketed the same runoff-producing storms.

Dataset Type	Date Acquired	Number of scans	Survey Epoch
TLS visit 1a	25 October 2018	10	1
UAV flight 1	25 October 2018	-	1
TLS visit 1b	30 October 2018	6	1
TLS visit 2a	18 December 2018	3	2
UAV flight 2	18 December 2018	-	2
TLS visit 2b	19 December 2018	12	2
TLS visit 3a	19 January 2019	4	3
TLS visit 3b	20 January 2019	9	3
UAV flight 3	30 January 2019	-	3
UAV flight 4	04 March 2019	-	4
TLS visit 4a	20 April 2019	7	4
TLS visit 4b	27 April 2019	8	4
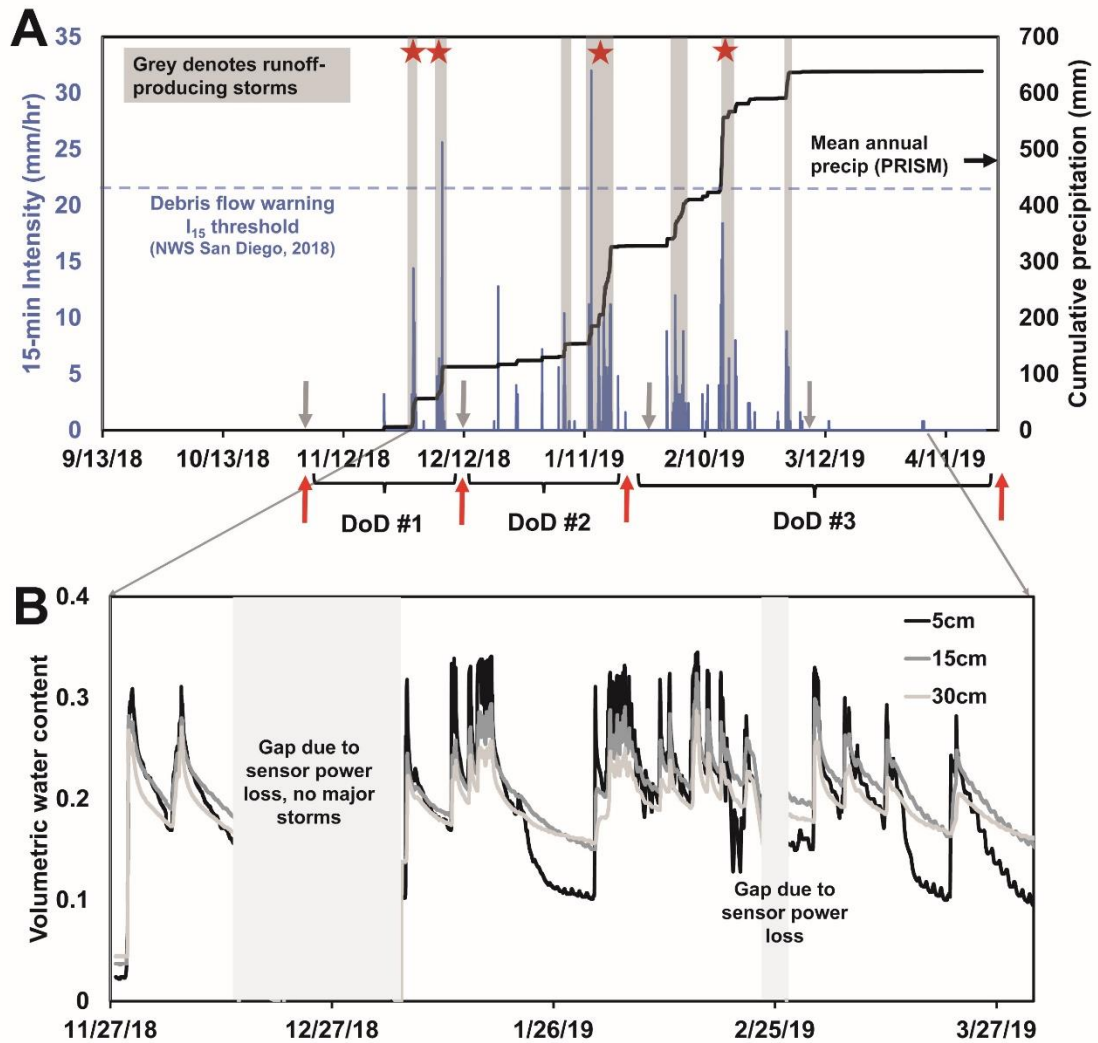
Figure 2.2. A. Cumulative rainfall time series with 15-minute intensities (I_{15}). Red arrows refer to the approximate time of TLS surveys (which was staggered over two days per survey but single arrow shown for simplicity), gray arrows denote the time of approximately coeval UAV-SfM acquisition and black brackets denote runoff-producing storms captured with change detection. Red stars indicate time periods with evidence of debris flow activity. Blue dashed line shows the I_{15} threshold for debris flow warning issued by the National Weather Service (2018) for the Holy Fire. Refer to Table 2.1 for more precise timing on dates of mapping data acquisition and Table 2.2 for more detailed information on hydrologic variables. **B.** Soil moisture time series from CS616 EC soil moisture probes at 5, 15, and 30 cm depths (location near runoff plot shown in Figure 1.1B).

2.5. Results
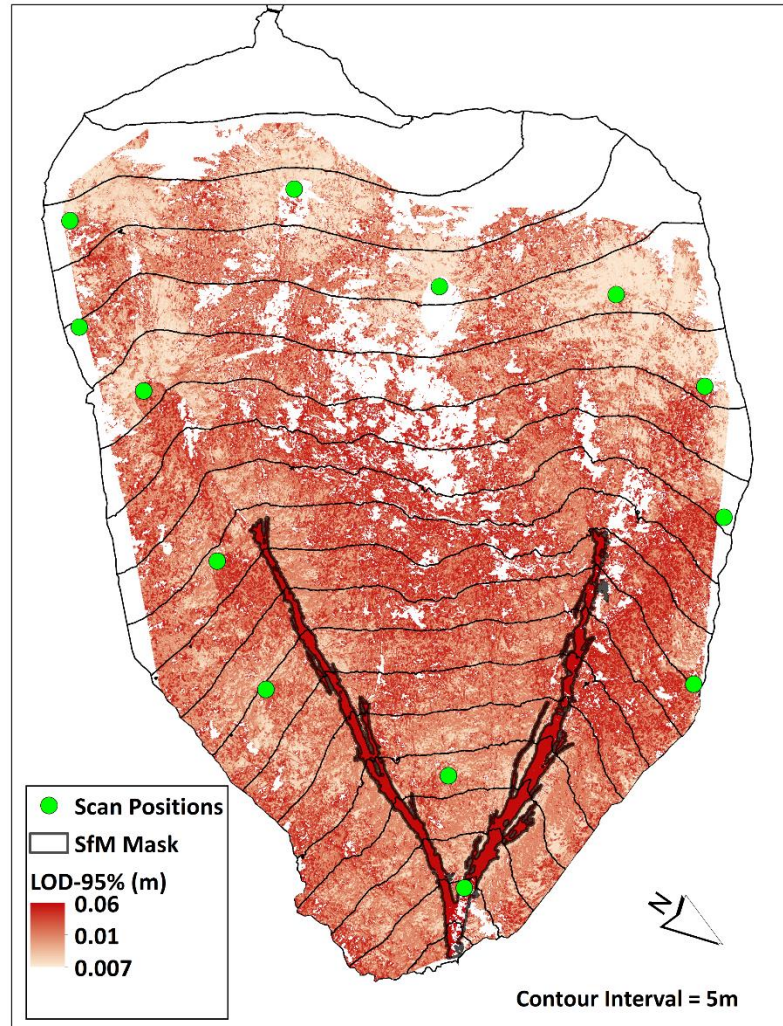
Figure 2.3. Spatially distributed limits of detection ($LOD_{95\%}$) for DoD_1 determined from the 95% confidence interval of fuzzy inference system (FIS) outputs using roughness, point density, and slope for TLS areas and a single error value for SfM zone (dark red areas with $LOD_{95\%} = 0.06$ m). In DoD1, SfM was not used for the baseline survey as there was sufficient TLS ground coverage. However, for DoD2, the SfM $LOD_{95\%} = 0.08$ because only SfM was used for differencing in the colluvial hollows. Green points are TLS scan positions. Otherwise, the error distribution is very similar to those in DoD_2 and DoD_3.
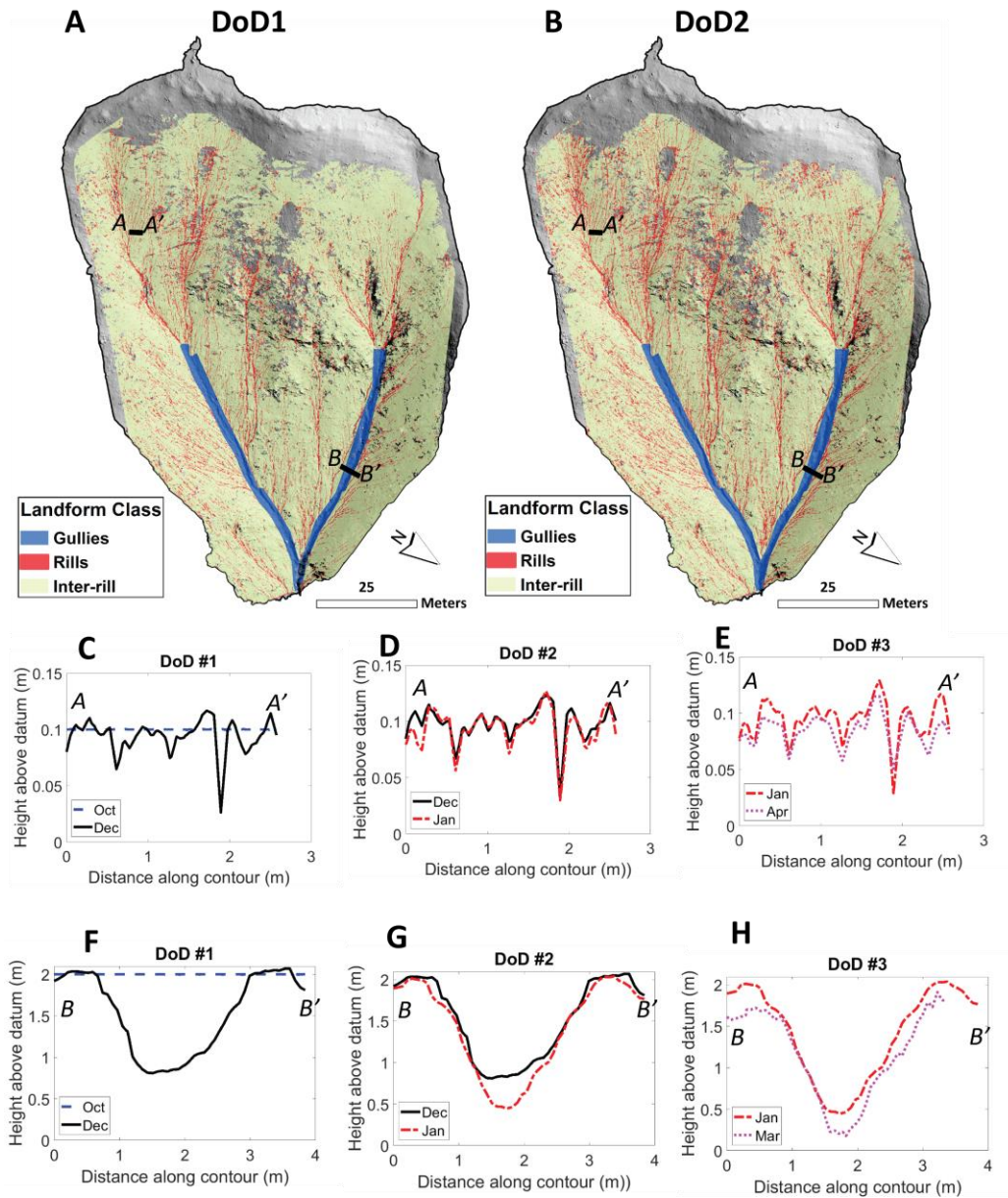
Figure 2.4. Delineated landscape features in plan view with example cross-sections of incisional features during DoD1 and DoD2. **A-B.** Landscape domains used for apportioning sediment flux for DoD1 and DoD2. No landscape delineation is completed for DoD3 because of significant ground occlusion from vegetation. Shaded relief map is derived from SfM surveys. **C-E.** Cross-sections of rill erosion over successive DoDs. During DoD #1 (**C**), it was noted that small levee deposition occurred along the boundary of a few rills. **F-H.** Cross-section of

Table 2.2. Hydrologic variables from runoff-producing storms over the study period.

Date	Total Rainfall (mm)	Peak I_{15} (mm hr^{-1})	Hp (m)	Peak Q_2 (mm hr^{-1})	Mean Q_2 (mm hr^{-1})	Cumulative Plot Runoff (mm)	VWC at 5cm* (m^3/m^3)	Plot Runoff Coefficient ($\Sigma I/ \Sigma Q$)**
29 November 2018	49	14.4	0.62	9.7	1.2	0.83	0.1	0.02
6 December 2018	56.4	25.6	0.97	3.9	1.8	0.3	0.28	0.01
5 January 2019	22	10.4	0.07	2	0.9	1.07	0.13	0.05
12 January 2019	31.4	32	0.33	22.5	4	5.1	0.22	0.16
15 January 2019	58	12.8	0.25	12	1.8	9	0.24	0.16
17 January 2019	62.6	11.2	0.33	24	2.7	16.6	0.34	0.27
2 February 2019	34	12	0.31	9.6	1.4	2.8	0.32	0.08
4 February 2019	23.8	8.8	0.14	7.7	1.7	3	0.31	0.13
10 February 2019	6.8	4	-	1.3	0.8	0.2	0.31	0.03
14 February 2019	133.4	18.4	0.46	32.1	5.4	57.5	0.32	0.43
2 March 2019	45.6	8.8	-	9	1.7	3.4	0.3	0.07

H_p = peak pressure transducer head, Q_2 = 2-min plot-scale runoff, Peak I_{15} = peak 15-min, VWC = volumetric water content from sensor

*VWC as measured at the start of hillslope hydrograph

**runoff coefficient as calculated from incoming rainfall vs. integral of Q_2 hydrograph
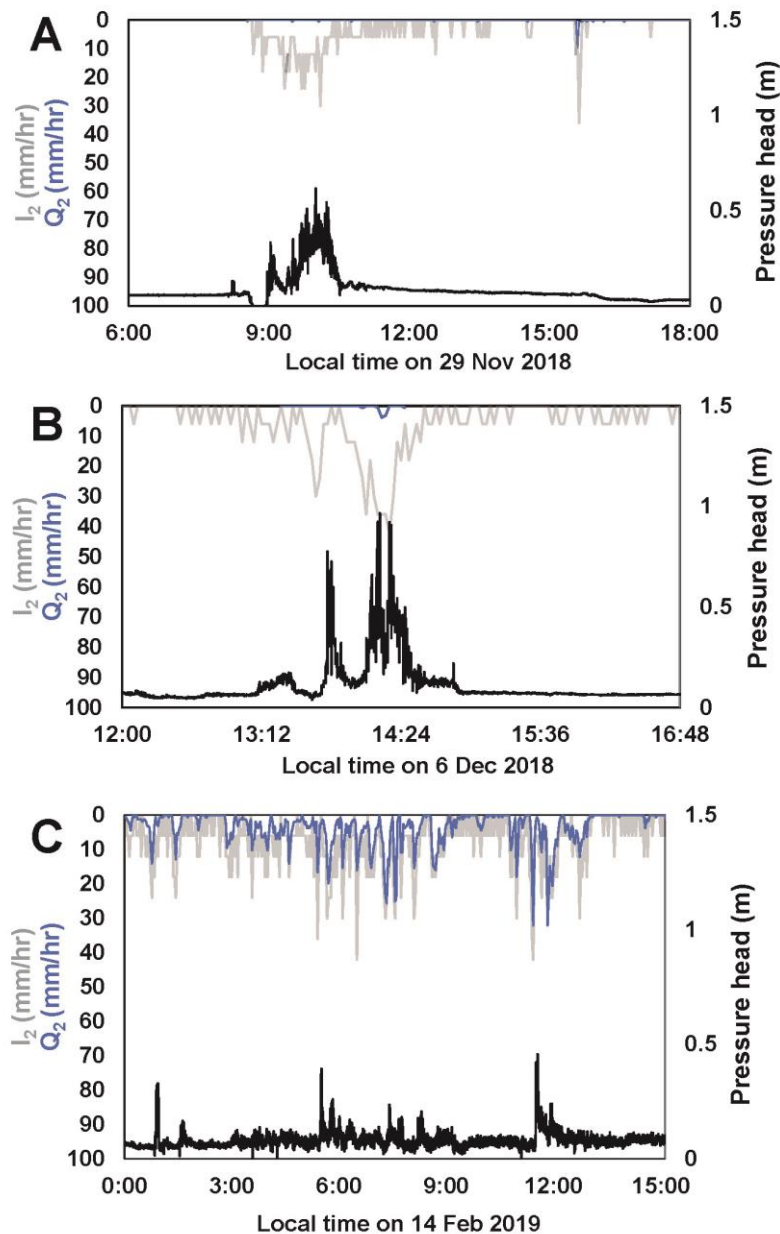
Figure 2.5. Hydrological response (2-minute rainfall intensity, grey, hillslope runoff plot data, blue, channel pressure head, black) for three representative storm events. **A.** First storm of the season (29 Nov 2018) showing minimal hillslope plot runoff but many surges in channel pressure head. **B.** Hydrological response for 6 Dec 2018 event, which recorded the single highest hydrostatic head peak with proportionately small responses from hillslope runoff plot **C.** Example hydrological response for a long-duration, high-magnitude storm event on 14 Feb 2019.
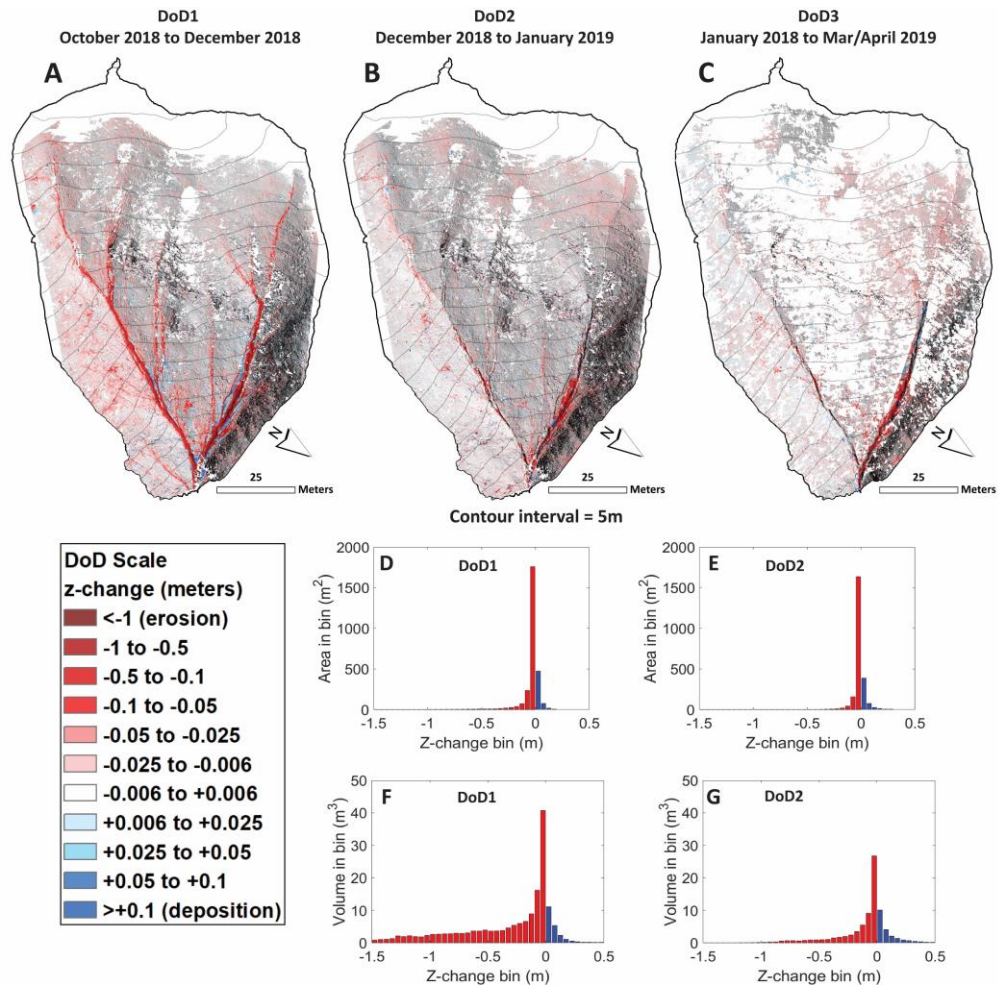
Figure 2.6. A-C: DEMs of difference for the 0.95 ha zero-order catchment overlying hillshade layer. White areas indicate ground with no point coverage. There is ~0.7 ha of coverage in DoD1 and DoD2. **C.** DoD3 had less coverage (~0.48 ha) due to ground occlusion from vegetation regrowth. Red colors indicate erosion, blue colors indicate deposition, and uncolored areas of the hillshade fall below the $LOD_{95\%}$. **D-E:** Histograms of area binned by surface elevation change exceeding limits of detection for DoD1 and DoD2. **F-G:** Histograms of volumetric change binned by surface elevation change exceeding limits of detection for DoD1 and DoD2. For all histograms, red indicates erosion and blue indicates deposition. Due to reduced ground coverage relative to DoDs 1-2, we did not complete area/volume histograms for DoD3.

45

Table 2.3. Estimates of erosion and deposition from thresholded DEMs of difference

	Area of interest	Un-occluded area (m^2)	Area with detectable change (m^2)	Gross Erosion (m^3)	Deposition (m^3)	Net erosion (m^3)	Average z-change (m)	Avg. z-change channels only (m)*
DoD 1	Zero-order catchment	6989	2838	148 ± 19	23 ± 4	125 ± 20	-0.02	-
	SfM valley bottoms	2026	928	479 ± 50	5 ± 2	474 ± 51	-0.23	-0.51
DoD 2	Zero-order catchment	6944	1998	61 ± 12	21 ± 5	40 ± 15	-0.006	-
	SfM valley bottoms	2026	257	61 ± 12	10 ± 3	51 ± 12	-0.02	-0.05
DoD 3**	Zero-order catchment**	4783	1658	45 ± 13	11 ± 3	34 ± 15	-0.007	-
	SfM valley bottoms	2011	272	64 ± 12	14 ± 4	51 ± 12	-0.03	-0.05

*change including only channel area from the area of scour identified in DoD1 and not adjacent masked area (assumes that system-wide channel widening is negligible in DoD2 and DoD3)

**due to significant occluded ground from low-growing vegetation and potential misclassification of near-ground vegetation points in areas of low point density, we are reporting values here but caution against using them for comparison against other DoDs and do not use them in morphologic budget apportionment.

2.5.1. First difference interval (DoD1): 25-30 October 2018 to 18-19 December 2018

Two effective storm events impacted the field site, the first on 29 November 2018 being a

moderate atmospheric river storm impacting southern California (Center for Western Weather

and Water Extremes, 2019) and the second being a cold front system on 6 December 2018. Both

had similar rainfall totals but the second storm on 6 December 2018 produced greater peak I_{15} of

27 mm hr^{-1}, exceeding National Weather Service warning thresholds estimates for debris flow

initiation (NWS San Diego, 2018) (Table 2.2; Figure 2.2A). Interestingly, runoff production from

the small hillslope plot was relatively modest, with very low plot runoff coefficients of 0.01-0.02

for the 29 November 2018 and 6 December 2018 storms (Table 2.2). This response is not

reflected downstream in the bedrock-floored channels, where transducer data revealed the largest

pressure heads of the season: $H_p = 0.62$ and 0.97 m (Figure 2.6A-B). The timing of hillslope-plot

and watershed-integrated runoff peaks generally lagged at ~2-min and ~10-15-min rainfall

intensity peaks respectively (Figure 2.5A-B), in a similar manner to Kean et al. (2011). Peak Q_2

was not temporally coincident with the largest surges in H_p (Table 1) during the 29 November

2018 storm. This implied that runoff response was likely spatially heterogeneous during this

storm towards the drainage divide but it is clear that runoff amplification occurred from the

extensive erosion that occurred in the watershed. The soil moisture probes near the runoff plot

remained well below saturation both at the surface and at depth (Fig 2B), implying any runoff

produced within this zone was likely from infiltration-excess mechanisms, as is commonly

observed in post-fire settings (e.g., Schmidt et al., 2011; Ebel and Moody, 2012).

Maps of change in the zero-order catchment show that rill erosion formed 0.01-0.1 m deep quasi-

parallel tracks nearly up to the upper divide (Figure 2.6A). Downslope these rill networks became

primarily steered into colluvial hollows through topographic convergence, but a prominent cliff

band in the central portion of the watershed did impose both flow divergence and convergence

(Figure 2.4; Figure 2.6). Gullies ranging from 0.1 m to > 1.5 m depth were carved into two primary colluvial hollows, with these two gullies eventually merging into a trunk channel at the outlet (Figure 2.6A). Total erosional volumes were 148 m^3 ± 19 m^3, depositional volumes were 23 m^3 ± 4 m^3, and resulting net erosion was 125 m^3 ± 20 m^3 (Table 2.3). This translates to a sediment delivery ratio = 0.85 and the equivalent of 0.02 m of surface lowering.

Out of the three morphologic units, gully formation in the two colluvial hollows (Figure 2.6A) accounted for 61% (77 m^3) of the net erosion during these runoff events (Figure 2.7A). Photographs of the gullies showed that flow accessed both post-fire ravel and older colluvial fill that had been stabilized by thick roots (Figure 2.8B). Incision within these gully systems cut down to bedrock (Figure 2.8, channel downcutting in Figures S10-12) and were observed to be impeded by thick root bundles further upslope. On surrounding hillslopes the formation of an extensive rill network (rill area drainage density = 0.055 m^2/m^2, see Figure 2.4A, 2.5A) and shallow inter-rill erosion both contributed approximately equally to the remaining 48 m^3 of net erosion.

Differencing in the SfM valley bottoms revealed a similar pattern of significant gully formation and channel scour (Table 2.3, Figure 2.9). Total erosion in these gullies and channels was 474 m^3 ± 51 m^3. Including the two gullies within the TLS zero-order catchment, total erosion of all channelized features is 550 m^3 ± 51 m^3 with about 63% of this erosion occurring in fluvial channels, highlighting the importance of both gully formation and channel evacuation in fueling flows in these initial storm events. Field observations show that material derived from gully and channel scour were composed of both post-fire dry ravel and pre-fire channel colluvial infill (Figure 2.8C, Figure A11).

Supported by field observations, we found decimeter-scale levee deposition along the gully tracts composed of matrix-supported gravels and cobbles (Figure 2.8B), with coarser debris deposits (up to the size of small boulders) further downstream of the pressure transducer (Figure A10). The presence of such levees commonly indicate the passage of debris flows (Iverson, 1997; McCoy et al., 2010). Additionally, we noted the formation of cm-scale levees in DoD1 bounding some rill networks (example cross-section Fig 2.4C), possibly indicative of sediment bulked flows occurring in the hillslope domain. Although pressure head measurements alone cannot distinguish debris flows from floods (Kean et al., 2012) (Figure 2.5A-B), the combination of levee development and elevated sediment flux indicates that debris flows were generated in the uplands. In contrast, timelapse cameras at the Riverside County sediment retention basin (drainage area = 380 ha) located 3 km downstream show water-dominated flow entering the basin, with most of the coarser material comprised of woody material (Figure A12). It appears that more debris-rich flows generated in the uplands had devolved into turbid water-dominated flows in the lower gradient mainstem channel of Leach Canyon.
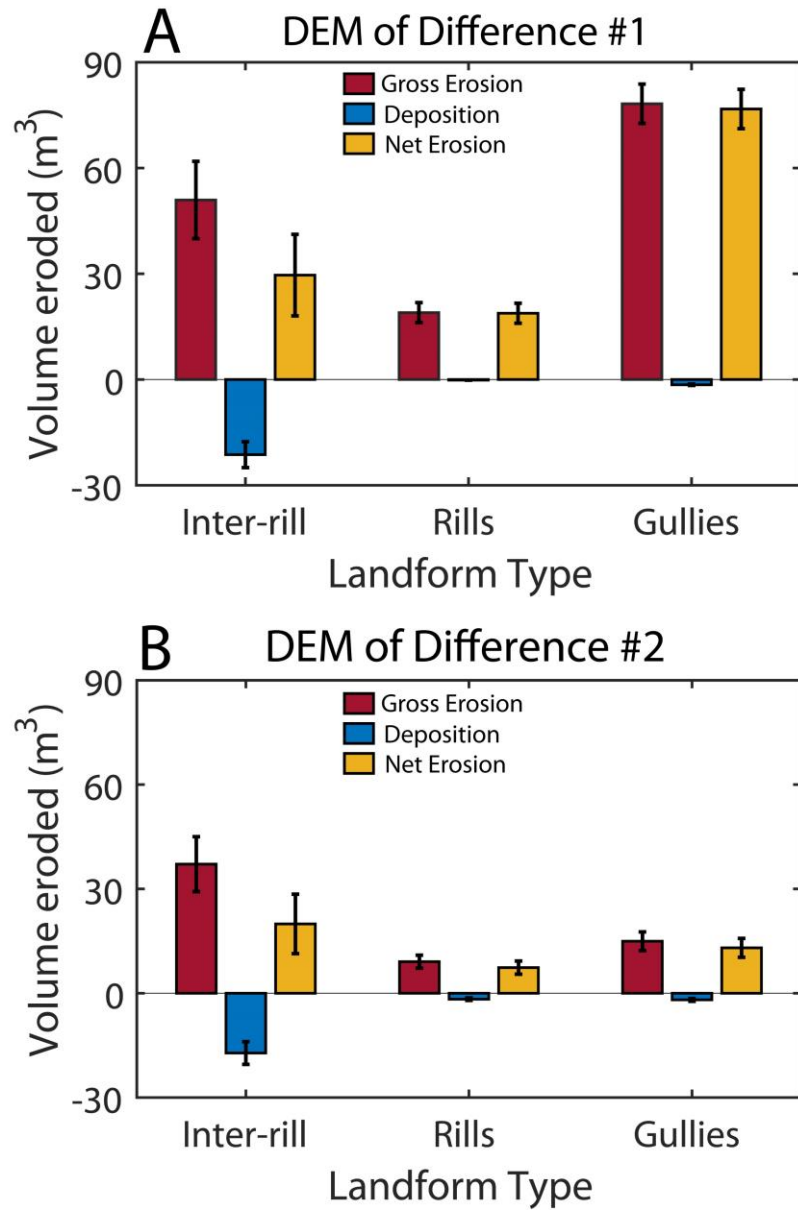
Figure 2.7. Sediment budgets apportioned to morphologic classes in the zero-order catchment for: **A.** DoD1 and **B.** DoD2. Red bar is erosion, blue bar is deposition (hence negative values of volume eroded), and yellow bar is net erosion. Uncertainty bars are propagated analytical uncertainty (σ_{DoD} of equation 3) from volume calculations.

Figure 2.8. Pictures taken from above and below confluence of two gully tracks on 19 December 2018 (just above outlet of watershed in Figures 6A-C). **A.** Arrow points to southern-most gully track showing bedrock unearthed by channel scour. **B.** Arrow shows small-scale levee deposition bounding the edge of the northern-most gully. Also note the circled area on the right side of the photo that shows coarse material overlying a slightly darkened ash layer. This is interpreted as post-fire dry-ravel overlying pre-fire colluvial fill, signifying the importance of both sources of material in the erosion of gullies and downstream channels. **C.** Photo taken from below the confluence showing extensive channel scour through post-fire ravel material and root-stabilized pre-fire colluvium.

2.5.2. Second difference interval (DoD2): 18-19 December to late January 2019

A sequence of four distinct storms (both frontal storms and the edge of atmospheric rivers storms, Table 2) struck the field site during DoD2, with much of the precipitation falling during the week of 11 January 2019. This sequence of storms elevated antecedent soil moisture levels (Table 2.1), but VWC still remained well below saturation (Figure 2.2B) and greater runoff coefficients of 0.16 and 0.27 were found for storms on 12 January 2019 and 17 January 2019, respectively (Table 2.2). At the watershed scale, H_p values for these two storms were 0.15 and 0.33 m. A small storm on 6 Jaunary produced a modest runoff response at both the hillslope plot and watershed-scale. Weighted mean Q_2 during this period was 2.6 mm hr^{-1}, greater than runoff produced during DoD1 within the headwater runoff plot. However, Hp values of the pressure transducer were less than in DoD1 (Table 2.2).

Inspection of maps of change for DoD2 in the zero-order catchment show reduced change from gully tracks, although the southern gully continued to erode via channel widening, and continued rill and inter-rill erosion (Figure 2.6B). Overall, total sediment yields were more subdued for DoD2, especially for erosion within our channelized morphometric classes relative to DoD1 (Figure 2.7B). Gross erosion volumes were 61 ± 12 m^3, deposition volumes were 21 ± 5 m^3, and resultant net erosion was 40 ± 15 m^3, resulting in a lower sediment delivery ratio = 0.66 (Table 3). When considering overlapping analytical uncertainty of all three morphologic domains, net erosion was approximately equivalent. However, we noted the highest gross erosion and deposition within the inter-rill domains. Rills expanded from a drainage density of 0.055 m^2/m^2 to 0.08 m^2/m^2.

SfM valley bottom differencing also revealed subdued and more localized erosion (Figure 2.9B) totaling 51 m^3 $\pm$ 12 m^3 (Table 2.3). Many of these erosive features occur along the boundary of channels where channel bank erosion, potentially through mass failures, occurred (Figure 2.9E).

Additionally, remaining bed sediment or saprolite could also be a source for sediment-laden flows along these flow paths. Upon inspection of length-normalized sediment net erosion over time, channels appear continue to act as both a source and conveyor of sediment (Figure 2.10) but eroded much less in DoD2 than DoD1 (differing on average by a factor of ten).

2.5.3. Third difference interval (DoD3): Late January 2019 to March/April 2019

DoD3 encompassed a period with the largest magnitude storm of the season on 2/14/2019, ranked as an "extreme AR-type storm" using metrics related to integrated vapor transport intensity and duration (Ralph et al., 2019). This storm inflicted widespread damage on southern California, with millions of dollars of damage to infrastructure in Riverside County alone (Horseman, 2019). Soil moisture conditions still did not reach saturation during this event (Table 1, Figure 2B). Rainfall gages including ours and those adjacent to Leach Canyon yielded consistently high (> 13 cm) but spatially heterogeneous storm totals. A National Oceanic and Atmospheric Administration (NOAA) rain gage (ID = LDYC) on the south divide of Leach Canyon reported 12-hr rainfall totals (22 cm) with a return interval close to 200 years (NOAA, 2019). Significant hillslope runoff was observed by the plot during this event with mean $Q2 = 4.9$ mm hr-1 and peak $Q2$ for this event $= 32.1$ mm hr-1 resulting in the highest plot runoff ratio of 0.43 (the largest of the season, Table 2).

The timelapse camera collocated with our pressure transducer showed the passage of multiple debris flows surges with contemporaneous Hp equal to or exceeding 0.3 m. Although the camera was operating at 1-minute frequency, it appears to have documented surges with coarser fronts and hyperconcentrated tails (Supplemental Video 1). Photo documentation of debris flows was also substantiated by field observations of small levees bounding channel pools and debris snouts leftover from this event. As was noted in earlier effective storm events, Riverside County Flood Control timelapse cameras at the canyon outlet debris basin in the hour following these surges

showed only muddy water-dominated flows filling the basin in a similar fashion to all previous storms in DoD1 and DoD2 (Figure A12), once again implying that any granular fronts produced in the uplands had devolved into very turbid streamflow.

Vegetation occlusion was very significant for DoD3 within the zero-order catchment when these scenes were acquired in late April 2019. A map of change on the non-occluded ground is shown to illustrate patterns of hillslope erosion in ground that was able to be sampled (Fig 2.5C), but we do not attempt to generate morphologic sediment budgets due to the more incomplete nature of these data and potential misclassification of low-lying vegetation as ground (especially in lower point density areas) resulting in artificially high deposition. Change in the SfM valley bottoms revealed similar patchy erosion (Fig 2.9C, 2.9E) with a few instances of local deposition along with strikingly similar net erosion values to DoD2 equivalent to 51 m3 ± 12 m3. This is again reflected in the patterns of length-normalized net erosion rates (Figure 2.10), where both gullies and channels are acting as effective conveyors and continued sediment sources, but at a much more modest rate than the initial flows that evacuated much of their material downstream at the beginning of the wet season.
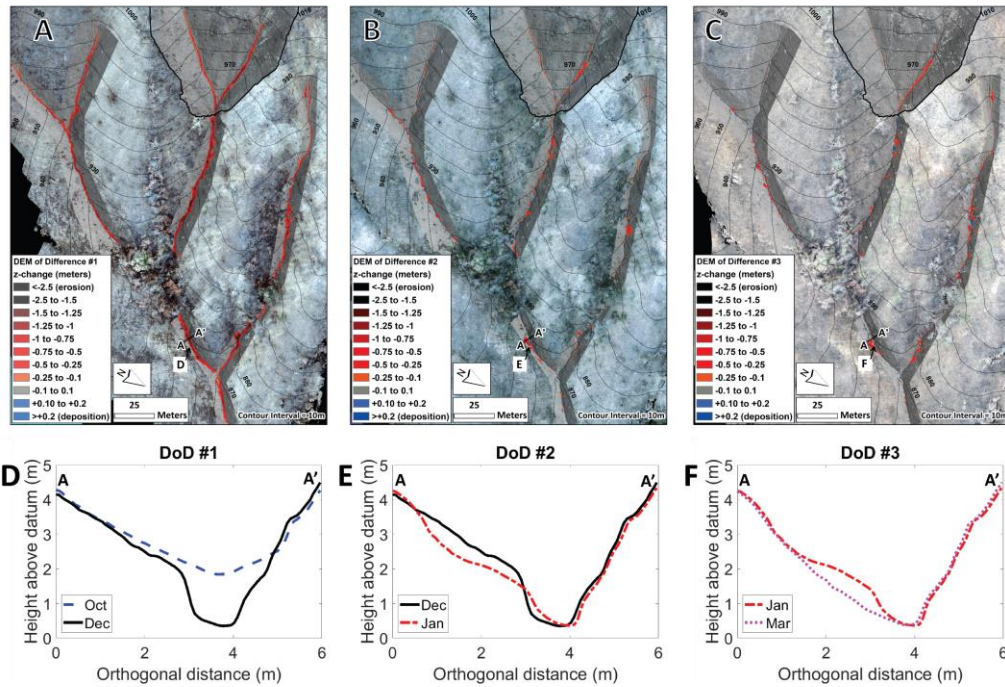
Figure 2.9. DEMs of difference for SfM surfaces showing valley bottom masks and orthoimagery showing both erosion in the zero-order catchment (top) and remainder of 6.5 ha catchment for: **A.** DoD#1 (October through December 2018), **B.** DoD#2 (December 2018 to January 2019), and **C.** DoD#3 (January 2019 to March 2019). Red values imply erosion and blue values imply deposition. **D-F:** Cross-sections for DoD1, DoD2, and DoD3 respectively along A to A' transect. Volumes of all SfM DoDs reported in Table 3.

2.5.4. Sources of Uncertainty in Sediment Budgets

Maps of propagated spatial uncertainty generated from the FIS (Figure 4) show patterns driven primarily by surface roughness and occlusion from standing skeletal biomass. Uncertainty by DoD is reported in Table S1, which fit within our range of FIS values. A common approach to the creation of a robust DoD is through thresholding, which discards all erosion and deposition
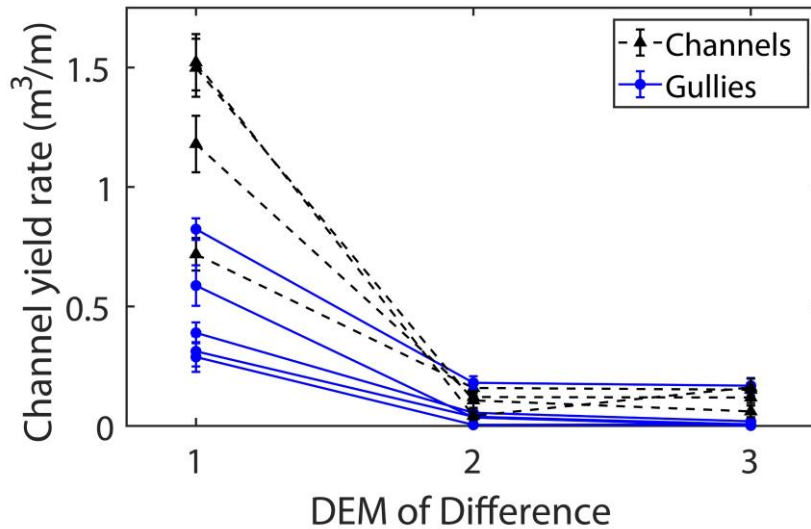
Figure 2.10. Channel yield normalized to length for gullies (blue circles and solid blue line) and fluvial channels (black triangles with dashed line) for all three DoDs. Error bars are propagated volumetric uncertainty from change detection.

values below the limits of detection. This approach presents issues if large swaths of the land surface experience change close to the limit of detection, resulting in either over or underestimation of the true sediment yield. An approach to assess this potential bias is to compare estimates of the raw and thresholded sediment yield estimates (DeLong et al., 2012; Wheaton et al., 2010). For DoD1, we found that net erosion from the raw map of change was 135 m³ compared to 125 m³ from thresholding, meaning that there is the possibility that some inter-rill erosion was excluded from our analysis. However, the raw estimate falls within the propagated volumetric uncertainty (± 16%) derived for this DoD and other DoDs analyzed.

Although we try to account for errors caused by undersampling the ground surface and slight misalignment by penalizing areas with lower point density and greater slope, there can still be artifacts present from differential sampling of surfaces. This could account for some of the apparent deposition observed on steep slopes (Figure 2.6A-C) that we find in our DoDs, though we verified many of these areas to be real from the existence of small-scale levee formation

adjacent to rill (Figure 4C) and gully features (Figure 2.4E, Figure 2.8B). Other factors unrelated to sediment redistribution can exist as well. For example, DeLong et al. (2018) found that over a winter period at their high elevation burn site, that the ground had become dilated through freeze-thaw and wet-dry cycles. At our site, we did note occasional overnight freezing of damp charred litter layers, so this could be a potential additional source of uncertainty and highlights the difficulty of obtaining sub-centimeter scale erosion measurements. Although it was impossible to complete a full TLS survey of our entire zero-order catchment in a single day given the amount of scan positions required and the time required to safely move heavy equipment across slopes, we acknowledge that spacing surveys out over two days could be an additional source of uncertainty due to dry weather sediment transport processes such as dry ravel and rockfall. In our assessments of sediment flux, we assume that most of the erosion that takes place is due to runoff-related processes and that most ravel processes are subdued relative to the initial post-fire ravel pulse (Lamb et al., 2011).

Additionally, there could be uncertainty from the fact that SfM-based measurements are unable to resolve finer-scale (sub-decimeter) sediment redistribution processes that could be occurring in sections of the channel during DoD2 and DoD3. This could include the subtle filling and flushing of low-gradient sections of channel, particularly during lower magnitude runoff events when upstream material may be delivered from the surrounding hillslopes. We do note that the SfM was effective in capturing bank erosion and continued downcutting during these time periods, which was likely an important process that fueled potential debris and sediment-laden flows later in the wet season.

2.6. Discussion

The initial goal of this study was to explore the evolution of sediment availability from different morphologic units on hillslopes and in low-order channels in a burned headwater catchment over a sequence of runoff events. Overall, we documented initial events with extensive inter-rill erosion, rill and gully formation, and intense scour of downstream channels from the generation of runoff-generated debris flows. Runoff events occurred with additional storms later in the season, and we saw evidence of continued rill and inter-rill erosion at similar rates. Gully and channel networks erosion rates decreased during these mid-season events, which resulted in overall lower sediment yields for the second series of storm events. We also note that the rill network expanded by a factor 1.6 between these epochs and underwent little deposition. We were unable to do a full accounting of hillslope erosion for the final, late-season series of storms because of ground occlusion from herbaceous vegetation that rapidly reestablished during the latter part of winter 2019. However, we did see observe continued rill and inter-rill erosion and debris flows later in this intervening period in response to intense rainfall. This rapid revegetation during a wetter-than-average post-fire year has implications for increasing hydraulic roughness on hillslopes, potentially increasing infiltration capacity, and decreasing rainsplash erosion (e.g., McGuire et al., 2017; Shakesby & Doerr, 2006).

Although our study is limited to a single basin subject to a unique post-fire storm cycle, we can consider our results among the growing body of literature utilizing high resolution monitoring to infer post-fire erosional processes. With access to high resolution change detection, this study revealed widespread inter-rill erosion as an important sediment source for post-fire sediment-laden flows, which has been highlighted in similar studies (e.g., DeLong et al., 2018; Orem & Pelletier, 2015; Rengers et al., 2016; Staley et al., 2014). Additionally, a similar shift of sediment sources over the first post-fire wet season have been observed in comparable settings in southern

California. The paired TLS studies of Schmidt et al. (2011) and Staley et al. (2014) were conducted in a 1.2 ha headwater basin along a flank of Mount Lukens in the San Gabriel Mountains, which was burned by the 2009 Station Fire. In the first runoff event following wildfire, Schmidt et al. (2011) found that sediment fluxes were dominated by the evacuation of fire-induced dry ravel and pre-fire material stored in the primary colluvial hollow of their study site. Staley et al. (2014) then demonstrated that inter-rill erosion dominated the sediment budget, and the newly-formed channel contributed zero sediment, transiently storing debris flow material and renewed dry ravel that were later evacuated in subsequent storm cycles (Jason W. Kean et al., 2011). This study clearly demonstrates a similar sediment availability trajectory to ours, which may be a characteristic evolutionary pathway of sediment sources in small, steep headwater catchments subject to repeated debris flow events. We also note that erosion in our differencing sequence of DoD1 and DoD2 resulted in somewhat lower basin-averaged erosion depths (DoD1 = 0.017, DoD2 = 0.006m) compared to 0.03 m reported by Schmidt et al. (2011) and 0.015 reported by Staley et al. (2014), which could highlight differences in the degree of erodibility, sediment supply, or wildfire-altered soil hydraulic properties between our site in the Santa Ana Mountains versus their burn site in the San Gabriel Mountains.

Using similar techniques to our study, Tang et al. (2019) used TLS and hydrologic field monitoring to calibrate and validate a numerical post-fire erosion model in a watershed burned by the 2016 Fish Fire in the San Gabriel foothills in which they found a relatively similar evolution of sediment sources to our study. They noted overall decreasing sediment supply following an initial storm event and increased relative hillslope erosion later in the season in response to high rainfall intensity that produced runoff at smaller drainage areas. Although we did not constrain the effects of individual storm events as did Tang et al. (2019), there is the possibility that much of the rill and inter-rill sediment generation during DoD2 could have occurred during the more

intense rainfall and concomitant hillslope plot runoff we observed during this period. Although beyond the scope of this present study, the additional insight provided by numerical modeling experiments (e.g., McGuire et al., 2016, 2017; Tang et al., 2019) that use high-resolution monitoring such as those presented here are a key step forward in exploring the mechanisms that drive post-fire erosion and debris flows. The exact processes controlling debris flow sediment sources and their relative importance can be challenging to extract from morphologically partitioned sediment budgets alone. This is because of the multitude of potential hydrogeomorphic processes acting simultaneously within the same morphologic domain (i.e., rainsplash and sheetflow in inter-rill areas; Staley et al., 2014; McGuire et al., 2016). It is also important to note that with our combination of soil moisture data and runoff measurements indicative of infiltration-excess overland flow and the lack of obvious landslide scarps, that our data strongly supports the characteristic post-fire mode of debris flows formed from runoff (e.g., Cannon et al., 2001, 2005; Kean et al., 2011) as opposed to saturation-induced mass wasting (e.g., Dietrich et al., 2001; Iverson, 2000).

Rill erosion within our study also experienced an interesting evolution from a sediment connectivity standpoint. Initially, we saw extensive rill formation (Figure 4A-5A) that yielded similar levels of sediment to surrounding inter-rill zones but we also note that some areas of small-scale levee deposition (cross section in Fig 2.4C), implying that rills likely experienced bulked sediment loads and behaved like 'leaky' conduits (Fryirs, 2013). Subsequently, expansion of the rill network between DoD1 and DoD2 additionally could have also provided additional structural connectivity to inter-rill erosional zones (e.g., Gabet & Bookter, 2008; Wester et al., 2014), which could have aided in routing inter-rill produced sediment downstream to the channel network.

In our downstream pressure transducer time series, we see a general pattern of decreasing H_p (peak pressure head) for successive storms throughout the season. For example, the 6 December 2018 (second effective storm) had the largest $H_p = 0.96$ m (Table 2.2) and the largest storm by overall depth on 14 February 2019 had similarly high (though shorter-duration) peaks in I_2 (exceeding 40-50 mm/hr) but had a smaller $H_p = 0.46$ (this peak is captured by timelapse photos in Supplemental Video A1). Although it is more difficult to interpret pressure head time series (Kean et al., 2012) compared to non-contact laser/sonic stage measurements (Kean et al., 2011) given the large variations in pore fluid pressures of debris flows and sediment-laden flows (McCoy et al., 2010), it is possible that this trend could represent smaller debris flow surges, or surges with high water content later in the season. This interpretation is supported by our TLS and SfM derived sediment budgets, where we note decreased net erosion over the season (Table 3). Kean et al. (2011) observed a similar trend in channel monitoring data that supported field observations of decreased sediment supply, particularly within their smallest basin (1.35 ha). There were differences in the rainfall profile (i.e. duration of higher-intensity peaks) between these storms (Figure 2.5) that could also exert a strong influence on debris flow surge behavior (Kean et al., 2013), but an analysis of this nature is beyond the scope of this study.

Additionally, we found puzzling differences between our small hillslope-bounded runoff plot and watershed-integrated pressure transducer data for earlier storm events (Figure 2.5, Table 2.2). Although this plot was a useful indicator of whether runoff was produced by the multitude of storms that impacted the field site, it is likely that the magnitude of runoff from the plot was not completely representative of hillslope runoff production throughout the whole watershed and represents only a patch of runoff produced at very low drainage areas at that particular location. This changed later in the season (January-February 2019 storms, Table 2.2) with storms of greater duration and equal or greater rainfall intensity, where there appeared to be greater spatiotemporal

coherence between the measurements (Figure 2.5C). It could be hypothesized that this is may

represent greater connectivity of runoff (Moody et al., 2013; Ebel & Moody 2012) during these

larger, longer-duration storms, which is supported by the fact that rill and inter-rill domains

remained important erosional sources for DoD2 and possibly DoD3, although rapid vegetation re-

growth (Figure A3; Figure 2.6C) likely impacted the latter. However, we did not have a fully

distributed hydrologic sensor network to affirm this. *In situ* overland flow detectors such as those

used in Schmidt et al. (2011) and Moody et al. (2015) show promise in further elucidating

spatiotemporal trends in runoff connectivity, though much like the runoff plots used in this study

they are only capable of sampling a small footprint that may not be representative of differences

in flow depth occurring in rill versus inter-rill domains. This spatiotemporal complexity could be

overcome by distributed techniques such as high-resolution multi-view stereo videos which are

now being successfully applied to understand landslide ground surface deformation (Rapstine et

al., 2020). Such a technique could be adapted to monitoring locations or burned plots subject to

experimental rainfall. Overall, this complex response involving multiple hydro-geomorphic and

biophysical processes controlling post-fire erosion and runoff highlights the continued need for

observational studies using multiple monitoring techniques (e.g., remote sensing paired with

distributed hydrologic monitoring) (Moody et al., 2013).

As noted from timelapse photography provided at the outlet retention basin of Leach Canyon by

Riverside County Flood Control and Water Conservation District (Figure A12), debris flows

produced in our headwaters (6.5 ha) devolved into water-dominated turbid flows prior to reaching

the canyon mouth (380 ha). Despite being a wetter than usual winter, this could be due to the fact

that rainfall intensities (max I_{15} = 32 mm/hr, Table 2) at our site were never more than 50% above

warning thresholds issued by the National Weather Service (I_{15} = 21 mm/hr) or USGS Debris

Flow Hazard Models (60-80% probability of debris flow from I_{15} = 24 mm/hr) (Staley et al.,

2017). Thus the debris flows produced were much smaller compared to more hazardous long run-out events such as the 2018 Montecito Debris Flows that were triggered by rainfall with peak 5-minute intensities ranging from 78-105 mm/hr (well in excess of warning thresholds), which tragically claimed 23 lives and damaged hundreds of homes in Santa Barbara county downstream of the Thomas Fire (Oakley et al., 2018; Kean et al., 2019). That event was the first major storm to make landfall over the burned coastal-facing Santa Ynez front (Oakley et al., 2018), highlighting both the importance of storm magnitude and timing relative to elevated sediment supply and decreased infiltration capacity (McGuire et al., 2019).

Our SfM channel and gully data revealed erosional patterns that are similar to Santi et al. (2008), where in that study they commonly observed increases in length-normalized erosion rates longitudinally along 46 channels scoured by debris flows. Our gully and headwater channels experienced erosion rates of 0.62 m^3/m and 1.45 m^3/m respectively (2.3-fold increase, see Figure 2.10) when summed over the course of the study, similar to their findings (Santi et al., 2008). Additionally, the SfM study by Ellett et al. (2019) showed channel scour accounted for most of the erosion in a single debris flow-producing event in a 95 ha Idaho batholith watershed, which could be analogous to our initial debris flow-producing event with significant channel scour (DoD1). Although our study is more limited in spatial scale (6.5 ha) than Ellet et al. (2019), the fact that we see a doubling of channel erosion rates from gullies to channels confirms the importance of increasing channelized erosion through debris flow scour at larger scales.

Our results are also consistent with work that has shown that once flows transition from colluvial hollows to headwater fluvial channels with significant channel fill, increases in sediment availability drive increased bulking of flow (Cannon and Gartner, 2005). In terms of the type of material accessed by these flows, fire-related ravel delivery was an important sediment source (e.g., DiBiase & Lamb, 2020; Gabet et al., 2003; Lamb et al., 2011), but it is clear from field

observations (Figure 2.8B-C) that significant material accessed from flows through these channelized features was also composed of root-stabilized pre-fire colluvial fill. Colluvial infilling is a process of long-term debris accumulation driven by soil creep, runoff, and ravel which outside of recently-burned areas can later be catastrophically mobilized through saturation-induced shallow landsliding during high-magnitude, long duration storm events (e.g., Dietrich and Dorn, 1984; Dietrich et al., 1986; Reneau et al., 1990). The process of colluvial evacuation in recently burned areas shown here is analogous to this, but instead of saturation-induced mass wasting, reductions in infiltration favoring amplified runoff production during intense rainfall are responsible for the mass wasting of these deposits, either through progressive bulking (Cannon et al., 2003; Gabet and Bookter, 2008) or channel bed failure (e.g., Gregoretti & Fontana, 2008; Prancevic et al., 2014). The clearing of longer-term accumulated deposits through these flows indicates that post-fire erosion may be an important process in longer-term sediment transfers and landscape evolution at this site, as has been highlighted regionally in southern California (Lavé & Burbank, 2004) and elsewhere in the western US (e.g., Pierce et al., 2004; Pierce and Meyer, 2008; Orem & Pelletier, 2016; Roering et al., 2005).

This study also highlighted the utility of employing UAV-SfM to sequentially document channel erosion processes, which used only a consumer-grade (DJI Mavic Pro) with a non-metric camera that was easily deployed into autonomous mode. Being able to rapidly deploy UAV to areas with survey control to quantify sediment flux in post-fire channels before and after storm events is a very useful tool, especially given increasing evidence that hydrodynamic thresholds leading to channel bed failure processes (e.g., Tillery & Rengers, 2019; Rengers et al., 2019; Tang et al., 2019) appear to be important in the generation of post-fire debris flows.

2.7. Conclusions

In this study, we used repeat TLS and UAV-SfM data in combination with hydrologic monitoring to examine how sediment sources fueling post-fire runoff and debris flows evolved in a burned headwater catchment in the Santa Ana Mountains, California, USA. During the first few storm events, more than half of the eroded sediment from a 0.95 ha zero-order catchment was derived from the formation of gullies in two colluvial hollows, and the remainder came from approximately equal amounts of rill and inter-rill erosion on surrounding hillslopes. Using coeval SfM measurements, we noted that these flows efficiently entrained and transported material in channels, with much of the material from these channels evacuated down to bedrock. Following these storms, overall sediment yields were subdued, despite equal or greater rainfall intensities, but inter-rill erosion continued at similar levels. Continued channel erosion occurred in the form of bank mass wasting and localized downcutting acted to convey material effectively downstream, but at a much smaller rate than during the first channel-clearing flows. Additionally, we noted rapid revegetation during the late winter that likely acted to increase hydraulic roughness and decrease rainsplash erosion. Overall, these results indicate that in the presence of repeated runoff events, sediment availability is a key control on event-scale sediment yield, and that the magnitude and rate of this availability was driven by depleted supply in the channelized domains and expanded hydrologic connectivity through intense rainfall for rill and inter-rill sources on the hillslopes. This study also highlights the utility of using nested scales of change detection and hydrologic monitoring to collect data that could be used in future studies to calibrate and validate numerical models of post-fire erosion.

Chapter 2 Acknowledgements

Chapter 2 Data Availability Statement

Geospatial data produced in this study is stored in the UNAVCO TLS and SfM archives. TLS data produced and used in this study can be found here: https://doi.org/10.7283/5vs7-xj27. SfM data produced and used in this study can be found here: https://doi.org/10.7283/p1ga-wj12. Hydrologic data produced and used in this study can be found in the CUAHSI HydroClient: https://data.cuahsi.org/ by searching "Holy Fire" in the data service filter and the data service

information page is located here: http://hiscentral.cuahsi.org/pub_network.aspx?n=5665. USGS

airborne lidar DEMs used for hillshades in this study can be found here:

https://www.sciencebase.gov/catalog/item/5eaa4caa82cefae35a21fee7. PRISM precipitation data

was provided by the PRISM Climate Group at Oregon State (http://prism.oregonstate.edu).

NOAA precipitation data at an additional rain gage (LDYC) was provided by NOAA NCDC

(https://www.ncdc.noaa.gov/cdo-web/). USGS debris flow hazard probability information was

accessed at: https://landslides.usgs.gov/hazards/postfire_debrisflow/.

Chapter 2 References

Atchley, A. L., Kinoshita, A. M., Lopez, S. R., Trader, L., & Middleton, R. (2018). Simulating Surface and Subsurface Water Balance Changes Due to Burn Severity. *Vadose Zone Journal*, *17*(1), 0. https://doi.org/10.2136/vzj2018.05.0099

Barnhart, T. B., & Crosby, B. T. (2013). Comparing two methods of surface change detection on an evolving thermokarst using high-temporal-frequency terrestrial laser scanning, Selawik River, Alaska. *Remote Sensing*, *5*(6), 2813–2837. https://doi.org/10.3390/rs5062813

Benavides-Solorio, J., & MacDonald, L. H. (2001). Post-fire runoff and erosion from simulated rainfall on small plots, Colorado Front Range. *Hydrological Processes*, *15*(15), 2931–2952. https://doi.org/10.1002/hyp.383

Bodí, M. B., Martin, D. A., Balfour, V. N., Santín, C., Doerr, S. H., Pereira, P., Cerdà, A., & Mataix-Solera, J. (2014). Wildland fire ash: Production, composition and eco-hydro-geomorphic effects. *Earth-Science Reviews*, *130*, 103–127. https://doi.org/10.1016/j.earscirev.2013.12.007

Bowman, D. M. J. S., Balch, J., Artaxo, P., Bond, W. J., Cochrane, M. A., D'Antonio, C. M., Defries, R., Johnston, F. H., Keeley, J. E., Krawchuk, M. A., Kull, C. A., Mack, M., Moritz, M. A., Pyne, S., Roos, C. I., Scott, A. C., Sodhi, N. S., & Swetnam, T. W. (2011). The human dimension of fire regimes on Earth. *Journal of Biogeography*, *38*(12), 2223–2236. https://doi.org/10.1111/j.1365-2699.2011.02595.x

Brogan, D. J., Nelson, P. A., & MacDonald, L. H. (2019). Spatial and temporal patterns of sediment storage and erosion following a wildfire and extreme flood. *Earth Surface Dynamics*, *7*(2), 563–590. https://doi.org/10.5194/esurf-7-563-2019

Campos, I., Vale, C., Abrantes, N., Keizer, J. J., & Pereira, P. (2015). Effects of wildfire on mercury mobilisation in eucalypt and pine forests. *Catena*, *131*, 149–159. https://doi.org/10.1016/j.catena.2015.02.024

Cannon, S. H., Kirkham, R. M., & Parise, M. (2001). Wildfire-related debris-flow initiation processes, Storm King Mountain, Colorado. *Geomorphology*, *39*(3–4), 171–188. https://doi.org/10.1016/S0169-555X(00)00108-2

Cannon, Susan H., Boldt, E. M., Laber, J. L., Kean, J. W., & Staley, D. M. (2011). Rainfall intensity-duration thresholds for postfire debris-flow emergency-response planning. *Natural Hazards*, *59*(1), 209–236. https://doi.org/10.1007/s11069-011-9747-2

Cannon, Susan H., Gartner, J. E., Rupert, M. G., Michael, J. A., Rea, A. H., & Parrett, C. (2010). Predicting the probability and volume of postwildfire debris flows in the intermountain western United States. *Bulletin of the Geological Society of America*, *122*(1–2), 127–144. https://doi.org/10.1130/B26459.1

Cannon, Susan H., Gartner, J. E., Wilson, R. C., Bowers, J. C., & Laber, J. L. (2008). Storm rainfall conditions for floods and debris flows from recently burned areas in southwestern Colorado and southern California. *Geomorphology*, *96*(3–4), 250–269. https://doi.org/10.1016/j.geomorph.2007.03.019

Cattau, M. E., Wessman, C., Mahood, A., & Balch, J. K. (2020). Anthropogenic and lightning-started fires are becoming larger and more frequent over a longer season length in the U.S.A. *Global Ecology and Biogeography*, *29*(4), 668–681. https://doi.org/10.1111/geb.13058

Chin, A., Solverson, A. P., O'Dowd, A. P., Florsheim, J. L., Kinoshita, A. M., Nourbakhshbeidokhti, S., Sellers, S. M., Tyner, L., & Gidley, R. (2019). Interacting geomorphic and ecological response of step-pool streams after wildfire. *Bulletin of the Geological Society of America*, *131*(9–10), 1480–1500. https://doi.org/10.1130/B35049.1

Collins, B. D., Oakley, N. S., Perkins, J. P., East, A. E., Corbett, S. C., & Hatchett, B. J. (2020). Linking Mesoscale Meteorology With Extreme Landscape Response: Effects of Narrow Cold Frontal Rainbands (NCFR). *Journal of Geophysical Research: Earth Surface*, *125*(10), 1–19. https://doi.org/10.1029/2020JF005675

Coombs, J. S., & Melack, J. M. (2013). Initial impacts of a wildfire on hydrology and suspended sediment and nutrient export in California chaparral watersheds. *Hydrological Processes*, *27*(26), 3842–3851. https://doi.org/10.1002/hyp.9508

Cox, R. D., Preston, K. L., Johnson, R. F., Minnich, R. A., & Allen, E. B. (2014). Influence of landscape-scale variables on vegetation conversion to exotic annual grassland in southern California, USA. *Global Ecology and Conservation*, *2*, 190–203. https://doi.org/10.1016/j.gecco.2014.09.008

Crozier, M. J. (1999). Prediction of rainfall-triggered landslides: A test of the antecedent water status model. *Earth Surface Processes and Landforms*, *24*(9), 825–833. https://doi.org/10.1002/(SICI)1096-9837(199908)24:9<825::AID-ESP14>3.0.CO;2-M

Dibiase, R. A., Heimsath, A. M., & Whipple, K. X. (2012). Hillslope response to tectonic forcing in threshold landscapes. *Earth Surface Processes and Landforms*, *37*(8), 855–865. https://doi.org/10.1002/esp.3205

Dibiase, R. A., & Lamb, M. P. (2013). Vegetation and wildfire controls on sediment yield in bedrock landscapes. *Geophysical Research Letters*, *40*(6), 1093–1097. https://doi.org/10.1002/grl.50277

DiBiase, R. A., & Lamb, M. P. (2020). Dry sediment loading of headwater channels fuels post-wildfire debris flows in bedrock landscapes. *Geology*, *48*(2), 189–193. https://doi.org/10.1130/G46847.1

DiBiase, R. A., Whipple, K. X., Heimsath, A. M., & Ouimet, W. B. (2010). Landscape form and millennial erosion rates in the San Gabriel Mountains, CA. *Earth and Planetary Science Letters*, *289*(1–2), 134–144. https://doi.org/10.1016/j.epsl.2009.10.036

Donato, D. C., Fontaine, J. B., Campbell, J. L., Robinson, W. D., Kauffman, J. B., & Law, B. E. (2006). Post-wildfire logging hinders regeneration and increases fire risk. *Science*, *311*(5759), 352. https://doi.org/10.1126/science.1122855

Ebel, B. A., & Martin, D. A. (2017). Meta-analysis of field-saturated hydraulic conductivity recovery following wildland fire: Applications for hydrologic model parameterization and resilience assessment. *Hydrological Processes*, *31*(21), 3682–3696. https://doi.org/10.1002/hyp.11288

Ebel, B. A., & Moody, J. A. (2020). Parameter estimation for multiple post-wildfire hydrologic models. *Hydrological Processes*, *34*(21), 4049–4066. https://doi.org/10.1002/hyp.13865

Ebel, B. A., Moody, J. A., & Martin, D. A. (2012). Hydrologic conditions controlling runoff generation immediately after wildfire. *Water Resources Research*, *48*(3), 1–13. https://doi.org/10.1029/2011WR011470

Ellett, N. G., Pierce, J. L., & Glenn, N. F. (2019). Partitioned by process: Measuring post-fire debris-flow and rill erosion with Structure from Motion photogrammetry. *Earth Surface Processes and Landforms*, *44*(15), 3128–3146. https://doi.org/10.1002/esp.4728

Florsheim, J. L., Pellerin, B. a., Oh, N. H., Ohara, N., Bachand, P. a M., Bachand, S. M., Bergamaschi, B. a., Hernes, P. J., & Kavvas, M. L. (2011). From deposition to erosion: Spatial and temporal variability of sediment sources, storage, and transport in a small agricultural watershed. *Geomorphology*, *132*(3–4), 272–286. https://doi.org/10.1016/j.geomorph.2011.04.037

Florsheim, Joan L, & Gaffney, K. (2013). *Thresholds of stability in incised " Anthropocene " landscapes. October*. https://doi.org/10.1016/j.ancene.2013.10.006

Furbish, D. J., Roering, J. J., Doane, T. H., Roth, D. L., Williams, S. G. W., & Abbott, A. M. (2021). Rarefied particle motions on hillslopes - Part 1: Theory. *Earth Surface Dynamics*, *9*(3), 539–576. https://doi.org/10.5194/esurf-9-539-2021

Gabet, E. J. (2003). Sediment transport by dry ravel. *Journal of Geophysical Research: Solid Earth*, *108*(B1), 1–8. https://doi.org/10.1029/2001JB001686

Gabet, E. J., & Dunne, T. (2002). Landslides on coastal sage-scrub and grassland hillslopes in a severe El Niño winter: The effects of vegetation conversion on sediment delivery. *Bulletin of the Geological Society of America*, *114*(8), 983–990. https://doi.org/10.1130/0016-7606(2002)114<0983:LOCSSA>2.0.CO;2

Gao, P. (2013). Rill and Gully Development Processes. *Treatise on Geomorphology*, *7*, 122–131. https://doi.org/10.1016/j.physc.2009.10.149

Gartner, J. E., Cannon, S. H., & Santi, P. M. (2014). Empirical models for predicting volumes of sediment deposited by debris flows and sediment-laden floods in the transverse ranges of southern California. *Engineering Geology*, *176*, 45–56. https://doi.org/10.1016/j.enggeo.2014.04.008

Guilinger, J. J., Gray, A. B., Barth, N. C., & Fong, B. T. (2020). The Evolution of Sediment Sources Over a Sequence of Postfire Sediment-Laden Flows Revealed Through Repeat High-Resolution Change Detection. *Journal of Geophysical Research: Earth Surface*, *125*(10), 1–23. https://doi.org/10.1029/2020JF005527

Hungr, O., McDougall, S., & Bovis, M. (2007). Entrainment of material by debris flows. *Debris-Flow Hazards and Related Phenomena*, 135–158. https://doi.org/10.1007/3-540-27129-5_7

Hunsinger, G. B., Mitra, S., Warrick, J. A., & Alexander, C. R. (2008). Oceanic loading of wildfire-derived organic compounds from a small mountainous river. *Journal of Geophysical Research: Biogeosciences*, *113*(2), 1–14. https://doi.org/10.1029/2007JG000476

Iverson, R. M. (1997). of Debris. *American Geophysical Union*, *97*, 245–296.

Jackson, M., & Roering, J. J. (2009). Post-fire geomorphic response in steep, forested landscapes: Oregon Coast Range, USA. *Quaternary Science Reviews*, *28*(11–12), 1131–1146. https://doi.org/10.1016/j.quascirev.2008.05.003

Kampf, S. K., Brogan, D. J., Schmeer, S., MacDonald, L. H., & Nelson, P. A. (2016). How do geomorphic effects of rainfall vary with storm type and spatial scale in a post-fire landscape? *Geomorphology*, *273*, 39–51. https://doi.org/10.1016/j.geomorph.2016.08.001

Kean, J. W., Staley, D. M., Lancaster, J. T., Rengers, F. K., Swanson, B. J., Coe, J. A., Hernandez, J. L., Sigman, A. J., Allstadt, K. E., & Lindsay, D. N. (2019). Inundation, flow dynamics, and damage in the 9 January 2018 Montecito debris-flow event, California, USA: Opportunities and challenges for post-wildfire risk assessment. *Geosphere*, *15*(4), 1140–1163. https://doi.org/10.1130/GES02048.1

Kean, Jason W., & Staley, D. M. (2021). Forecasting the Frequency and Magnitude of Postfire Debris Flows Across Southern California. *Earth's Future*, *9*(3). https://doi.org/10.1029/2020EF001735

Kean, Jason W., Staley, D. M., & Cannon, S. H. (2011). In situ measurements of post-fire debris flows in southern California: Comparisons of the timing and magnitude of 24 debris-flow events with rainfall and soil moisture conditions. *Journal of Geophysical Research: Earth Surface*, *116*(4), 1–21. https://doi.org/10.1029/2011JF002005

Kean, Jason W., Staley, D. M., Leeper, R. J., Schmidt, K. M., & Gartner, J. E. (2012). A low-cost method to measure the timing of postfire flash floods and debris flows relative to rainfall. *Water Resources Research*, *48*(5), 1–8. https://doi.org/10.1029/2011WR011460

Keeley, J. E., & Fotheringham, C. J. (2001). Historic fire regime in southern California shrublands. *Conservation Biology*, *15*(6), 1536–1548. https://doi.org/10.1046/j.1523-1739.2001.00097.x

Keeley, J. E., Franklin, J., & Antonio, C. D. (2011). *The Landscape Ecology of Fire | Donald McKenzie | Springer*. 193–221. https://doi.org/10.1007/978-94-007-0301-8

Keeley, J. E., & Pausas, J. G. (2019). Distinguishing disturbance from perturbations in fire-prone ecosystems. *International Journal of Wildland Fire*, *28*(4), 282–287. https://doi.org/10.1071/WF18203

Keeley, J. E., & Syphard, A. D. (2019). Twenty-first century California, USA, wildfires: fuel-dominated vs. wind-dominated fires. *Fire Ecology*, *15*(1). https://doi.org/10.1186/s42408-019-0041-0

Kinoshita, A. M., & Hogue, T. S. (2015). Increased dry season water yield in burned watersheds in Southern California. *Environmental Research Letters*, *10*(1). https://doi.org/10.1088/1748-9326/10/1/014003

Kirby, M. E., Poulsen, C. J., Lund, S. P., Patterson, W. P., Reidy, L., & Hammond, D. E. (2004). Late Holocene lake level dynamics inferred from magnetic susceptibility and stable oxygen isotope data: Lake Elsinore, southern California (USA). *Journal of Paleolimnology*, *31*(3), 275–293. https://doi.org/10.1023/B:JOPL.0000021710.39800.f6

Lague, D., Brodu, N., Leroux, J., Rennes, G., Rennes, U., & Beaulieu, C. De. (n.d.). *Accurate 3D comparison of complex topography with terrestrial laser scanner : application to the Rangitikei canyon (N-Z). February 2013*, 1–28.

Lamb, M. P., Scheingross, J. S., Amidon, W. H., Swanson, E., & Limaye, A. (2011). A model for fire-induced sediment yield by dry ravel in steep landscapes. *Journal of Geophysical Research: Earth Surface*, *116*(3), 1–13. https://doi.org/10.1029/2010JF001878

Larsen, I. J., MacDonald, L. H., Brown, E., Rough, D., Welsh, M. J., Pietraszek, J. H., Libohova, Z., de Dios Benavides-Solorio, J., & Schaffrath, K. (2009). Causes of Post-Fire Runoff and Erosion: Water Repellency, Cover, or Soil Sealing? *Soil Science Society of America Journal*, *73*(4), 1393. https://doi.org/10.2136/sssaj2007.0432

Lavé, J., & Burbank, D. W. (2004). Denudation processes and rates in the Transverse Ranges, southern California: Erosional response of a transitional landscape to external and anthropogenic forcing. *Journal of Geophysical Research*, *109*(F1), F01006. https://doi.org/10.1029/2003JF000023

Liu, T., McGuire, L. A., Wei, H., Rengers, F. K., Gupta, H., Ji, L., & Goodrich, D. C. (2021). The timing and magnitude of changes to Hortonian overland flow at the watershed scale during the post-fire recovery process. *Hydrological Processes*, *35*(5), 1–18. https://doi.org/10.1002/hyp.14208

Lu, M., Ikejiri, T., & Lu, Y. H. (2021). A synthesis of the Devonian wildfire record: Implications for paleogeography, fossil flora, and paleoclimate. *Palaeogeography, Palaeoclimatology, Palaeoecology*, *571*(February), 110321. https://doi.org/10.1016/j.palaeo.2021.110321

MacDonald, L. H., & Larsen, I. J. (2009). Runoff and Erosion from Wildfires and Roads: Effects and Mitigation, ch 9. *Land Restoration to Combat Desertification: Innovative Approaches, Quality Control and Project Evaluation , Dissmeyer 2000*, 145–167.

Martinez, D., & Anderson, M. A. (2013). Methane production and ebullition in a shallow, artificially aerated, eutrophic temperate lake (Lake Elsinore, CA). *Science of the Total Environment*, *454–455*, 457–465. https://doi.org/10.1016/j.scitotenv.2013.03.040

McCoy, S. W., Kean, J. W., Coe, J. A., Staley, D. M., Wasklewicz, T. A., & Tucker, G. E. (2010). Evolution of a natural debris flow: In situ measurements of flow dynamics, video imagery, and terrestrial laser scanning. *Geology*, *38*(8), 735–738. https://doi.org/10.1130/G30928.1

McGuire, L. A., Kean, J. W., Staley, D. M., Rengers, F. K., & Wasklewicz, T. A. (2016). Constraining the relative importance of raindrop- and flow-driven sediment transport mechanisms in postwildfire environments and implications for recovery time scales. *Journal of Geophysical Research: Earth Surface*, *121*(11), 2211–2237. https://doi.org/10.1002/2016JF003867

McGuire, L. A., Rengers, F. K., Kean, J. W., & Staley, D. M. (2017). Debris flow initiation by runoff in a recently burned basin: Is grain-by-grain sediment bulking or en masse failure to blame? *Geophysical Research Letters*, *44*(14), 7310–7319. https://doi.org/10.1002/2017GL074243

McGuire, L. A., Rengers, F. K., Kean, J. W., Staley, D. M., & Mirus, B. B. (2018). Incorporating spatially heterogeneous infiltration capacity into hydrologic models with applications for simulating post-wildfire debris flow initiation. *Hydrological Processes*, *32*(9), 1173–1187. https://doi.org/10.1002/hyp.11458

Mensing, S. A., Michaelsen, J., & Byrne, R. (1999). *142-1999-A 560-year record of Santa Ana fires reconstructed from charcoal deposited in the Santa Barbara Basin.pdf*. *305*, 295–305.

Miller, M. E., MacDonald, L. H., Robichaud, P. R., & Elliot, W. J. (2011). Predicting post-fire hillslope erosion in forest lands of the western United States. *International Journal of Wildland Fire*, *20*(8), 982–999. https://doi.org/10.1071/WF09142

Minnich, R. A. (1983). Fire Mosaics in Southern California and Northern Baja California. In *Science* (Vol. 219, Issue 4590, pp. 1287–1294). https://doi.org/10.1126/science.219.4590.1287

Mirus, B. B., & Loague, K. (2013). How runoff begins (and ends): Characterizing hydrologic response at the catchment scale. *Water Resources Research*, *49*(5), 2987–3006. https://doi.org/10.1002/wrcr.20218

Montgomery, D. R., & Dietrich, W. E. (1994). A physically based model for the topographical control on shallow landsliding. *Water Resources Research*, *30*(4), 1153–1171. https://doi.org/10.1029/93WR02979

Montgomery, D. R., Schmidt, K. M., Greenberg, H. M., & Dietrich, W. E. (2000). Forest clearing and regional landsliding. *Geology*, *28*(4), 311–314. https://doi.org/10.1130/0091-7613(2000)28<311:FCARL>2.0.CO;2

Moody, J. A. (2017). Residence times and alluvial architecture of a sediment superslug in response to different flow regimes. *Geomorphology*, *294*(April), 40–57. https://doi.org/10.1016/j.geomorph.2017.04.012

Moody, J. A., & Ebel, B. A. (2014). Infiltration and runoff generation processes in fire-affected soils. *Hydrological Processes*, *28*(9), 3432–3453. https://doi.org/10.1002/hyp.9857

Moody, J. A., Ebel, B. A., Nyman, P., Martin, D. A., Stoof, C., & Mckinley, R. (2016). Relations between soil hydraulic properties and burn severity. *International Journal of Wildland Fire*, *25*(3), 279–293. https://doi.org/10.1071/WF14062

Moody, J. A., & Martin, D. A. (2001). Initial hydrologic and geomorphic response following a wildfire in the Colorado front range. *Earth Surface Processes and Landforms*, *26*(10), 1049–1070. https://doi.org/10.1002/esp.253

Moody, J. A., & Martin, D. A. (2009). Synthesis of sediment yields after wildland fire in different rainfall regimes in the western United States. *International Journal of Wildland Fire*, *18*(1), 96–115. https://doi.org/10.1071/WF07162

Moody, J. A., & Martin, R. G. (2015). Measurements of the initiation of post-wildfire runoff during rainstorms using in situ overland flow detectors. *Earth Surface Processes and Landforms*, *40*(8), 1043–1056. https://doi.org/10.1002/esp.3704

Moody, J. A., Shakesby, R. A., Robichaud, P. R., Cannon, S. H., & Martin, D. A. (2013). Current research issues related to post-wildfire runoff and erosion processes. *Earth-Science Reviews*, *122*, 10–37. https://doi.org/10.1016/j.earscirev.2013.03.004

Murphy, B. P., Czuba, J. A., & Belmont, P. (2019). Post-wildfire sediment cascades: A modeling framework linking debris flow generation and network-scale sediment routing. *Earth Surface Processes and Landforms*, *44*(11), 2126–2140. https://doi.org/10.1002/esp.4635

Murphy, B. P., Yocom, L. L., & Belmont, P. (2018). Beyond the 1984 Perspective: Narrow Focus on Modern Wildfire Trends Underestimates Future Risks to Water Security. *Earth's Future*, *6*(11), 1492–1497. https://doi.org/10.1029/2018EF001006

Murphy, S. F., McCleskey, R. B., Martin, D. A., Holloway, J. A. M., & Writer, J. H. (2020). Wildfire-driven changes in hydrology mobilize arsenic and metals from legacy mine waste. *Science of the Total Environment*, *743*, 140635. https://doi.org/10.1016/j.scitotenv.2020.140635

Neely, A. B., & DiBiase, R. A. (2020). Drainage Area, Bedrock Fracture Spacing, and Weathering Controls on Landscape-Scale Patterns in Surface Sediment Grain Size. *Journal of Geophysical Research: Earth Surface*, *125*(10), 1–22. https://doi.org/10.1029/2020JF005560

Neris, J., Santin, C., Lew, R., Robichaud, P. R., Elliot, W. J., Lewis, S. A., Sheridan, G., Rohlfs, A. M., Ollivier, Q., Oliveira, L., & Doerr, S. H. (2021). Designing tools to predict and mitigate impacts on water quality following the Australian 2019/2020 wildfires: Insights from Sydney's largest water supply catchment. *Integrated Environmental Assessment and Management*, *00*(00), 1–11. https://doi.org/10.1002/ieam.4406

Nyman, P., Sheridan, G. J., Moody, J. A., Smith, H. G., Noske, P. J., & Lane, P. N. J. (2013). Sediment availability on burned hillslopes. *Journal of Geophysical Research: Earth Surface*, *118*(4), 2451–2467. https://doi.org/10.1002/jgrf.20152

Nyman, P., Sheridan, G. J., Smith, H. G., & Lane, P. N. J. (2014). Modeling the effects of surface storage, macropore flow and water repellency on infiltration after wildfire. *Journal of Hydrology*, *513*, 301–313. https://doi.org/10.1016/j.jhydrol.2014.02.044

Odigie, K. O., & Flegal, A. R. (2011). Pyrogenic remobilization of historic industrial lead depositions. *Environmental Science and Technology*, *45*(15), 6290–6295. https://doi.org/10.1021/es200944w

Odigie, K. O., Khanis, E., Hibdon, S. A., Jana, P., Araneda, A., Urrutia, R., & Flegal, A. R. (2016). Remobilization of trace elements by forest fire in Patagonia, Chile. *Regional Environmental Change*, *16*(4), 1089–1096. https://doi.org/10.1007/s10113-015-0825-y

Orem, C. A., & Pelletier, J. D. (2015). Quantifying the time scale of elevated geomorphic response following wildfires using multi-temporal LiDAR data: An example from the Las Conchas fire, Jemez Mountains, New Mexico. *Geomorphology*, *232*, 224–238. https://doi.org/10.1016/j.geomorph.2015.01.006

Overpeck, J. T., & Udall, B. (2020). Climate change and the aridification of North America. *Proceedings of the National Academy of Sciences of the United States of America*, *117*(22), 11856–11858. https://doi.org/10.1073/pnas.2006323117

Palucis, M. C., Ulizio, T. P., & Lamb, M. P. (2021). Debris flow initiation from ravel-filled channel bed failure following wildfire in a bedrock landscape with limited sediment supply. *GSA Bulletin*, 1–18. https://doi.org/10.1130/b35822.1

Parsons, A., Robichaud, P. R., Lewis, S. A., Napper, C., & Clark, J. T. (2010). Field guide for mapping post-fire soil burn severity. *USDA Forest Service - General Technical Report RMRS-GTR*, *243*, 1–49. https://doi.org/10.2737/RMRS-GTR-243

Passalacqua, P., Belmont, P., Staley, D. M., Simley, J. D., Arrowsmith, J. R., Bode, C. A., Crosby, C., Delong, S. B., Glenn, N. F., Kelly, S. A., Lague, D., Sangireddy, H., Schaffrath, K., Tarboton, D. G., Wasklewicz, T., & Wheaton, J. M. (2015). Earth-Science Reviews Analyzing high resolution topography for advancing the understanding of mass and energy transfer through landscapes : A review. *Earth Science Reviews*, *148*, 174–193. https://doi.org/10.1016/j.earscirev.2015.05.012

Pelletier, J. D., & Orem, C. A. (2014). How do sediment yields from post-wildfire debris-laden flows depend on terrain slope, soil burn severity class, and drainage basin area? Insights from airborne-LiDAR change detection. *Earth Surface Processes and Landforms*, *39*(13), 1822–1832. https://doi.org/10.1002/esp.3570

Pierce, J. L., Meyer, G. a, & Jull, a J. T. (2004). Fire-induced erosion and millennial- scale climate change in northern ponderosa pine forests. *Nature*, *432*(November), 87–90. https://doi.org/10.1038/nature03028.Published

Pierce, J. M. G. (2008). Long-term fire history from alluvial fan sediments: the role of drought and climate. *International Journal of Wildland Fire; 2008*, *17*(1), 84–95.

Poon, P. K., & Kinoshita, A. M. (2018). Spatial and temporal evapotranspiration trends after wildfire in semi-arid landscapes. *Journal of Hydrology*, *559*, 71–83. https://doi.org/10.1016/j.jhydrol.2018.02.023

Radeloff, V. C., Helmers, D. P., Kramer, H. A., Mockrin, M. H., Alexandre, P. M., Bar-Massada, A., Butsic, V., Hawbaker, T. J., Martinuzzi, S., Syphard, A. D., & Stewart, S. I. (2018). Rapid growth of the US wildland-urban interface raises wildfire risk. *Proceedings of the National Academy of Sciences*, *115*(13), 3314–3319. https://doi.org/10.1073/pnas.1718850115

Ralph, F. M., & Dettinger, M. D. (2011). Storms, floods, and the science of atmospheric rivers. *Eos*, *92*(32), 265–266. https://doi.org/10.1029/2011EO320001

Raymond, C. A., McGuire, L. A., Youberg, A. M., Staley, D. M., & Kean, J. W. (2020). Thresholds for post-wildfire debris flows: Insights from the Pinal Fire, Arizona, USA. *Earth Surface Processes and Landforms*, *45*(6), 1349–1360. https://doi.org/10.1002/esp.4805

Reneau, S. L. (2007). *Sediment delivery after a wildfi re*. *2*, 151–154. https://doi.org/10.1130/G23288A.1

Rengers, F. K., McGuire, L. A., Kean, J. W., Staley, D. M., Dobre, M., Robichaud, P. R., & Swetnam, T. (2021). Movement of Sediment Through a Burned Landscape: Sediment Volume Observations and Model Comparisons in the San Gabriel Mountains, California, USA. *Journal of Geophysical Research: Earth Surface*, *126*(7), 1–25. https://doi.org/10.1029/2020jf006053

Rengers, Francis K., McGuire, L. A., Oakley, N. S., Kean, J. W., Staley, D. M., & Tang, H. (2020). Landslides after wildfire: initiation, magnitude, and mobility. *Landslides*, *17*(11), 2631–2641. https://doi.org/10.1007/s10346-020-01506-3

Rickson, R. J. (2010). Fire Effects on Soils and Restoration Strategies. Edited by A. Cerda and P. R. Robichaud. Enfield, NH, USA: Science Publishers (2009), pp. 589, £85.00. ISBN 978-1-57808-526-2. *Experimental Agriculture*, *46*(02), 260. https://doi.org/10.1017/S0014479709990913

Riley, K., Pierce, J., & Meyer, G. A. (2015). Vegetative and climatic controls on Holocene wildfire and erosion recorded in alluvial fans of the Middle Fork Salmon River, Idaho. *Holocene*, *25*(5), 857–871. https://doi.org/10.1177/0959683615571423

Robinne, F. N., Hallema, D. W., Bladon, K. D., Flannigan, M. D., Boisramé, G., Bréthaut, C. M., Doerr, S. H., Di Baldassarre, G., Gallagher, L. A., Hohner, A. K., Khan, S. J., Kinoshita, A. M., Mordecai, R., Nunes, J. P., Nyman, P., Santín, C., Sheridan, G., Stoof, C. R., Thompson, M. P., … Wei, Y. (2021). Scientists' warning on extreme wildfire risks to water supply. *Hydrological Processes*, *35*(5), 0–3. https://doi.org/10.1002/hyp.14086

Roth, D. L., Doane, T. H., Roering, J. J., Furbish, D. J., & Zettler-Mann, A. (2020). Particle motion on burned and vegetated hillslopes. *Proceedings of the National Academy of Sciences of the United States of America*, *117*(41), 25335–25343. https://doi.org/10.1073/pnas.1922495117

Sankey, J. B., Germino, M. J., & Glenn, N. F. (2009). Aeolian sediment transport following wildfire in sagebrush steppe. *Journal of Arid Environments*, *73*(10), 912–919. https://doi.org/10.1016/j.jaridenv.2009.03.016

Sankey, Joel B., Kreitler, J., Hawbaker, T. J., McVay, J. L., Miller, M. E., Mueller, E. R., Vaillant, N. M., Lowe, S. E., & Sankey, T. T. (2017). Climate, wildfire, and erosion ensemble foretells more sediment in western USA watersheds. *Geophysical Research Letters*, *44*(17), 8884–8892. https://doi.org/10.1002/2017GL073979

Santi, P. M., deWolfe, V. G., Higgins, J. D., Cannon, S. H., & Gartner, J. E. (2008). Sources of debris flow material in burned areas. *Geomorphology*, *96*(3–4), 310–321. https://doi.org/10.1016/j.geomorph.2007.02.022

Santi, P. M., & MacAulay, B. (2019). Rainfall intensity limitation and sediment supply independence of post-wildfire debris flows in the western U.S. *Debris-Flow Hazards Mitigation: Mechanics, Monitoring, Modeling, and Assessment - Proceedings of the 7th International Conference on Debris-Flow Hazards Mitigation*, *2005*, 539–547.

Schmidt, K. M., Roering, J. J., Stock, J. D., Dietrich, W. E., Montgomery, D. R., & Schaub, T. (2001). The variability of root cohesion as an influence on shallow landslide susceptibility in the Oregon Coast Range. *Canadian Geotechnical Journal*, *38*(5), 995–1024. https://doi.org/10.1139/cgj-38-5-995

Schmidt, Kevin M., Hanshaw, M. N., Howle, J. F., Kean, J. W., Staley, D. M., Stock, J. D., & Bawden, G. W. (2011). Hydrologic Conditions and Terrestrial Laser Scanning of Post-fire Debris Flows in the San Gabriel Mountains, CA, U.S.A. *Debris-Flow Hazards Mitigation, Mechanics, Prediction, and Assessment*, 583–593. https://doi.org/10.4408/IJEGE.2011-03.B-064

Schwanghart, W., & Kuhn, N. J. (2010). TopoToolbox: A set of Matlab functions for topographic analysis. *Environmental Modelling and Software*, *25*(6), 770–781. https://doi.org/10.1016/j.envsoft.2009.12.002

Shakesby, R. a., & Doerr, S. H. (2006). Wildfire as a hydrological and geomorphological agent. *Earth-Science Reviews*, *74*(3–4), 269–307. https://doi.org/10.1016/j.earscirev.2005.10.006

Shakesby, R. A., & Doerr, S. H. (2006). *Wildfire as a hydrological and geomorphological agent*. *74*, 269–307. https://doi.org/10.1016/j.earscirev.2005.10.006

Sklar, L. S., Riebe, C. S., Marshall, J. A., Genetti, J., Leclere, S., Lukens, C. L., & Merces, V. (2017). The problem of predicting the size distribution of sediment supplied by hillslopes to rivers. *Geomorphology*, *277*, 31–49. https://doi.org/10.1016/j.geomorph.2016.05.005

Staley, D. M., Kean, J. W., & Rengers, F. K. (2020). The recurrence interval of post-fire debris-flow generating rainfall in the southwestern United States. *Geomorphology*, *370*, 107392. https://doi.org/10.1016/j.geomorph.2020.107392

Staley, D. M., Negri, J. A., Kean, J. W., Laber, J. L., Tillery, A. C., & Youberg, A. M. (2017). Prediction of spatially explicit rainfall intensity–duration thresholds for post-fire debris-flow generation in the western United States. *Geomorphology*, *278*, 149–162. https://doi.org/10.1016/j.geomorph.2016.10.019

Staley, D. M., Wasklewicz, T. A., & Kean, J. W. (2014a). Characterizing the primary material sources and dominant erosional processes for post-fire debris-flow initiation in a headwater basin using multi-temporal terrestrial laser scanning data. *Geomorphology*, *214*, 324–338. https://doi.org/10.1016/j.geomorph.2014.02.015

Staley, D. M., Wasklewicz, T. A., & Kean, J. W. (2014b). Characterizing the primary material sources and dominant erosional processes for post-fire debris-flow initiation in a headwater basin using multi-temporal terrestrial laser scanning data. *Geomorphology*, *214*, 324–338. https://doi.org/10.1016/j.geomorph.2014.02.015

Steeplands, C., California, S., Wohlgemuth, P. M., & Hubbert, K. R. (2008). *The Effects of Fire on Soil Hydrologic Properties and Sediment Fluxes in*. 115–122.

Stein, E. D., Brown, J. S., Hogue, T. S., Burke, M. P., & Kinoshita, A. (2012). Stormwater contaminant loading following southern California wildfires. *Environmental Toxicology and Chemistry*, *31*(11), 2625–2638. https://doi.org/10.1002/etc.1994

Swain, D. L., Langenbrunner, B., Neelin, J. D., & Hall, A. (2018). Increasing precipitation volatility in twenty-first-century California. *Nature Climate Change*, *8*(5), 427–433. https://doi.org/10.1038/s41558-018-0140-y

Syphard, A. D., & Keeley, J. E. (2015). Location, timing and extent of wildfire vary by cause of ignition. *International Journal of Wildland Fire*, *24*(1), 37–47. https://doi.org/10.1071/WF14024

Syphard, A. D., & Keeley, J. E. (2020). Mapping fire regime ecoregions in California. *International Journal of Wildland Fire*, *29*(7), 595–601. https://doi.org/10.1071/WF19136

Terwilliger, V. J., & Waldron, L. J. (1991). Effects of root reinforcement on soil-slip patterns in the Transverse Ranges of southern California. *Geological Society of America Bulletin*, *103*(6), 775–785. https://doi.org/10.1130/0016-7606(1991)103<0775:EORROS>2.3.CO;2

Thomas, M. A., Rengers, F. K., Kean, J. W., McGuire, L. A., Staley, D. M., Barnhart, K. R., & Ebel, B. A. (2021). Postwildfire Soil-Hydraulic Recovery and the Persistence of Debris Flow Hazards. *Journal of Geophysical Research: Earth Surface*, *126*(6), 1–25. https://doi.org/10.1029/2021JF006091

Thompson, J. R., Spies, T. A., & Ganio, L. M. (2007). Reburn severity in managed and unmanaged vegetation in a large wildfire. *Proceedings of the National Academy of Sciences of the United States of America*, *104*(25), 10743–10748. https://doi.org/10.1073/pnas.0700229104

Warrick, J. A., Hatten, J. A., Pasternack, G. B., Gray, A. B., Goni, M. A., & Wheatcroft, R. A. (2012). The effects of wildfire on the sediment yield of a coastal California watershed. *Bulletin of the Geological Society of America*, *124*(7–8), 1130–1146. https://doi.org/10.1130/B30451.1

Warrick, Jonathan A., Melack, J. M., & Goodridge, B. M. (2015). Sediment yields from small, steep coastal watersheds of California. *Journal of Hydrology: Regional Studies*, *4*, 516–534. https://doi.org/10.1016/j.ejrh.2015.08.004

Wester, T., Wasklewicz, T., & Staley, D. (2014). Functional and structural connectivity within a recently burned drainage basin. *Geomorphology*, *206*, 362–373. https://doi.org/10.1016/j.geomorph.2013.10.011

Westerling, A. L., Hidalgo, H. G., Cayan, D. R., & Swetnam, T. W. (2006). Warming and earlier spring increase Western U.S. forest wildfire activity. *Science*, *313*(5789), 940–943. https://doi.org/10.1126/science.1128834

Wheaton, J. M., Brasington, J., Darby, S. E., & Sear, D. A. (2010). Accounting for uncertainty in DEMs from repeat topographic surveys: Improved sediment budgets. *Earth Surface Processes and Landforms*, *35*(2), 136–156. https://doi.org/10.1002/esp.1886

Wheaton, J. M., Brasington, J., Darby, S. E., Sear, D. A., Sciences, W., & Hill, O. M. (2010). *Accounting for uncertainty in DEMs from repeat topographic surveys : improved sediment budgets*. *156*(December 2009), 136–156. https://doi.org/10.1002/esp.1886

Wilder, B. A., Lancaster, J. T., Cafferata, P. H., Coe, D. B. R., Swanson, B. J., Lindsay, D. N., Short, W. R., & Kinoshita, A. M. (2021). An analytical solution for rapidly predicting post-fire peak streamflow for small watersheds in southern California. *Hydrological Processes*, *35*(1), 1–14. https://doi.org/10.1002/hyp.13976

Williams, A. P., Abatzoglou, J. T., Gershunov, A., Guzman-Morales, J., Bishop, D. A., Balch, J. K., & Lettenmaier, D. P. (2019). Observed Impacts of Anthropogenic Climate Change on Wildfire in California. *Earth's Future*, *7*(8), 892–910. https://doi.org/10.1029/2019EF001210

Williams, A. P., Abatzoglou, J. T., Gershunov, A., Guzman-Morales, J., Bishop, D. A., Balch, J. K., & Lettenmaier, D. P. (2019). Observed impacts of anthropogenic climate change on wildfire in California. *Earth's Future*, 2019EF001210. https://doi.org/10.1029/2019EF001210

Wilson, C., Kampf, S. K., Ryan, S., Covino, T., MacDonald, L. H., & Gleason, H. (2021). Connectivity of post-fire runoff and sediment from nested hillslopes and watersheds. *Hydrological Processes*, *35*(1), 1–17. https://doi.org/10.1002/hyp.13975

Chapter 3. Channel sediment availability patterns ranging from event to decadal timescales revealed by surface differencing across hundreds of small burned mountain headwater channels, southern California, USA

Abstract

In the western US and other similar semiarid environments, wildfire is increasing both in its severity and frequency as climate change progresses, thus wildland-adjacent communities will need to increasingly contend with postfire sedimentation hazards. Considering this, additional tools are needed to understand, plan for, and mitigate postfire hazards. One large uncertainty that remains is being able to predict the volume of sediment produced from burn scars and transported downstream during rainstorms immediately following fire. In this study we focus on channelized erosion, an important component of postfire sediment budgets, and ask the following questions: (1) does erosion of headwater channel sediments become supply-limited and if it does, (2) does headwater channel supply relate to previous fire disturbance history? In order to answer these questions, we used repeat airborne lidar surface differencing in concert with additional remote sensing, burn history datasets from CALFire, and hydrometerological monitoring across a large suite (n=1551) of small (0.6-30 hectare) headwater catchments in five burn scars in southern California. In the 2018 Holy Fire, we found that wildfire-initiated dry ravel constitutes a fraction (~12%) of the total volume of channel sediments. Additionally, we observed that amplified postfire channel erosion accesses pre-fire accumulations and that this stock of sediment becomes supply-limited even in response to a sequence of rainfall intensities at 1-3 year return intervals and found that runoff-driven loading of low-order steep channel networks is very small and likely not a significant hazard. We also found that empirical models of sediment yield from similar

80

settings in southern California and Australia fit our observations and constrained hillslope erosion estimates most closely. Building off these results, we found that the magnitude of contemporary post-fire erosion increases with elapsed time since the last previous fire and that the confidence of this relationship is partially governed by the magnitude of associated previous postfire erosion. At shorter timescales of reburn (<20 years), we note that more subdued erosional responses may be controlled by lower overall burn severities using BARC data. At longer reburn timescales (>20 years), channel sediment availability becomes more pronounced with increasing hillslope angle, likely a consequence of greater coupling between steeper hillslopes and valley bottoms along with increased incidence of debris flow initiation in steep terrain. Given the readily available nature of fire history, these results can be used to inform predictions about channel sediment supplies in the state of California and beyond.

Keywords: pyrogeomorphology; debris flows; wildfire; airborne lidar; SfM; M3C2; hillslope-channel coupling

3.1. Introduction

Wildfire is a major hydrogeomorphic disturbance agent in mountainous settings worldwide (Moody et al., 2013; Shakesby & Doerr, 2006). The extent and severity of wildfire in many semiarid climates such as the western US in this study has increased in recent decades (Williams, Abatzoglou, Gershunov, Guzman-Morales, et al., 2019). Much of this driven by more prolonged and intense fire seasons due to a warming climate (Westerling et al., 2006; Williams, Abatzoglou et al., 2019), increasing incidence of drought (Swain et al., 2018), increase in anthropogenic ignition rates (Cattau et al., 2020), and in some regions, fuel buildup from prolonged fire exclusion practices during the 20th century (Murphy et al., 2018). Wildland fire intensification is concomitant with an increase in human populations along the wildland urban interface, thus

markedly increasing the exposure of infrastructure and human lives to the hazardous impacts of fire itself and the transformation of the landscape in its wake (Radeloff et al., 2018).

Wildfire greatly increases the amount of noncohesive sediment available for erosion, decreases canopy interception, reduces surface cover and roughness, and reduces the water infiltration capacity of soil, with these impacts particularly pronounced at moderate to high burn severities (Shakesby and Doerr, 2006). In steep landscapes, these conditions greatly increase the likelihood flash floods, hyperconcentrated flows, and debris flows (destructive flows composed of 50:50 water to sediment) (Cannon et al., 2010; Kean et al., 2011). Alarmingly, it has been shown that most postfire debris flows in the western US have been initiated by rainfall intensities that are likely to occur every 1-2 years (Staley et al., 2020). This is also exacerbated by projections of increased rainfall intensity as the climate warms and atmospheric water holding capacities increase (Kean & Staley, 2021; Swain et al., 2018). Therefore, wildland-bounding foothill communities will need to increasingly contend with postfire sediment hazards.

Postfire debris flows can be classified by as being triggered by runoff (Cannon et al., 2008; 2001) or infiltration-driven instabilities (e.g., Montgomery et al., 2000; Rengers et al., 2020). Runoff-generated debris flows are most common in the first year following fire when runoff partitioning of rainfall is highest and once rainfall thresholds are met during short-duration, high intensity bursts of rainfall (e.g., Cannon et al., 2008; Staley et al., 2017; Tang et al., 2019). Processes that transition runoff into debris flows include progressive bulking from hillslope erosion (Orem & Pelletier, 2015; Rengers et al., 2021; Staley et al., 2014) and channel bed/bank erosion (Ellett et al., 2019; Santi et al., 2008). Because runoff production can occur across much of the burned landscape, a diversity of hillslope and channel erosion processes can contribute sediment to these flows (Guilinger et al., 2020; McGuire et al., 2017; Staley et al., 2014a), which makes sediment source attribution for these events difficult. Some studies have found shallow hillslope erosion (F.

82

K. Rengers et al., 2021; Staley et al., 2014a) to be a primary contributor whereas others have found channelized erosion to dominate sediment source budgets (Ellett et al., 2019; Santi et al., 2008). Another class of debris flow is initiated via soil saturation by longer-duration rainfall that acts to decrease the shear strength of soils, leading to discrete shallow landslides which may undergo liquefaction and transition into debris flows (Hungr et al., 2007). Infiltration-driven landsliding has been shown to also trigger debris flows in recently burned settings, although usually a few years following fire (Jackson & Roering, 2009; Rengers et al., 2020). This time lag is caused by fire-induced tree and shrub mortality with attendant decreases in root reinforcement of hillslope soils, reduced evapotranspiration increasing antecedent soil moisture, and recovery of soil infiltration capacity (Thomas et al., 2021).

Although regionally-derived statistical models exist for estimating debris flow hazard (USGS DF Model, Staley et al., 2017), there are many difficulties in developing hazard frameworks for postfire sedimentation across fire-affected regions due to wide-varying hydrogeomorphic state variables related to debris and sediment-laden flow initiation and magnitude (Moody et al., 2013). These factors include sediment availability (Guilinger et al., 2020; Tang et al. 2019), lowered infiltration capacity (e.g., Ebel & Moody, 2020; Larsen et al., 2009), reduced evapotranspiration (Poon & Kinoshita, 2018), reduced root stability (Jackson and Roering, 2009), loss of ground cover (Benavides-Solorio & MacDonald, 2001), and reduced canopy interception (Moody & Martin, 2001). These processes are also inherently non-steady in time and can have wide-ranging timescales of recovery depending on the ecosystem and magnitude of hydrologic events following fire, making these processes difficult to parameterize (Ebel & Martin, 2017). There is evidence that very steep settings prone to episodic wildfire and postfire debris flows such as Southern California considered in the study verge towards supply-limitation due to the patchiness of soil and sediment on hillslopes and headwater channel networks. For example, in the San

Gabriel Mountains, angles are maintained above their stability limit (angle of repose ≈ 32 degrees), with vegetation acting as sediment dams (Dibiase & Lamb, 2013; Lamb et al., 2011). When biomass is combusted in these settings, soil is no longer stable and cohesionless sediment rapidly cascades downslope in a process referred to as dry ravel (e.g., Florsheim et al., 2011; Gabet, 2003; Lamb et al., 2011)). Commonly these dry ravel pulses end up in topographic low points and may subsequently fuel debris flows during even relatively modest rainstorms prior to hydrologic recovery (DiBiase & Lamb, 2020). Studies have shown that weathering products that fuel dry ravel could be limited by soil production rates, thus if fire return intervals decrease below this dry ravel rejuvenation period, there may be a reduction in sediment available for postfire sediment-laden flows (Lamb et al., 2011). Postfire debris flows commonly sweep headwater channels down to bedrock, reducing that material for subsequent debris flows. Thus, much in the same way dry ravel supply may be sensitive to timescales of fire return intervals, it is possible that inter-fire channel fill may be sensitive to the timescales of channel filling between fire-associated channel clearing flows. However, few studies have examined these effects (Loomis et al., 2003; DiBiase and Lamb, 2020), with one study finding correspondence between volumes of postfire material delivered to debris basins (Loomis et al., 2003) and another study finding little correlation between fire history and channel sediment flux (DiBiase and Lamb, 2020). Therefore, more work is needed to understand sediment supply dynamics both at the postfire seasonal and inter-fire timescales, especially in a warming climate where fire return frequency may increase (Westerling et al., 2006).

In this study, we explicitly consider processes related to sediment availability at multiple spatial and temporal scales across five different burn scars. The primary area we focus on is the 2018 Holy Fire, in which we exploit a unique dataset consisting of six repeat airborne lidar (light detection and ranging) campaigns acquired before wildfire and between major runoff events in

southern California in order to quantify spatial and temporal patterns of erosion in burned

headwater catchments (Table 1). This builds off a previous study of a 6.5 ha debris flow-

producing headwater catchment in the same region that was the subject of repeat ground-based

lidar and unmanned aerial vehicle-based structure-from-motion surveys to assess the degree of

net erosion from hillslope and upper channel network domains (Guilinger et al., 2020). In that

study, it was found that sediment supply diminished over the course of the first post-fire wet

season, driven by declining sediment supply in colluvial hollows and valley bottoms. Because the

length scale of surface change in channels is large enough (10^{-1} to 10^1 meters) to be detected with

airborne lidar, changes in channelized domains can be readily sensed across the scale of full

upland watersheds (up to tens of square kilometers) (e.g., Brogan et al., 2019; DiBiase and Lamb,

2020; Rengers et al., 2021). Thus, we set out to utilize repeat surface change detection with

airborne lidar along with other lines of evidence from hydro-geomorphic monitoring to answer

the following questions: 1. How do patterns of initial dry ravel sediment loading relate to postfire

sediment yields? 2. Are sediment depletion patterns evident in channel erosion typical features of

the studied postfire settings? 3. Does the movement of sediment into transient depositional zones

in headwater streams affect erosional risk of subsequent runoff events? Through answering these

questions with the Holy Fire dataset, we expand our scope to test the following hypothesis:

sediment availability in channels will increase with time since previous fire in steep catchments

as material accumulates in valley bottoms during inter-fire periods. In this study, we demonstrate

that a majority of channel erosion accesses pre-fire accumulations and that this stock of sediment

becomes supply-limited even in response to a sequence of rainfall intensities at 1-3 year return

intervals. Additionally, we find that runoff-driven loading of low order steep channel networks is

very small and likely not a significant hazard. Finally, expanding out over all four burn scars

using a century-long previous fire record, we find that the amount of contemporary post-fire

erosion is positively correlated to time between fires, with this correlation much stronger for areas that likely experienced higher magnitude fire-flood cycles. Importantly, we find that this effect becomes more pronounced with increasing hillslope angle, likely a consequence of greater coupling between steeper hillslopes and valley bottoms along with increased incidence of debris flow initiation in steep terrain.

3.2. Study Areas

This study included fires that burned in steep (slope: 20-45 degrees) chaparral-dominated terrain in the Santa Ana, San Gabriel, and Santa Monica Mountains (Fig 1A). Mean annual precipitation totals across the study areas ranged from 309 mm in the Elsinore Trough of the leeward side of Holy Fire burn scar to 904 mm at higher elevations in the San Gabriel front, with much of this variation driven by orographic effects (PRISM, 2021). Southern California hosts a Mediterranean climate with summer drought and most precipitation falling from November-April. All study sites are primarily classified as chaparral-dominated ecosystems with some areas of coastal sage scrub, oak woodlands, and conifers at high elevation (LANDFIRE, 2016). Chaparral is adapted to episodic wildfire regimes characterized by burn intervals of approximately 30-80 years (Minnich, 1983, Keeley refs). The study focused primarily on the 2018 Holy Fire as this burn scar had the most comprehensive remote sensing and sediment retention basin datasets. An important factor for determining the volume of sediment of postfire debris flows is short-duration bursts of rainfall intensity (Staley et al., 2017). Rainfall intensities of sufficient magnitude were evaluated across these burn scars and it was found that two or more storms were at or above thresholds for probable debris flow production (USGS, 2018) (Figure 3.1B).

3.2.1. Holy Fire (2018)

The primary focus of this study is the 2018 Holy Fire, which burned 30,000 acres of the Cleveland National Forest in the Santa Ana Mountains (Figures 3.1-2), a subrange of the Peninsular Ranges of southern California, USA. The underlying geology is composed of Cretaceous Peninsular Range granitic rocks in the core of the study area with northern and southern flanks underlain primarily by Jurassic metasedimentary strata (Morton and Miller, 2006). Inactive, Quaternary deep-seated landslide complexes have also been mapped in some zones of the field area (Morton and Miller, 2006). There were observations of widespread dry ravel loading and soil water repellency (Schwarz and Stempniewicz, 2018). USGS logistic regression debris flow predictions estimated the production of debris flows as likely in response to 1-2 year return rainfall intensities (24 mm/hr over 15 minutes, USGS 2018).

3.2.2. Woolsey Fire (2018)

The Woolsey Fire burned 39,234 ha of the Santa Monica Mountains (Figure 3.2) in November 2018. Repeat airborne lidar was collected in the central portion of the burn scar above the city of Malibu, CA. The dominant lithology is an assemblage of sandstone, shale, and andesitic-to-basaltic volcanic rocks (Yerkes and Campbell, 2005). The area experienced the same wet winter of 2018-2019 and it was noted both through local reports (NWS) and repeat imagery that debris and sediment-laden flows were triggered by intense rainfall during winter storms. Repeat lidar coverage was available for the principal canyons of Zuma, Trancas, and Ramirez drainages draining to the beaches around Malibu. Many upland catchments within these drainages were ranked as likely debris flow production zones in response to ~1 year return rainfall intensities (USGS, 2018).

3.2.3. San Gabriel Complex: Fish and Reservoir Fires (2016)

The Fish and Reservoir Fires (formally known as San Gabriel Complex) burned along the San Gabriel Mountain rangefront (Figure 2) in June 2016. The Fish Fire burned chaparral-dominated uplands above the city of Duarte, CA. Large portions of both scars fire burned at moderate to high severity (MTBS, 2021). Significant dry ravel loading and soil water repellency was present in the Fish Fire, as noted by many postfire studies of various catchments in the burn scar (Tang et al., 2019; Palucis et al., 2021; Rengers et al., 2021). Winter 2016-2017 was approximately average (rainfall intensity and duration = 1-2 year returns, Rengers et al., 2021), with rainfall intensities sufficient to produce multiple debris flows over many storm cycles (Staley et al. 2017; Tang et al., 2019). The Reservoir Fire burned steep topography above Morris Reservoir and was a repeat burn of the 2009 Morris Fire, providing an example of steep topography burned repeatedly in less than a decade. The underlying geology of the Fish and Reservoir Fires is composed of orthogneisses and granitic crystalline rock. Of all burn areas assessed, the San Gabriel Complex fires burned the steepest terrain (mean = 40 degrees) and maintains a thin and patchy soil mantle (DiBiase et al., 2010; Lavé & Burbank, 2004). Upland catchments within this burn scar were ranked as highly likely debris flow production zones in response to 0.5-1 year return rainfall intensities (USGS, 2018).

3.2.4. Blue Cut (2016)

The Blue Cut Fire (2016) burned the Cajon Pass area between the San Bernardino and San Gabriel Mountains. Repeat airborne lidar was available for the far eastern San Gabriel mountains north and east of Lytle Creek, CA along the Lone Pine Canyon drainage which is cut down the middle by the San Andreas Fault (Morton and Miller, 2006b). Within this area Google Earth Imagery show evidence of debris flow initiation following the wildfire (supplement), part of which buried railway lines in debris fans (which were cleared by the time of image acquisition).

The previous burn history of the burn scar is very complex and hosts significant areas which reburned within 7 years. The underlying geology is primarily Proterozoic metamorphic rocks (Morton and Miller, 2006b). The area with best coverage of lidar across steep terrain was in the burn scar around Lytle Creek where repeat lidar was available (Fig 3.2B), debris flow production was likely in response to ~1-2 year return 15-minute rainfall intensities.

3.3. Materials and Methods

3.3.1. ALS analysis and hillslope erosion constraints

Airborne lidar swath (ALS) mapping was performed by multiple agencies, which we detail below (Table 3.1). In the Holy Fire, five flights encompassed most of the burn scar (see Table 1 and Figure 3.1). As part of an effort funded by FEMA and the USGS to assist with wildfire-related hazards, the first dataset was advantageously acquired in late July/early August 2018 immediately prior to the wildfire. Riverside County Flood Control and Water Conservation District acquired postfire lidar prior to the first major rainfall and in between runoff events for the first year following fire, water year 2019 (WY2019: October 1 2018- 30 Sept 2019). Because four out of the five lidar datasets were from a single source that used NAD83 California State Plane VI, we projected the remaining datasets (3DEP, both NAD 83 11N) into CA State Plane using LAStools (Table 1).

Multitemporal ALS data for the 2018 Woolsey Fire was obtained prior the fire by Los Angeles County through their Los Angeles Regional Imagery Acquisition Consortium (LARIAC) in 2016. Repeat ALS data for the 2016 San Gabriel Complex Fires was obtained prior to the fire through the same LARIAC effort in 2016 and following the postfire wet season by the USGS in 2017. Similar to the Woolsey Fire, LARIAC ALS was transformed into the same reference as the USGS dataset (UTM NAD 1983 11N) reference frame (Table 3.1). ALS data for the 2016 Blue Cut Fire

was obtained before the fire by San Bernardino County in 2013 and following two winters post-fire in 2018. Both of these datasets were collected within the UTM NAD 1983 11N reference frame. A source of uncertainty for the Blue Cut methods could be the fact that five years had passed between lidar acquisitions and that other geomorphic processes could occur, but it was assumed that most of the sediment mobilization and deposition in steep catchments occurred due to postfire erosion. This assumption was validated by comparing maps of change against repeat imagery in Google Earth (Fig S1) that showed correspondence of erosion with wildfire.

Using LAStools, we extracted ground-classified clouds for all subsequent analyses. Fine registration was performed by utilizing iterative closest point between survey epochs on ~1000x1000 m tiles in CloudCompare (ver. 2.11.3). This generally resulted in RMSE registration errors of ~0.05 to 0.1 m, similar to vertical deviations reported by check points from the vendors of each dataset. We also checked these against stable road surfaces to validate the accuracy of this alignment procedure (Figures B2-5), which yielded adequate surface differencing results within reported accuracies.

We performed surface change detection directly between fine-registered point clouds using multi-scale model to model cloud comparison (M3C2, Lague et al., 2013) in CloudCompare. This tool defines surface change based on surface normal instead of the z-axis only and is less prone to interpolation errors induced by gaps within point cloud coverage. Following the tool developer's guidance and other similar studies (Barnhart & Crosby, 2013; DiBiase & Lamb, 2020; F. K. Rengers et al., 2021), we defined a projection scale (2.5 meters) in which >95% of cylinders used to define M3C2 distance had 4 or more points. M3C2 distinguishes real differences from noise by defining a 95% confidence interval by the propagated errors of registration (~0.06 m in our case), surface roughness, and point cloud density. This resulted in spatially-variable propagated errors

on the order of 0.1-0.3 meters across the landscape in which the standard error term was used to estimate pixel-by-pixel error volumes (Wheaton, et al. 2010).

Outputs were rasterized into a 1-m grid and outputs with statistically significant change (values greater than 95% CI) were retained for analysis. We also generated digital elevation models (DEMs) of every epoch using triangular irregular networks in LAStools to generate watersheds and derive slope values (LAStools, 2020). Recognizing that ALS is most accurate in capturing incisional erosion of colluvial hollows and valley bottoms, we generate flowpaths from digital elevation models using TopoToolbox using the D8 algorithm and included change within 7.5 meters of these flow lines to avoid incorporating artifacts that arise due to noise, which could arise due to differences in ground classification between different epochs, lidar vendors, or differences in vegetation regrowth, something we observed within our datasets (DiBiase and Lamb, 2020; Brogan et al., 2019). Negative values imply surface lowering (erosion) and positive values imply surface rising (deposition). Signed volumes of erosion and deposition were computed by multiplying surface changes by their respective pixel areas (1 m^2) but for the sake of measuring erosion we transformed negative volume values into positive values of erosion and positive values of deposition into negative values of erosion (e.g., Figures 3B and 5).

Using Topotoolbox (Schwanghart & Kuhn, 2010), we also delineated stream order in selected watersheds in the Holy Fire burn scar using a 1000 m^2 threshold for drainage area required for channelization (Schwanghart & Kuhn, 2010). This drainage area was verified using GEONET 2.0 (Passalacqua et al., 2010) and has also been found to be the approximate drainage area for channelization in the San Gabriel Mountains (DiBiase et al., 2012; Rengers et al., 2019). Because small headwater catchments (0.01-1km^2) situated above higher-order stream channels are zones of debris flow generation with a smaller likelihood of large deposition (Gartner et al., 2014), we took a standardized approach of delineating 3rd-order catchments as our fundamental hydrologic

units for determining the distribution of headwater postfire sediment production. Areas for these headwater catchments ranged from 0.007 to 0.3 km^2, with a mean size of 0.05 km^2. We verified that there was not a strong relationship between drainage area in which there was a very small positive effect size, though there was significantly greater variability at smaller drainage areas (Figure A6).

We recognize that not all surface changes are captured due to surface occlusion and change magnitudes below the limit of detection, which can result in significant bias from a skewed distribution of non-detects (Helsel and Hirsch, 2002; Rengers et al., 2021). Therefore, we made a direct comparison between volumes derived from ALS and that from a previous study utilizing SfM and TLS in a representative subcatchment (Guilinger et al., 2020) to understand the degree which our ALS-derived values underestimate total sediment flux from headwater catchments (Table 2). Upon comparison of collocated coeval ALS erosion volume and TLS/SfM, we found that ALS could only account for ~40% (79 m^3 of the 199 m^3 estimated) of the erosion in the zero-order subcatchment (0.95 ha) studied in Guilinger et al. 2020. Therefore, assuming this underestimation scaling applies across all studied catchments, we estimate net lowering in areas that did not have surface changes detected and were less than 45 degrees, which corresponds to slope stability threshold in which bedrock is likely to exist and appeared to work well for our the Holy Fire burn scar (DiBiase et al., 2012; Rengers et al., 2021). We checked these against independent estimates of sediment budgets for Leach and McVicker Canyons through a sediment budget mass balance closure:

$$Y_h = (V_{cd} + V_d - V_{ce})/A_S \qquad (1)$$

Where Y_h is the hillslope yield below LOD, V_{cd} is the volume of ALS-derived channel deposition, V_d is the volume of deposition into sediment retention basins, V_e is the amount of erosion above the LOD, and As is the area (m^2) of the catchment mantled by soil that did not have detected erosion (<45 degrees), which is a majority of the total contributing area. We obtained V_d values from debris basin sediment removal estimates, which are derived from a combination of truckload counts and repeat SfM from Riverside County's Flood Control and Water Conservation District (Table 3.3). This dataset consisted of truckload counts which used a conversion factor of 7 cubic yards of wet sediment per truckload. Additionally, Riverside County collected UAV SfM data from which we estimated volumes using 2.5D surface differencing in Cloudcompare (Table 3.2). We took the approach of averaging these two values and deriving an uncertainty estimate as the standard error of these two methods.

Finally, we compiled both estimates of volume from ALS channel erosion and net erosion per headwater watershed (represented as volume over contributing area or area-normalized net lowering in mm) across the study area for each time epoch and compare these to modeled estimates for debris flow production as described below.

Comparison to empirical debris flow models

We compared our estimates of erosion due to debris flows and sediment-laden flooding in headwater catchments in the Holy Fire to various empirically-derived debris production models. These models ranged in complexity from a three-parameter model to single parameter area-volume scaling relationships. We started by using arguably one of the most widely-used debris flow volume prediction models for emergency assessments, that of Gartner et al., (2014):

$$Ln(V) = 4.22 + 0.39\text{sqrt}(I_{15p}) + 0.36Ln(Bmh) + 0.13\text{sqrt}(R) \qquad (2)$$

Where V is volume (m³), I_{15p} is storm peak 15-minute rainfall intensity (mm/hr), *Bmh* is

watershed area burned at moderate and high severity (km²), and R is basin relief (m). Equation 1

is a statistical model derived from estimates of debris flow delivery to sediment retention basins

primarily in the Transverse Ranges of southern California, USA.

We also modeled sediment volumes using the approach of Pelletier and Orem (2014), who

derived debris volume estimates from airborne lidar in a burn area in the Valles Caldera area of

New Mexico, USA:

$$V = 1.53S^{1.6}B^{1.7}\,1000A \tag{3}$$

where V is volume (m³) S is catchment-averaged slope (m/m), B is the catchment-averaged

BARC reflectance class (1 = low, 2 = moderate, 3 = high) for which the product of S and B yields

sediment yield in mm (converted to m by the 1000 (mm/m) coefficient), and A is area (m²).

the remaining models we used as a basis of comparison were simple power law best-fit

relationships. First, we used a model developed using surveying and modeling of sediment efflux

from debris flows in burned Eucalypt forest in SE Australia (Nyman et al., 2020):

$$V = 0.35A^{0.73} \tag{4}$$

where A is catchment area (m²). Similarly, we used the equation that Rengers et al. (2021)

developed from a combination of airborne and terrestrial laser scanning estimates of erosion in

the San Gabriel Mountains of southern California:

$$V = 0.19A^{0.93} \tag{5}$$

where A is catchment area (m²). Finally, as a point of comparison, we ran a power law regression

between our hillslope erosion-adjusted volumes and catchment area along with raw estimates

from our channels above the limit of detection.

In order to assess the influence of lithology, we obtained digitized 30' x 60' geologic maps for Los Angeles (Yerkes and Campbell, 2005), San Bernardino (Morton and Miller, 2006a), and Santa Ana (Morton and Miller, 2006b). Quadrangles from the USGS GIS databases and geologic unit information was spatially joined using a majority function in ArcMap (ESRI). Burn area reflectance analysis products were obtained from the USGS Monitoring Trends in Burn Severity (MTBS) group (https://www.mtbs.gov/direct-download) and also joined the headwater catchments with these datasets.

3.3.2. Time since previous fire analysis

We obtained fire history information for all five burn scars from the California Department of Forestry and Fire Protection's Fire and Resource Assessment Program fire perimeter database (https://frap.fire.ca.gov/frap-projects/fire-perimeters/). The database is the product of a multi-agency effort to map burn scars with participation from the US Forest Service (dating back as far as 1878), the Bureau of Land Management (dating back to 2002), and the National Park Service (dating back to 1921). Using ArcGIS, we clipped previous burn perimeters to current fire perimeters, determined the years since previous burn, and rasterized the outputs at a 10m resolution by using a ranking scheme that overlaid the most recent burn scars. Burn areas ranged from 0 years post-fire (less than a year re-burned) up to 105 years (Figure 3.2). From this, we used a zonal statistics 'majority' function in using the R package *exactextractr*. Most catchments (>98%) had much of their area burned previously and the small number of watersheds with no record of burn history were not assigned a year but assigned a value of >105 years. Because our headwater catchments have a small spatial extent relative to most of the previous individual burn history classes, there were very few watersheds where burn history was nearly evenly split between two previous scars, justifying the simple approach of assigning time since previous fire through a majority function.

We determined that erosion magnitudes were spatially autocorrelated, through an assessment of Moran's I (Moran, 1950), that there was strong evidence for spatial autocorrelation of erosion across the full dataset. This effect is common in GIS data and likely extends to our datasets through geographically-clustered controls on erosion (e.g., rainfall patterns, relief structures, aspect, etc.). Additionally, we noted very significant non-constant variance in our erosion magnitudes across our watersheds that would lead to heteroscedasticity. Thus, to explore the amount of erosion as a function of burn history, we ran linear regressions using a generalized least squares (*GLS*) approach. GLS regression frameworks relax the assumptions of homoscedasticity (constant variance) and independence of residuals through incorporation of variance weights and correct for spatial autocorrelation (Kariya and Kurata, 2004). Using geostatistical packages in R (*nlme, gstat*), we ran a GLS regression by using variance weights modeled as a power function of the independent variable (time since previous fire) and an exponential spatial autocorrelation structure. This regression was stratified across differing slope classes: <20, 20-25, 25-30, 30-35, and 40-50 degrees. To assess the degree to which postfire erosion in the first year following fire may control the amount of sediment supply remaining in channel and hollow networks due to incomplete evacuation of postfire dry ravel or interfire accumulation (e.g., Florsheim et al., 2017; Wester et al., 2014), we queried Western Regional Climate Center data on PRISM-based precipitation indices for the initial water year of each burn scar (WRCC, 2021). Though this dataset provides a coarse analysis of interpolation precipitation (annual timescales, 4km grid sizes), it has continuous spatial and temporal scope (dating back to 1896). We chose a simple ranking of wet (>100% 1980-2011 normal) and dry (<100% 1980-2011 normal) for each initial postfire to further divide the data. The justification for including only the first year following fire is due to work that has shown that debris flow initiation probability and associated rainfall-runoff partitioning is greatest in the first year (e.g., Liu et al., 2021; McGuire

96

et al., 2021; Staley et al., 2017), thus this time period represents the most critical disturbance window for postfire headwater channel flushing. Following this stratification, we ran a maximum likelihood-based analysis of covariance (ANCOVA) across each slope strata by testing for differences between slope terms and whether y-intercepts were significantly different from zero.
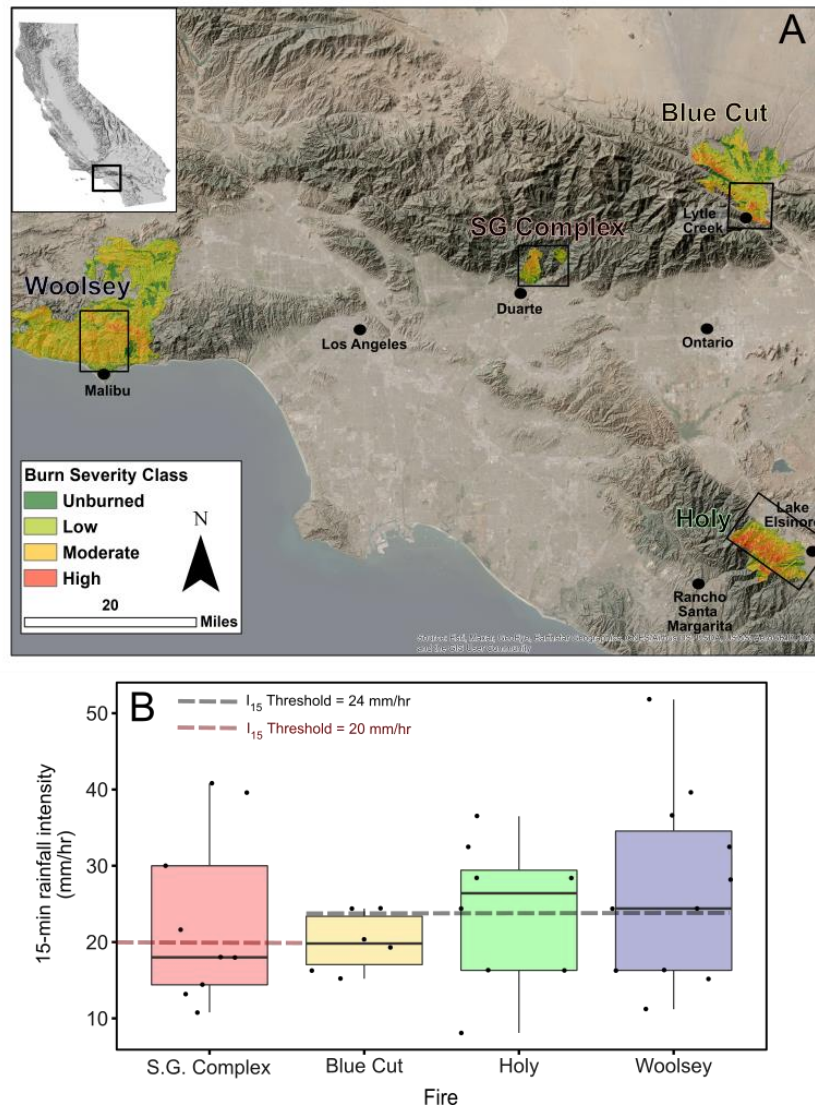
Figure 3.1. A. Regional study map of southern California showing the four burn areas and their soil burn severity. Black rectangles highlight approximate extents of repeat airborne lidar data. B. Boxplots of peak 15 minute rainfall intensity from co-located rain gages for all four burn areas. Each burn scar had rainfall intensities at or above debris flow thresholds (defined here as >50% of watersheds with high likelihood of debris flow based on USGS Debris Flow Hazard Model).

Table 3.1. Lidar datasets used in this study along with metadata.

Fire	Flight Number	Date acquired	Dataset Source	Ground point density (pts/m²)	Cumulative Rainfall During or Following First Wet Season (mm)	Horizontal Reference Used in Collection
Holy	1	July 26-27 2018	USGS 3DEP LPC SoCal Wildfires B1 2018	2.5	0	NAD 83 Zone 11N
Holy	2	September 14 2018	Riverside County Flood Control and Water Conservation District	5.5	0	NAD 83 State Plane VI
Holy	3	December 08 2018	Riverside County Flood Control and Water Conservation District	5.5	151	NAD 83 State Plane VI
Holy	4	Feb 11 2019	Riverside County Flood Control and Water Conservation District	5.7	544	NAD 83 State Plane VI
Holy	5	Feb 22 2019	Riverside County Flood Control and Water Conservation District	5.9	725	NAD 83 State Plane VI
Blue Cut	1	March 19 2013	San Bernardino County	2.0	0	NAD 83 State Plane V
Blue Cut	2	July 20-21 2018	USGS 3DEP LPC SoCal Wildfires B1 2018	2.5	406	NAD 83 Zone 11N
Woolsey	1	Jan 29-30 2016	Los Angeles Region Imagery Acquisition Consortium	1.7	0	NAD 83 State Plane V
Woolsey	2	Sep 25-26 2019	National Center for Airborne Laser Altimetry Seed Project (PI: K. Townsend)	2.1	635	WGS 84 Zone 11N
San Gabriel Complex	1	March 6 2016	Los Angeles Region Imagery Acquisition Consortium	1.7	0	NAD 83 State Plane V
San Gabriel Complex	2	Aug 11-24 2017	USGS 3DEP CA SE Fault Zone 2017	2.5	975	NAD 83 Zone 11N
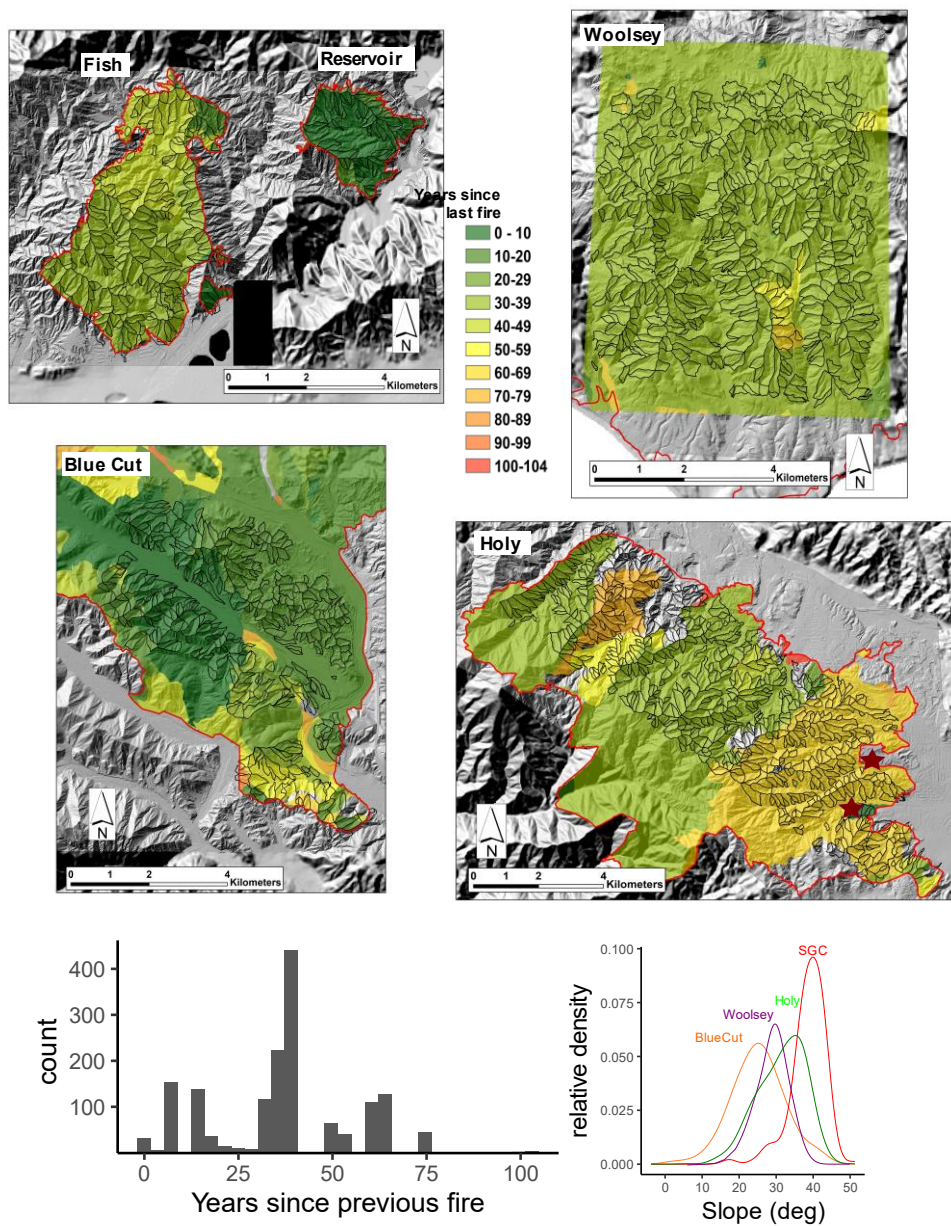
Figure 3.2. Zoomed in maps showing shaded relief for each burn scar, burn history, and delineated 3rd-order headwater catchments. Red stars in Holy Fire scar show location of Leach and McVicker retention basins (Table 2). Note that shaded relief resolution corresponds to areas with repeat lidar coverage. Red lines indicate the burn perimeter of the contemporary fire (note that given the large extent of the Woolsey Fire (>90,000 acres), burn history was masked to the rectangular extent of watershed delineation). Bottom panes show distributions of headwater burn history and headwater catchment average slopes by burn scar.

3.4. Results

3.4.1. Holy Fire: Supply Limited Channel Erosion and the Dominance of Pre-fire Channel Sediment Sources

Following containment of the Holy Fire in September, no significant rainfall occurred until November 29 2018. During this initial dry post-fire period, dry ravel in many colluvial hollows and channels was observed. Extensive runoff-induced erosion occurred across the burn scar during the two initial storm events on November 29 and December 5 2018. This erosion resulted in extensive sediment-laden flooding that was observed on Riverside County Flood Control timelapse cameras, though we note that none of these flows exhibited strong debris flow behavior. Continued erosion and sediment-laden runoff exiting the range occurred for the remainder of the season, with the largest storm event of the season occurring during an atmospheric river event on Feb 14 2019 (Fig 3.3). Unless otherwise noted, we report erosion magnitudes below as area-normalized erosion magnitudes below.

Epoch 1 encompassed the period in which fire occurred but prior to rainfall and area-normalized changes were attributed to dry ravel loading of hollows and valley bottoms throughout the Holy Fire burn area (Figure 3). Erosion was the most effective during Epoch 2 which encompassed the first two storm events on November 29 and Dec 5 2018. There was widespread channelized erosion across most of the burn scar sensed by ALS-derived surface changes, resulting in area-normalized net erosion values as high as 50mm. There were instances of net depositional upland catchments (negative values of erosion in Fig 3), though most watersheds were net erosional. The following storm cycles captured in Epoch 3, notably storms during the week of January 13 2019 and a storm on Feb 4 2019, show subdued channel erosion relative to the initial storm cycle with a greater instances of net deposition across many more catchments. Finally, net erosion slightly increased from Epoch 3 to Epoch 4 for the final storm

cycles, which included the largest single storm event, a longer-duration atmospheric river event on Feb 14 2019. There were instances of erosion magnitudes on the order of >80 mm (Fig 3). Closer inspection of these highly eroded catchments revealed that they were subject to shallow landsliding that was likely triggered by the long-duration atmospheric river storm on Feb 14 2019 (Fig S7), with one of these landslides identified as an outlier (>200 mm of erosion in a smaller headwater catchment, Figure 2, Fig S7).

Inspection of channel cross sections showed initial dry ravel loading prior to rainfall, meter-scale incision of valley bottoms, and meter-scale infilling reaches downstream in higher-order fluvial channels (Figure 4). These changes were also observable in orthoimagery taken during the lidar flights, from UAV-acquired imagery, and upstream erosional patterns were generally commensurate with estimates of sediment retention basin volumes in Leach and McVicker canyons (Table 3).

Plots of net erosion vs mean catchment slope (Figure 3.5) show a significant positive relationship, as has been found across many post-fire studies (e.g., Staley et al., 2017). Within the Holy Fire burn scar, watersheds underlain by landslide deposits and granitic terrain experienced greater dry ravel loading on average (Figure 3.5A), particularly at higher slopes at or above the angle of repose (>30 degrees). It should be noted that this somewhat larger dry ravel loading did not appear to result in increased erosion for granitic rock types. This is consistent with the observation that dry ravel loading overall accounted for only a fraction (12% across all watersheds) of the total gross channel erosion volumes detected by ALS (Figure 3.5C).
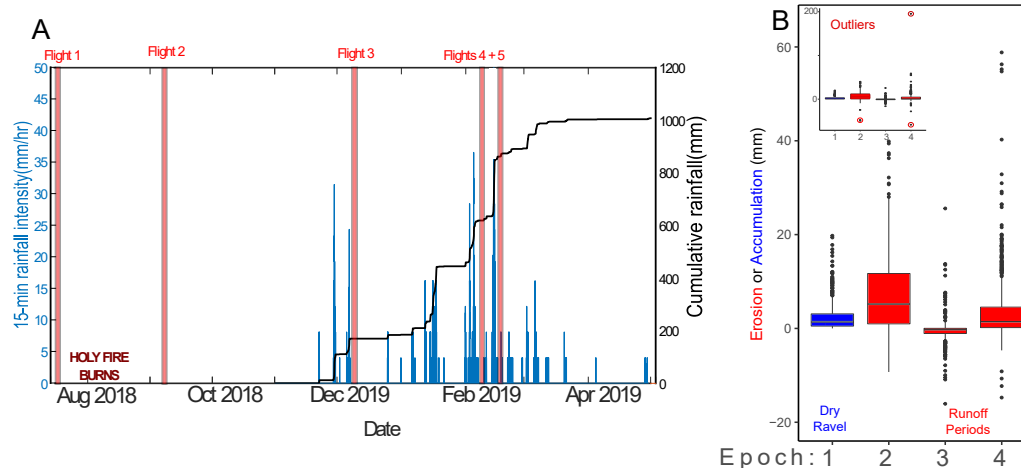
Figure 3.3.**A.** Rainfall time series from Horsethief Canyon rain gauge in Holy Fire burn scar showing cumulative and 15-minute rainfall intensity. **B.** Box plots of channel ravel accumulation (blue) and subsequent erosional periods (red) for burned 3rd order headwater catchments (area range: 0.6-30 ha) throughout the Holy Fire. Solid lines in interior of boxplots = median and dots are outside of 10 and 90 percentile range. Inset plot shows outliers that were selected for removal, including a very high erosional value caused by a large shallow landslide in a small catchment (~200 mm of area normalized erosion).

3.4.2. Remobilization of Transient Sediment Stocks Occurs in Less Hazardous Reaches

When analyzing the movement of sediment through the channelized network of an example catchment, Leach Canyon, it appeared that the largest depositional zones were in the higher-order reaches of the main axial channels (Fig 3.7). Though some deposition occurred in the lower-order portion of the headwater networks, much of the deposition and subsequent remobilization was focused in the trunk axial channels (Fig 3.7). Thus, the upper headwater portion of the channelized network appeared to efficiently entrain and transport material downstream during higher-magnitude runoff events, especially during the initial November and December 2018 storm cycle. These reaches maintain slopes (<0.1 m/m) well within what is generally classified as the fluvial channel domain where debris flow initiation is very unlikely. This is also supported by observations of water-dominated sediment-laden flows entering both Leach and McVicker sediment retentions by Riverside County Flood Control timelapse imagery.
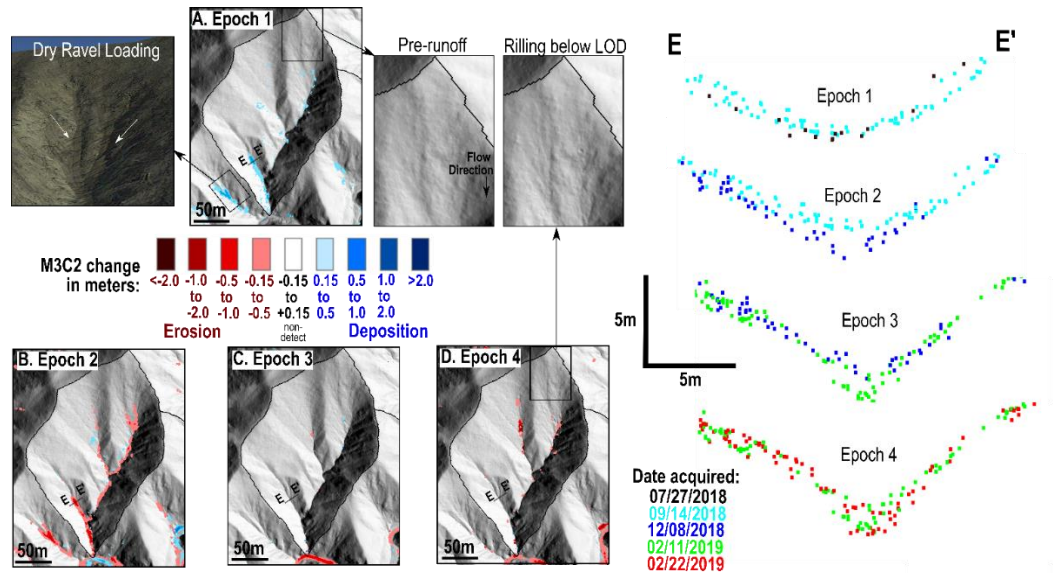
Figure 3.4. Maps of surface change from a selected headwater catchment (area = 4.6 ha). **A.** Epoch 1 showing dry ravel loading of hollows and channels, with corresponding Google Earth image confirming deposits. **B**. Epoch 2 showing initial erosional events. **C.** Epoch 3 showing modest erosion during middle time period of study**. D.** Epoch 4 shows renewed erosion corresponding to largest storm of the monitoring period. E to E' (line right of center in map view) is corresponding cross-sectional slice of point clouds composing channel network.

Table 3.2. Estimates of hillslope sediment yields below limit of detection and propagated analytical uncertainties.

Hillslope Budget Closure Method	Hillslope Sediment Yield Below ALS LOD (mm)
Unaccounted erosion from TLS and SfM in Leach Canyon (Guilinger et al. 2020)	20 (+/- 5)
Hillslope Erosional Balance from Leach Canyon Assuming 100% Detection of Channel Deposition	8 (+/- 13)
Hillslope Erosional Balance from McVicker Canyon Assuming 100% Detection of Channel Deposition	10 (+/- 9)
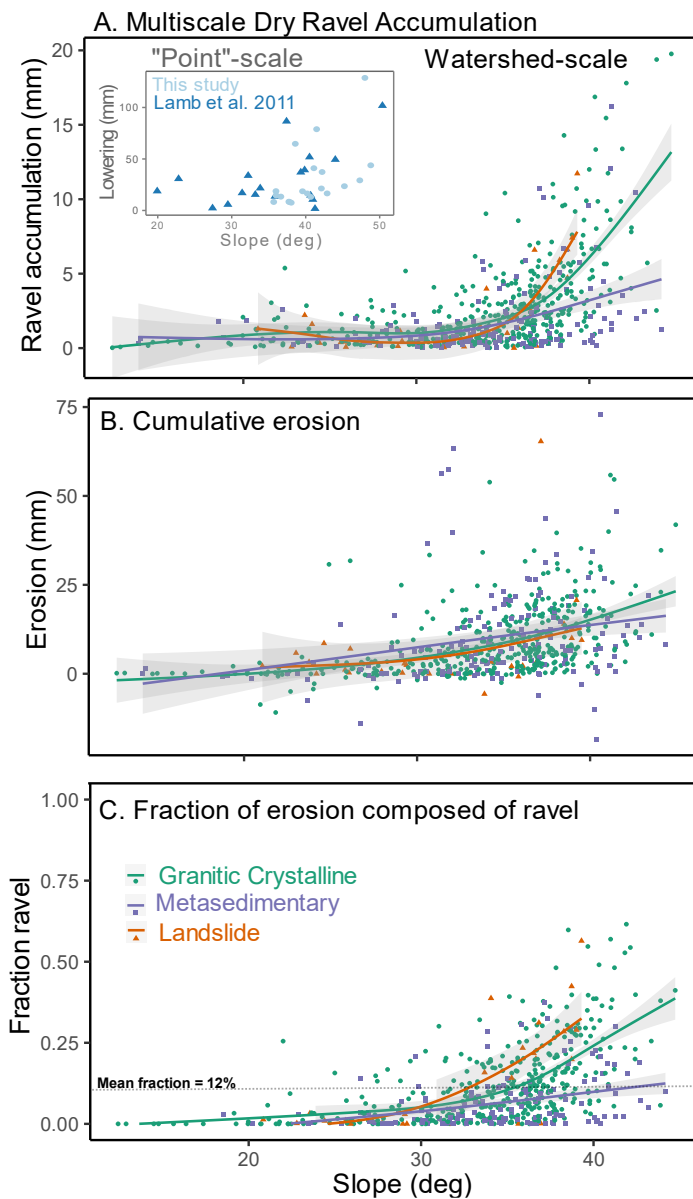
Figure 3.5. A. Holy Fire dry ravel loading at two scales: point-scale is from measurements of dry ravel-induced lowering above fan apex ("point"-scale). Ravel cone derived lowering measurements from Lamb et al., 2011 are plotted as well. Dry ravel accumulation volumes normalized to catchment area for headwater basins with generalized additive model (GAM) fits. Plots of dominant geologic units shown: granitic, metasedimentary, and landslide (green, purple, and red respectively), with granitic and landslide units having the greatest response above 30 degrees. **B.** Cumulative runoff net erosion across Epochs 2-4. Note that there are no significant lithologic differences with GAM fits shown. **C.** Fraction of total erosion due to erosion of dry ravel deposits with GAM fits. Geologic unit trends scale according to available ravel in pane A.

Table 3.3. Riverside County retention basin and ALS volume comparison

	Watershed-Integrated Net Erosion Estimates from ALS M3C2 (m³)	*Truckload Count Estimate (m³)*	*UAV SfM Differencing Estimate of Debris Basins (m³)*	*Average Between Debris Basin Estimates (m³)*	*Debris Basin Estimate Standard Error (m³)*
McVicker Epoch 2	22511	30203	26177	28190	2847
McVicker Epoch 3	-12030*	3499	7532	5515	2852
McVicker Epoch 4	-2016*	21016	29257	25137	5827
Leach Pre-runoff	N/A	15291	19811	17551	3196
Leach Epoch 2	15887	37748	27176	32462	7476
Leach Epoch 3	-3233*	12276	7249	9762	3554
Leach Epoch 4	15487	18961	16964	17963	1412

*indicates net depositional

3.4.3. Shallow soil erosion estimates and model comparisons

There were missing areas for the lidar flight in area for Flight #4 (Feb 11 2019), which were removed by the ALS vendor because of snow cover in the uplands above approximately 850-900 mASL, reducing coverage by ~20%. The portions of the watershed area that were missing due to transient snow cover for Epochs 2-3 were estimated. We noted that net ALS-derived erosion, which represent either net erosive (positive in our scheme) or net depositional (negative in our scheme) were in all cases well-below estimates of sediment flux to retention basins (Table 3). This observation is also consistent in upland watersheds that had greater deposition than erosion (Figure 3.6, negative erosion values), meaning that these catchments "gained" material (a physical impossibility). Assuming this is not due to alignment uncertainty, which was largely mitigated by our alignment and filtering methods, this implies that a significant portion of hillslope erosion in these catchments is below the limit of detection as has been found in other multitemporal ALS erosion studies (e.g., DiBiase and Lamb, 2020; Rengers et al., 2021). From a process-based perspective, much of this erosion is likely from various forms of shallow soil

erosion that inevitably occurs on steep burned hillslopes, which was confirmed by a previous study using TLS and SfM in this burn scar (Guilinger et al., 2020). There is also evidence of widespread rilling present in hillshades across many catchments when comparing pre-runoff to post-runoff surface model textures (Figure 3.4).

Using TLS-derived erosion from Guilinger et al. 2020 and maps of soil mantle estimated from a thresholded slope map (>45 degree angles), we estimated the amount of hillslope erosion across the burn scar. A comparison of the area-volume relationships for the raw ALS channel erosion data and hillslope erosion estimates is shown in Figure 3.7A. Using a best fit line for this ALS channel erosion + hillslope erosion estimate, we derive an area power law scaling relationship with similar exponent (approximately linear scaling, ~1) to Rengers et al 2021 and Nyman et al 2020 (Fig 3.7A). We compared our models to various empirical models used in Australia and the western US and found that most models either under or over-predicted erosion volumes, but that Rengers et al. 2021 and Nyman et al. 2020 provided the closest fits (Fig 3.7B).
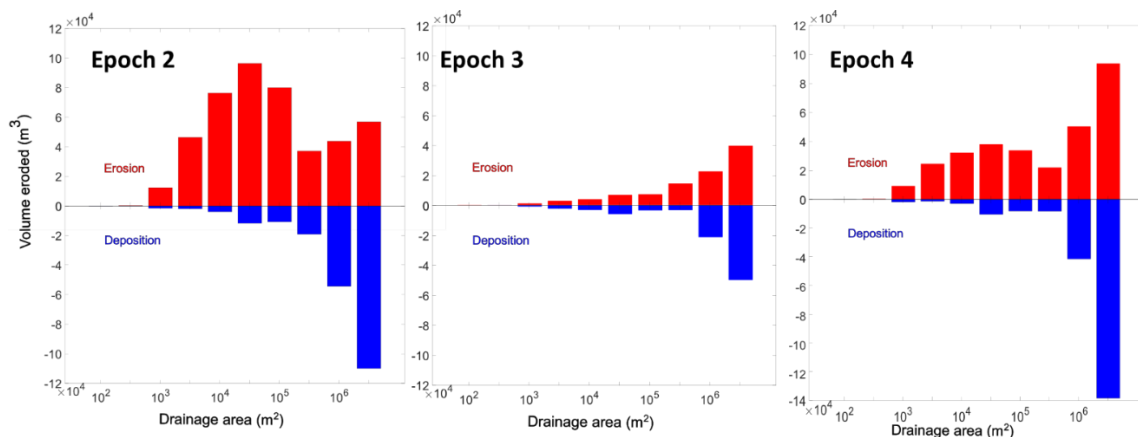
Figure 3.6. Combined sediment flux from ALS M3C2 differencing binned by drainage area for multiple catchments in the Holy Fire burn scar. Consistent with maps of change (Figure 4), Epoch 2 showed the greatest amount of channel erosion. Deposition for all epochs occurred mostly in the highest order axial channels which generally had much gentler slopes and floodplain connectivity compared to more hazardous debris and sediment-laden flow producing reaches upstream.

3.4.4. Most recent fire history and probable postfire response magnitude reveals systematic but complex slope-dependent channel supply dynamics

Because initial lidar data for the San Gabriel Complex, Woolsey, and Blue Cut fires were collected prior to wildfire, these data do not capture dry ravel channel loading in steep terrain. Thus, contributions to dry ravel loading were removed from the Holy Fire dataset for a less biased comparison. When catchment erosion across all fires is plotted against time since previous fire (Fig 3.8), we noted a consistent increase in the regression slope-intercept (representing channel accumulation rates) coincident with hillslope gradient bins (Fig 3.9). Overall, for the steepest catchments (>35 degrees), this relationship is stronger in watersheds which experienced wet years (>100% of normal) for their most recent incipient postfire year than those that were classified as dry (<100% of normal). In a comparison of distributions of wet vs dry groups, median watershed response was significantly greater for steeper (>30 degrees) watersheds. Part of these observations are likely explained by the degree of erosion above ALS LODs, which likely suppressed the amount of detection of erosion and internal redistribution in less steep (<30 degree) catchments. Additionally, there is likely a greater coupling between hillslopes and channels with increasing hillslope angle in the steepest. It is notable that the strongest relationships approximately correspond to watershed-average angles above the angle of repose determined for soils in the region (~30-32 degrees; Lamb et al., 2011). Additionally, it is important to note that most regression analysis revelated that the y-intercept term, which would represent erosional responses and/or incipient sediment supply in the most recent burns, were not significantly different from zero for most analyses (i.e., negligible response from areas that re-burned most rapidly).

To investigate a potential fuel and burn severity linkage to this muted response for areas that re-burned quickly, we show plots of MTBS burn area reflectance classification (BARC), we noted

that areas that had repeat burns in under 20 years appeared to have subdued burn intensity (Fig 3.10). This can likely be interpreted as a fuel limitation where at shorter timescales prior to robust vegetation regrowth, resultant biomass is not sufficient to produce moderate or high soil burn severity. This burn severity limitation, along with potential channel sediment supply limitations we noted using the Holy Fire dataset and evidence from other burn scars (see Fig B8), likely explains the more limited erosional response in areas burned less than 20 years apart.
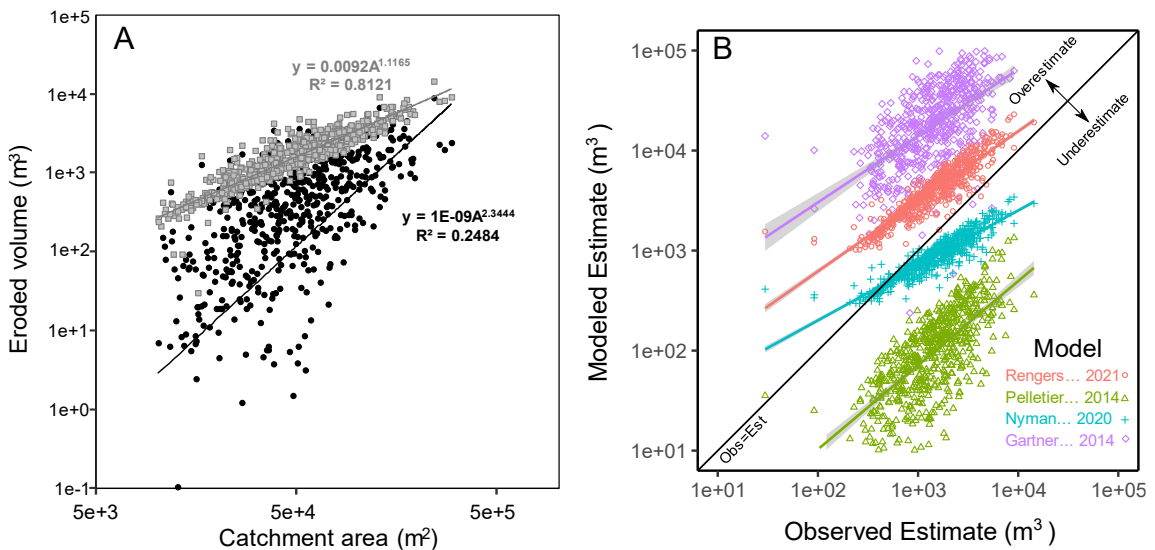
Figure 3.7. A. Bivariate plots of catchment area vs erosion from headwater catchments in the Holy Fire. Black circles are raw ALS erosion volumes while gray squares includes both ALS volumes and erosion scaled by constrained uniform hillslope erosion values with resulting volume. Power-law scaling regressions also shown. **B.** Model estimates from four additional debris-flow volume models as indicated by first author surname plotted. 1:1 line shown for reference.
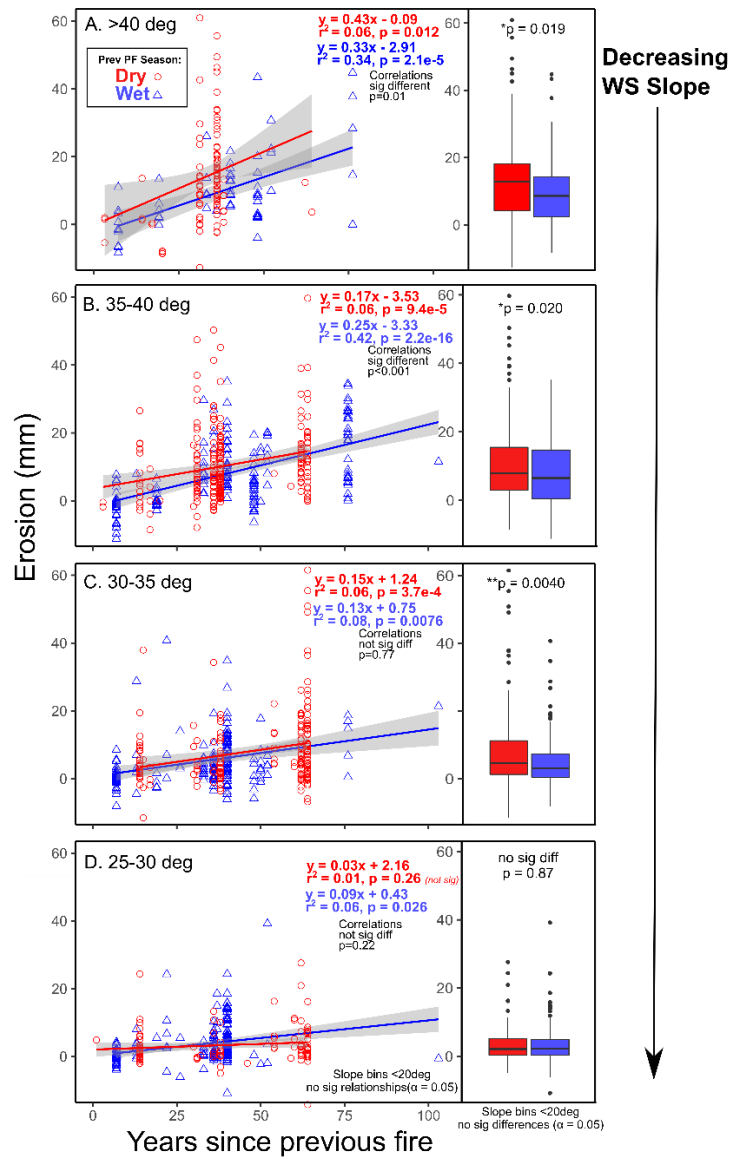
Figure 3.8. Plot showing time since previous fire versus area-normalized erosion for headwater catchments from all five burn scars. Analysis is stratified by slope bins (**A-D)** and within-bin comparisons between wet (blue) and dry (red) previous postfire years, with significant relationships for >25 deg bins shown (see Fig 3.9). Box plots shown on right with comparison of medians (Wilcoxon rank-sum test single-tailed test for dry greater than wet) results shown. Differences in correlations were tested by Fisher's r-z transformation test, with results shown (significant only for >35 degrees). Regression coefficients and significance of relationships shown in each bin panel. Regression slope term (e.g. channel accumulation rate estimate) and y-intercept terms and associated 95% confidence intervals for all bins shown in Fig 3.9.

110
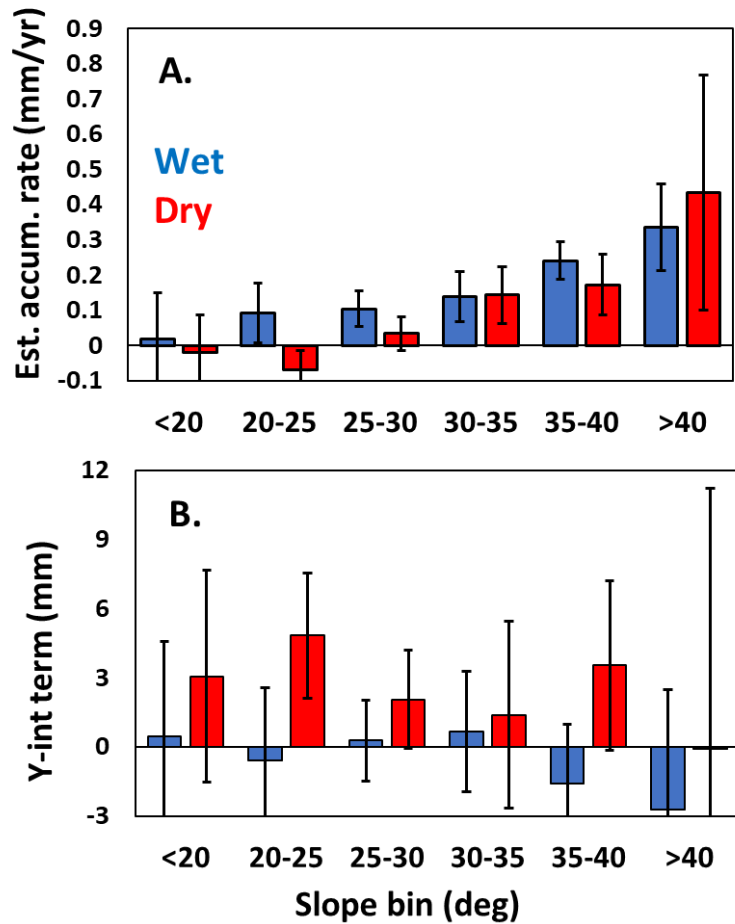
Figure 3.9. ANCOVA plot showing regression terms for wet vs dry groupings (A. channel accumulation rate term and B. Y-intercept terms, by slope term) from analysis in Fig 3.8, including additional non-significant estimates for slope bins 20-25 and <20 degrees. **A.** Note, there are no significant positive rate terms in slope bins below 25 degrees and that consistent relationships exist in bins above 30 degrees. Though, the wet group contains higher confidence in the rate terms, there are no significant differences between wet vs dry channel accumulation rate estimates. **B.** All Y-intercept terms were not significantly different from zero, except for the dry 20-25 degree bin, indicating very little response from watersheds that burned very recently.
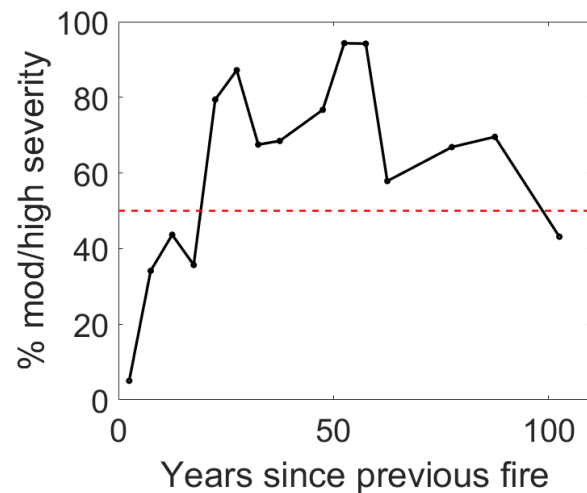
Figure 3.10. Plot of fraction of burn area in **all five burn scars** at moderate or high severity according to MTBS (USGS) Dnbr-6 reflectance classes binned by 5 year windows. Plot shows a cross over into majority higher severity burn at approximately 25 years, which levels off between 70-95% until dropping back down at burned highly mature vegetation stands. Note however that this 100-105 bin contains very few data points (n= 4).

3.5. Discussion

Wildfire is a very important disturbance in mountainous systems worldwide and in regions such as California considered in this study, episodic postfire erosion is an important long-term erosion and sediment transfer agent (e.g., Lave and Burbank, 2004; Orem and Pelletier, 2016; Rengers et al., 2021). The goal of this study was to further understand these sediment production and transfer dynamics over multiple scales at the nexus of hillslopes and upland channel networks. In doing so, we used multitemporal ALS data of eroding burned upland watersheds in the Holy Fire to answer the following questions: 1). Does erosion of headwater channel networks and colluvial hollows become supply limited? 2). What proportion of eroded material is dry ravel and how does the vary across slope and geology? 3). Are there significant hazards due to remobilization of channel depocenters during storm sequences? Expanding out to regional scales across four burn scars covering a wide range of burn history, we tested the following hypothesis: sediment availability in channels will increase with time since previous fire

112

in steep catchments as material accumulates in valley bottoms during inter-fire periods and that this relationship will be stronger in areas that more likely

3.5.1. Holy Fire: channel sediment supply limitations and slope-varying dry ravel inputs

We found that that despite a sequence of rainstorms with rainfall intensities at or above rainfall thresholds needed to generate debris flows and significant runoff there was a seasonal-scale decline in erosion in colluvial hollows and valley bottoms across the Holy Fire. These observations are largely consistent with gully and channel evacuation documented by smaller-scale surveying work in a 6.5-ha catchment in the burn scar (Guilinger et al., 2020). Similar supply dynamics have also been found in other postfire erosion studies in very steep (> 35 degrees) burned catchments in southern California (e.g., Lamb et al., 2011; DiBiase and Lamb, 2020; Palucis et al., 2021). In these settings, soil mantle is only maintained by vegetation and local lower-slope (<~32 degrees) zones, which are exhausted via fire-initiated dry ravel processes and they are subsequently eroded by amplified runoff (Lamb et al., 2011). This contrasts with lower slope (<32 degrees) burned landscapes which have a continuous soil mantle, where it has been found that shallow soil erosion via rainsplash and overland flow are majority components of sediment budgets for debris flows (Rengers et al., 2021; Staley et al., 2014) and postfire sediment-laden floods (Rengers et al., 2016; DeLong et al., 2018). The topography burned by the Holy Fire spanned a large slope range (13-44 degrees, mean = 33 degrees), thus it would be expected that a diverse suite of erosional processes ranging from deep erosion of channel fill in the steepest bedrock-dominated watersheds to shallower hillslope erosion on lower gradient soil-mantled slopes.

An important assumption we make in this study is that practically all of the erosion occurring in our ALS difference maps is due to the erosion of weathering products accumulated in the channel and not from direct bedrock incision or plucking. In field visits to the site, we did

113

note some evidence of bedrock erosion following the passage of debris and sediment-laden flows including plucking of blocks from channels floored by fractured metasedimentary units, but we did not see this at a scale that would invalidate this assumption. Additionally, evidence from ALS differencing and observations from Guilinger et al. (2020) showed that continued erosion following initial sediment evacuations to bedrock in Epoch 2 was driven by channel bank erosion and sideslope failure processes (Figure 4D) which has been found in other similar studies (Santi & MacAulay, 2019). Thus, we largely rule out bedrock erosion following sediment cover evacuation as a surface change mechanism significant enough to be detectable with airborne lidar over these events.

In addition to multitemporal ALS and UAV-SfM data previously collected on the burn scar showing soil erosion, multiple lines of evidence point to significant soil erosion below our limit of detection across the burn scar. First, net volume changes derived from lidar were below our estimates to combined SfM and truckload counts from clear outs in sediment retention basins operated by Riverside County. This is to be expected if much of the distribution of erosion depths were below the LOD (mean = 0.2 meters), where substantial fractions of eroded sediments could be conveyed to the outlet of the watershed. Second, we noted erosional roughness patterns resembling rills evident in 50cm hillshades in regions with no change indicated (Figure 4). A transition to channel-dominated fluxes is also evident in the steepest catchments as indicated by the steepest catchments where significant fractions of hillslopes are likely bedrock-dominated (>45 degrees) and dry ravel loading constitutes a significant fraction of material eroded (Fig 5C). Thus, processes controlling sediment redistribution and erosion are highly slope dependent in these terrains and a single "one-size fits all" approach to physically modeling watershed-scale sediment fluxes is unwarranted. Instead, assuming all other factors equal, it appears that the

114

distribution and mean of hillslope angles within a watershed could be used as a first order prediction of the dominant erosive processes.

3.5.2. Holy Fire: empirical models from similar climate and geomorphology fit most closely

Comparisons of ALS + hillslope estimates from this study show a clear separation between the different models assessed (Figure 3.7). Pelletier and Orem (2014)'s two-parameter model developed from post-fire erosion in New Mexico was a clear under-predicter for the Holy Fire dataset. The Valles Caldera, where that model was developed is a portion of the tectonically-quiescent southern Rocky Mountains (Orem & Pelletier, 2015) and thus likely has much lower long-term erosion rates relative to actively-uplifting Santa Ana Mountains and is also located within a completely different biome and climate. The model that under-predicted our model but did overlap at lower drainage area portions of the domain was Nyman et al. (2020), which was derived from debris flow modeling and observations in SE Australia. The closer correspondence between the Nyman et al. (2020) model and ours, compared to Pelleteier and Orem (2014), is consistent with the fact that Australia also hosts a semiarid Mediterranean climate and their specific study domain was also steep (30-45 degrees). The next model in the ranking, Rengers et al (2021), which was developed in the Fish Fire using the same ALS dataset along with additional TLS data (McGuire and Rengers, 2018) showed a slight over-prediction, though it had a similar scaling exponent (0.9 vs our 1.1). Finally, the three-parameter USGS emergency assessment model of Gartner et al. (2014) clearly over-predicted. Both the Gartner et al. (2014) and Rengers et al. (2021) models were developed in the San Gabriel Mountains, which maintain steeper modal slopes than the Santa Ana Mountains of our study (Figure 2), thus it is not surprising that there is over-prediction. We note that in an emergency-assessment scenario the continued use of the USGS model does appear to provide safe conservative prediction of sediment flux along with the Rengers et al. (2021) model which was a better fit than the USGS dataset. We also note that our

best-fit model could potentially be used to predict sediment volume for small, burned headwater catchments in the Peninsular Ranges of similar slope, vegetation type, and burn severity.

Although the empirical models assessed and developed here can provide approximate order-of-magnitude sediment volumes useful for hazard assessment, it is clear from datasets in this study and many others (e.g., DiBiase and Lamb, 2020; Pelletier and Orem, 2014; list others) that there is significant variability (~2-3 orders of magnitude, Figures 5 and 7) in sediment yields across terrain with broadly similar burn severity, topographic, and biophysical characteristics. This can be a function of multiple factors including (but not limited to) heterogeneity in forcing driven by small-scale variations in rainfall intensity that can be common to steep terrain or narrow rainfall structures (Moody et al., 2013, Oakley refs) and subtle lithologic differences related to fracture spacing and grain size of weathering products (DiBiase and Lamb, 2020) along with larger-scale controls such as topographic relief-lithologic strength feedbacks (Townsend et al., 2020). Ravel production datasets which showed (Figure 3.5) within this study also point to potential systematic geologic-driven differences whose controls have yet to be elucidated. Through an identification of systematic controls on hillslope-to-channel transfer functions, more physically based models could be refined for predicting postfire sediment availability across a broader range of fire-prone mountainous landscapes (e.g., McGuire et al., 2017; DiBiase et al., 2017).

3.5.3. Timing and relative magnitude of previous fire-flood cycles is an effective proxy for channel sediment availability

An important finding in this study was the statistically significant positive association found between area-normalized erosion and time since previous fire in the steepest catchments. This relationship had greater correlations in regions where the most recent postfire disturbance had an incipient wetter than average compared to those with drier incipient postfire seasons. We

interpret these results to be driven by two hydrogeomorphic processes: 1. channel infilling processes over inter-fire periods which are most enhanced by increased coupling between channels and hillslopes in the steepest catchments (>35 degrees) and 2. burn severity limitations in areas undergoing frequent reburns (<20 years). This first factor related to sediment availability is supported by observations of channel sediment depletion via flushing flows in the Holy Fire analysis, greater confidence in regression models in areas that likely experienced higher magnitude postfire disturbance, and high levels of burn severity in areas burned at a frequency of 20 years or beyond in the dataset. In areas burned at more frequent timescales (<20 years), levels of moderate or high soil burn severity are likely limited by vegetation regrowth rates in chaparral and shrubland communities of southern California. This finding is supported by a study using debris basin data from LA County Flood Control (Loomis et al., 2003). Our results contrast with DiBiase and Lamb (2020), who found no significant correlation between fire history and sediment yields using multitemporal ALS differencing across the 2009 Station Fire in the San Gabriel Mountains. Instead, they suggest that erosion in this burn scar could be controlled by lithologic differences related to fracture spacing and rock strength possibly associated with differing tectonic history across the burn footprint. In that study, and others in the San Gabriel Mountains (e.g., Lamb et al., 2011; Palucis et al., 2021), it has been shown that large fractions of sediment stored in channels sourced by debris flows can be derived from postfire dry ravel pulses. The hillslope angles in the San Gabriels can commonly exceed the angle of repose (>35 degrees, see Fig 3.1 SGC slopes) and we also found that within the Holy Fire (Fig 3.4) many catchments in these slope domains where dry ravel constituted greater than 50% of the channel mass balance. Thus, given that most lidar was not collected for the purpose of capturing dry ravel (and this effect was removed for consistency from the Holy Fire dataset), a direct comparison to our results in that study may be obfuscated. Although it was beyond the scope of this study to develop

multivariate approaches, many of these processes are likely augmented by other potential geologic or biophysical differences, such as fine-scale lithologic differences controlling grain size distribution (e.g., Neely & DiBiase, 2020; Sklar et al., 2017) and vegetation cover characteristics (DiBiase & Lamb, 2013; Roth et al., 2020). More studies and targeted datasets are needed to understand the impact of these characteristics on sediment volume, flow type, and relationships to grain size (particularly coarse fractions for hazard assessments).

Inter-fire channel sediment infilling rates (represented by the slope of stratified regression lines) appeared to monotonically increase with watershed slope angles beyond 25 degrees. This is consistent with a model of increasing connectivity between hillslopes and channels with increasing slope (DiBiase et al., 2013). Sedimentation of channels in steep semiarid mountain chains like those in southern California are driven by a multitude of processes such as dry weather loading (Wohlgemuth and Hubbert, 2008), wet diffusive processes (e.g., overland flow, rainsplash), soil creep (Deshpande et al., 2021) and shallow landsliding (Schmidt et al., 2001). Most notably, there is a coupling between severe wildfire and shallow land sliding driven by tree and shrub root mortality in a timescale 3-5years following fire (Rengers et al., 2020; Thomas et al., 2021). In fact, it was found that this process occurred on south-facing slopes in the Fish Fire burn scar 3-5 years following fire, (Rengers et al., 2020), post-dating the final lidar dataset for this burn scar. These landslides were less hazardous than the initial runoff-generated debris flows and instead acted to replenish in-stream sediment stocks (Rengers et al., 2020). Thus, among many potential sources of variability, there may be significant spatiotemporal variability in channel re-loading driven by events such as shallow landsliding triggered by long-duration rainfall beyond the previous incipient postfire wet season evaluated in this study. Additionally, we note that hillslope sediment supply and its potential redistribution to channel networks, which could not be measured directly in this study, is also an important process that could be augmented

by postfire and inter-fire. This study highlights the headwater channel and colluvial hollow network as an important nexus and more studies explicitly exploring the connectivity of hillslopes to the channels in the context of fire and other disturbances is needed.

Given the potentially short timing between fire and potentially hazardous rainfall in regions like California (Kean & Staley, 2021), metrics such as those described here that are not already integrated into quantitative risk models could be useful for improving hazard pre-prediction and scenario planning. Notably from this study the broad correspondence between time since previous fire, previous incipient wet season magnitude, and erosional volumes across multiple burn scars does indicate that this metric could be used for postfire hazard pre-planning (e.g., Staley et al., 2017; Kean et al., 2021). In fact, the California Watershed Emergency Response Teams qualitatively use burn history as part of their reactive hazard analysis (D. Coe, personal communication). Thus, we argue for continued use of such metrics for aiding in reactive and proactive risk assessments of postfire sedimentation risk and given the significant variability in these trends additional studies should be done looking more closely at postfire sediment availability patterns using study designs that can further address fundamental biophysical controls.

The finding of a correspondence between inter-fire timescales and sediment availability is relevant to forecasting future postfire sedimentation patterns over the remaining 21st-century. Broadly speaking for wildlands in the western United States and many semiarid regions globally, fire extent and frequency is predicted to increase (Sankey et al., 2017; Westerling et al., 2006). Additionally, in many regions fire suppression can also be an important factor (Minnich, 1983), though there is evidence that southern California chaparral is ignition-limited and that any active suppression policies may be outweighed by human ignition along the WUI (Keeley & Fotheringham, 2001). However, we did note that the Holy Fire burn scar may have had a signal of

suppression relative to the other burn scars evaluated, which could be a function of its relative isolation from population centers (and thus potential ignitions) (Radeloff et al., 2018; Syphard & Keeley, 2015). Regardless, climate change will likely increase fire frequency in this region and these findings indicate potential sediment availability limitations. In addition to frequency, a warming climate sustains a warmer atmosphere that can sustain greater rainfall intensities, thus the incidence and magnitude of debris flows could increase (Kean et al., 2021). One additional process not considered in this study that was not quantified but may impact our results is vegetation type conversion from shrubland to invasive annual grassland. This phenomenon has also increased in light of increased fire frequency driven by human activity along with other anthropogenic environmental stressors such as pollution, invasive forbs/grasses, and climate change (e.g.,Cox et al., 2014; Keeley et al., 2011). The potential hydrogeomorphic impacts of grassland type conversion both through a shift in fire regime and permanent reorganization of eco-hydrogeomorphic processes (Gabet & Dunne, 2002) should be further explored.

3.4.5. Future Work

Further work should explore sediment availability patterns as they relate to burn history and we discuss a few independent approaches below. A more direct field method for exploring this could be interrogation of headwater sediment deposits that fuel postfire sediment-laden flows in similar catchments with differing burn histories. Similar approaches have been taken to explore postfire deposits downstream on alluvial fans which has been much more widely employed in the Intermountain West (Pierce et al., 2004; Riley et al., 2015).

Additionally, in recently burned areas monitoring and/or experimental approaches to estimate the amount of material entering channel networks while re-vegetation is occurring would be warranted. Wildfire completely transforms surface roughness characteristics, allowing for less constrained particle travel distances (Roth et al., 2020) and exploring the timescales by which the

120

reestablishment of roughness resets to a background mean state would be useful in predicting channel sediment availability.

More work should also be done at broader scales to explore feedbacks between burn frequency, burn severity, and vegetation type conversion/stability in the context of hydrogeomorphic impacts. In our assessment, we found that shorter fire return intervals reduced burn severity of subsequent fires at a threshold of about ~20 years and that this effect, coupled with potential channel clearing from the most recent fires, could be an important control on hydrogeomorphic response in steep catchments. However, we made no effort to assess the degree that burn severity limitations could be caused by type conversion. There is evidence in settings that undergo conversion from shrub to grassland due to fire and other factors (e.g., pollution, grazing) that hillslopes can become destabilized as roots decay and infiltration-induced shallow landsliding may become more common (Gabet & Dunne, 2002; Terwilliger & Waldron, 1991). Additionally, this paradigm of burn severity limitations is likely only applicable to chaparral communities. For example, different relationships have been found in forested systems of northern California and southern Oregon, where more managed approaches to postfire salvage logging can inadvertently increase near-ground fine fuel loading which can increase burn severity and frequency inadvertently (Donato et al., 2006; Thompson et al., 2007). Thus, an exploration of reburning dynamics and its hydrogeomorphic impacts should be done in the context of land management and ecosystem type.

3.6. Conclusions

In this study, we investigated controls on channel sediment availability and evaluated existing models of sediment yield. We specifically asked: 1. How do patterns of initial dry ravel sediment loading relate to postfire sediment yields? 2. Do we see sediment depletion patterns

evident in channel erosion across a broader spatial scale over the course of the study period? 3. Does the movement of sediment into transient depositional zones in headwater streams affect erosional risk of subsequent runoff events? Through answering these questions with the Holy Fire dataset, we expand our scope to test the following hypothesis: sediment availability in channels is partially governed by the amount of time since previous fire and the probable magnitude of postfire erosion following this most recent fire. In this study, we demonstrate that a majority of channel erosion accesses pre-fire accumulations as opposed to dry ravel delivery and that this stock of sediment becomes supply-limited over the course of the wet season. Additionally, we find that runoff-driven loading of low order steep channel networks is very small and likely not a significant hazard. In our model evaluation, we find that empirical models developed in similar physiographic and climatic regimes fit our observations but that there were some systematic biases that could likely explained by differences in landscape factors. Finally, expanding out over all four burn scars using a century-long previous fire record, we find that the amount of contemporary post-fire erosion relates to time between fires that there is greater confidence in these relationships for steep catchments which experienced higher-magnitude postfire erosion during a previous fire disturbance. Broadly, we find a systematic increase in this relationship with increasing watershed average slope, likely a consequence of greater coupling between steeper hillslopes and valley bottoms along with increased incidence of debris flow initiation in steep terrain. This study provides an additional empirical sediment volume production model for steep burned terrain outside of the Transverse Ranges of southern California and shows that previous postfire disturbance exhibits a legacy effect on contemporary postfire erosional responses.

Chapter 3 References

Atchley, A. L., Kinoshita, A. M., Lopez, S. R., Trader, L., & Middleton, R. (2018). Simulating Surface and Subsurface Water Balance Changes Due to Burn Severity. *Vadose Zone Journal*, *17*(1), 0. https://doi.org/10.2136/vzj2018.05.0099

Barnhart, T. B., & Crosby, B. T. (2013). Comparing two methods of surface change detection on an evolving thermokarst using high-temporal-frequency terrestrial laser scanning, Selawik River, Alaska. *Remote Sensing*, *5*(6), 2813–2837. https://doi.org/10.3390/rs5062813

Benavides-Solorio, J., & MacDonald, L. H. (2001). Post-fire runoff and erosion from simulated rainfall on small plots, Colorado Front Range. *Hydrological Processes*, *15*(15), 2931–2952. https://doi.org/10.1002/hyp.383

Bodí, M. B., Martin, D. A., Balfour, V. N., Santín, C., Doerr, S. H., Pereira, P., Cerdà, A., & Mataix-Solera, J. (2014). Wildland fire ash: Production, composition and eco-hydro-geomorphic effects. *Earth-Science Reviews*, *130*, 103–127. https://doi.org/10.1016/j.earscirev.2013.12.007

Bowman, D. M. J. S., Balch, J., Artaxo, P., Bond, W. J., Cochrane, M. A., D'Antonio, C. M., Defries, R., Johnston, F. H., Keeley, J. E., Krawchuk, M. A., Kull, C. A., Mack, M., Moritz, M. A., Pyne, S., Roos, C. I., Scott, A. C., Sodhi, N. S., & Swetnam, T. W. (2011). The human dimension of fire regimes on Earth. *Journal of Biogeography*, *38*(12), 2223–2236. https://doi.org/10.1111/j.1365-2699.2011.02595.x

Brogan, D. J., Nelson, P. A., & MacDonald, L. H. (2019). Spatial and temporal patterns of sediment storage and erosion following a wildfire and extreme flood. *Earth Surface Dynamics*, *7*(2), 563–590. https://doi.org/10.5194/esurf-7-563-2019

Campos, I., Vale, C., Abrantes, N., Keizer, J. J., & Pereira, P. (2015). Effects of wildfire on mercury mobilisation in eucalypt and pine forests. *Catena*, *131*, 149–159. https://doi.org/10.1016/j.catena.2015.02.024

Cannon, S. H., Kirkham, R. M., & Parise, M. (2001). Wildfire-related debris-flow initiation processes, Storm King Mountain, Colorado. *Geomorphology*, *39*(3–4), 171–188. https://doi.org/10.1016/S0169-555X(00)00108-2

Cannon, Susan H., Boldt, E. M., Laber, J. L., Kean, J. W., & Staley, D. M. (2011). Rainfall intensity-duration thresholds for postfire debris-flow emergency-response planning. *Natural Hazards*, *59*(1), 209–236. https://doi.org/10.1007/s11069-011-9747-2

Cannon, Susan H., Gartner, J. E., Rupert, M. G., Michael, J. A., Rea, A. H., & Parrett, C. (2010). Predicting the probability and volume of postwildfire debris flows in the intermountain western United States. *Bulletin of the Geological Society of America*, *122*(1–2), 127–144. https://doi.org/10.1130/B26459.1

Cannon, Susan H., Gartner, J. E., Wilson, R. C., Bowers, J. C., & Laber, J. L. (2008). Storm rainfall conditions for floods and debris flows from recently burned areas in southwestern Colorado and southern California. *Geomorphology*, *96*(3–4), 250–269. https://doi.org/10.1016/j.geomorph.2007.03.019

Cattau, M. E., Wessman, C., Mahood, A., & Balch, J. K. (2020). Anthropogenic and lightning-started fires are becoming larger and more frequent over a longer season length in the U.S.A. *Global Ecology and Biogeography*, *29*(4), 668–681. https://doi.org/10.1111/geb.13058

Chin, A., Solverson, A. P., O'Dowd, A. P., Florsheim, J. L., Kinoshita, A. M., Nourbakhshbeidokhti, S., Sellers, S. M., Tyner, L., & Gidley, R. (2019). Interacting geomorphic and ecological response of step-pool streams after wildfire. *Bulletin of the Geological Society of America*, *131*(9–10), 1480–1500. https://doi.org/10.1130/B35049.1

Collins, B. D., Oakley, N. S., Perkins, J. P., East, A. E., Corbett, S. C., & Hatchett, B. J. (2020). Linking Mesoscale Meteorology With Extreme Landscape Response: Effects of Narrow Cold Frontal Rainbands (NCFR). *Journal of Geophysical Research: Earth Surface*, *125*(10), 1–19. https://doi.org/10.1029/2020JF005675

Coombs, J. S., & Melack, J. M. (2013). Initial impacts of a wildfire on hydrology and suspended sediment and nutrient export in California chaparral watersheds. *Hydrological Processes*, *27*(26), 3842–3851. https://doi.org/10.1002/hyp.9508

Cox, R. D., Preston, K. L., Johnson, R. F., Minnich, R. A., & Allen, E. B. (2014). Influence of landscape-scale variables on vegetation conversion to exotic annual grassland in southern California, USA. *Global Ecology and Conservation*, *2*, 190–203. https://doi.org/10.1016/j.gecco.2014.09.008

Crozier, M. J. (1999). Prediction of rainfall-triggered landslides: A test of the antecedent water status model. *Earth Surface Processes and Landforms*, *24*(9), 825–833. https://doi.org/10.1002/(SICI)1096-9837(199908)24:9<825::AID-ESP14>3.0.CO;2-M

Dibiase, R. A., Heimsath, A. M., & Whipple, K. X. (2012). Hillslope response to tectonic forcing in threshold landscapes. *Earth Surface Processes and Landforms*, *37*(8), 855–865. https://doi.org/10.1002/esp.3205

Dibiase, R. A., & Lamb, M. P. (2013). Vegetation and wildfire controls on sediment yield in bedrock landscapes. *Geophysical Research Letters*, *40*(6), 1093–1097. https://doi.org/10.1002/grl.50277

DiBiase, R. A., & Lamb, M. P. (2020). Dry sediment loading of headwater channels fuels post-wildfire debris flows in bedrock landscapes. *Geology*, *48*(2), 189–193. https://doi.org/10.1130/G46847.1

DiBiase, R. A., Whipple, K. X., Heimsath, A. M., & Ouimet, W. B. (2010). Landscape form and millennial erosion rates in the San Gabriel Mountains, CA. *Earth and Planetary Science Letters*, *289*(1–2), 134–144. https://doi.org/10.1016/j.epsl.2009.10.036

Donato, D. C., Fontaine, J. B., Campbell, J. L., Robinson, W. D., Kauffman, J. B., & Law, B. E. (2006). Post-wildfire logging hinders regeneration and increases fire risk. *Science*, *311*(5759), 352. https://doi.org/10.1126/science.1122855

Ebel, B. A., & Martin, D. A. (2017). Meta-analysis of field-saturated hydraulic conductivity recovery following wildland fire: Applications for hydrologic model parameterization and resilience assessment. *Hydrological Processes*, *31*(21), 3682–3696. https://doi.org/10.1002/hyp.11288

Ebel, B. A., & Moody, J. A. (2020). Parameter estimation for multiple post-wildfire hydrologic models. *Hydrological Processes*, *34*(21), 4049–4066. https://doi.org/10.1002/hyp.13865

Ebel, B. A., Moody, J. A., & Martin, D. A. (2012). Hydrologic conditions controlling runoff generation immediately after wildfire. *Water Resources Research*, *48*(3), 1–13. https://doi.org/10.1029/2011WR011470

Ellett, N. G., Pierce, J. L., & Glenn, N. F. (2019). Partitioned by process: Measuring post-fire debris-flow and rill erosion with Structure from Motion photogrammetry. *Earth Surface Processes and Landforms*, *44*(15), 3128–3146. https://doi.org/10.1002/esp.4728

Florsheim, J. L., Pellerin, B. a., Oh, N. H., Ohara, N., Bachand, P. a M., Bachand, S. M., Bergamaschi, B. a., Hernes, P. J., & Kavvas, M. L. (2011). From deposition to erosion: Spatial and temporal variability of sediment sources, storage, and transport in a small agricultural watershed. *Geomorphology*, *132*(3–4), 272–286. https://doi.org/10.1016/j.geomorph.2011.04.037

Florsheim, Joan L, & Gaffney, K. (2013). *Thresholds of stability in incised " Anthropocene " landscapes. October*. https://doi.org/10.1016/j.ancene.2013.10.006

Gabet, E. J. (2003). Sediment transport by dry ravel. *Journal of Geophysical Research: Solid Earth*, *108*(B1), 1–8. https://doi.org/10.1029/2001JB001686

Gabet, E. J., & Dunne, T. (2002). Landslides on coastal sage-scrub and grassland hillslopes in a severe El Niño winter: The effects of vegetation conversion on sediment delivery. *Bulletin of the Geological Society of America*, *114*(8), 983–990. https://doi.org/10.1130/0016-7606(2002)114<0983:LOCSSA>2.0.CO;2

Gao, P. (2013). Rill and Gully Development Processes. *Treatise on Geomorphology*, *7*, 122–131. https://doi.org/10.1016/j.physc.2009.10.149

Gartner, J. E., Cannon, S. H., & Santi, P. M. (2014). Empirical models for predicting volumes of sediment deposited by debris flows and sediment-laden floods in the transverse ranges of southern California. *Engineering Geology*, *176*, 45–56. https://doi.org/10.1016/j.enggeo.2014.04.008

Guilinger, J. J., Gray, A. B., Barth, N. C., & Fong, B. T. (2020). The Evolution of Sediment Sources Over a Sequence of Postfire Sediment-Laden Flows Revealed Through Repeat High-Resolution Change Detection. *Journal of Geophysical Research: Earth Surface*, *125*(10), 1–23. https://doi.org/10.1029/2020JF005527

Hungr, O., McDougall, S., & Bovis, M. (2007). Entrainment of material by debris flows. *Debris-Flow Hazards and Related Phenomena*, 135–158. https://doi.org/10.1007/3-540-27129-5_7

Hunsinger, G. B., Mitra, S., Warrick, J. A., & Alexander, C. R. (2008). Oceanic loading of wildfire-derived organic compounds from a small mountainous river. *Journal of Geophysical Research: Biogeosciences*, *113*(2), 1–14. https://doi.org/10.1029/2007JG000476

Iverson, R. M. (1997). of Debris. *American Geophysical Union*, *97*, 245–296.

Jackson, M., & Roering, J. J. (2009). Post-fire geomorphic response in steep, forested landscapes: Oregon Coast Range, USA. *Quaternary Science Reviews*, *28*(11–12), 1131–1146. https://doi.org/10.1016/j.quascirev.2008.05.003

Kampf, S. K., Brogan, D. J., Schmeer, S., MacDonald, L. H., & Nelson, P. A. (2016). How do geomorphic effects of rainfall vary with storm type and spatial scale in a post-fire landscape? *Geomorphology*, *273*, 39–51. https://doi.org/10.1016/j.geomorph.2016.08.001

Kean, J. W., Staley, D. M., Lancaster, J. T., Rengers, F. K., Swanson, B. J., Coe, J. A., Hernandez, J. L., Sigman, A. J., Allstadt, K. E., & Lindsay, D. N. (2019). Inundation, flow dynamics, and damage in the 9 January 2018 Montecito debris-flow event, California, USA: Opportunities and challenges for post-wildfire risk assessment. *Geosphere*, *15*(4), 1140–1163. https://doi.org/10.1130/GES02048.1

Kean, Jason W., & Staley, D. M. (2021). Forecasting the Frequency and Magnitude of Postfire Debris Flows Across Southern California. *Earth's Future*, *9*(3). https://doi.org/10.1029/2020EF001735

Kean, Jason W., Staley, D. M., & Cannon, S. H. (2011). In situ measurements of post-fire debris flows in southern California: Comparisons of the timing and magnitude of 24 debris-flow events with rainfall and soil moisture conditions. *Journal of Geophysical Research: Earth Surface*, *116*(4), 1–21. https://doi.org/10.1029/2011JF002005

Kean, Jason W., Staley, D. M., Leeper, R. J., Schmidt, K. M., & Gartner, J. E. (2012). A low-cost method to measure the timing of postfire flash floods and debris flows relative to rainfall. *Water Resources Research*, *48*(5), 1–8. https://doi.org/10.1029/2011WR011460

Keeley, J. E., & Fotheringham, C. J. (2001). Historic fire regime in southern California shrublands. *Conservation Biology*, *15*(6), 1536–1548. https://doi.org/10.1046/j.1523-1739.2001.00097.x

Keeley, J. E., Franklin, J., & Antonio, C. D. (2011). *The Landscape Ecology of Fire | Donald McKenzie | Springer*. 193–221. https://doi.org/10.1007/978-94-007-0301-8

Keeley, J. E., & Pausas, J. G. (2019). Distinguishing disturbance from perturbations in fire-prone ecosystems. *International Journal of Wildland Fire*, *28*(4), 282–287. https://doi.org/10.1071/WF18203

Keeley, J. E., & Syphard, A. D. (2019). Twenty-first century California, USA, wildfires: fuel-dominated vs. wind-dominated fires. *Fire Ecology*, *15*(1). https://doi.org/10.1186/s42408-019-0041-0

Kinoshita, A. M., & Hogue, T. S. (2015). Increased dry season water yield in burned watersheds in Southern California. *Environmental Research Letters*, *10*(1). https://doi.org/10.1088/1748-9326/10/1/014003

Kirby, M. E., Poulsen, C. J., Lund, S. P., Patterson, W. P., Reidy, L., & Hammond, D. E. (2004). Late Holocene lake level dynamics inferred from magnetic susceptibility and stable oxygen isotope data: Lake Elsinore, southern California (USA). *Journal of Paleolimnology*, *31*(3), 275–293. https://doi.org/10.1023/B:JOPL.0000021710.39800.f6

Lague, D., Brodu, N., Leroux, J., Rennes, G., Rennes, U., & Beaulieu, C. De. (n.d.). *Accurate 3D comparison of complex topography with terrestrial laser scanner : application to the Rangitikei canyon (N-Z). February 2013*, 1–28.

Lamb, M. P., Scheingross, J. S., Amidon, W. H., Swanson, E., & Limaye, A. (2011). A model for fire-induced sediment yield by dry ravel in steep landscapes. *Journal of Geophysical Research: Earth Surface*, *116*(3), 1–13. https://doi.org/10.1029/2010JF001878

Larsen, I. J., MacDonald, L. H., Brown, E., Rough, D., Welsh, M. J., Pietraszek, J. H., Libohova, Z., de Dios Benavides-Solorio, J., & Schaffrath, K. (2009). Causes of Post-Fire Runoff and Erosion: Water Repellency, Cover, or Soil Sealing? *Soil Science Society of America Journal*, *73*(4), 1393. https://doi.org/10.2136/sssaj2007.0432

Lavé, J., & Burbank, D. W. (2004). Denudation processes and rates in the Transverse Ranges, southern California: Erosional response of a transitional landscape to external and anthropogenic forcing. *Journal of Geophysical Research*, *109*(F1), F01006. https://doi.org/10.1029/2003JF000023

Liu, T., McGuire, L. A., Wei, H., Rengers, F. K., Gupta, H., Ji, L., & Goodrich, D. C. (2021). The timing and magnitude of changes to Hortonian overland flow at the watershed scale during the post-fire recovery process. *Hydrological Processes*, *35*(5), 1–18. https://doi.org/10.1002/hyp.14208

Lu, M., Ikejiri, T., & Lu, Y. H. (2021). A synthesis of the Devonian wildfire record: Implications for paleogeography, fossil flora, and paleoclimate. *Palaeogeography, Palaeoclimatology, Palaeoecology*, *571*(February), 110321. https://doi.org/10.1016/j.palaeo.2021.110321

MacDonald, L. H., & Larsen, I. J. (2009). Runoff and Erosion from Wildfires and Roads: Effects and Mitigation, ch 9. *Land Restoration to Combat Desertification: Innovative Approaches, Quality Control and Project Evaluation , Dissmeyer 2000*, 145–167.

Martinez, D., & Anderson, M. A. (2013). Methane production and ebullition in a shallow, artificially aerated, eutrophic temperate lake (Lake Elsinore, CA). *Science of the Total Environment*, *454–455*, 457–465. https://doi.org/10.1016/j.scitotenv.2013.03.040

McCoy, S. W., Kean, J. W., Coe, J. A., Staley, D. M., Wasklewicz, T. A., & Tucker, G. E. (2010). Evolution of a natural debris flow: In situ measurements of flow dynamics, video imagery, and terrestrial laser scanning. *Geology*, *38*(8), 735–738. https://doi.org/10.1130/G30928.1

McGuire, L. A., Kean, J. W., Staley, D. M., Rengers, F. K., & Wasklewicz, T. A. (2016). Constraining the relative importance of raindrop- and flow-driven sediment transport mechanisms in postwildfire environments and implications for recovery time scales. *Journal of Geophysical Research: Earth Surface*, *121*(11), 2211–2237. https://doi.org/10.1002/2016JF003867

McGuire, L. A., Rengers, F. K., Kean, J. W., & Staley, D. M. (2017). Debris flow initiation by runoff in a recently burned basin: Is grain-by-grain sediment bulking or en masse failure to blame? *Geophysical Research Letters*, *44*(14), 7310–7319. https://doi.org/10.1002/2017GL074243

McGuire, L. A., Rengers, F. K., Kean, J. W., Staley, D. M., & Mirus, B. B. (2018). Incorporating spatially heterogeneous infiltration capacity into hydrologic models with applications for simulating post-wildfire debris flow initiation. *Hydrological Processes*, *32*(9), 1173–1187. https://doi.org/10.1002/hyp.11458

Mensing, S. A., Michaelsen, J., & Byrne, R. (1999). *142-1999-A 560-year record of Santa Ana fires reconstructed from charcoal deposited in the Santa Barbara Basin.pdf. 305*, 295–305.

Miller, M. E., MacDonald, L. H., Robichaud, P. R., & Elliot, W. J. (2011). Predicting post-fire hillslope erosion in forest lands of the western United States. *International Journal of Wildland Fire*, *20*(8), 982–999. https://doi.org/10.1071/WF09142

Minnich, R. A. (1983). Fire Mosaics in Southern California and Northern Baja California. In *Science* (Vol. 219, Issue 4590, pp. 1287–1294). https://doi.org/10.1126/science.219.4590.1287

Mirus, B. B., & Loague, K. (2013). How runoff begins (and ends): Characterizing hydrologic response at the catchment scale. *Water Resources Research*, *49*(5), 2987–3006. https://doi.org/10.1002/wrcr.20218

Montgomery, D. R., & Dietrich, W. E. (1994). A physically based model for the topographical control on shallow landsliding. *Water Resources Research*, *30*(4), 1153–1171. https://doi.org/10.1029/93WR02979

Montgomery, D. R., Schmidt, K. M., Greenberg, H. M., & Dietrich, W. E. (2000). Forest clearing and regional landsliding. *Geology*, *28*(4), 311–314. https://doi.org/10.1130/0091-7613(2000)28<311:FCARL>2.0.CO;2

Moody, J. A. (2017). Residence times and alluvial architecture of a sediment superslug in response to different flow regimes. *Geomorphology*, *294*(April), 40–57. https://doi.org/10.1016/j.geomorph.2017.04.012

Moody, J. A., & Ebel, B. A. (2014). Infiltration and runoff generation processes in fire-affected soils. *Hydrological Processes*, *28*(9), 3432–3453. https://doi.org/10.1002/hyp.9857

Moody, J. A., Ebel, B. A., Nyman, P., Martin, D. A., Stoof, C., & Mckinley, R. (2016). Relations between soil hydraulic properties and burn severity. *International Journal of Wildland Fire*, *25*(3), 279–293. https://doi.org/10.1071/WF14062

Moody, J. A., & Martin, D. A. (2001). Initial hydrologic and geomorphic response following a wildfire in the Colorado front range. *Earth Surface Processes and Landforms*, *26*(10), 1049–1070. https://doi.org/10.1002/esp.253

Moody, J. A., & Martin, D. A. (2009). Synthesis of sediment yields after wildland fire in different rainfall regimes in the western United States. *International Journal of Wildland Fire*, *18*(1), 96–115. https://doi.org/10.1071/WF07162

Moody, J. A., & Martin, R. G. (2015). Measurements of the initiation of post-wildfire runoff during rainstorms using in situ overland flow detectors. *Earth Surface Processes and Landforms*, *40*(8), 1043–1056. https://doi.org/10.1002/esp.3704

Moody, J. A., Shakesby, R. A., Robichaud, P. R., Cannon, S. H., & Martin, D. A. (2013). Current research issues related to post-wildfire runoff and erosion processes. *Earth-Science Reviews*, *122*, 10–37. https://doi.org/10.1016/j.earscirev.2013.03.004

Murphy, B. P., Czuba, J. A., & Belmont, P. (2019). Post-wildfire sediment cascades: A modeling framework linking debris flow generation and network-scale sediment routing. *Earth Surface Processes and Landforms*, *44*(11), 2126–2140. https://doi.org/10.1002/esp.4635

Murphy, B. P., Yocom, L. L., & Belmont, P. (2018). Beyond the 1984 Perspective: Narrow Focus on Modern Wildfire Trends Underestimates Future Risks to Water Security. *Earth's Future*, *6*(11), 1492–1497. https://doi.org/10.1029/2018EF001006

Murphy, S. F., McCleskey, R. B., Martin, D. A., Holloway, J. A. M., & Writer, J. H. (2020). Wildfire-driven changes in hydrology mobilize arsenic and metals from legacy mine waste. *Science of the Total Environment*, *743*, 140635. https://doi.org/10.1016/j.scitotenv.2020.140635

Neely, A. B., & DiBiase, R. A. (2020). Drainage Area, Bedrock Fracture Spacing, and Weathering Controls on Landscape-Scale Patterns in Surface Sediment Grain Size. *Journal of Geophysical Research: Earth Surface*, *125*(10), 1–22. https://doi.org/10.1029/2020JF005560

Neris, J., Santin, C., Lew, R., Robichaud, P. R., Elliot, W. J., Lewis, S. A., Sheridan, G., Rohlfs, A. M., Ollivier, Q., Oliveira, L., & Doerr, S. H. (2021). Designing tools to predict and mitigate impacts on water quality following the Australian 2019/2020 wildfires: Insights from Sydney's largest water supply catchment. *Integrated Environmental Assessment and Management*, *00*(00), 1–11. https://doi.org/10.1002/ieam.4406

Nyman, P., Sheridan, G. J., Moody, J. A., Smith, H. G., Noske, P. J., & Lane, P. N. J. (2013). Sediment availability on burned hillslopes. *Journal of Geophysical Research: Earth Surface*, *118*(4), 2451–2467. https://doi.org/10.1002/jgrf.20152

Nyman, P., Sheridan, G. J., Smith, H. G., & Lane, P. N. J. (2014). Modeling the effects of surface storage, macropore flow and water repellency on infiltration after wildfire. *Journal of Hydrology*, *513*, 301–313. https://doi.org/10.1016/j.jhydrol.2014.02.044

Odigie, K. O., & Flegal, A. R. (2011). Pyrogenic remobilization of historic industrial lead depositions. *Environmental Science and Technology*, *45*(15), 6290–6295. https://doi.org/10.1021/es200944w

Odigie, K. O., Khanis, E., Hibdon, S. A., Jana, P., Araneda, A., Urrutia, R., & Flegal, A. R. (2016). Remobilization of trace elements by forest fire in Patagonia, Chile. *Regional Environmental Change*, *16*(4), 1089–1096. https://doi.org/10.1007/s10113-015-0825-y

Orem, C. A., & Pelletier, J. D. (2015). Quantifying the time scale of elevated geomorphic response following wildfires using multi-temporal LiDAR data: An example from the Las Conchas fire, Jemez Mountains, New Mexico. *Geomorphology*, *232*, 224–238. https://doi.org/10.1016/j.geomorph.2015.01.006

Overpeck, J. T., & Udall, B. (2020). Climate change and the aridification of North America. *Proceedings of the National Academy of Sciences of the United States of America*, *117*(22), 11856–11858. https://doi.org/10.1073/pnas.2006323117

Palucis, M. C., Ulizio, T. P., & Lamb, M. P. (2021). Debris flow initiation from ravel-filled channel bed failure following wildfire in a bedrock landscape with limited sediment supply. *GSA Bulletin*, 1–18. https://doi.org/10.1130/b35822.1

Parsons, A., Robichaud, P. R., Lewis, S. A., Napper, C., & Clark, J. T. (2010). Field guide for mapping post-fire soil burn severity. *USDA Forest Service - General Technical Report RMRS-GTR*, *243*, 1–49. https://doi.org/10.2737/RMRS-GTR-243

Passalacqua, P., Belmont, P., Staley, D. M., Simley, J. D., Arrowsmith, J. R., Bode, C. A., Crosby, C., Delong, S. B., Glenn, N. F., Kelly, S. A., Lague, D., Sangireddy, H., Schaffrath, K., Tarboton, D. G., Wasklewicz, T., & Wheaton, J. M. (2015). Earth-Science Reviews Analyzing high resolution topography for advancing the understanding of mass and energy transfer through landscapes : A review. *Earth Science Reviews*, *148*, 174–193. https://doi.org/10.1016/j.earscirev.2015.05.012

Pelletier, J. D., & Orem, C. A. (2014). How do sediment yields from post-wildfire debris-laden flows depend on terrain slope, soil burn severity class, and drainage basin area? Insights from airborne-LiDAR change detection. *Earth Surface Processes and Landforms*, *39*(13), 1822–1832. https://doi.org/10.1002/esp.3570

Pierce, J. L., Meyer, G. a, & Jull, a J. T. (2004). Fire-induced erosion and millennial- scale climate change in northern ponderosa pine forests. *Nature*, *432*(November), 87–90. https://doi.org/10.1038/nature03028.Published

Pierce, J. M. G. (2008). Long-term fire history from alluvial fan sediments: the role of drought and climate. *International Journal of Wildland Fire; 2008*, *17*(1), 84–95.

Poon, P. K., & Kinoshita, A. M. (2018). Spatial and temporal evapotranspiration trends after wildfire in semi-arid landscapes. *Journal of Hydrology*, *559*, 71–83. https://doi.org/10.1016/j.jhydrol.2018.02.023

Radeloff, V. C., Helmers, D. P., Kramer, H. A., Mockrin, M. H., Alexandre, P. M., Bar-Massada, A., Butsic, V., Hawbaker, T. J., Martinuzzi, S., Syphard, A. D., & Stewart, S. I. (2018). Rapid growth of the US wildland-urban interface raises wildfire risk. *Proceedings of the National Academy of Sciences*, *115*(13), 3314–3319. https://doi.org/10.1073/pnas.1718850115

Ralph, F. M., & Dettinger, M. D. (2011). Storms, floods, and the science of atmospheric rivers. *Eos*, *92*(32), 265–266. https://doi.org/10.1029/2011EO320001

Raymond, C. A., McGuire, L. A., Youberg, A. M., Staley, D. M., & Kean, J. W. (2020). Thresholds for post-wildfire debris flows: Insights from the Pinal Fire, Arizona, USA. *Earth Surface Processes and Landforms*, *45*(6), 1349–1360. https://doi.org/10.1002/esp.4805

Reneau, S. L. (2007). *Sediment delivery after a wildfi re*. *2*, 151–154. https://doi.org/10.1130/G23288A.1

Rengers, F. K., McGuire, L. A., Kean, J. W., Staley, D. M., Dobre, M., Robichaud, P. R., & Swetnam, T. (2021). Movement of Sediment Through a Burned Landscape: Sediment Volume Observations and Model Comparisons in the San Gabriel Mountains, California, USA. *Journal of Geophysical Research: Earth Surface*, *126*(7), 1–25. https://doi.org/10.1029/2020jf006053

Rengers, Francis K., McGuire, L. A., Oakley, N. S., Kean, J. W., Staley, D. M., & Tang, H. (2020). Landslides after wildfire: initiation, magnitude, and mobility. *Landslides*, *17*(11), 2631–2641. https://doi.org/10.1007/s10346-020-01506-3

Rickson, R. J. (2010). Fire Effects on Soils and Restoration Strategies. Edited by A. Cerda and P. R. Robichaud. Enfield, NH, USA: Science Publishers (2009), pp. 589, £85.00. ISBN 978-1-57808-526-2. *Experimental Agriculture*, *46*(02), 260. https://doi.org/10.1017/S0014479709990913

Riley, K., Pierce, J., & Meyer, G. A. (2015). Vegetative and climatic controls on Holocene wildfire and erosion recorded in alluvial fans of the Middle Fork Salmon River, Idaho. *Holocene*, *25*(5), 857–871. https://doi.org/10.1177/0959683615571423

Robinne, F. N., Hallema, D. W., Bladon, K. D., Flannigan, M. D., Boisramé, G., Bréthaut, C. M., Doerr, S. H., Di Baldassarre, G., Gallagher, L. A., Hohner, A. K., Khan, S. J., Kinoshita, A. M., Mordecai, R., Nunes, J. P., Nyman, P., Santín, C., Sheridan, G., Stoof, C. R., Thompson, M. P., … Wei, Y. (2021). Scientists' warning on extreme wildfire risks to water supply. *Hydrological Processes*, *35*(5), 0–3. https://doi.org/10.1002/hyp.14086

Roth, D. L., Doane, T. H., Roering, J. J., Furbish, D. J., & Zettler-Mann, A. (2020). Particle motion on burned and vegetated hillslopes. *Proceedings of the National Academy of Sciences of the United States of America*, *117*(41), 25335–25343. https://doi.org/10.1073/pnas.1922495117

Sankey, J. B., Germino, M. J., & Glenn, N. F. (2009). Aeolian sediment transport following wildfire in sagebrush steppe. *Journal of Arid Environments*, *73*(10), 912–919. https://doi.org/10.1016/j.jaridenv.2009.03.016

Sankey, Joel B., Kreitler, J., Hawbaker, T. J., McVay, J. L., Miller, M. E., Mueller, E. R., Vaillant, N. M., Lowe, S. E., & Sankey, T. T. (2017). Climate, wildfire, and erosion ensemble foretells more sediment in western USA watersheds. *Geophysical Research Letters*, *44*(17), 8884–8892. https://doi.org/10.1002/2017GL073979

Santi, P. M., deWolfe, V. G., Higgins, J. D., Cannon, S. H., & Gartner, J. E. (2008). Sources of debris flow material in burned areas. *Geomorphology*, *96*(3–4), 310–321. https://doi.org/10.1016/j.geomorph.2007.02.022

Santi, P. M., & MacAulay, B. (2019). Rainfall intensity limitation and sediment supply independence of post-wildfire debris flows in the western U.S. *Debris-Flow Hazards Mitigation: Mechanics, Monitoring, Modeling, and Assessment - Proceedings of the 7th International Conference on Debris-Flow Hazards Mitigation*, *2005*, 539–547.

Schmidt, K. M., Roering, J. J., Stock, J. D., Dietrich, W. E., Montgomery, D. R., & Schaub, T. (2001). The variability of root cohesion as an influence on shallow landslide susceptibility in the Oregon Coast Range. *Canadian Geotechnical Journal*, *38*(5), 995–1024. https://doi.org/10.1139/cgj-38-5-995

Schmidt, Kevin M., Hanshaw, M. N., Howle, J. F., Kean, J. W., Staley, D. M., Stock, J. D., & Bawden, G. W. (2011). Hydrologic Conditions and Terrestrial Laser Scanning of Post-fire Debris Flows in the San Gabriel Mountains, CA, U.S.A. *Debris-Flow Hazards Mitigation, Mechanics, Prediction, and Assessment*, 583–593. https://doi.org/10.4408/IJEGE.2011-03.B-064

Schwanghart, W., & Kuhn, N. J. (2010). TopoToolbox: A set of Matlab functions for topographic analysis. *Environmental Modelling and Software*, *25*(6), 770–781. https://doi.org/10.1016/j.envsoft.2009.12.002

Shakesby, R. a., & Doerr, S. H. (2006). Wildfire as a hydrological and geomorphological agent. *Earth-Science Reviews*, *74*(3–4), 269–307. https://doi.org/10.1016/j.earscirev.2005.10.006

Shakesby, R. A., & Doerr, S. H. (2006). *Wildfire as a hydrological and geomorphological agent*. *74*, 269–307. https://doi.org/10.1016/j.earscirev.2005.10.006

Sklar, L. S., Riebe, C. S., Marshall, J. A., Genetti, J., Leclere, S., Lukens, C. L., & Merces, V. (2017). The problem of predicting the size distribution of sediment supplied by hillslopes to rivers. *Geomorphology*, *277*, 31–49. https://doi.org/10.1016/j.geomorph.2016.05.005

Staley, D. M., Kean, J. W., & Rengers, F. K. (2020). The recurrence interval of post-fire debris-flow generating rainfall in the southwestern United States. *Geomorphology*, *370*, 107392. https://doi.org/10.1016/j.geomorph.2020.107392

Staley, D. M., Negri, J. A., Kean, J. W., Laber, J. L., Tillery, A. C., & Youberg, A. M. (2017). Prediction of spatially explicit rainfall intensity–duration thresholds for post-fire debris-flow generation in the western United States. *Geomorphology*, *278*, 149–162. https://doi.org/10.1016/j.geomorph.2016.10.019

Staley, D. M., Wasklewicz, T. A., & Kean, J. W. (2014a). Characterizing the primary material sources and dominant erosional processes for post-fire debris-flow initiation in a headwater basin using multi-temporal terrestrial laser scanning data. *Geomorphology*, *214*, 324–338. https://doi.org/10.1016/j.geomorph.2014.02.015

Staley, D. M., Wasklewicz, T. A., & Kean, J. W. (2014b). Characterizing the primary material sources and dominant erosional processes for post-fire debris-flow initiation in a headwater basin using multi-temporal terrestrial laser scanning data. *Geomorphology*, *214*, 324–338. https://doi.org/10.1016/j.geomorph.2014.02.015

Wohlgemuth, P. M., & Hubbert, K. R. (2008). *The Effects of Fire on Soil Hydrologic Properties and Sediment Fluxes in*. 115–122.

Stein, E. D., Brown, J. S., Hogue, T. S., Burke, M. P., & Kinoshita, A. (2012). Stormwater contaminant loading following southern California wildfires. *Environmental Toxicology and Chemistry*, *31*(11), 2625–2638. https://doi.org/10.1002/etc.1994

Swain, D. L., Langenbrunner, B., Neelin, J. D., & Hall, A. (2018). Increasing precipitation volatility in twenty-first-century California. *Nature Climate Change*, *8*(5), 427–433. https://doi.org/10.1038/s41558-018-0140-y

Syphard, A. D., & Keeley, J. E. (2015). Location, timing and extent of wildfire vary by cause of ignition. *International Journal of Wildland Fire*, *24*(1), 37–47. https://doi.org/10.1071/WF14024

Syphard, A. D., & Keeley, J. E. (2020). Mapping fire regime ecoregions in California. *International Journal of Wildland Fire*, *29*(7), 595–601. https://doi.org/10.1071/WF19136

Terwilliger, V. J., & Waldron, L. J. (1991). Effects of root reinforcement on soil-slip patterns in the Transverse Ranges of southern California. *Geological Society of America Bulletin*, *103*(6), 775–785. https://doi.org/10.1130/0016-7606(1991)103<0775:EORROS>2.3.CO;2

Thomas, M. A., Rengers, F. K., Kean, J. W., McGuire, L. A., Staley, D. M., Barnhart, K. R., & Ebel, B. A. (2021). Postwildfire Soil-Hydraulic Recovery and the Persistence of Debris Flow Hazards. *Journal of Geophysical Research: Earth Surface*, *126*(6), 1–25. https://doi.org/10.1029/2021JF006091

Thompson, J. R., Spies, T. A., & Ganio, L. M. (2007). Reburn severity in managed and unmanaged vegetation in a large wildfire. *Proceedings of the National Academy of Sciences of the United States of America*, *104*(25), 10743–10748. https://doi.org/10.1073/pnas.0700229104

Warrick, J. A., Hatten, J. A., Pasternack, G. B., Gray, A. B., Goni, M. A., & Wheatcroft, R. A. (2012). The effects of wildfire on the sediment yield of a coastal California watershed. *Bulletin of the Geological Society of America*, *124*(7–8), 1130–1146. https://doi.org/10.1130/B30451.1

Warrick, Jonathan A., Melack, J. M., & Goodridge, B. M. (2015). Sediment yields from small, steep coastal watersheds of California. *Journal of Hydrology: Regional Studies*, *4*, 516–534. https://doi.org/10.1016/j.ejrh.2015.08.004

Wester, T., Wasklewicz, T., & Staley, D. (2014). Functional and structural connectivity within a recently burned drainage basin. *Geomorphology*, *206*, 362–373. https://doi.org/10.1016/j.geomorph.2013.10.011

Westerling, A. L., Hidalgo, H. G., Cayan, D. R., & Swetnam, T. W. (2006). Warming and earlier spring increase Western U.S. forest wildfire activity. *Science*, *313*(5789), 940–943. https://doi.org/10.1126/science.1128834

Wheaton, J. M., Brasington, J., Darby, S. E., & Sear, D. A. (2010). Accounting for uncertainty in DEMs from repeat topographic surveys: Improved sediment budgets. *Earth Surface Processes and Landforms*, *35*(2), 136–156. https://doi.org/10.1002/esp.1886

Wheaton, J. M., Brasington, J., Darby, S. E., Sear, D. A., Sciences, W., & Hill, O. M. (2010). *Accounting for uncertainty in DEMs from repeat topographic surveys : improved sediment budgets*. *156*(December 2009), 136–156. https://doi.org/10.1002/esp.1886

Wilder, B. A., Lancaster, J. T., Cafferata, P. H., Coe, D. B. R., Swanson, B. J., Lindsay, D. N., Short, W. R., & Kinoshita, A. M. (2021). An analytical solution for rapidly predicting post-fire peak streamflow for small watersheds in southern California. *Hydrological Processes*, *35*(1), 1–14. https://doi.org/10.1002/hyp.13976

Williams, A. P., Abatzoglou, J. T., Gershunov, A., Guzman-Morales, J., Bishop, D. A., Balch, J. K., & Lettenmaier, D. P. (2019). Observed Impacts of Anthropogenic Climate Change on Wildfire in California. *Earth's Future*, *7*(8), 892–910. https://doi.org/10.1029/2019EF001210

Williams, A. P., Abatzoglou, J. T., Gershunov, A., Guzman-Morales, J., Bishop, D. A., Balch, J. K., & Lettenmaier, D. P. (2019). Observed impacts of anthropogenic climate change on wildfire in California. *Earth's Future*, 2019EF001210. https://doi.org/10.1029/2019EF001210

Wilson, C., Kampf, S. K., Ryan, S., Covino, T., MacDonald, L. H., & Gleason, H. (2021). Connectivity of post-fire runoff and sediment from nested hillslopes and watersheds. *Hydrological Processes*, *35*(1), 1–17. https://doi.org/10.1002/hyp.13975

Chapter 4. Source to Sink Dynamics: A Case Study of Postfire Runoff Impacts on an Arid Managed Terminal Lake, Lake Elsinore, CA, USA

4.1. Abstract

Wildfire is increasingly impacting many parts of the world as the climate warms, including the semiarid western United States. Water resources in semiarid regions are already pressured by the onset of drought, demographic shifts, and a more uncertain hydroclimate, in addition to which postfire runoff represents a serious and increasing risk to water quality that has been little studied. The goal of this study is to evaluate time-dependent effects on sediment-associated water quality parameters (TSS, total P and N, and metals) and additionally understand broader geomorphic and flow infrastructure controls on postfire sediment delivery. We used a unique opportunity of coeval hydro-geomorphic monitoring, remote sensing, and sediment sampling in Lake Elsinore, a partially endorheic system in southern California, USA, which was impacted by runoff from the burn scar of the 2018 Holy Fire. During the first post-fire wet season it was found that water quality concentrations were highly elevated relative to a nearby unburned control site, such as an 10 to 10^4 fold difference in metal concentrations. There was also some evidence of first-flush dynamics in the smaller catchment of two monitored catchments in the burn scar. Additionally, we found that much of the sediment and nutrient delivery to Lake Elsinore is likely from two small, undammed catchments with high sediment transfer efficiency and that sediment control infrastructure held back ~50-70% of material exports from the burned terrain draining to the lake. This case study highlights a unique source-to-sink perspective on post-fire sediment pulses in an intensively-managed wildland-urban lake system and provides a context for understanding, planning for, and mitigating postfire impacts on water resources.

4.2. Introduction

The impact of wildfire is increasing in many regions worldwide due to increasing fire severity and frequency as the climate warms. There is a growing incidence of fire-enhancing conditions such as droughts, intense heat waves, and rainfall volatility (e.g., Swain et al., 2018; Westerling et al., 2006; Williams et al., 2019). Post-wildfire landscapes can produce and export immense amounts of sediment and associated constituents, as well as dissolved inorganic and organic compounds, particularly following high severity fire in mountainous terrain (e.g., Moody & Martin, 2001; Shakesby & Doerr, 2006). Because forest and shrubland-dominated headwaters in semiarid temperate settings are the primary source areas of freshwater to downstream communities, the dual threat of greater wildfire disturbance and increasing rainfall intensity in a warming climate represents a serious threat to surface water supplies across much of the western United States (Bladon et al.,2014; Emelko et al., 2011; Robinne et al., 2021; Sankey et al., 2017). These impacts are important to understand and quantify, particularly at a time when these resources are already at risk in the face of increased drought and aridification (Overpeck & Udall, 2020). Yet, even in the state of California, which is arguably one of the most well-studied environments for post-wildfire impacts in the world, there have not been enough studies on water resources impacts from wildfire, which are needed in order to inform land managers on how to best anticipate and mitigate impacts of post-wildfire runoff on water resources. Many studies on postfire sediment and constituent transfers exist at either very large scales (10-1000 km^2) where investigation of specific processes in postfire sediment cascades are much more difficult (Kampf et al., 2016; Wilson et al., 2021), or at very small hillslope scales (e.g. Benavides-Solorio & MacDonald, 2001; Schmidt et al., 2011) where it may be difficult to upscale findings to scales relevant to management. Thus, additional studies linking these scales will like required to bridge

this gap (Moody et al., 2013) and inform management of wildfire impacts on surface water resources.

Wildfire impacts water quantity and quality by altering rainfall-runoff partitioning to produce greater amounts of runoff (e.g., Ebel et al., 2012; Larsen et al., 2009; Moody & Ebel, 2014) and also increases the erodibility of soil through a variety of processes including destabilizing surface soil texture, removing surface cover and reduces other hydraulic roughness elements (e.g., MacDonald & Larsen, 2009; Reneau, 2007; Shakesby & Doerr, 2006). Fire also produces a large amount of ash , which can be readily mobilized by wind and water, and can contain elevated concentrations of nutrients and contaminants such as heavy metals (Campos et al., 2015; Odigie et al., 2016; Odigie & Flegal, 2011) and polyaromatic hydrocarbons (PAHs) released by plant matter combustion (Hunsinger et al., 2008; Stein et al., 2012). There can be additional onlapping impacts of wildfire with other disturbances such as the postfire mobilization of mine tailings and flow through old workings, which can deliver levels of heavy metals above maximum contaminant levels to downstream waterbodies (S. F. Murphy et al., 2020). Increased suspended load of post-wildfire itself is a significant stressor through increases turbidity and rapid sedimentation of benthic habitats. Finally, one of the most important long-term impacts on water management is through reservoir sedimentation (Murphy et al., 2018, 2019), which can greatly reduce reservoir capacity without very costly interventions.

To our knowledge, there are no studies that have investigated contemporary post-wildfire runoff and sedimentation impacts specifically on an endorheic (terminal, land-locked) lake system. These lakes are especially sensitive to upstream influences on their water quality, given that hydrologic losses occur through evapotranspiration and/or percolation rather than surface water outlets (Sawe, 2017; Yapiyev et al., 2017). Endorheic drainages constitute ~25% of the world's ice-free continental catchment area (Hostetler, 1995), and are commonly found in

137

semiarid to arid regions, making them prone to wildfire. The focus of this study is to document and understand impacts of post-wildfire runoff on an intensively-managed partially endorheic lake in southern California as a case study for other similar regions that are prone to post-fire impacts. In this study, we focus on erosional dynamics and the transfer of sediment, sediment-associated metals, and particulate and dissolved nutrients (e.g., nitrate and nitrite) from steep mountainous terrain burned in the 2018 Holy Fire to Lake Elsinore in the Santa Ana watershed of southern California, USA. We particularly wanted to better understand the time-dependent characteristics of first-flush effects of these water quality parameters. Another goal of this study was to understand how sediment and sediment-associated constituent transfer dynamics to the lake were controlled by both built infrastructure and the geomorphology of the system. Finally, we wanted to contextualize postfire sediment and nutrient transfers to the lake through a comparison of fluxes to lake sedimentation rates at centennial (100-yr) timescales (Kirby et al., 2004) and a previously derived annual nutrient budget (Anderson, 2001). Proximal inputs to Lake Elsinore from steep basins burned by the wildfire are intensively-managed by sediment retention basins and other control infrastructure, and this study provided an opportunity to evaluate their impacts on sediment, nutrient and heavy metal efflux from the burn scar. Using sediment budgets derived from remote sensing and hydrosedimentological monitoring in combination with stream sampling, we found that total metals, and total nitrogen (N) and phosphorus (P) were orders of magnitude higher than an unburned control during the same storm event. There was also evidence of a first-flush and depletion signal in the smallest monitored catchment (0.25 km^2). Using a combination of remote sensing, sediment volume estimations, and lake-bottom sampling, we found that sediment control infrastructure was very effective at preventing large sediment pulses (~50-70% of the total flux) from entering the lake from the two largest catchments feeding Lake Elsinore, and that much of the delivered sediment and nutrients came from small undammed

138

catchments in the burn area. When we compared sediment inputs to previous published

sedimentation rates averaged much of the 20th century, there was an equivalent almost half a year

of area-normalized lake infill from sources that compose less than 1% of the total catchment of

area of the lake. Nutrient loading to the lake was also very high relative to previous non-fire

estimates during a relatively dry year (Anderson, 2001), where it was found that standing stock

estimates of nutrients delivered in the emplaced postfire plume were ~105-fold and ~78-fold

greater for total N and P respectively. These results highlight the large magnitude changes of

postfire runoff draining steep burned terrain and provide a source-to-sink snapshot of postfire

stormflow pulses that could be useful in planning for and mitigating postfire stormflow impacts in

similar lake and reservoir environments prone to wildfire.

4.3. Study Area

Lake Elsinore is a shallow, polymictic partial terminal lake basin 75 miles southeast of

Los Angeles, CA located in western Riverside County managed by the City of Lake Elsinore in

southern California USA (Figure 1.1) (Anderson, 2001). The lake is in a graben rift valley formed

by trans-tensional extension of strands of the active right-lateral Elsinore Fault (Morton and

Miller, 2006; Figure 1). The lake naturally overflows during high rainfall years through Temescal

Wash an ephemeral drainage that connects it to the larger downstream Santa Ana River basin

(reports of at least 20 major overflows between 1769 and 1933 AD according to Lynch [1931]).

The lake has been site of many algal blooms and resultant fish kills and is managed by the Santa

Ana Regional Water Quality Control Board through the total maximum daily load (TMDL)

process where it is listed as 303(d) impaired for N+P nutrient loading and low dissolved oxygen

(RWQCB, 2019). In response to these water quality issues, the lake was equipped with aeration

systems in 2006 (Martinez & Anderson, 2013). Phosphorus and nitrogen nutrient loading

monitoring indicate that much of the lake is internally loaded through nutrient cycling processes

with smaller relative inputs from runoff and atmospheric sources (Anderson, 2001; 2010), although the initial 2001 study that estimated total nutrient fluxes was during a relatively inflow discharge year.

The drainage area of Lake Elsinore is ~2000 km^2 with the primary inflows being the San Jacinto River via Canyon Lake Reservoir (>95% of upstream contributing area) and drainage from Leach, McVicker, and Dickey canyons along the eastern escarpment of the northern Santa Ana Mountains. Leach, McVicker, and Dickey canyons burned at predominantly moderate-to-high severity during the 2018 Holy Fire (Figure 1.1A). Leach McVicker Canyons are primarily underlain by Jurassic metasedimentary lithology and Dickey Canyon is underlain primarily by Cretaceous granitic intrusive rocks. Owing to this high burn severity and very steep hillslopes (>30 degrees), these drainages experienced debris and sediment-laden flows during winter storms of the active season of 2018-2019 with ~120% of annual rainfall and rain gages reported 15-minute rainfall intensities ranging from 1-3 year return intervals (Guilinger et al., 2020; Wilder et al., 2021). Previous work (Chapter 2) found that burned hillslopes were severely eroded during this period, with sediment yields (area-normalized erosion magnitudes) of steep hillslopes and headwater channel networks on the order of 20-40 mm and observations of significant storage of material in less confined valley bottoms in higher drainage areas above the canyon mouth fan apexes (Chapter 2).

4.4. Methods

4.4.1 Stream and Retention Basin Sampling

Through a joint effort by Riverside County Flood Control and Water Conservation District (RCFCWCD) and Alta-NV5, Inc. (ANV5), postfire runoff from the Holy Fire was sampled on November 30 2018 and January 14 2019 was sampled at two locations located at the mouths of

two headwater drainages: McVicker Sediment Retention Basin (MVB) and Horsethief Canyon (HC) (Figure 1A). Additionally, a control site unaffected by wildfire approximately 2 to the southwest of the burn scar, Adobe Creek (AC) (Figure 4.1A), was sampled during the initial November 30 2018 runoff event. At each location, flow-integrated samples were collected using 1L bottles attached to a long pole and a flowmeter was deployed to estimate flow. Additionally, a YSI multiparameter water quality sonde was deployed for ambient measurements of temperature, TDS, and turbidity. Individual 1L samples were taken and all samples were composited per event for subsequent chemical and physical analyses. The stream sampling design was modeled after approaches of Stein and Brown (2009) as part of an effort to standardize postfire monitoring approaches by the Southern California Coastal Water Research Project. This methodology highlights importance of sampling and testing for a full suite of water quality parameters that could be impactful to downstream aquatic habitat or human health. Sampling was cut short on November 29 2018 due to safety concerns and evacuation orders issued by the County of Riverside. These samples were analyzed for general water quality parameters, nutrients, and metals (Table 1). Water quality parameters which we focus on include total suspended solids and organic carbon. Nutrients we focused on included total Nitrogen and total Phosphorus. Metals that we focus on are Al, Cd, Cu, Fe, Pb, Mn, Ni, and Zn for which total and dissolved concentrations were quantified. For additional information on specific laboratory measurement techniques of these constituents, the reader is referred to Engelhorn and Guill (2019). Using mean discharge of the composite sampling periods, we evaluated discharge-concentration relationships of these various constituents for the four stormwater sampling events and compared them to the controls.

4.4.2. Lake Postfire Sediment and Chemistry Characterization

As part of a process to characterize postfire runoff and sediment plume inputs to Lake Elsinore for the Lake Elsinore and San Jacinto Watershed Project Authority, the consulting group Wood Environment and Infrastructure Solutions, Inc. was contracted to characterize sediment and water physical and chemical characteristics via boat sampling along transects on April 15-16 2019 following postfire winter rainstorms (see Table 4.2). We focus specifically on their characterization of plume deposits, which was achieved by ponar sediment grab sampling and sediment coring along four transects radiating out from the mouth of Leach Canyon channel where a delta composed of postfire sediments had been deposited (Figure 1.1B). Additionally, a sample was taken at the mouth of the channel, generating an estimate of sediment postfire deposit depth at the apex of the delta and a reference sample was taken beyond the influence of the postfire delta (North Reference, Figure 4.1B). For each sample, depth was estimated through visual estimation with a ruler. Using these depth estimates (n=17), we determined the volume of sediment deposited in the channel from the Leach Canyon channel by interpolating an isopach model of the postfire delta using Empricial Bayesian Kriging techniques, using an analytical error estimate of +/-1cm across the estimate of the delta area (resulting in a relative error volume of 22%). We assumed a symmetrical conical shape for the delta extending out 1000 m, the approximate distance which all samples along the transect verged to zero. Additional samples (n=4) were taken along the transect for chemical and physical analysis. These analyses were largely identical to water quality measurements and included grain size distribution, nutrients, and metals. Water samples were taken at these stations and dissolved constituents were determined. For more details on laboratory analytical techniques, the reader is referred to Stransky and Rudolph (2019).

4.4.3. Estimates of Postfire-Associated Sediment and Constituent Yields

Sediment was sampled from Leach and McVicker debris basins (Fig 1A). These samples were analyzed as part of an effort to estimate sediment-associated nutrient (N and P) reductions by the Riverside County retention basins (Table 3). These samples were devoid of any coarse (>2mm) rock clasts, which from observations of inflow to the debris basin (Guilinger et al., 2020 – Chapter 1 of this dissertation) was likely primarily composed of fines. However, we try to account for the fraction of coarse clasts later in the methods below.

Because P and heavy metals partition more strongly to fine sediments, in which there was a significant moderate correlation with %mud (e.g., As vs. %mud, $r^2= 0.2$, p=0.004), we attempted to estimate the amount of material exported from the uplands to the retention basins and Lake Elsinore that was composed of the <2mm fraction. Sediments had to be cleared quickly from the debris basin, thus it was not possible to assess the bulk grain size distribution greater than (> 2 mm). Although debris flows did not extend down into the debris basin, there was field evidence of bedload containing cobbles and small boulders reaching the debris basins, thus it is important to try to estimate the potential mass fractions of this material for estimating fine sediment-associated constituent yield. To do this, we used samples of hillslope soils (n=12) and channel material (n=9) in Leach Canyon that underwent traditional sieving analysis. Because we had evidence that material within these channels were swept down to bedrock (Guilinger et al., 2020 – Chapter 1), we defined an envelope of possibilities for the grain size distribution of exported sediment. To define the lower range of fine fraction export, we assumed a scenario in which the competence of flows were sufficient to entrain a majority of the channel grain size distribution scaled to the average amount of channel erosion (~34% on average for the Holy Fire burn scar using estimates from Guilinger et al., 2021 – Chapter 2) in our remote sensing derived sediment budgets, which results in an estimate of 85% fine material (< 2 mm) exported. In the

upper limit, we assume that export of coarse material (> 2 mm) is negligible due to a greater probability of deposition of these fractions, thus export is 100% fine material. For both scenarios, we assume that in general the competence of erosion on hillslopes is insufficient to transport large quantities of material of coarse clasts (> 2 mm). This is supported by the observation that there was significant residual gravel/cobble armoring (or pedastaling) as observed in Guilinger et al., 2020 (Chapter 1) in inter-rill zones.

Building off work from Guilinger et al. (2020;2021, Chapters 1-2 of this dissertation), we used sediment volumetric flux and yield (area-normalized flux) estimates derived from ground-based and airborne-based repeat laser scanning to estimate sediment-associated nutrient and metal yields adjusted to our envelope of %fines delivery above. Finally, we contextualize these with schematic sediment budgets to determine sources and sinks of sediment (and constituent) yield from the burned uplands to Lake Elsinore.
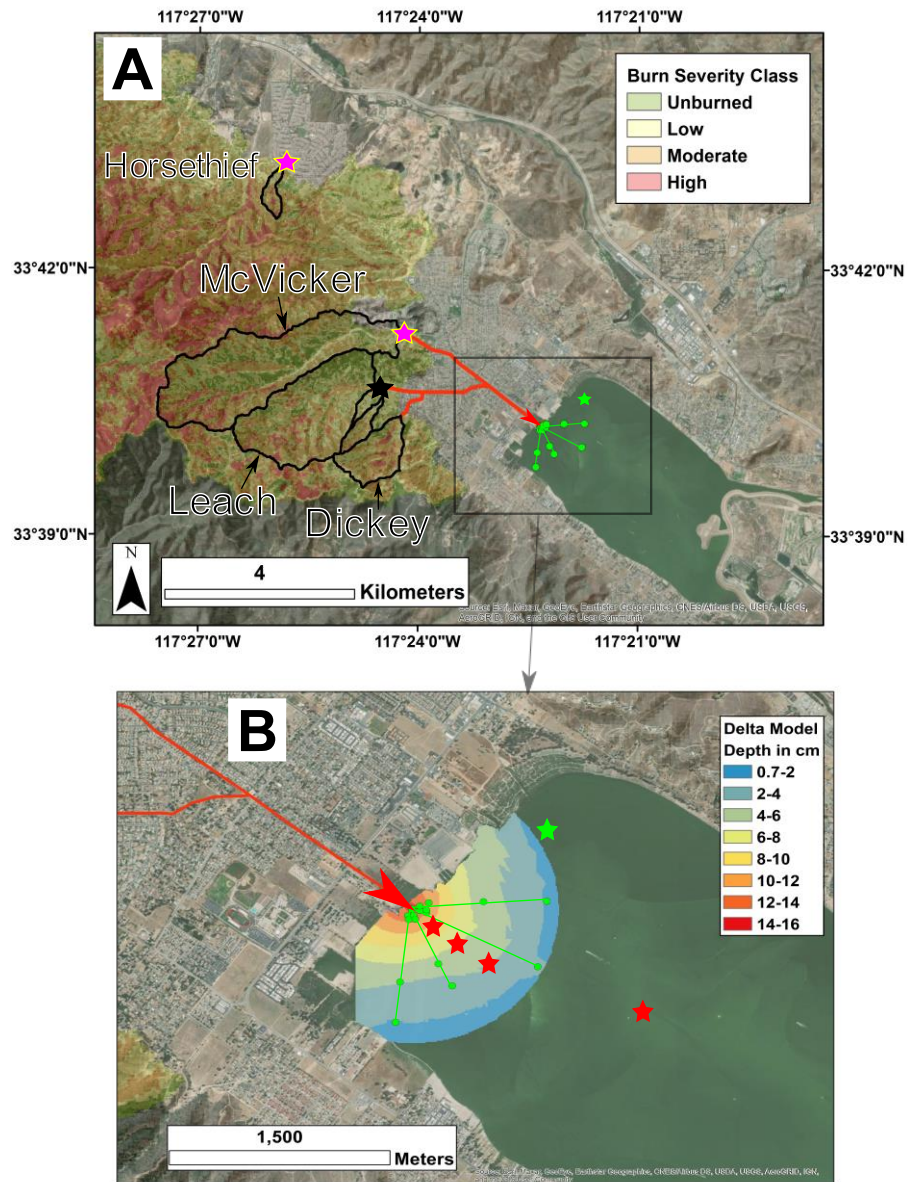
Figure 4.1. A. Larger-scale image-overlayed hillshade of study area showing Holy Fire burn scar with associated soil burn severity classes (USGS, 2021) and watersheds of interest (black outlines). Stream sample locations (McVicker and Horsethief mouths) are shown as magenta stars, red lines are the urbanized stream network feeding Lake Elsinore, black star is the Leach sediment retention basin, and green circle on green lines are boat transect delta depth samples along with a reference (star). **B.** Zoomed in map showing estimated extent and kriged isopach model of the postfire delta along with boat transect sample points and red stars showing samples taken for chemical and physical analysis. *Note: Adobe Reference is off the map, located approximately 24km south of McVicker sediment retention basin.*

145

Figure 4.2. Photos of sampling campaigns. **A.** UAV image of the plume taken on Jan 8 2019 showing prograding postfire delta (credit: Alta Env NV5) with associated color/texture of samples taken from mouth (red), proximal sample of sediment plume (green), and non-Holy Fire sample taken from center of the lake (red star Fig 1B) (sample photo credit: Stransky and Rudolph, 2019). **B.** Image of inflamed red gills of carp from cold season fish kill in Lake Elsinore during postfire runoff period linked to Golden Algal bloom, also pictured (credit: Stransky and Rudolph, 2019). **C.** Image of sampling location spillway downstream of McVicker retention basin showing hyper-concentrated runoff during first-flush event on Nov 29 2018. **D.** Image of slotted drain outlet sampling location for Horsethief outlet take on Nov 29 2018. **E.** Control sampling site at Adobe Creek showing unburned chaparral catchment taken on Nov 29 2018. (photo credit for C-E: Guill and Engelhorn, 2019).
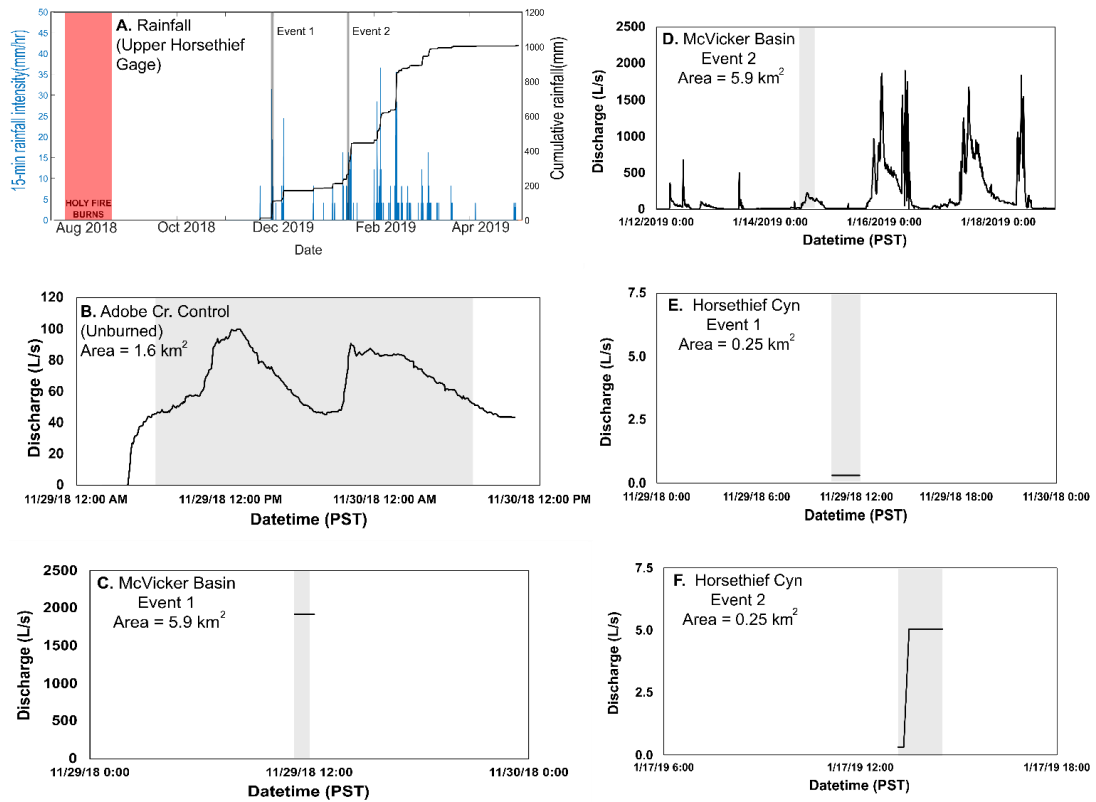
Figure 4.3. A. Overview plot of rainfall patterns and timing of sampling during postfire wet period. B-F: Plots of sampling times and available discharge measurements, where grey regions show sample compositing time periods. B shows unburned control, C-D shows McVicker retention basin site, E-F shows Horsethief Canyon site. Note that for Event 1, sampling staff was evacuated due to debris flow hazard warnings.

4.5. Results

4.5.1. Concentration-Discharge Relationships Show Major Postfire Influence

During the initial sampling effort, it was found that all constituents and water quality parameters in postfire runoff (except orthophosphate) had concentrations far exceeding the control group (Fig 3C). For example, for the first event, total P was 60-130 times greater in the postfire runoff compared to control group. Differences in many metals were much starker, with many non-detects in the control site runoff and overall 10 to 10^4-fold differences in metal concentrations. We noted that total suspended solids (TSS) values for the initial Event 1

McVicker sample of 130 g/L were very high. Depending on the organic content of this sample (which was not evaluated), this flow is almost hyper-concentrated (>139 g/L of mineral sediment), which appeared to be consistent with observations of very sediment-rich floodwaters and turbidity levels well above the range of the deployed sensor (Figure 4.2C; Table 4.1).

Considering the bulk trends of all constituents, it was found that there was a general positive trend between discharge and concentration, as expected. However, we noted interesting trends between sites and through the two successive runoff events. In Horsethief Canyon it appeared as though there was a slight decrease in metals, TSS, and nutrients between event 1 and 2 (Fig 4.4). This was confirmed by also plotting concentrations against peak rainfall intensity of the closest rain gage. The high discharge value for the first runoff event in McVicker Canyon corresponded to a relatively high rainfall intensity (which led to an evacuation of the field site) and the second event had more much more modest rainfall intensities (22 vs. 8 mm/hr over 15 min). Thus, because the first event at McVicker Canyon produced the highest discharge and rainfall intensities relative to the second event, it could be that the decrease in most constituents was due to overall lower runoff and connectivity to sediment and nutrient sources. However, we outline below evidence that there was likely an overall decrease in sediment-associated constituent loading from an inferred flux-based perspective.

4.5.2. Sediment Retention Basin Flux Data Consistent with First-Flush Mechanism

Volumes of sediment in both the Leach and McVicker retention basins showed similar trends with the largest export of material into the basins occurring during the initial sampling period and dropping off dramatically during the second event (despite somewhat similar rainfall intensities) (Figure 4.5). We interpret this as evidence that the flux of sediment-associated constituents (e.g., total metals) was much greater during Event 1 compared to Event 2, supporting the idea of a first-flush event. This is also supported by work in Chapters 1 and 2 (Guilinger et al.,

2020; 2021) where it was found that erosion in source zones of the headwater networks were highest for the initial event and decreased relative to storm rainfall intensities during the season.

4.5.3. Estimates of Sediment and Nutrient Loading Across the System

A sediment budget based on debris basin and remote sensing data (Figs 4.5-6) showed significant erosion of the burned uplands and variation in sediment delivery efficiency and dynamics between the three principal catchment systems feeding Lake Elsinore (Figure 4.7). Most strikingly, it was found that Dickey Canyon (and its unnamed neighbor, lumped into the estimate) had no major depositional zones. This appears to be consistent with the size and geomorphology of these relatively small catchments (120 hectares of Dickey Canyon vs 590 hectares for McVicker) where there was relatively less unconfined valley bottom area along the principal stream of these catchments. This contrasted with McVicker basin, where there was a large amount of deposition (and sediment redistribution) that occurred in the channels. Despite the visual appearance of significant bank erosion, much of the volume of sediment appeared to be balanced out by deposition in the downstream alluvial system linking the uplands to Lake Elsinore (Fig 4.6-7).

There were major differences between Total P and Total N dynamics as inferred from our flux estimates within the system (Figure 4.8). For the most part, Total P load estimates (Fig 4.8B) tracked well with estimates of sediment volumes, with export from undammed catchments (Diceky and Unnamed Canyon) likely composing much of this. It is clear from mass balance estimates that a significant amount of Total N was not conserved across this sedimentation system. Assuming conservative transport of N from upland runoff to Lake Elsinore, the difference between delivery and standing stock of material at the time of sampling in Lake Elsinore results in a value of -2707 (+/- 40%) tons of N that is unaccounted for. If we estimate the water volume of Lake Elsinore and estimate the total suspended/dissolved standing stock of N

(4.1 mg/L of total N primarily composed of TKN, with little to no ammonia-nitrate detected, see Table 4) in the water column at time of sampling, the estimate falls between 211 to 455 tons N, with the range representing normal lake volumes up to full capacity. It is not likely that all the N in the water column is derived completely from external postfire inputs, as there already exists a large pool of internal N (Anderson, 2001). Therefore, if these values are all accurate, a significant amount of N has left the system, which we discuss mechanisms of below. Finally, contextualizing these results to longer timescales, if we normalize estimates of the total Holy Fire sediment plume to the lake surface area this results in an infill rate of 5mm. When we compare this to 20th-century estimates of sedimentation rates from a profundal zone sediment core of 12 mm/yr (Kirby et al., 2004), the emplacement of this postfire sediment pulse represents ~0.4 years of equivalent catchment area sedimentation to the lake, the implications of which we discuss below.

Table 4.1a. Water quality parameters estimated from streamflow sampling

Parameter	Units	Event #1 11/29/2018			Event #2 1/14/2019	Event #2 1/17/2019
		Adobe	McVicker Debris Basin	Horsethief Canyon	McVicker Debris Basin	Horsethief Canyon
General						
Temperature	°C	11.6	13.6	14.3	10.5	12.6
pH	SU	7.51	7.44	7.23	7.79	7.96
Specific Conductance	mS/cm	0.470	0.680	0.557	0.238	0.127
Dissolved Oxygen	mg/L	8.12	8.58	8.65	9.78	8.25
Turbidity	NTU	0.8	OR (>4,000)	49.1	945.28	1940.06
Biochemical Oxygen Demand	mg/L	ND(<5.0)	<498	55	<50	ND(<10)
Chemical Oxygen Demand	mg/L	23	10,000	500	5,900	470
Total Dissolved Solids	mg/L	300	1,500	830	290	300
Total Hardness	mg/L	180	16,000	770	930	160
Total Suspended Solids	mg/L	ND(<2)	130,000	6,900	15,000	2,200
Total Organic Carbon	mg/L	7.7	780	100	43	15
Dissolved Organic Carbon	mg/L	6.9	330	77	15	8.1
Nutrients						
Ammonia-Nitrogen	mg/L	ND(<0.048)	8.9	3.8	0.81	0.14
Kjeldahl Nitrogen	mg/L	0.25	50	28	23	8.4

Table 4.1b. Water quality parameters estimated from streamflow sampling (cont.)

Parameter	Units	Event #1 11/29/2018			Event #2 1/14/2019	Event #2 1/17/2019
		Adobe	McVicker Debris Basin	Horsethief Canyon	McVicker Debris Basin	Horsethief Canyon
Nitrate as N	mg/L	ND(<0.055)	6.2	4.7	1.8	1.2
Nitrite as N	mg/L	ND(<0.0042)	1.2	0.11	0.053	0.027
Organic Nitrogen	mg/L	0.2	41	24	22	8.3
Total Nitrogen	mg/L	(0.25)J	58	33	25	9.6
Total Phosphorus	mg/L	0.12	7.3	16	16	4.6
Ortho Phosphate	mg/L	0.083	0.052	0.25	0.12	0.37
Sulfate	mg/L	51	170	53	28	2.8
Metals						
Aluminum, Total	ug/L	ND(<74)	3,400,000	97,000	320,000	67,000
Aluminum, Dissolved	ug/L	N/A[1]	N/A[1]	N/A[1]	ND(<37)	ND(<37)
Cadmium, Total	ug/L	ND(<0.12)	680	3.8	33	1.7
Cadmium, Dissolved	ug/L	N/A[1]	N/A[1]	N/A[1]	ND(<0.12)	ND(<0.12)
Copper, Total	ug/L	1.5	7,900	120	450	24
Copper, Dissolved	ug/L	N/A[1]	N/A[1]	N/A[1]	4.4	1.8
Iron, Total	ug/L	65	3,600,000	93,000	300,000	74,000
Iron, Dissolved	ug/L	N/A[1]	N/A[1]	N/A[1]	15	15
Lead, Total	ug/L	ND(<0.2)	5,100	200	210	64
Lead, Dissolved	ug/L	N/A[1]	N/A[1]	N/A[1]	ND(<0.2)	ND(<0.2)
Manganese, Total	ug/L	17	210,000	7,000	9,300	3,300
Manganese, Dissolved	ug/L	N/A[1]	N/A[1]	N/A[1]	96	ND(<5.0)
Nickel, Total	ug/L	1.9	5,700	45	300	13
Nickel, Dissolved	ug/L	N/A[1]	N/A[1]	N/A[1]	2.4	0.6
Zinc, Total	ug/L	6.2	39,000	730	1,700	200
Zinc, Dissolved	ug/L	N/A[1]	N/A[1]	N/A[1]	1.6	2.8

1. The analytical laboratory did not analyze dissolved metals from Event #1.

Table 4.2. Lake bottom sediment characterization

Analyte	Plume-1	Plume-2	Plume-3	Beach	LE02	Units	TEL (mg/kg)	PEL (mg/kg)
Total Solids	53.8	45.3	27.4	76.7	10.3	%	-	-
Total Phosphorus	1000	430	510	180	650	mg/kg	-	-
Total Kjeldahl Nitrogen	2300	5900	6100	370	5400	mg/kg	-	-
Total Nitrogen[1]	2200[a]	6000	6200	370	5400	mg/kg	-	-
2,6-Dimethylnaphthalene	<0.037	<0.043	0.49	<0.065	<0.97	mg/kg	-	-
Naphthalene	0.045	<0.043	<0.36	<0.065	<0.97	mg/kg	0.0346	0.391
Ammonia (as N)	2.6	6.8	20	0.37	71	mg/kg	-	-
Carbon, Total Organic	2.3	2.8	3.2	0.38	6.2	%	-	-
TPH as Diesel	<9.2	<11	<18	13	<48	mg/kg	-	-
TPH as Motor Oil	<9.2	<11	<18	62	<48	mg/kg	-	-
Arsenic	13.6*	5.13	17.7**	2.31	9.32*	mg/kg	5.9	17.0
Cadmium	1.19*	0.397	1.32*	<0.13	<0.97	mg/kg	0.60	3.5
Chromium	53.5*	19.5	65.9*	8.71	29.8	mg/kg	37.3	90
Copper	39.9*	14.9	57.4*	4.78	37.6*	mg/kg	35.7	197
Lead	13.3	4.43	19.2	2.62	19.2	mg/kg	35.0	91.3
Nickel	20.8*	7.90	29.9*	3.58	17.4	mg/kg	18.0	36.0
Selenium	0.953	<0.22	1.18	<0.13	4.82	mg/kg	-	-
Silver	0.273	0.279	0.374	<0.13	<0.97	mg/kg	-	-
Zinc	141*	49.5	193*	29.3	132*	mg/kg	123	315

ND – not detected; * - exceeds TEL; ** - exceeds PEL

Table 4.3. Estimates of total N and P for sediments stored in Leach and McVicker retention basins.

Sample Location	Leach Canyon Dam (LC)	McVicker Canyon Basin (MV)
TN (mg/kg)	20,000	47,000
TP (mg/kg)	368	689

Table 4.4. Water column sampling and analysis

Analyte	Plume - 1	Plume- 2	Plume - 3	Beach	LE02	WQO (mg/L)	CTR (ug/L)
Conventional Constituents (mg/L)							
Calcium	34	37	36	38	34	-	-
Potassium	33	35	33	34	33	-	-
Magnesium	55	59	56	58	56	-	-
Sodium	540	580	550	560	560	-	-
Chloride	710	710	710	710	710	-	-
Sulfate	380	380	380	380	380	-	-
Total Kjeldahl Nitrogen	3.8	4.2	4.1	4.3	9.5[a]	-	-
Total Nitrogen[1, 2]	3.8	4.2	4.1	4.3	9.5[a]	-	-
Total Dissolved Solids	2000	2000	2000	2000	2000	2000	-
Total Suspended Solids	38	28	24	50	30	-	-
Total Phosphorus[3]	0.26	0.25	0.25	0.30	0.25	-	-
Ortho Phosphate Phosphorus	0.044	0.041	0.018	0.048	0.048	-	-
Total Organic Carbon	27	25	23	25	25	-	-
Dissolved Organic Carbon	21	21	21	20	20	-	-
Ammonia-Nitrogen	<0.044	<0.044	0.086	<0.044	<0.044	-	-
Chlorophyll a (µg/L)[4]	90	105	83	91	89	-	-
Total Metals (ug/L)							
Arsenic	19.7	15.3	17.5	18.7	18.8	-	-
Copper	2.2	1.6	1.9	2.6	1.9	-	-
Lead	1.2	<1	<1	<1	<1	-	-
Nickel	1.6	1.5	1.6	1.8	1.6	-	-
Selenium	1.9	4.0	3.3	2.9	2.3	-	-
Zinc	<5	<5	6.6	5.5	5.2	-	-
Dissolved Metals (ug/L)							
Arsenic	14.2	16.0	17.4	19.3	20.2	-	150
Chromium	<1	<1	1.0	<1	<1	-	180
Copper	1.2	1.4	1.8	1.8	1.7	-	90
Nickel	1.5	1.6	1.6	1.5	1.5	-	52
Selenium	4.7	4.3	4.5	3.3	3.1	-	5.0
Zinc	<5	<5	22.3	<5	<5	-	120

Notes:

[1] Total nitrogen = TKN +NO2 + NO3

[2] 2020 TMDL target for Total Nitrogen is 0.75 mg/L

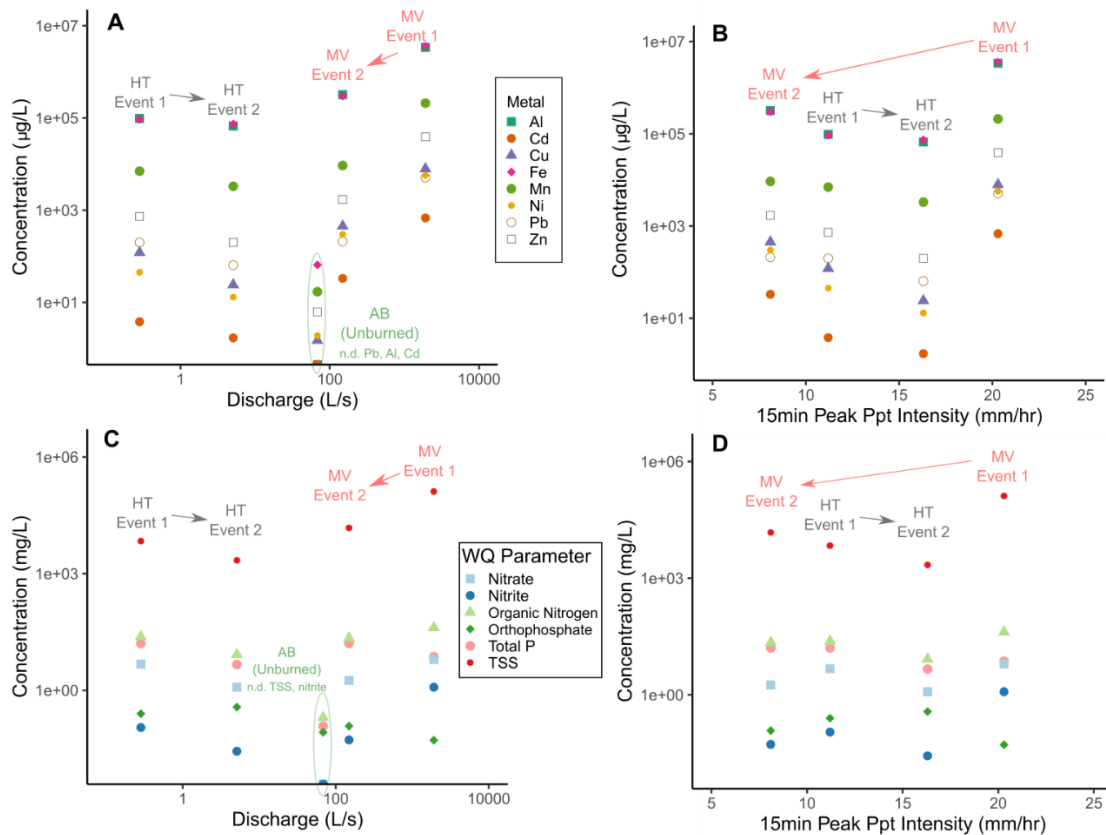[3] 2020 TMDL target for Total Phosphorous is 0.1 mg/L

Figure 4.4. Concentration of metals (A,C) and other water quality parameters (C,D) plotted against mean discharge over sampling period (compositing timescale) and inferred peak 15-min rainfall triggering intensity of the nearest rain gage. Sampling periods and locations are annotated in red (MV = McVicker) and black (HT = Horsethief) Note that the unburned control sample taken only during Event 1 (circled in green in A and C, AB = Adobe Creek) was not plotted because there was not a sufficiently close gage to estimate an associated rainfall intensity, but it is clear from the concentration-discharge relationships that the unburned control was orders of magnitude lower in all metals and non-metal constituents except orthophosphate. (note that TSS = total suspended solids and Total P = total Phosphorus and n.d. = non-detects of constituents for AB).
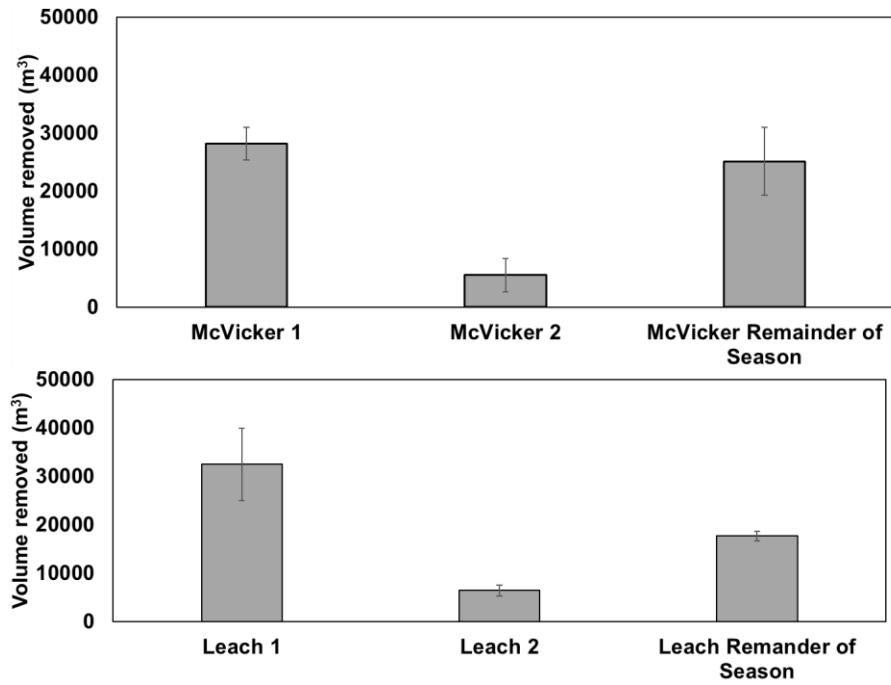
Figure 4.5. Volume of material removed attributed to sediment sampling periods of this study inferred from UAV-based SfM surface differencing and truckload counts. For example, Leach 1 refers to storm cycles associated with sampling Event 1 (Fig 3A). Uncertainty bars refer to analytical uncertainty based on standard error differences between SfM and truckload estimates.
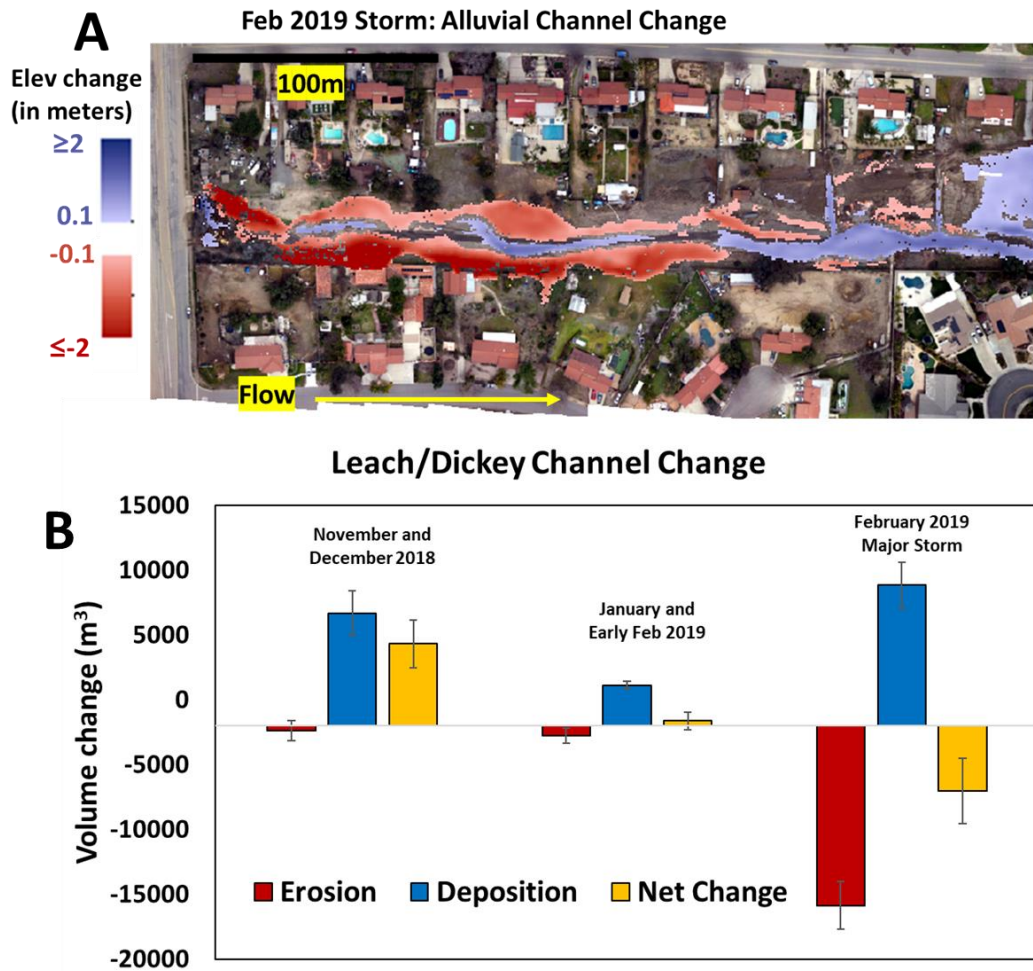
Figure 4.6. A. Example surface differencing along Leach alluvial channel (downstream of retention basin) for a large storm event during the season with high resolution UAV basemap and **B.** full volumetric mass balance for alluvial channel. Despite significant bank erosion along reaches of the Leach alluvial channel (red), cumulative net change over the full season was very minor ("minor net bank erosion" term in Figure 4.7).
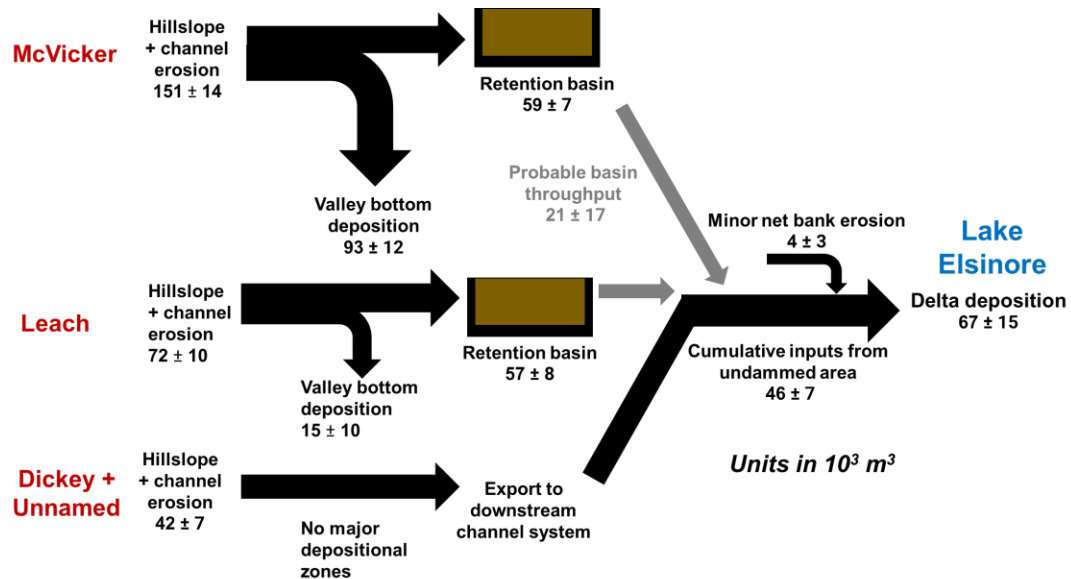
Figure 4.7. Cumulative seasonal sediment budget diagram for burned uplands and Lake Elsinore depositional system using multi-method approach of airborne and ground-based laser scanning estimates of uplands and downstream bank erosion in Leach alluvial channel (Chapters 1 and 2), retention basin yields (Table 1 of Chapter 2), and kriged isopach model of Lake Elsinore delta deposit based on boat transect samples. Note that sediment volume units are in 1000 m^3 and errors represent propagated analytical uncertainty.
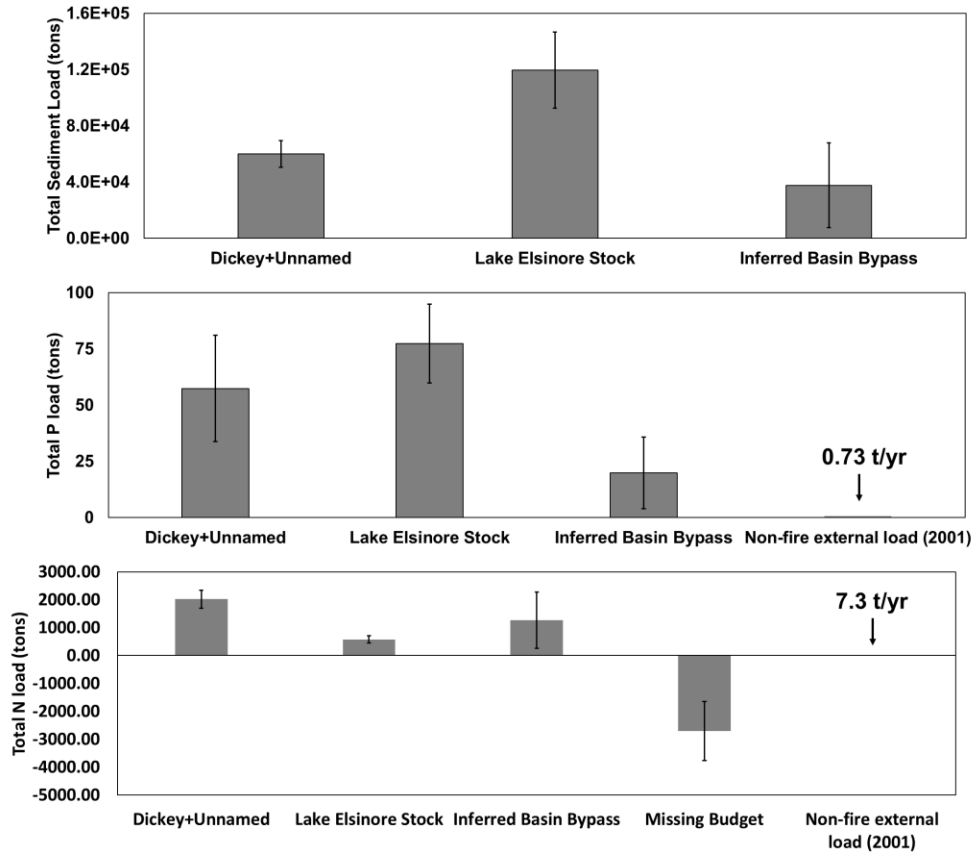
Figure 4.8. Estimated mass balances for sediment (A), total Phosphorus (B), and total Nitrogen (C). Lake Elsinore Stock refers to the standing stock of material estimated across the delta body and the other terms refer to upstream inputs. Note that in 7C, there are large differences in standing stock of nitrogen, assuming non-reactive inputs from the retention basin bypass and undammed flows which result in a large negative imbalance of nitrogen. External loading (including runoff and atmospheric sources) estimated from Anderson (2001) for WY2001 are also shown (with values indicated due to small relative scales).

4.6. Discussion

4.6.1. High magnitude loading of runoff from the Holy Fire

All of these results highlight order-of-magnitude increased responses across many water quality parameters when values are considered against baselines and controls. This study highlights the importance of wildfire in delivering significant quantities of sediment and nutrients to this lake. Considering our comparison to average sedimentation rates over longer-term (100yr) timescales,

we note that Holy Fire-associated runoff over the 5-month period delivered a tremendous amount of material to Lake Elsinore despite material being held up by debris basins. This equivalent of 0.4 years of sedimentation was sourced from a burn area that composes less than one percent of the drainage area of Lake Elsinore. This is despite winter rains being only slightly above average both in terms of rainfall totals (~120% above 30-year normal) and rainfall intensities (1-3 year return intervals, Chapters 1-2). Undoubtedly the effective delivery of postfire sediments to the lake is a reflection of the short stream length distance from burned catchments but is also illustrative of the immense geomorphic work accomplished by episodic disturbances such as wildfire (Orem & Pelletier, 2016). Other studies have found similar punctuated geomorphic disturbances with relatively small footprints, such as a study by Collins et al. (2020) who found that an extreme rainfall landslide event delivered sediments to a river system equivalent to the whole basin annual sediment load. From a nutrients perspective, it is also clear that this event was well above non-fire baselines. Compared to a previous study that estimated nutrient budgets during a relatively drier water year with no upstream wildfire influence (Anderson 2001), our external nutrient estimates were many times greater. Although if these baseline values were taken during a wetter year with larger inputs from the San Jacinto River (Anderson, 2001), the relative difference would probably not be as extreme, it nonetheless highlights the importance of wildfire-associated fluxes to lakes in semiarid climates.

4.6.2. Wildfire impacts on aquatic life and TMDL targets

It was expected that sediment-laden flows may be a major setback to TMDL targets for the lake (Stransky and Rudolph, 2019), however it was found that there were no major increases beyond TMDLs that could be solely attributed to postfire impacts. For example, total N and P mass concentrations of postfire sediments did not grossly exceed values determined by recent studies (Anderson, 2001; 2010) which showed amount of nutrients were internally recycled through

various biogeochemical processes. Though there were somewhat noticeably higher metals in postfire sediments (Table 4.2), this did not translate to concerning levels of more bioavailable dissolved metals in the water column (Table 4.4). The greatest single impact was a fish kill that occurred in winter 2019 following delivery of sediments to the lake. Stransky and Rudolph (2019) determined that the source of this fish kill was likely elevated levels of golden algae (*Prymnesium parvum*) that produced elevated cyanotoxins. Though Lake Elsinore is the site of previous eutrophication fish die-off events (Anderson, 2001), they noted that golden algae is not common to this system and must have been triggered by postfire runoff loading in Lake Elsinore. A more mechanistic understanding of this golden algal bloom event is likely warranted given its likely linkage to these runoff events, with implications for other similar systems.

4.6.3. Comparisons to other postfire water quality studies

Additional studies commensurate with the spatial scale and physiography of watersheds characterized in this study have shown high-magnitude responses in sediments and other constituents relative to baseline or adjacent baseline conditions. A study done in small mountainous catchments burned in Santa Barbara showed similar highly elevated sediment/particulate concentrations (suspended sediment concentrations 10-200 g/L) (Coombs & Melack, 2013). A study analyzing nutrient fluxes in small (136-244 ha) severely burned Eucalypt catchment in SE Australia found a 5-6 fold increase in Total P and N, with peak nutrient yields of 1.7 kg/ha of P and 15.3 kg/ha of N immediately following fire , compared to our cumulative estimates of 0.1 to 0.2 kg/ha of P and 3.4 to 11.7 kg/ha of N. Differences in Total P could be driven by lithologic differences between the sites but there is overall similar values in Total N export. We note that there was a mass balance deficit of total N in the system. Much of the N analytes both in sources and sinks (Tables 1-2) was composed of total organic nitrogen and ammonia (there was very little nitrite+nitrate detected in the water column and sediments) thus a

162

large portion could have been bound to sediments initially and could have underwent reactions such as denitrification (i.e., N_2 gas losses from the system) while in the lake (Grantz, 2011).

A growing number of studies have collected data on and highlighted the importance of postfire runoff impacts on water quality at large catchment (>10 km^2) scales (e.g., Stein et al., 2012; Rust et al., 2019; Warrick et al., 2012). A comprehensive analysis of streamflows in wildfire-impacted watersheds across the western United States (Rust et al., 2019) found noticeable impacts in up to half of wildfire-affected watersheds, with this effect particularly evident in sediment-associated constituents (P and metals). A direct comparison between the compiled results in Rust et al. (2019) and our study reveal large differences. For example, total P estimates from their database were 0.3 (+/-0.4) mg/L; much smaller than mean total P concentrations in this study (11 mg/L). This is likely a result of dilution in the much larger catchment sizes evaluated in that study (tens to hundreds of km^2) and partial burn area (~18% on average). These differences highlight the importance of understanding the scaling of postfire water quality disturbance signals taken immediately downstream of burn areas versus those integrating a larger drainage area and network further downstream. Additionally, Stein et al. (2012) highlighted the importance of ashfall on affecting downwind air quality, especially for ash-associated parameters like total metals. There is likely a tradeoff between existing infrastructure and baseline measurements at larger scales downstream of wildfire-affected uplands and signal detection of wildfire perturbations on watershed processes and water quality parameters, especially against a backdrop of many other disturbances and nonstationary hydrogeomorphic processes that act to alter sediment dynamics (e.g., Warrick et al. 2009; Gray et al., 2016; Gray, 2018). We argue that studies at multiple scales (ideally at nested scales where possible) are needed to understand these impacts and how wildfire associated signals are propagated or attenuated downstream (Wilson et al., 2020).

4.6.4. Land management implications

This study provided a unique opportunity to evaluate impacts of post-fire runoff from source-to-sink and explore the efficacy of flow and sediment control infrastructure on reducing postfire impacts. A significant amount of sediment and nutrients were held back (approximately two-thirds as measured at canyon mouth exports) by sediment retention infrastructure, which were carefully dredged in order to maintain capacity. Estimates derived in this study show that much of the sediment and Total P flux to the reservoir was likely from steep small, undammed catchments. Generalizing these findings to other fire-prone regions, it begs the question: what is the fate of other lake and reservoir systems that do not have significant sediment control infrastructure? Undoubtedly, if the full sediment pulses from the Holy Fire had entered Lake Elsinore uncontrolled, the fate of the lake from the standpoint of TMDL standards and its status recreational beneficial uses and overall ecosystem services may have been severely affected. But Southern California has a long history of dealing with fire-flood cycles and many wildland-urban interface communities have invested in significant flow and sediment control infrastructure (LADWP, 2015). This mitigation approach is well-tailored to the hazard profile of the region: the very steep (>32 degrees) and erodible nature of hillslopes (Lamb et al., 2011) and propensity for severe stand-replacing chaparral crown fire (Keeley & Fotheringham, 2001) limit the effectiveness of hillslope mitigation treatments at watershed-scales in many mountainous regions of southern California (Robichaud et al., 2010; Wohlgemuth et al., 2002). But, for other regions with overall lower slope and less severe erodibility, the costs of targeted hillslope treatments could be justified if downstream water quality risk is very high, though more work is needed to assess these across various hydroclimatic regimes (e.g., Cole et al., 2021). Given fire's increasing role in the western US, managers of water resources should plan for and not just react to wildfire and the assessment of effective mitigation strategies on a regional basis, for which there are

increasing amount of predictive tools for estimating postfire sediment and constituent delivery in the years following wildfire (e.g., WEPP, Miller et al., 2011; WATAR, Neris et al., 2021).

Additionally, we note the difficulty of obtaining datasets of this nature in which safety considerations need to be taken very seriously in very fast-moving and dynamic postfire runoff environments. Postfire science and management is generally very reactive to a wildfire hazard and needs to move at very fast speeds, which makes the presence of solid monitoring and management plans ahead of time very important (e.g., Stein and Brown, 2009). The most recent plan for the southern California region, developed in 2009 (Stein and Brown, 2009) was an effective tool for generating the study design used for stream sampling in this work. Given the significant amount of work happening in the postfire community and the increasing issue of postfire impacts, we recommend that these guidelines be updated frequently with the most up-to-date science and integrate recommendations from previous monitoring campaigns. Additionally, this study and previous chapters highlight the use of other tools beyond traditional in-stream monitoring (which may be too dangerous in postfire environments) including the use of UAVs and airborne lidar to quantify material fluxes.

We also emphasize that while this study is short-lived, it points to the potential that the Holy Fire disturbance to the hydro-sedimentological system could be protracted to many years or even decades. We note significant sediment infilling of unconfined valley bottoms (McVicker, Fig 4.7). The sediment stock provided to these higher drainage areas could be reworked by less sediment-rich flows and aggravate sediment (and sediment and/or ash-associated constituent) fluxes somewhat above pre-fire background levels during stormflow periods for potentially many years as has been found in other studies that monitor postfire alluvial deposits directly (Moody, 2017) or investigated periods of elevated suspended sediment yields in fire-affected river basins (e.g., Jumps, 2020; Warrick et al., 2012). Although there is evidence that chaparral systems

165

recover quickly to wildfire at the hillslope-scale (McGuire et al., 2019, also observed in Chapter 2), continued monitoring of Lake Elsinore and sediment retention basins could provide a longer-term perspective on the evolution of sediment yields and sediment-associated constituents, as more longer-term studies at this scale are needed to elucidate these dynamics.

4.7. Conclusions

Using a unique dataset of remote sensing, hydrosedimentological monitoring, and lake sediment sampling, we sought to understand postfire stormflow impacts on an intensively managed partial terminal lake basin. Our goals were to understand potential time-dependent patterns in water quality parameters in wildfire-affected runoff, understand broader geomorphic controls on sediment production and delivery from burned headwater catchments above the lake, and evaluate the effectiveness of sediment retention infrastructure on mitigating water resource impacts. We found that there were $10\text{-}10^4$ fold increases in water quality parameter concentrations (e.g., 78-fold increase in external P loading) in both streamflow and mass flux estimates relative to baseline conditions or unburned control samples. We also found that there was some evidence of time-dependent decreases in concentrations from the first flush event to the second event in the smallest catchment ($0.25\ \text{km}^2$). Our analysis found that much of the postfire delivery of sediments to Lake Elsinore were from smaller undammed catchments and that sediment control infrastructure held back an estimated ~50-70% of material and nutrient fluxes to the lake. This total sediment flux accounted for almost one-half of the lake's total sediment annual sediment flux despite the source area covering less than 1% of the catchment area. This case study provides a basis for understanding, planning for, and mitigating postfire impacts to other similar lake and reservoir basins that will increasingly experience wildfire disturbance in the coming century.

Chapter 4 References

Atchley, A. L., Kinoshita, A. M., Lopez, S. R., Trader, L., & Middleton, R. (2018). Simulating Surface and Subsurface Water Balance Changes Due to Burn Severity. *Vadose Zone Journal*, *17*(1), 0. https://doi.org/10.2136/vzj2018.05.0099

Barnhart, T. B., & Crosby, B. T. (2013). Comparing two methods of surface change detection on an evolving thermokarst using high-temporal-frequency terrestrial laser scanning, Selawik River, Alaska. *Remote Sensing*, *5*(6), 2813–2837. https://doi.org/10.3390/rs5062813

Benavides-Solorio, J., & MacDonald, L. H. (2001). Post-fire runoff and erosion from simulated rainfall on small plots, Colorado Front Range. *Hydrological Processes*, *15*(15), 2931–2952. https://doi.org/10.1002/hyp.383

Bodí, M. B., Martin, D. A., Balfour, V. N., Santín, C., Doerr, S. H., Pereira, P., Cerdà, A., & Mataix-Solera, J. (2014). Wildland fire ash: Production, composition and eco-hydro-geomorphic effects. *Earth-Science Reviews*, *130*, 103–127. https://doi.org/10.1016/j.earscirev.2013.12.007

Bowman, D. M. J. S., Balch, J., Artaxo, P., Bond, W. J., Cochrane, M. A., D'Antonio, C. M., Defries, R., Johnston, F. H., Keeley, J. E., Krawchuk, M. A., Kull, C. A., Mack, M., Moritz, M. A., Pyne, S., Roos, C. I., Scott, A. C., Sodhi, N. S., & Swetnam, T. W. (2011). The human dimension of fire regimes on Earth. *Journal of Biogeography*, *38*(12), 2223–2236. https://doi.org/10.1111/j.1365-2699.2011.02595.x

Brogan, D. J., Nelson, P. A., & MacDonald, L. H. (2019). Spatial and temporal patterns of sediment storage and erosion following a wildfire and extreme flood. *Earth Surface Dynamics*, *7*(2), 563–590. https://doi.org/10.5194/esurf-7-563-2019

Campos, I., Vale, C., Abrantes, N., Keizer, J. J., & Pereira, P. (2015). Effects of wildfire on mercury mobilisation in eucalypt and pine forests. *Catena*, *131*, 149–159. https://doi.org/10.1016/j.catena.2015.02.024

Cannon, S. H., Kirkham, R. M., & Parise, M. (2001). Wildfire-related debris-flow initiation processes, Storm King Mountain, Colorado. *Geomorphology*, *39*(3–4), 171–188. https://doi.org/10.1016/S0169-555X(00)00108-2

Cannon, Susan H., Boldt, E. M., Laber, J. L., Kean, J. W., & Staley, D. M. (2011). Rainfall intensity-duration thresholds for postfire debris-flow emergency-response planning. *Natural Hazards*, *59*(1), 209–236. https://doi.org/10.1007/s11069-011-9747-2

Cannon, Susan H., Gartner, J. E., Rupert, M. G., Michael, J. A., Rea, A. H., & Parrett, C. (2010). Predicting the probability and volume of postwildfire debris flows in the intermountain western United States. *Bulletin of the Geological Society of America*, *122*(1–2), 127–144. https://doi.org/10.1130/B26459.1

Cannon, Susan H., Gartner, J. E., Wilson, R. C., Bowers, J. C., & Laber, J. L. (2008). Storm rainfall conditions for floods and debris flows from recently burned areas in southwestern Colorado and southern California. *Geomorphology*, *96*(3–4), 250–269. https://doi.org/10.1016/j.geomorph.2007.03.019

Cattau, M. E., Wessman, C., Mahood, A., & Balch, J. K. (2020). Anthropogenic and lightning-started fires are becoming larger and more frequent over a longer season length in the U.S.A. *Global Ecology and Biogeography*, *29*(4), 668–681. https://doi.org/10.1111/geb.13058

Chin, A., Solverson, A. P., O'Dowd, A. P., Florsheim, J. L., Kinoshita, A. M., Nourbakhshbeidokhti, S., Sellers, S. M., Tyner, L., & Gidley, R. (2019). Interacting geomorphic and ecological response of step-pool streams after wildfire. *Bulletin of the Geological Society of America*, *131*(9–10), 1480–1500. https://doi.org/10.1130/B35049.1

Collins, B. D., Oakley, N. S., Perkins, J. P., East, A. E., Corbett, S. C., & Hatchett, B. J. (2020). Linking Mesoscale Meteorology With Extreme Landscape Response: Effects of Narrow Cold Frontal Rainbands (NCFR). *Journal of Geophysical Research: Earth Surface*, *125*(10), 1–19. https://doi.org/10.1029/2020JF005675

Coombs, J. S., & Melack, J. M. (2013). Initial impacts of a wildfire on hydrology and suspended sediment and nutrient export in California chaparral watersheds. *Hydrological Processes*, *27*(26), 3842–3851. https://doi.org/10.1002/hyp.9508

Cox, R. D., Preston, K. L., Johnson, R. F., Minnich, R. A., & Allen, E. B. (2014). Influence of landscape-scale variables on vegetation conversion to exotic annual grassland in southern California, USA. *Global Ecology and Conservation*, *2*, 190–203. https://doi.org/10.1016/j.gecco.2014.09.008

Crozier, M. J. (1999). Prediction of rainfall-triggered landslides: A test of the antecedent water status model. *Earth Surface Processes and Landforms*, *24*(9), 825–833. https://doi.org/10.1002/(SICI)1096-9837(199908)24:9<825::AID-ESP14>3.0.CO;2-M

Dibiase, R. A., Heimsath, A. M., & Whipple, K. X. (2012). Hillslope response to tectonic forcing in threshold landscapes. *Earth Surface Processes and Landforms*, *37*(8), 855–865. https://doi.org/10.1002/esp.3205

Dibiase, R. A., & Lamb, M. P. (2013). Vegetation and wildfire controls on sediment yield in bedrock landscapes. *Geophysical Research Letters*, *40*(6), 1093–1097. https://doi.org/10.1002/grl.50277

DiBiase, R. A., & Lamb, M. P. (2020). Dry sediment loading of headwater channels fuels post-wildfire debris flows in bedrock landscapes. *Geology*, *48*(2), 189–193. https://doi.org/10.1130/G46847.1

DiBiase, R. A., Whipple, K. X., Heimsath, A. M., & Ouimet, W. B. (2010). Landscape form and millennial erosion rates in the San Gabriel Mountains, CA. *Earth and Planetary Science Letters*, *289*(1–2), 134–144. https://doi.org/10.1016/j.epsl.2009.10.036

Donato, D. C., Fontaine, J. B., Campbell, J. L., Robinson, W. D., Kauffman, J. B., & Law, B. E. (2006). Post-wildfire logging hinders regeneration and increases fire risk. *Science*, *311*(5759), 352. https://doi.org/10.1126/science.1122855

Ebel, B. A., & Martin, D. A. (2017). Meta-analysis of field-saturated hydraulic conductivity recovery following wildland fire: Applications for hydrologic model parameterization and resilience assessment. *Hydrological Processes*, *31*(21), 3682–3696. https://doi.org/10.1002/hyp.11288

Ebel, B. A., & Moody, J. A. (2020). Parameter estimation for multiple post-wildfire hydrologic models. *Hydrological Processes*, *34*(21), 4049–4066. https://doi.org/10.1002/hyp.13865

Ebel, B. A., Moody, J. A., & Martin, D. A. (2012). Hydrologic conditions controlling runoff generation immediately after wildfire. *Water Resources Research*, *48*(3), 1–13. https://doi.org/10.1029/2011WR011470

Ellett, N. G., Pierce, J. L., & Glenn, N. F. (2019). Partitioned by process: Measuring post-fire debris-flow and rill erosion with Structure from Motion photogrammetry. *Earth Surface Processes and Landforms*, *44*(15), 3128–3146. https://doi.org/10.1002/esp.4728

Florsheim, J. L., Pellerin, B. a., Oh, N. H., Ohara, N., Bachand, P. a M., Bachand, S. M., Bergamaschi, B. a., Hernes, P. J., & Kavvas, M. L. (2011). From deposition to erosion: Spatial and temporal variability of sediment sources, storage, and transport in a small agricultural watershed. *Geomorphology*, *132*(3–4), 272–286. https://doi.org/10.1016/j.geomorph.2011.04.037

Florsheim, Joan L, & Gaffney, K. (2013). *Thresholds of stability in incised " Anthropocene " landscapes. October*. https://doi.org/10.1016/j.ancene.2013.10.006

Furbish, D. J., Roering, J. J., Doane, T. H., Roth, D. L., Williams, S. G. W., & Abbott, A. M. (2021). Rarefied particle motions on hillslopes - Part 1: Theory. *Earth Surface Dynamics*, *9*(3), 539–576. https://doi.org/10.5194/esurf-9-539-2021

Gabet, E. J. (2003). Sediment transport by dry ravel. *Journal of Geophysical Research: Solid Earth*, *108*(B1), 1–8. https://doi.org/10.1029/2001JB001686

Gabet, E. J., & Dunne, T. (2002). Landslides on coastal sage-scrub and grassland hillslopes in a severe El Niño winter: The effects of vegetation conversion on sediment delivery. *Bulletin of the Geological Society of America*, *114*(8), 983–990. https://doi.org/10.1130/0016-7606(2002)114<0983:LOCSSA>2.0.CO;2

Gao, P. (2013). Rill and Gully Development Processes. *Treatise on Geomorphology*, *7*, 122–131. https://doi.org/10.1016/j.physc.2009.10.149

Gartner, J. E., Cannon, S. H., & Santi, P. M. (2014). Empirical models for predicting volumes of sediment deposited by debris flows and sediment-laden floods in the transverse ranges of southern California. *Engineering Geology*, *176*, 45–56. https://doi.org/10.1016/j.enggeo.2014.04.008

Gray, A. B. (2018). The impact of persistent dynamics on suspended sediment load estimation. Geomorphology, 322, 132-147.

Gray, A. B., Pasternack, G. B., Watson, E. B., Warrick, J. A., & Goñi, M. A. (2015). Effects of antecedent hydrologic conditions, time dependence, and climate cycles on the suspended sediment load of the Salinas River, California. *Journal of Hydrology*, *525*, 632-649.

Guilinger, J. J., Gray, A. B., Barth, N. C., & Fong, B. T. (2020). The Evolution of Sediment Sources Over a Sequence of Postfire Sediment-Laden Flows Revealed Through Repeat High-Resolution Change Detection. *Journal of Geophysical Research: Earth Surface*, *125*(10), 1–23. https://doi.org/10.1029/2020JF005527

Hungr, O., McDougall, S., & Bovis, M. (2007). Entrainment of material by debris flows. *Debris-Flow Hazards and Related Phenomena*, 135–158. https://doi.org/10.1007/3-540-27129-5_7

Hunsinger, G. B., Mitra, S., Warrick, J. A., & Alexander, C. R. (2008). Oceanic loading of wildfire-derived organic compounds from a small mountainous river. *Journal of Geophysical Research: Biogeosciences*, *113*(2), 1–14. https://doi.org/10.1029/2007JG000476

Iverson, R. M. (1997). of Debris. *American Geophysical Union*, *97*, 245–296.

Jackson, M., & Roering, J. J. (2009). Post-fire geomorphic response in steep, forested landscapes: Oregon Coast Range, USA. *Quaternary Science Reviews*, *28*(11–12), 1131–1146. https://doi.org/10.1016/j.quascirev.2008.05.003

Kampf, S. K., Brogan, D. J., Schmeer, S., MacDonald, L. H., & Nelson, P. A. (2016). How do geomorphic effects of rainfall vary with storm type and spatial scale in a post-fire landscape? *Geomorphology*, *273*, 39–51. https://doi.org/10.1016/j.geomorph.2016.08.001

Kean, J. W., Staley, D. M., Lancaster, J. T., Rengers, F. K., Swanson, B. J., Coe, J. A., Hernandez, J. L., Sigman, A. J., Allstadt, K. E., & Lindsay, D. N. (2019). Inundation, flow dynamics, and damage in the 9 January 2018 Montecito debris-flow event, California, USA: Opportunities and challenges for post-wildfire risk assessment. *Geosphere*, *15*(4), 1140–1163. https://doi.org/10.1130/GES02048.1

Kean, Jason W., & Staley, D. M. (2021). Forecasting the Frequency and Magnitude of Postfire Debris Flows Across Southern California. *Earth's Future*, *9*(3). https://doi.org/10.1029/2020EF001735

Kean, Jason W., Staley, D. M., & Cannon, S. H. (2011). In situ measurements of post-fire debris flows in southern California: Comparisons of the timing and magnitude of 24 debris-flow events with rainfall and soil moisture conditions. *Journal of Geophysical Research: Earth Surface*, *116*(4), 1–21. https://doi.org/10.1029/2011JF002005

Kean, Jason W., Staley, D. M., Leeper, R. J., Schmidt, K. M., & Gartner, J. E. (2012). A low-cost method to measure the timing of postfire flash floods and debris flows relative to rainfall. *Water Resources Research*, *48*(5), 1–8. https://doi.org/10.1029/2011WR011460

Keeley, J. E., & Fotheringham, C. J. (2001). Historic fire regime in southern California shrublands. *Conservation Biology*, *15*(6), 1536–1548. https://doi.org/10.1046/j.1523-1739.2001.00097.x

Keeley, J. E., Franklin, J., & Antonio, C. D. (2011). *The Landscape Ecology of Fire | Donald McKenzie | Springer*. 193–221. https://doi.org/10.1007/978-94-007-0301-8

Keeley, J. E., & Pausas, J. G. (2019). Distinguishing disturbance from perturbations in fire-prone ecosystems. *International Journal of Wildland Fire*, *28*(4), 282–287. https://doi.org/10.1071/WF18203

Keeley, J. E., & Syphard, A. D. (2019). Twenty-first century California, USA, wildfires: fuel-dominated vs. wind-dominated fires. *Fire Ecology*, *15*(1). https://doi.org/10.1186/s42408-019-0041-0

Kinoshita, A. M., & Hogue, T. S. (2015). Increased dry season water yield in burned watersheds in Southern California. *Environmental Research Letters*, *10*(1). https://doi.org/10.1088/1748-9326/10/1/014003

Kirby, M. E., Poulsen, C. J., Lund, S. P., Patterson, W. P., Reidy, L., & Hammond, D. E. (2004). Late Holocene lake level dynamics inferred from magnetic susceptibility and stable oxygen isotope data: Lake Elsinore, southern California (USA). *Journal of Paleolimnology*, *31*(3), 275–293. https://doi.org/10.1023/B:JOPL.0000021710.39800.f6

Lague, D., Brodu, N., Leroux, J., Rennes, G., Rennes, U., & Beaulieu, C. De. (n.d.). *Accurate 3D comparison of complex topography with terrestrial laser scanner : application to the Rangitikei canyon (N-Z). February 2013*, 1–28.

Lamb, M. P., Scheingross, J. S., Amidon, W. H., Swanson, E., & Limaye, A. (2011). A model for fire-induced sediment yield by dry ravel in steep landscapes. *Journal of Geophysical Research: Earth Surface*, *116*(3), 1–13. https://doi.org/10.1029/2010JF001878

Larsen, I. J., MacDonald, L. H., Brown, E., Rough, D., Welsh, M. J., Pietraszek, J. H., Libohova, Z., de Dios Benavides-Solorio, J., & Schaffrath, K. (2009). Causes of Post-Fire Runoff and Erosion: Water Repellency, Cover, or Soil Sealing? *Soil Science Society of America Journal*, *73*(4), 1393. https://doi.org/10.2136/sssaj2007.0432

Lavé, J., & Burbank, D. W. (2004). Denudation processes and rates in the Transverse Ranges, southern California: Erosional response of a transitional landscape to external and anthropogenic forcing. *Journal of Geophysical Research*, *109*(F1), F01006. https://doi.org/10.1029/2003JF000023

Liu, T., McGuire, L. A., Wei, H., Rengers, F. K., Gupta, H., Ji, L., & Goodrich, D. C. (2021). The timing and magnitude of changes to Hortonian overland flow at the watershed scale during the post-fire recovery process. *Hydrological Processes*, *35*(5), 1–18. https://doi.org/10.1002/hyp.14208

Lu, M., Ikejiri, T., & Lu, Y. H. (2021). A synthesis of the Devonian wildfire record: Implications for paleogeography, fossil flora, and paleoclimate. *Palaeogeography, Palaeoclimatology, Palaeoecology*, *571*(February), 110321. https://doi.org/10.1016/j.palaeo.2021.110321

MacDonald, L. H., & Larsen, I. J. (2009). Runoff and Erosion from Wildfires and Roads: Effects and Mitigation, ch 9. *Land Restoration to Combat Desertification: Innovative Approaches, Quality Control and Project Evaluation , Dissmeyer 2000*, 145–167.

Martinez, D., & Anderson, M. A. (2013). Methane production and ebullition in a shallow, artificially aerated, eutrophic temperate lake (Lake Elsinore, CA). *Science of the Total Environment*, *454–455*, 457–465. https://doi.org/10.1016/j.scitotenv.2013.03.040

McCoy, S. W., Kean, J. W., Coe, J. A., Staley, D. M., Wasklewicz, T. A., & Tucker, G. E. (2010). Evolution of a natural debris flow: In situ measurements of flow dynamics, video imagery, and terrestrial laser scanning. *Geology*, *38*(8), 735–738. https://doi.org/10.1130/G30928.1

McGuire, L. A., Kean, J. W., Staley, D. M., Rengers, F. K., & Wasklewicz, T. A. (2016). Constraining the relative importance of raindrop- and flow-driven sediment transport mechanisms in postwildfire environments and implications for recovery time scales. *Journal of Geophysical Research: Earth Surface*, *121*(11), 2211–2237. https://doi.org/10.1002/2016JF003867

McGuire, L. A., Rengers, F. K., Kean, J. W., & Staley, D. M. (2017). Debris flow initiation by runoff in a recently burned basin: Is grain-by-grain sediment bulking or en masse failure to blame? *Geophysical Research Letters*, *44*(14), 7310–7319. https://doi.org/10.1002/2017GL074243

McGuire, L. A., Rengers, F. K., Kean, J. W., Staley, D. M., & Mirus, B. B. (2018). Incorporating spatially heterogeneous infiltration capacity into hydrologic models with applications for simulating post-wildfire debris flow initiation. *Hydrological Processes*, *32*(9), 1173–1187. https://doi.org/10.1002/hyp.11458

Mensing, S. A., Michaelsen, J., & Byrne, R. (1999). *142-1999-A 560-year record of Santa Ana fires reconstructed from charcoal deposited in the Santa Barbara Basin.pdf. 305*, 295–305.

Miller, M. E., MacDonald, L. H., Robichaud, P. R., & Elliot, W. J. (2011). Predicting post-fire hillslope erosion in forest lands of the western United States. *International Journal of Wildland Fire*, *20*(8), 982–999. https://doi.org/10.1071/WF09142

Minnich, R. A. (1983). Fire Mosaics in Southern California and Northern Baja California. In *Science* (Vol. 219, Issue 4590, pp. 1287–1294). https://doi.org/10.1126/science.219.4590.1287

Mirus, B. B., & Loague, K. (2013). How runoff begins (and ends): Characterizing hydrologic response at the catchment scale. *Water Resources Research*, *49*(5), 2987–3006. https://doi.org/10.1002/wrcr.20218

Montgomery, D. R., & Dietrich, W. E. (1994). A physically based model for the topographical control on shallow landsliding. *Water Resources Research*, *30*(4), 1153–1171. https://doi.org/10.1029/93WR02979

Montgomery, D. R., Schmidt, K. M., Greenberg, H. M., & Dietrich, W. E. (2000). Forest clearing and regional landsliding. *Geology*, *28*(4), 311–314. https://doi.org/10.1130/0091-7613(2000)28<311:FCARL>2.0.CO;2

Moody, J. A. (2017). Residence times and alluvial architecture of a sediment superslug in response to different flow regimes. *Geomorphology*, *294*(April), 40–57. https://doi.org/10.1016/j.geomorph.2017.04.012

Moody, J. A., & Ebel, B. A. (2014). Infiltration and runoff generation processes in fire-affected soils. *Hydrological Processes*, *28*(9), 3432–3453. https://doi.org/10.1002/hyp.9857

Moody, J. A., Ebel, B. A., Nyman, P., Martin, D. A., Stoof, C., & Mckinley, R. (2016). Relations between soil hydraulic properties and burn severity. *International Journal of Wildland Fire*, *25*(3), 279–293. https://doi.org/10.1071/WF14062

Moody, J. A., & Martin, D. A. (2001). Initial hydrologic and geomorphic response following a wildfire in the Colorado front range. *Earth Surface Processes and Landforms*, *26*(10), 1049–1070. https://doi.org/10.1002/esp.253

Moody, J. A., & Martin, D. A. (2009). Synthesis of sediment yields after wildland fire in different rainfall regimes in the western United States. *International Journal of Wildland Fire*, *18*(1), 96–115. https://doi.org/10.1071/WF07162

Moody, J. A., & Martin, R. G. (2015). Measurements of the initiation of post-wildfire runoff during rainstorms using in situ overland flow detectors. *Earth Surface Processes and Landforms*, *40*(8), 1043–1056. https://doi.org/10.1002/esp.3704

Moody, J. A., Shakesby, R. A., Robichaud, P. R., Cannon, S. H., & Martin, D. A. (2013). Current research issues related to post-wildfire runoff and erosion processes. *Earth-Science Reviews*, *122*, 10–37. https://doi.org/10.1016/j.earscirev.2013.03.004

Murphy, B. P., Czuba, J. A., & Belmont, P. (2019). Post-wildfire sediment cascades: A modeling framework linking debris flow generation and network-scale sediment routing. *Earth Surface Processes and Landforms*, *44*(11), 2126–2140. https://doi.org/10.1002/esp.4635

Murphy, B. P., Yocom, L. L., & Belmont, P. (2018). Beyond the 1984 Perspective: Narrow Focus on Modern Wildfire Trends Underestimates Future Risks to Water Security. *Earth's Future*, *6*(11), 1492–1497. https://doi.org/10.1029/2018EF001006

Murphy, S. F., McCleskey, R. B., Martin, D. A., Holloway, J. A. M., & Writer, J. H. (2020). Wildfire-driven changes in hydrology mobilize arsenic and metals from legacy mine waste. *Science of the Total Environment*, *743*, 140635. https://doi.org/10.1016/j.scitotenv.2020.140635

Neely, A. B., & DiBiase, R. A. (2020). Drainage Area, Bedrock Fracture Spacing, and Weathering Controls on Landscape-Scale Patterns in Surface Sediment Grain Size. *Journal of Geophysical Research: Earth Surface*, *125*(10), 1–22. https://doi.org/10.1029/2020JF005560

Neris, J., Santin, C., Lew, R., Robichaud, P. R., Elliot, W. J., Lewis, S. A., Sheridan, G., Rohlfs, A. M., Ollivier, Q., Oliveira, L., & Doerr, S. H. (2021). Designing tools to predict and mitigate impacts on water quality following the Australian 2019/2020 wildfires: Insights from Sydney's largest water supply catchment. *Integrated Environmental Assessment and Management*, *00*(00), 1–11. https://doi.org/10.1002/ieam.4406

Nyman, P., Sheridan, G. J., Moody, J. A., Smith, H. G., Noske, P. J., & Lane, P. N. J. (2013). Sediment availability on burned hillslopes. *Journal of Geophysical Research: Earth Surface*, *118*(4), 2451–2467. https://doi.org/10.1002/jgrf.20152

Nyman, P., Sheridan, G. J., Smith, H. G., & Lane, P. N. J. (2014). Modeling the effects of surface storage, macropore flow and water repellency on infiltration after wildfire. *Journal of Hydrology*, *513*, 301–313. https://doi.org/10.1016/j.jhydrol.2014.02.044

Odigie, K. O., & Flegal, A. R. (2011). Pyrogenic remobilization of historic industrial lead depositions. *Environmental Science and Technology*, *45*(15), 6290–6295. https://doi.org/10.1021/es200944w

Odigie, K. O., Khanis, E., Hibdon, S. A., Jana, P., Araneda, A., Urrutia, R., & Flegal, A. R. (2016). Remobilization of trace elements by forest fire in Patagonia, Chile. *Regional Environmental Change*, *16*(4), 1089–1096. https://doi.org/10.1007/s10113-015-0825-y

Orem, C. A., & Pelletier, J. D. (2015). Quantifying the time scale of elevated geomorphic response following wildfires using multi-temporal LiDAR data: An example from the Las Conchas fire, Jemez Mountains, New Mexico. *Geomorphology*, *232*, 224–238. https://doi.org/10.1016/j.geomorph.2015.01.006

Overpeck, J. T., & Udall, B. (2020). Climate change and the aridification of North America. *Proceedings of the National Academy of Sciences of the United States of America*, *117*(22), 11856–11858. https://doi.org/10.1073/pnas.2006323117

Palucis, M. C., Ulizio, T. P., & Lamb, M. P. (2021). Debris flow initiation from ravel-filled channel bed failure following wildfire in a bedrock landscape with limited sediment supply. *GSA Bulletin*, 1–18. https://doi.org/10.1130/b35822.1

Parsons, A., Robichaud, P. R., Lewis, S. A., Napper, C., & Clark, J. T. (2010). Field guide for mapping post-fire soil burn severity. *USDA Forest Service - General Technical Report RMRS-GTR*, *243*, 1–49. https://doi.org/10.2737/RMRS-GTR-243

Passalacqua, P., Belmont, P., Staley, D. M., Simley, J. D., Arrowsmith, J. R., Bode, C. A., Crosby, C., Delong, S. B., Glenn, N. F., Kelly, S. A., Lague, D., Sangireddy, H., Schaffrath, K., Tarboton, D. G., Wasklewicz, T., & Wheaton, J. M. (2015). Earth-Science Reviews Analyzing high resolution topography for advancing the understanding of mass and energy transfer through landscapes : A review. *Earth Science Reviews*, *148*, 174–193. https://doi.org/10.1016/j.earscirev.2015.05.012

Pelletier, J. D., & Orem, C. A. (2014). How do sediment yields from post-wildfire debris-laden flows depend on terrain slope, soil burn severity class, and drainage basin area? Insights from airborne-LiDAR change detection. *Earth Surface Processes and Landforms*, *39*(13), 1822–1832. https://doi.org/10.1002/esp.3570

Pierce, J. L., Meyer, G. a, & Jull, a J. T. (2004). Fire-induced erosion and millennial- scale climate change in northern ponderosa pine forests. *Nature*, *432*(November), 87–90. https://doi.org/10.1038/nature03028.Published

Pierce, J. M. G. (2008). Long-term fire history from alluvial fan sediments: the role of drought and climate. *International Journal of Wildland Fire; 2008*, *17*(1), 84–95.

Poon, P. K., & Kinoshita, A. M. (2018). Spatial and temporal evapotranspiration trends after wildfire in semi-arid landscapes. *Journal of Hydrology*, *559*, 71–83. https://doi.org/10.1016/j.jhydrol.2018.02.023

Radeloff, V. C., Helmers, D. P., Kramer, H. A., Mockrin, M. H., Alexandre, P. M., Bar-Massada, A., Butsic, V., Hawbaker, T. J., Martinuzzi, S., Syphard, A. D., & Stewart, S. I. (2018). Rapid growth of the US wildland-urban interface raises wildfire risk. *Proceedings of the National Academy of Sciences*, *115*(13), 3314–3319. https://doi.org/10.1073/pnas.1718850115

Ralph, F. M., & Dettinger, M. D. (2011). Storms, floods, and the science of atmospheric rivers. *Eos*, *92*(32), 265–266. https://doi.org/10.1029/2011EO320001

Raymond, C. A., McGuire, L. A., Youberg, A. M., Staley, D. M., & Kean, J. W. (2020). Thresholds for post-wildfire debris flows: Insights from the Pinal Fire, Arizona, USA. *Earth Surface Processes and Landforms*, *45*(6), 1349–1360. https://doi.org/10.1002/esp.4805

Reneau, S. L. (2007). *Sediment delivery after a wildfi re*. *2*, 151–154. https://doi.org/10.1130/G23288A.1

Rengers, F. K., McGuire, L. A., Kean, J. W., Staley, D. M., Dobre, M., Robichaud, P. R., & Swetnam, T. (2021). Movement of Sediment Through a Burned Landscape: Sediment Volume Observations and Model Comparisons in the San Gabriel Mountains, California, USA. *Journal of Geophysical Research: Earth Surface*, *126*(7), 1–25. https://doi.org/10.1029/2020jf006053

Rengers, Francis K., McGuire, L. A., Oakley, N. S., Kean, J. W., Staley, D. M., & Tang, H. (2020). Landslides after wildfire: initiation, magnitude, and mobility. *Landslides*, *17*(11), 2631–2641. https://doi.org/10.1007/s10346-020-01506-3

Rickson, R. J. (2010). Fire Effects on Soils and Restoration Strategies. Edited by A. Cerda and P. R. Robichaud. Enfield, NH, USA: Science Publishers (2009), pp. 589, £85.00. ISBN 978-1-57808-526-2. *Experimental Agriculture*, *46*(02), 260. https://doi.org/10.1017/S0014479709990913

Riley, K., Pierce, J., & Meyer, G. A. (2015). Vegetative and climatic controls on Holocene wildfire and erosion recorded in alluvial fans of the Middle Fork Salmon River, Idaho. *Holocene*, *25*(5), 857–871. https://doi.org/10.1177/0959683615571423

Robinne, F. N., Hallema, D. W., Bladon, K. D., Flannigan, M. D., Boisramé, G., Bréthaut, C. M., Doerr, S. H., Di Baldassarre, G., Gallagher, L. A., Hohner, A. K., Khan, S. J., Kinoshita, A. M., Mordecai, R., Nunes, J. P., Nyman, P., Santín, C., Sheridan, G., Stoof, C. R., Thompson, M. P., … Wei, Y. (2021). Scientists' warning on extreme wildfire risks to water supply. *Hydrological Processes*, *35*(5), 0–3. https://doi.org/10.1002/hyp.14086

Roth, D. L., Doane, T. H., Roering, J. J., Furbish, D. J., & Zettler-Mann, A. (2020). Particle motion on burned and vegetated hillslopes. *Proceedings of the National Academy of Sciences of the United States of America*, *117*(41), 25335–25343. https://doi.org/10.1073/pnas.1922495117

Sankey, J. B., Germino, M. J., & Glenn, N. F. (2009). Aeolian sediment transport following wildfire in sagebrush steppe. *Journal of Arid Environments*, *73*(10), 912–919. https://doi.org/10.1016/j.jaridenv.2009.03.016

Sankey, Joel B., Kreitler, J., Hawbaker, T. J., McVay, J. L., Miller, M. E., Mueller, E. R., Vaillant, N. M., Lowe, S. E., & Sankey, T. T. (2017). Climate, wildfire, and erosion ensemble foretells more sediment in western USA watersheds. *Geophysical Research Letters*, *44*(17), 8884–8892. https://doi.org/10.1002/2017GL073979

Santi, P. M., deWolfe, V. G., Higgins, J. D., Cannon, S. H., & Gartner, J. E. (2008). Sources of debris flow material in burned areas. *Geomorphology*, *96*(3–4), 310–321. https://doi.org/10.1016/j.geomorph.2007.02.022

Santi, P. M., & MacAulay, B. (2019). Rainfall intensity limitation and sediment supply independence of post-wildfire debris flows in the western U.S. *Debris-Flow Hazards Mitigation: Mechanics, Monitoring, Modeling, and Assessment - Proceedings of the 7th International Conference on Debris-Flow Hazards Mitigation*, *2005*, 539–547.

Schmidt, K. M., Roering, J. J., Stock, J. D., Dietrich, W. E., Montgomery, D. R., & Schaub, T. (2001). The variability of root cohesion as an influence on shallow landslide susceptibility in the Oregon Coast Range. *Canadian Geotechnical Journal*, *38*(5), 995–1024. https://doi.org/10.1139/cgj-38-5-995

Schmidt, Kevin M., Hanshaw, M. N., Howle, J. F., Kean, J. W., Staley, D. M., Stock, J. D., & Bawden, G. W. (2011). Hydrologic Conditions and Terrestrial Laser Scanning of Post-fire Debris Flows in the San Gabriel Mountains, CA, U.S.A. *Debris-Flow Hazards Mitigation, Mechanics, Prediction, and Assessment*, 583–593. https://doi.org/10.4408/IJEGE.2011-03.B-064

Schwanghart, W., & Kuhn, N. J. (2010). TopoToolbox: A set of Matlab functions for topographic analysis. *Environmental Modelling and Software*, *25*(6), 770–781. https://doi.org/10.1016/j.envsoft.2009.12.002

Shakesby, R. a., & Doerr, S. H. (2006). Wildfire as a hydrological and geomorphological agent. *Earth-Science Reviews*, *74*(3–4), 269–307. https://doi.org/10.1016/j.earscirev.2005.10.006

Shakesby, R. A., & Doerr, S. H. (2006). *Wildfire as a hydrological and geomorphological agent*. *74*, 269–307. https://doi.org/10.1016/j.earscirev.2005.10.006

Sklar, L. S., Riebe, C. S., Marshall, J. A., Genetti, J., Leclere, S., Lukens, C. L., & Merces, V. (2017). The problem of predicting the size distribution of sediment supplied by hillslopes to rivers. *Geomorphology*, *277*, 31–49. https://doi.org/10.1016/j.geomorph.2016.05.005

Staley, D. M., Kean, J. W., & Rengers, F. K. (2020). The recurrence interval of post-fire debris-flow generating rainfall in the southwestern United States. *Geomorphology*, *370*, 107392. https://doi.org/10.1016/j.geomorph.2020.107392

Staley, D. M., Negri, J. A., Kean, J. W., Laber, J. L., Tillery, A. C., & Youberg, A. M. (2017). Prediction of spatially explicit rainfall intensity–duration thresholds for post-fire debris-flow generation in the western United States. *Geomorphology*, *278*, 149–162. https://doi.org/10.1016/j.geomorph.2016.10.019

Staley, D. M., Wasklewicz, T. A., & Kean, J. W. (2014a). Characterizing the primary material sources and dominant erosional processes for post-fire debris-flow initiation in a headwater basin using multi-temporal terrestrial laser scanning data. *Geomorphology*, *214*, 324–338. https://doi.org/10.1016/j.geomorph.2014.02.015

Staley, D. M., Wasklewicz, T. A., & Kean, J. W. (2014b). Characterizing the primary material sources and dominant erosional processes for post-fire debris-flow initiation in a headwater basin using multi-temporal terrestrial laser scanning data. *Geomorphology*, *214*, 324–338. https://doi.org/10.1016/j.geomorph.2014.02.015

Wohlgemuth, P. M., & Hubbert, K. R. (2008). *The Effects of Fire on Soil Hydrologic Properties and Sediment Fluxes in*. 115–122.

Stein, E. D., Brown, J. S., Hogue, T. S., Burke, M. P., & Kinoshita, A. (2012). Stormwater contaminant loading following southern California wildfires. *Environmental Toxicology and Chemistry*, *31*(11), 2625–2638. https://doi.org/10.1002/etc.1994

Swain, D. L., Langenbrunner, B., Neelin, J. D., & Hall, A. (2018). Increasing precipitation volatility in twenty-first-century California. *Nature Climate Change*, *8*(5), 427–433. https://doi.org/10.1038/s41558-018-0140-y

Syphard, A. D., & Keeley, J. E. (2015). Location, timing and extent of wildfire vary by cause of ignition. *International Journal of Wildland Fire*, *24*(1), 37–47. https://doi.org/10.1071/WF14024

Syphard, A. D., & Keeley, J. E. (2020). Mapping fire regime ecoregions in California. *International Journal of Wildland Fire*, *29*(7), 595–601. https://doi.org/10.1071/WF19136

Terwilliger, V. J., & Waldron, L. J. (1991). Effects of root reinforcement on soil-slip patterns in the Transverse Ranges of southern California. *Geological Society of America Bulletin*, *103*(6), 775–785. https://doi.org/10.1130/0016-7606(1991)103<0775:EORROS>2.3.CO;2

Thomas, M. A., Rengers, F. K., Kean, J. W., McGuire, L. A., Staley, D. M., Barnhart, K. R., & Ebel, B. A. (2021). Postwildfire Soil-Hydraulic Recovery and the Persistence of Debris Flow Hazards. *Journal of Geophysical Research: Earth Surface*, *126*(6), 1–25. https://doi.org/10.1029/2021JF006091

Thompson, J. R., Spies, T. A., & Ganio, L. M. (2007). Reburn severity in managed and unmanaged vegetation in a large wildfire. *Proceedings of the National Academy of Sciences of the United States of America*, *104*(25), 10743–10748. https://doi.org/10.1073/pnas.0700229104

Warrick, J. A., Hatten, J. A., Pasternack, G. B., Gray, A. B., Goni, M. A., & Wheatcroft, R. A. (2012). The effects of wildfire on the sediment yield of a coastal California watershed. *Bulletin of the Geological Society of America*, *124*(7–8), 1130–1146. https://doi.org/10.1130/B30451.1

Warrick, Jonathan A., Melack, J. M., & Goodridge, B. M. (2015). Sediment yields from small, steep coastal watersheds of California. *Journal of Hydrology: Regional Studies*, *4*, 516–534. https://doi.org/10.1016/j.ejrh.2015.08.004

Wester, T., Wasklewicz, T., & Staley, D. (2014). Functional and structural connectivity within a recently burned drainage basin. *Geomorphology*, *206*, 362–373. https://doi.org/10.1016/j.geomorph.2013.10.011

Westerling, A. L., Hidalgo, H. G., Cayan, D. R., & Swetnam, T. W. (2006). Warming and earlier spring increase Western U.S. forest wildfire activity. *Science*, *313*(5789), 940–943. https://doi.org/10.1126/science.1128834

Wheaton, J. M., Brasington, J., Darby, S. E., & Sear, D. A. (2010). Accounting for uncertainty in DEMs from repeat topographic surveys: Improved sediment budgets. *Earth Surface Processes and Landforms*, *35*(2), 136–156. https://doi.org/10.1002/esp.1886

Wheaton, J. M., Brasington, J., Darby, S. E., Sear, D. A., Sciences, W., & Hill, O. M. (2010). *Accounting for uncertainty in DEMs from repeat topographic surveys : improved sediment budgets*. *156*(December 2009), 136–156. https://doi.org/10.1002/esp.1886

Wilder, B. A., Lancaster, J. T., Cafferata, P. H., Coe, D. B. R., Swanson, B. J., Lindsay, D. N., Short, W. R., & Kinoshita, A. M. (2021). An analytical solution for rapidly predicting post-fire peak streamflow for small watersheds in southern California. *Hydrological Processes*, *35*(1), 1–14. https://doi.org/10.1002/hyp.13976

Williams, A. P., Abatzoglou, J. T., Gershunov, A., Guzman-Morales, J., Bishop, D. A., Balch, J. K., & Lettenmaier, D. P. (2019). Observed Impacts of Anthropogenic Climate Change on Wildfire in California. *Earth's Future*, *7*(8), 892–910. https://doi.org/10.1029/2019EF001210

Williams, A. P., Abatzoglou, J. T., Gershunov, A., Guzman-Morales, J., Bishop, D. A., Balch, J. K., & Lettenmaier, D. P. (2019). Observed impacts of anthropogenic climate change on wildfire in California. *Earth's Future*, 2019EF001210. https://doi.org/10.1029/2019EF001210

Wilson, C., Kampf, S. K., Ryan, S., Covino, T., MacDonald, L. H., & Gleason, H. (2021). Connectivity of post-fire runoff and sediment from nested hillslopes and watersheds. *Hydrological Processes*, *35*(1), 1–17. https://doi.org/10.1002/hyp.13975

Chapter 5. Conclusions

5.1. Summative conclusions of dissertation

This dissertation is a source-to-sink investigation of postfire sediment cascades and their downstream impacts with an explicit aim of understanding time-varying controls on sediment supply in source areas and comparing impacts of postfire sediments and nutrients on downstream waterbodies to historical baselines. Beginning with Chapters 2 and 3, the goal of this dissertation was to evaluate the spatial scaling and temporal evolution of postfire erosion and sediment transfers in burned steep headwater catchments in southern California. Spatiotemporal scales ranged from event-scale analyses in a single headwater catchment up to an investigation of potential legacy controls of previous postfire disturbance on channel erosion across hundreds (n=1551) of small burned headwater catchments in five separate burn scars. In Chapter 3, we also evaluate easily parameterized empirical models for postfire sediment yield using sediment budget inversions from sediment trapping and change detection methods. In the case study presented in Chapter 4, the goal was to determine how postfire runoff impacted the water quality of a downstream terminal lake and contextualize these impacts against baseline nutrient and sediment loading estimates. In these studies, we utilized lidar and structure-from-motion surface change detection, hydrogeomorphic monitoring, field sampling, and publicly-available geospatial databases (e.g., MTBS, CALFRAP Fire Perimeters, USGS Geologic Maps, PRISM). By investigating temporal dependence and spatial scaling of postfire erosion and its downstream impacts, this dissertation advances a more nuanced understanding of postfire sediment cascades from source to sink. Below, we provide more detailed discussions of each chapter and contextualize their most impactful findings in the scientific literature.

Chapter 2 presents results from an intensive change detection monitoring campaign over first-year storm cycles in a 6.5 ha headwater catchment burned by the 2018 Holy Fire near Lake Elsinore, CA. In this study, we were specifically interested in understanding the relative contributions of shallower hillslope erosion (rill and interill erosion) compared to deeper channelized incision over the course of multiple storm cycles. Over the course of the wet season (~120% of average precipitation), we documented evidence of multiple smaller debris flows throughout the season. It was found that the sediment budgets of these events were dominated by deeper incisional erosion during initial storm events, which depleted channels and gullies of sediment, whereby hillslope erosion became a dominant sediment source during subsequent events. This study demonstrated the importance of declining sediment availability, particularly in gully and channel networks in steep catchments, over the course of an initial postfire wet season. Not only does this study advance a greater understanding of complex sediment source dynamics in burned headwaters within a single study, it confirms and contextualizes results from other similar studies in the region. For example, investigations of a 1-ha catchment burned in the 2009 Station Fire in the San Gabriel Mountains, CA by Schmidt et al. (2011) and subsequently by Staley et al. (2014) found a similar sequence of deeper incisional erosion in an initial storm event followed by shallow hillslope erosion dominated sourcing for a cycle of postfire debris flows. Similar findings of declining sediment supply were also replicated in a field-validated modeling study by Tang et al. (2019) in the 2016 Fish Fire in the San Gabriel Mountains. Tang et al. (2019) were able to determine that despite evidence of declining sediment supply, there was a tighter coupling between rainfall intensity-driven responses through increased runoff partitioning, which allowed multiple debris flows to be generated throughout the season. In our study, we also documented persistent debris flow hazards that extended later in the wet season despite numerous runoff-generating storms and obvious declines in sediment supply. But importantly, our study

180

demonstrated that overall sediment volumes in late-season flows likely decreased from the initial events. Results from our study and those of others highlight the particularly hazardous nature of initial larger volumes generated by the first storms immediately following fire and shifting sediment supply parameters that could be incorporated into dynamic hazard modeling frameworks. In summary, this contribution demonstrates that sediment supply can undergo rapid shifts and declines during a single wet season in steep postfire environments and that this process is an important control on the magnitude of postfire debris and sediment-laden flows.

Building off the results found in Chapter 2 of effective flushing of headwater channel networks, in Chapter 3 we used an extensive database of repeat airborne lidar both in the 2018 Holy Fire and four additional burn scars that experienced near or above average cumulative precipitation and rainfall intensities sufficient to generate postfire debris flows in their first wet season. This expanded scope allowed us to scale-up observations of channel erosion to hundreds of headwater catchments to evaluate whether previous postfire disturbance modulates contemporary postfire export, as well as the efficacy of existing models of postfire sediment export. We found evidence of declining sediment supply in headwater channel networks across the Holy Fire and that longer-term accumulations of sediment pre-dating (as opposed to dry ravel) were by far the largest channel sediment stock. In a multi-model evaluation, we found that models developed in similar climate and physiography (those of Rengers et al., 2021 in the San Gabriel Mountains and Nyman et al., 2020 in Australia) performed the best against our datasets. Across all burn scars, we found evidence of a significant dependence of contemporary postfire channel erosion on time since previous fire. When previous burn disturbances were grouped by first-year precipitation normalized to PRISM 30 year means, this relationship was significantly stronger in wetter first years, particularly with increasing catchment-averaged slope (>30 degrees). This study is among the first to show a direct legacy effect in a coupled biotic-geomorphic system (e.g., Lamb et al.,

2011; Monger et al., 2015) in the context of wildfire, by demonstrating that previous postfire disturbance can influence subsequent sediment yields in steep shrublands. Additionally, this study also demonstrates increasing hillslope-channel coupling (e.g., DiBiase et al., 2017; Michaelides et al., 2014) with increasing slope effectively partitions greater amounts of sediment into channelized domains at faster rates between fires. Results from this study are an important step towards prediction of steepland sediment supply responses to amplifications in fire regimes such as decreasing fire frequency (Westerling, 2006) due to a warming climate.

Finally in Chapter 4, we expanded our spatial scope of inquiry to the watershed scale and investigated the impacts of runoff from the Holy Fire on Lake Elsinore, a shallow terminal lake that is 303(d)-listed for excessive nutrients, organic material, and eutrophication events associated with these conditions. Through a multitude of approaches including change detection employed in previous chapters, lake and stream sampling, and sediment basin trapping estimates, we quantified stream discharge and rainfall intensity concentrations relationships for metals and nutrients (nitrogen and phosphorus) and developed a sediment and nutrient mass balance budget for the first postfire wet season. Results from postfire stream sampling showed constituent concentrations elevated 10-10,000 times above the control, as well as evidence of declining concentrations in nutrients and metals following the first-flush event. This followed the pattern of reduced sediment fluxes over the course of the season with increasing sediment source limitation found in Chapters 2 and 2, which was expected since most of investigate constituents were sediment-associated. Source-to-lake sediment budgets revealed significant retention (~50-70% of the total) of sediments in Riverside County debris basins, with most of the material constituting the postfire delta of Lake Elsinore being sourced from undammed catchment area upstream. The nutrient budget showed that phosphorus appeared to be largely conserved during delivery and sequestration in Lake Elsinore while a significant loss of nitrogen either during transport or

182

following accretion in the postfire delta, which may reflect losses due to denitrification. Most strikingly, it was found that the flux of these sediments and nutrients are well above baseline levels, with a ~80-100 fold increase in nutrients compared to a relatively dry year (Anderson, 2001) and surface area-normalized sediment delivery from the Holy Fire constituting nearly half of a year of 20th-century lake sediment accumulation (Kirby et al., 2004) despite the burn area constituting only a small fraction of the total catchment area of Lake Elsinore. Interestingly, it was found that water column estimates of dissolved (and more bioavailable) metals did not constitute a major public health or ecological risk and that postfire runoff did not result in a major setback in TMDL targets for the lake as might be expected. However, there was a moderate-sized novel golden algae bloom that led to a cold season fish kill event, the mechanisms behind which were beyond the scope of this study but warrant further investigation.

This last study contributes to a greater understanding of postfire sediment delivery to intensively managed lake systems and highlights the importance of fire as an extremely important agent of episodic high magnitude sediment and nutrient transfers in semiarid systems such as southern California (e.g., Lave and Burbank, 2004; Rengers et al., 2021; Rulli and Rosso, 2005)

Among the most important takeaways of this dissertation is the finding that there are limitations in the amount of postfire channel erosion in steep shrublands like those studied here due to sediment supply limitations (Chapters 2-3) and at shorter reburn timescales, potentially dampened hydrologic responses driven by lower burn severity due to more limited time for fuel regrowth (Chapter 3) (see Figure 5.1). As discussed above, other studies in the region have highlighted similar headwater sediment supply evolution patterns (e.g., Tang et al., 2019) and supply limitations, with analogous findings for dry ravel accumulation and delivery in the San Gabriel Mountains (e.g., Lamb et al., 2011; DiBiase and Lamb, 2020). However, there are workers who have observed that sediment availability in steep catchments is practically unlimited during the

early fire disturbance window (Cannon and Gartner, 2005; Gartner, 2004; Santi and MacAulay, 2019). Santi and MacAulay (2019) utilized an extensive dataset of observations of debris flows across the western US and provide pictures of many meters of colluvium in channels in burned watersheds where successive debris flows occurred prior to hydrologic recovery. This study included observations of thick colluvium of a repetitive debris flow-producing catchment in Utah and other studies have indicated that some settings which maintain thin colluvial fill may only produce debris flows during the first intense rainfall event postfire (Cannon and Gartner, 2005). Assuming other factors were equal, we posit that a potential difference in these supply differences could be related to fire return interval, such as longer timescales between higher-severity fires in montane forests of the interior southwestern US (>100 years, LANDFIRE, 2016). Our observations of channel supply limitations were obtained from systems that are dominated by chaparral, which experiences repeat stand-replacing fire every 30-80 years (Minnich, 1983, mean time since previous fire is 37 years in this study) with frequent observations of postfire debris flows in steep areas documented in the historical record (Cannon et al., 2008). Assuming postfire sediment transfers out of these catchments are a major long-term driver of headwater channel sediment supply (Orem and Pelletier, 2016), these sediment supply differences could be partially explained by the length of inter-fire accumulation periods both through naturally longer return intervals or areas affected by fire exclusion practices in since the 20th-century in steep forested systems across the western US (Murphy et al., 2017).

The observed differences in postfire channel sediment supply dynamics highlighted above and those found through our model comparison in Chapter 3 highlight the need for more observations of postfire erosion and debris flows outside of southern California. In addition to differences in modern fire return interval between southern California chaparral and other shrub and forest vegetation communities in the western US, there are major differences in the soils, geology,

climatology, land use history (e.g., logging, grazing), and other physiographic factors which

would likely exert a strong control on postfire runoff partitioning and sediment supply. Building

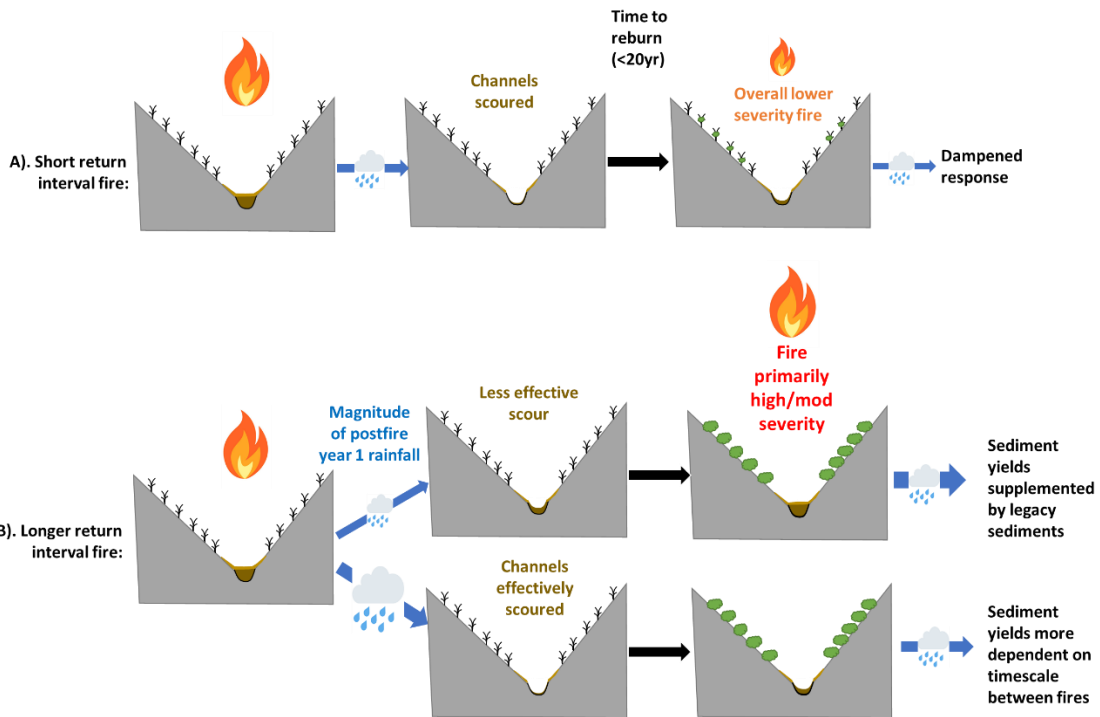off this discussion, we detail directions for future research below.

Figure 5.1. Conceptual models of reburning effects in steep chaparral terrain on postfire channel sediment yields based on findings in Chapters 3 and 4 of this dissertation. **A).** Conceptual model of fuel limitation controls on hydrogeomorphic responses from reburning at shorter return intervals. **B).** Conceptual model of sediment yield due to timescale since previous postfire disturbance and precipitation magnitude during previous postfire disturbance.

5.2. Future Directions

Indicated below is a (non-exhaustive) list of future work and additional lines of inquiry building

off research in this dissertation organized by general research theme related to postfire erosion.

5.2.1. Sediment Supply

- How do the rates of channel and colluvial hollow rejuvenation in steep headwater catchments vary during vegetation recovery periods in steep catchments and what processes are responsible for this infilling? Recommended methods to evaluate this would likely require longer-term occupation and monitoring of recovering postfire settings. Specifically, rock-tracer experiments during re-vegetation periods or across a chronosequence of recovering sites (e.g., DiBiase et al., 2017; Roth et al., 2020) or longer-term (>3 years) passive monitoring through SfM-based methods or traditional surveying of channel networks could be employed.

- How do channel sediment supplies vary across different lithologies, vegetation types, disturbance histories, climatology, and other physiographic factors? Where feasible in either burned or unburned settings, direct measurement of channel sediment supply by soil pits, soil augers, or novel methods using UAV-mounted ground-penetrating radar (e.g., UGCS DJI systems) using a study design stratified by variation in each of these variables could be very useful. Additionally, methods used in dating downstream postfire debris flow deposits of C-14 based charcoal dating (e.g., Pierce et al., 2004; Ellett et al., 2019) or other long-lasting sediment tracer isotopic systems (e.g., Cs-137, bomb effect C-14) could be employed in headwater systems to estimate dates of sediment emplacement/accumulation in debris flow-prone colluvial hollows and channels.

- Are there sediment supply limitations further upstream on hillslope soils? Few studies (e.g., Chapter 2 of this dissertation, Nyman et al., 2013; Cole et al., 2020) have evaluated this effect and more work is needed. One difficulty in evaluating this is that soil erosion is not easily detectable with airborne lidar, for which much more pre-fire data is available. However, the continued refinement of advanced UAV-based lidar and ultra-

high precision SfM could make more limited and labor-intensive ground-based laser scanning an obsolete technology in plot-to-watershed scale geomorphic change studies.

- How does type conversion from shrublands to annual grasses alter geomorphic responses? Few studies have examined the impacts of type conversion from shrublands to grasses on surface processes in southern California (e.g., Gabet and Dunne, 2002; Terwilliger et al., 1991; Rice and Foggin, 1971). These studies suggest that shallow landslides are much more common in shrub to grass converted landscapes due to loss of apparent soil cohesion due in the absence of deeper root systems. Gabet and Dunne (2002) suggest that especially voluminous shallow landsliding could occur in response to longer-duration storm events due to unstable over-thickened soils, thus type conversion dynamics could represent a serious geologic hazard. This impact is important to understand both locally for California and in the broader context of landscape evolution as vegetation shifts due to climate change could represent one of the largest impacts of climate change on surface processes in the semiarid western US (e.g., East and Sankey, 2021; Gabet and Dunne, 2002).

5.2.2. Hydrogeomorphic Recovery

- How do soil hydraulic properties vary over time? Additional longer-term (3+ years) studies of the recovery rates of soil hydraulic properties across a wider range of physiographic settings and postfire recovery conditions (i.e., drought or wet year) are needed. We note that additional work involved with the coauthors and additional collaborators is being done to evaluate this specifically for the Holy Fire over a 2-year period.

- In addition to sediment supply evolution, how do postfire recovery parameters alter postfire sediment volume exports during the initial postfire period? Additional operative

processes during the initial disturbance period (1-year postfire) evaluated in this study include changes in soil hydraulic properties, canopy interception, and hydraulic roughness, which were evaluated in other studies (2016 Fish Fire: Tang et al., 2019; McGuire et al., 2019), undoubtedly impact the hydrogeomorphic response of catchments experiencing multiple rainfall-runoff events. A promising means of understanding the relative importance of recovery processes is with hydrologic process-based modeling frameworks (e.g., McGuire et al., 2017; Tang et al., 2019; Raymond et al., 2020). Potential integration of insights from this dissertation and other similar studies into these modeling frameworks that quantify sediment supply states could include: longer-term legacy effects of previous disturbance on sediment supply (Chapter 3), declines in erodible soil stocks as a function of the cumulative seasonal precipitation forcing (inferred from Chapter 2), and constraints on soil erodibility as a function of soil type and burn severity (e.g., Nyman et al., 2013).

5.2.3. Downstream Impacts

- Specific to Chapter 4, we strongly urge a more mechanistic understanding of the postfire runoff mechanisms that were conducive to a novel golden algae bloom during the cold season in Lake Elsinore. Elevated suspended sediment and nutrient loading and shifts in towards warmer water in burned catchments create conditions that can favor toxic algae blooms in receiving freshwater systems (Bladon et al., 2014). Thus, given the detailed accounting of constituent loading (Chapter 3) and additional data on golden algal census through time in the lake (Stransky and Rudolph, 2019), further analysis and experimentation through analogs could yield useful mechanistic results on ecological impacts of postfire runoff on lake systems in semiarid settings.

- What are the longer-term effects of a postfire sediment slug on downstream fluvial and lacustrine systems? If possible, we recommend further monitoring of the sediment slug studied in Chapter 4 both in the Lake Elsinore delta and the upstream fluvial system. In the delta system, the primary concern would be the potential release of nutrients and heavy metals into more bioavailable forms as the material is potentially reworked by biotic and abiotic processes (i.e., wind, future runoff) or the lake water chemistry shifts to favor reactions towards these more bioavailable forms. In the upstream higher-order fluvial system, sediment pulses from upstream have been transiently stored, as has been found in other studies (e.g., Moody, 2017; Murphy et al., 2019). From a practical standpoint it is likely much of this material will be held up by debris basins, however, sediment excavation (and potential nutrient levels) in subsequent water years could be instructive in providing estimates on sediment yield relaxation times for a mountain range outside of the Transverse Ranges. Additionally, these estimates could be compared against estimates of upstream channel deposition to understand the amount of subsequent reworking and export of the postfire sediment slug.

Chapter 5 References

Bladon, K. D., Emelko, M. B., Silins, U., & Stone, M. (2014). Wildfire and the Future of Water Supply. *Environmental Science & Technology*, *48*, 8936–8943. Retrieved from dx.doi.org/10.1021/es500130g

Cole, R. P., Bladon, K. D., Wagenbrenner, J. W., & Coe, D. B. R. (2020). Hillslope sediment production after wildfire and post-fire forest management in northern California. *Hydrological Processes*, *34*(26), 5242–5259. https://doi.org/10.1002/hyp.13932

DiBiase, R., Lamb, M. P., & Vam. (2017). Journal of Geophysical Research : Planets, 295–328. https://doi.org/10.1002/2016JE005195.Received

DiBiase, R. A., & Lamb, M. P. (2020). Dry sediment loading of headwater channels fuels post-wildfire debris flows in bedrock landscapes. *Geology*, *48*(2), 189–193. https://doi.org/10.1130/G46847.1

East, A. E., & Sankey, J. B. (2020). Geomorphic and Sedimentary Effects of Modern Climate Change: Current and Anticipated Future Conditions in the Western United States. *Reviews of Geophysics*, *58*(4). https://doi.org/10.1029/2019RG000692

Ellett, N. G., Pierce, J. L., & Glenn, N. F. (2019). Partitioned by process: Measuring post-fire debris-flow and rill erosion with Structure from Motion photogrammetry. *Earth Surface Processes and Landforms*, *44*(15), 3128–3146. https://doi.org/10.1002/esp.4728

Gabet, E. J., & Dunne, T. (2002). Landslides on coastal sage-scrub and grassland hillslopes in a severe El Niño winter: The effects of vegetation conversion on sediment delivery. *Bulletin of the Geological Society of America*, *114*(8), 983–990. https://doi.org/10.1130/0016-7606(2002)114<0983:LOCSSA>2.0.CO;2

Keeley, J. E., & Syphard, A. D. (2019). Twenty-first century California, USA, wildfires: fuel-dominated vs. wind-dominated fires. *Fire Ecology*, *15*(1). https://doi.org/10.1186/s42408-019-0041-0

Kirby, M. E., Poulsen, C. J., Lund, S. P., Patterson, W. P., Reidy, L., & Hammond, D. E. (2004). Late Holocene lake level dynamics inferred from magnetic susceptibility and stable oxygen isotope data: Lake Elsinore, southern California (USA). *Journal of Paleolimnology*, *31*(3), 275–293. https://doi.org/10.1023/B:JOPL.0000021710.39800.f6

Lamb, M. P., Scheingross, J. S., Amidon, W. H., Swanson, E., & Limaye, A. (2011). A model for fire-induced sediment yield by dry ravel in steep landscapes. *Journal of Geophysical Research: Earth Surface*, *116*(3), 1–13. https://doi.org/10.1029/2010JF001878

McGuire, L. A., Rengers, F. K., Kean, J. W., Staley, D. M., & Mirus, B. B. (2018). Incorporating spatially heterogeneous infiltration capacity into hydrologic models with applications for simulating post-wildfire debris flow initiation. *Hydrological Processes*, *32*(9), 1173–1187. https://doi.org/10.1002/hyp.11458

Moody, J. A. (2017). Residence times and alluvial architecture of a sediment superslug in response to different flow regimes. *Geomorphology*, *294*(April), 40–57. https://doi.org/10.1016/j.geomorph.2017.04.012

Murphy, B. P., Yocom, L. L., & Belmont, P. (2018). Beyond the 1984 Perspective: Narrow Focus on Modern Wildfire Trends Underestimates Future Risks to Water Security. *Earth's Future*, *6*(11), 1492–1497. https://doi.org/10.1029/2018EF001006

Murphy, B. P., Czuba, J. A., & Belmont, P. (2019). Post-wildfire sediment cascades: A modeling framework linking debris flow generation and network-scale sediment routing. *Earth Surface Processes and Landforms*, *44*(11), 2126–2140. https://doi.org/10.1002/esp.4635

Nyman, P., Sheridan, G. J., Moody, J. A., Smith, H. G., Noske, P. J., & Lane, P. N. J. (2013). Sediment availability on burned hillslopes. *Journal of Geophysical Research: Earth Surface*, *118*(4), 2451–2467. https://doi.org/10.1002/jgrf.20152

Nyman, P., Box, W. A. C., Stout, J. C., Sheridan, G. J., Keesstra, S. D., Lane, P. N. J., & Langhans, C. (2020). Debris-flow-dominated sediment transport through a channel network after wildfire. *Earth Surface Processes and Landforms*, *45*(5), 1155–1167. https://doi.org/10.1002/esp.4785

Pierce, J. L., Meyer, G. a, & Jull, a J. T. (2004). Fire-induced erosion and millennial- scale climate change in northern ponderosa pine forests. *Nature*, *432*(November), 87–90. https://doi.org/10.1038/nature03028.Published

Raymond, C. A., McGuire, L. A., Youberg, A. M., Staley, D. M., & Kean, J. W. (2020). Thresholds for post-wildfire debris flows: Insights from the Pinal Fire, Arizona, USA. *Earth Surface Processes and Landforms*, *45*(6), 1349–1360. https://doi.org/10.1002/esp.4805

Rengers, F. K., McGuire, L. A., Kean, J. W., Staley, D. M., Dobre, M., Robichaud, P. R., & Swetnam, T. (2021). Movement of Sediment Through a Burned Landscape: Sediment Volume Observations and Model Comparisons in the San Gabriel Mountains, California, USA. *Journal of Geophysical Research: Earth Surface*, *126*(7), 1–25. https://doi.org/10.1029/2020jf006053

Robinne, F. N., Hallema, D. W., Bladon, K. D., Flannigan, M. D., Boisramé, G., Bréthaut, C. M., et al. (2021). Scientists' warning on extreme wildfire risks to water supply. *Hydrological Processes*, *35*(5), 0–3. https://doi.org/10.1002/hyp.14086

Roth, D. L., Doane, T. H., Roering, J. J., Furbish, D. J., & Zettler-Mann, A. (2020). Particle motion on burned and vegetated hillslopes. *Proceedings of the National Academy of Sciences of the United States of America*, *117*(41), 25335–25343. https://doi.org/10.1073/pnas.1922495117

Santi, P. M., & MacAulay, B. (2019). Rainfall intensity limitation and sediment supply independence of post-wildfire debris flows in the western U.S. *Debris-Flow Hazards Mitigation: Mechanics, Monitoring, Modeling, and Assessment - Proceedings of the 7th International Conference on Debris-Flow Hazards Mitigation*, (2005), 539–547.

Schmidt, K. M., Hanshaw, M. N., Howle, J. F., Kean, J. W., Staley, D. M., Stock, J. D., & Bawdeng, W. (2011). Hydrologic conditions and terrestrial laser scanning of post-firedebris flows in the San Gabriel Mountains, CA, U.S.A. *International Conference on Debris-Flow Hazards Mitigation: Mechanics, Prediction, and Assessment, Proceedings*, 583–593. https://doi.org/10.4408/IJEGE.2011-03.B-064

Staley, D. M., Wasklewicz, T. A., & Kean, J. W. (2014). Characterizing the primary material sources and dominant erosional processes for post-fire debris-flow initiation in a headwater basin using multi-temporal terrestrial laser scanning data. *Geomorphology*, *214*, 324–338. https://doi.org/10.1016/j.geomorph.2014.02.015

Tang, H., McGuire, L. A., Rengers, F. K., Kean, J. W., Staley, D. M., & Smith, J. B. (2019a). Evolution of Debris-Flow Initiation Mechanisms and Sediment Sources During a Sequence of Postwildfire Rainstorms. *Journal of Geophysical Research: Earth Surface*, *124*(6), 1572–1595. https://doi.org/10.1029/2018JF004837

Tang, H., McGuire, L. A., Rengers, F. K., Kean, J. W., Staley, D. M., & Smith, J. B. (2019b). Evolution of Debris-Flow Initiation Mechanisms and Sediment Sources During a Sequence of Postwildfire Rainstorms. *Journal of Geophysical Research: Earth Surface*, 1572–1595. https://doi.org/10.1029/2018JF004837

Terwilliger, V. J., & Waldron, L. J. (1991). Effects of root reinforcement on soil-slip patterns in the Transverse Ranges of southern California. *Geological Society of America Bulletin*, *103*(6), 775–785. https://doi.org/10.1130/0016-7606(1991)103<0775:EORROS>2.3.CO;2

Westerling, A. L., Hidalgo, H. G., Cayan, D. R., & Swetnam, T. W. (2006). Warming and earlier spring increase Western U.S. forest wildfire activity. *Science*, *313*(5789), 940–943. https://doi.org/10.1126/science.1128834

Appendix A. Supplement for Chapter 2. The evolution of sediment sources over a sequence of post-fire sediment-laden flows revealed through repeat high-resolution change detection

James J. Guilinger[1], Andrew B. Gray[1], Nicolas C. Barth[2], Brandon T. Fong[1]

[1]Department of Environmental Sciences, University of California-Riverside, Riverside, CA 92521

[2]Department of Earth and Planetary Sciences, University of California-Riverside, Riverside, CA 92521
Contents of this file

Remote Sensing Data Processing

Following Rengers et al (2016), cumulative distributions of point density in the masked areas were generated for potential grid sizes (2.5-15 cm) and a 7.5 cm DEM was found to adequately represent the surface of interest, avoid interpolating significant areas (~5%), and had a median point density of 34 (Figure A3). These DEMs were constructed from the thinned ground-classified points using a triangular irregular network from meshes produced on the octree-filtered cloud in

CloudCompare. No TIN-based gridding was performed on the DEMs for the third epoch (DoD_3) because of these larger areas of occlusion. Instead, differencing was performed using 2.5D volumes directly on the January and April clouds in CloudCompare and any changes visually determined to be residual leftover vegetation points following iterative treatments with CANUPO were discarded using a distance filter. Identical uncertainty analysis to DoD_1 and DoD_2 were performed on this gridded difference product.

As is common practice with TLS, a Fuzzy Inference System (Wheaton et al., 2010) for uncertainty was developed using point density, slope, and roughness. For example, a pixel that

contained low slope (< 22 degrees), moderate roughness (0.02 - 0.1 m), and medium point density

(7-24 pts) would be assigned an uncertainty value close to 0.004 m. For simplicity, we used the

single 0.03 m error term for our SfM surveys within the headwater TLS zone (Figure A6, Table

S2) and 0.04 m error term for SfM outside of the TLS region (Table S3). The error term of each

pixel was propagated according to Equation 2 (Lane, 2003; Wheaton et al. 2010) to estimate

change detection uncertainty (σ_{DoD}) on a pixel-by-pixel basis. To determine our spatially

distributed limit of detection (LOD), we evaluated change using Equation 3 according to the 95%

confidence interval of σ_{DoD} where any value of $t_{0.95} > 1.96$ was kept as a thresholded DoD and all

other values were ignored.

The instrumental accuracy of the laser scanner used (Riegl VZ-400) is 0.005m for the

scanning ranges we used (Riegl, 2014), therefore a well-calibrated LOD should not be less than

this value. In the best possible case scenario of low slope, low roughness, and high point density

our FIS would assign a $\sigma_{DoD} = 0.0028$. This best-case σ_{DoD} can be convolved as $LOD_{0.95} = \sigma_{DoD} *$

1.96, with $LOD_{0.95} = 0.0055$, greater than instrumental uncertainty. It should be noted that in our

landscape this model yielded a conservative error surface with $LOD_{0.95}$ values ranging from

0.006-0.02m, matching error distributions from many other studies that used similar techniques

(DeLong et al., 2018; Nourbakhshbeidokhti et al., 2019; Rengers et al., 2016; Staley et al., 2014).

Figure A1. Picture of fixed cylindrical monument fixed on ½" rebar used as tiepoints used in this study. Laptop on the right shown for scale.

A. 25 October 2018
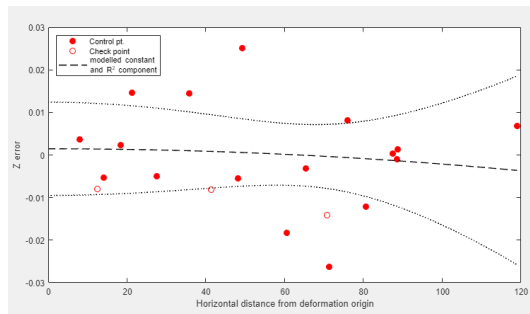
B. 18 December 2018
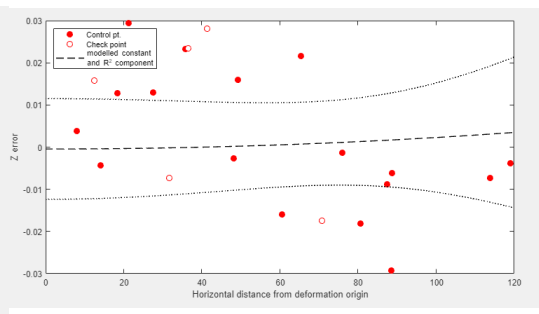
C. 30 January 2019
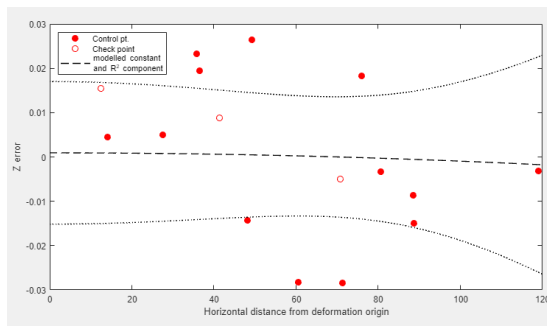
D. 4 March 2019
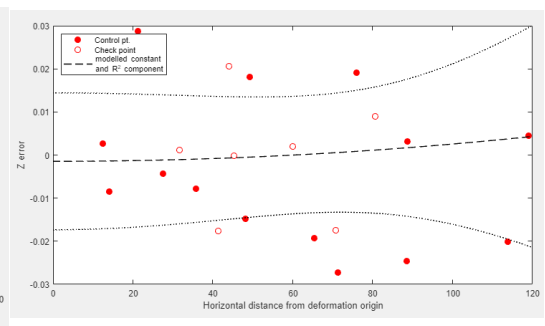
Figure A2. Plot of elevation residuals for control and check tie points for all four UAV-SfM surveys using Doming Analysis Toolbox of James et al. (2020). Deformation center refers to the centroid of tie points. There is no statistically significant trend in z-error, implying there is no detectable distortion within the point cloud models.
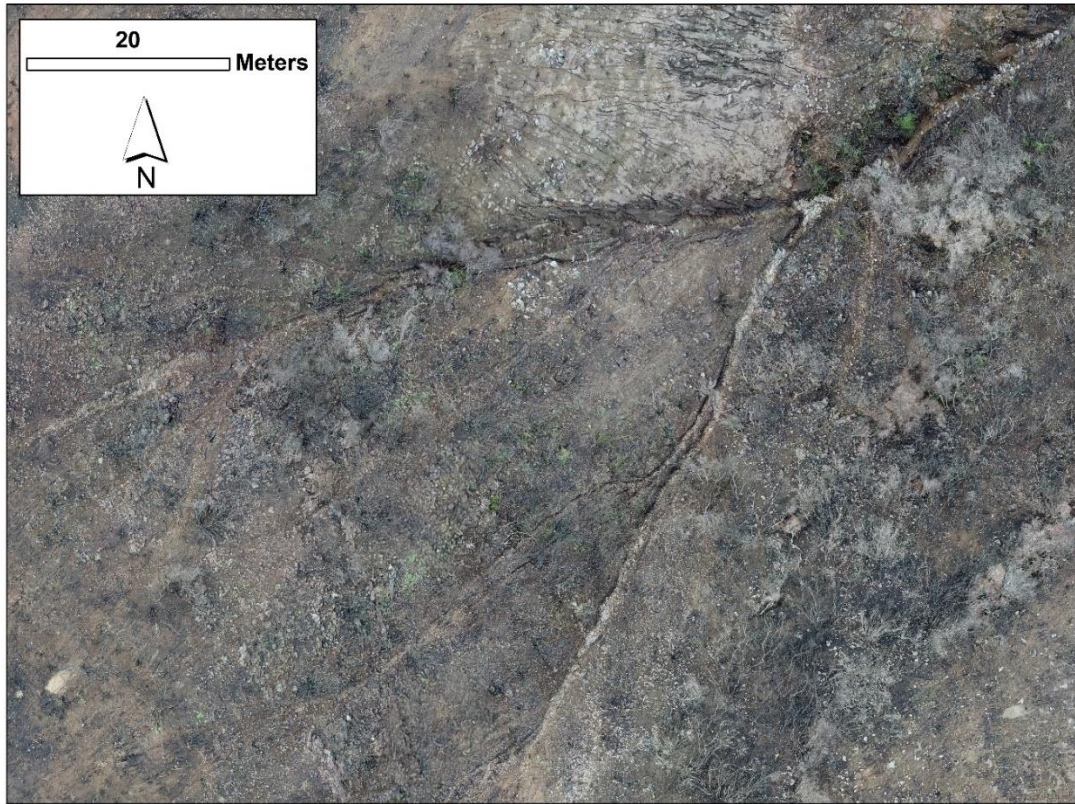
Figure A3. Orthoimagery of zero-order catchment with shaded relief taken on 4 March 2019 following all major runoff events showing revegetation of the field site. Note that vegetation regrowth increased greatly between this photo and the equivalent TLS scans taken later in April 2019.
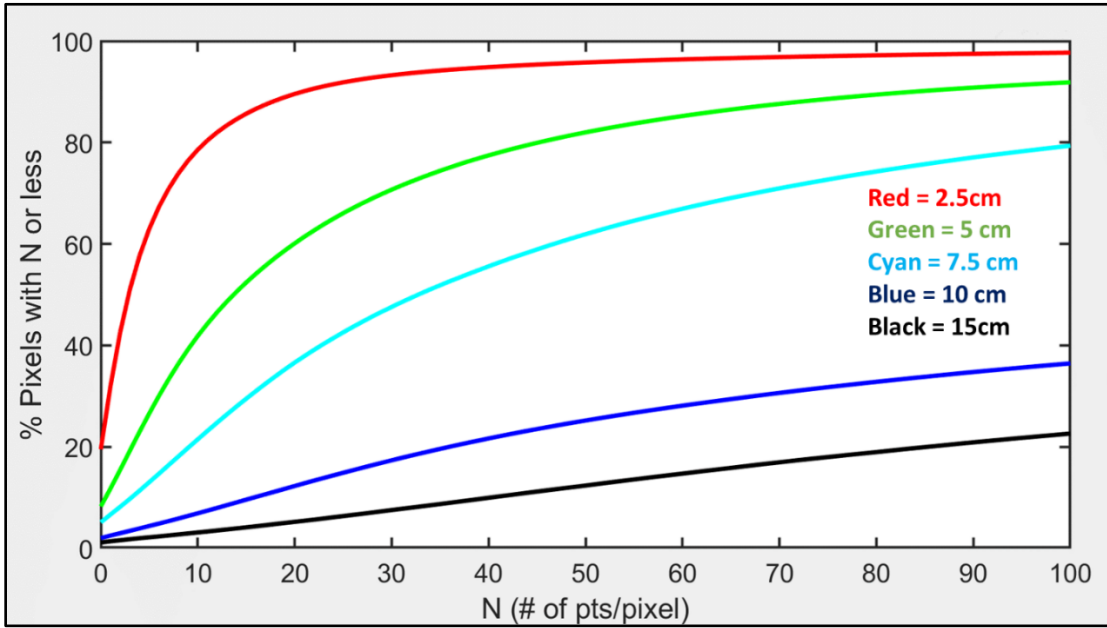
Figure A4. Cumulative distribution of points per pixel created for different resolutions of digital terrain model. Points only include ground and low debris points used for rendering the digital terrain model. We selected a grid size of 7.5 cm as a tradeoff between resolution and sufficient point density which had cell sizes with more adequate coverage and was not too coarse as to inadequately represent small-scale erosional features such as rills.
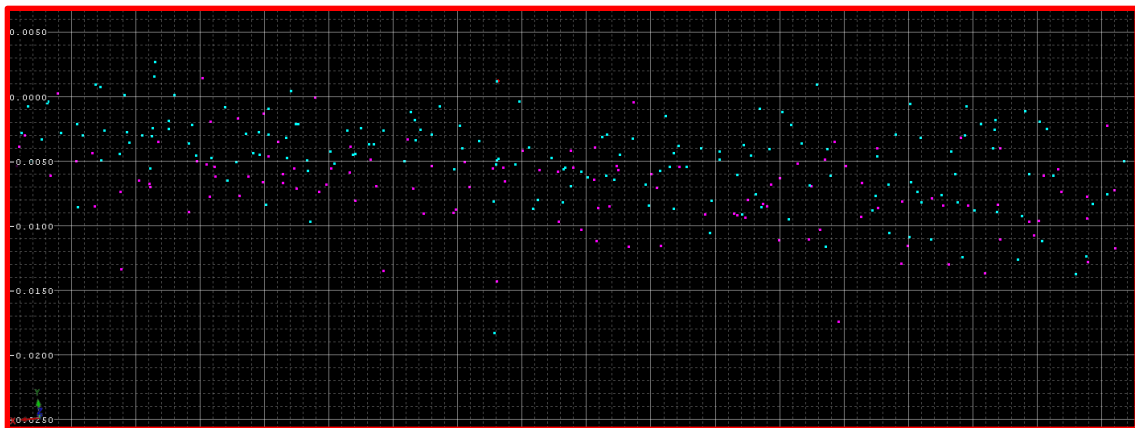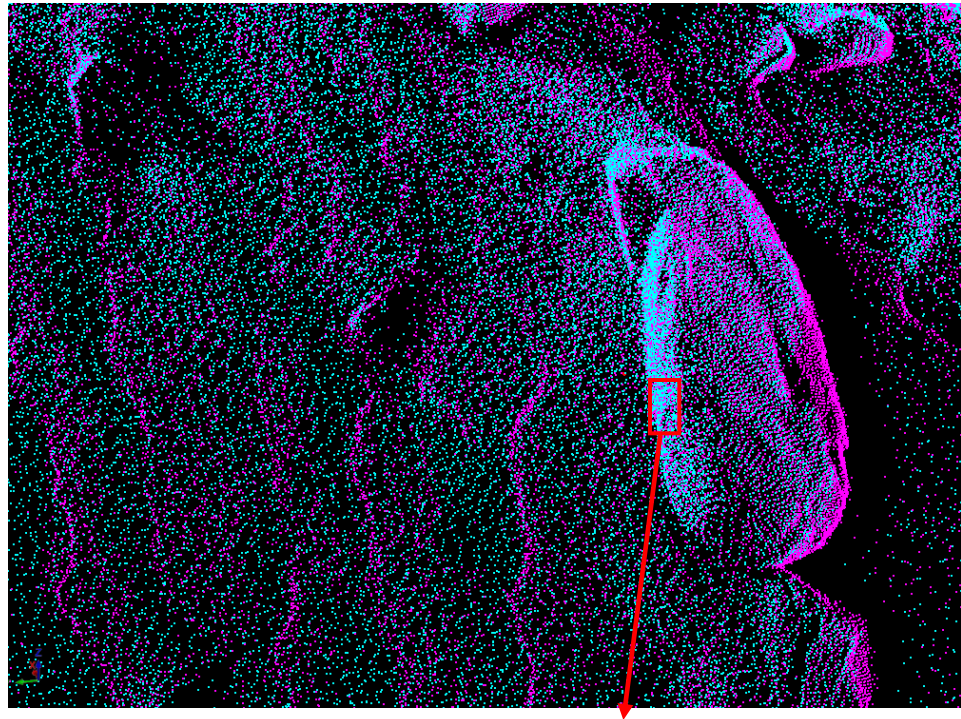
Figure A5. Point clouds of scans for DoD_1 (teal points = 25 October 2018 and magenta points = 18 December 2018) showing alignment on stable boulder surface. Lower inset (red box) shows zoomed in surfaces with grid spacing of 0.005 m.
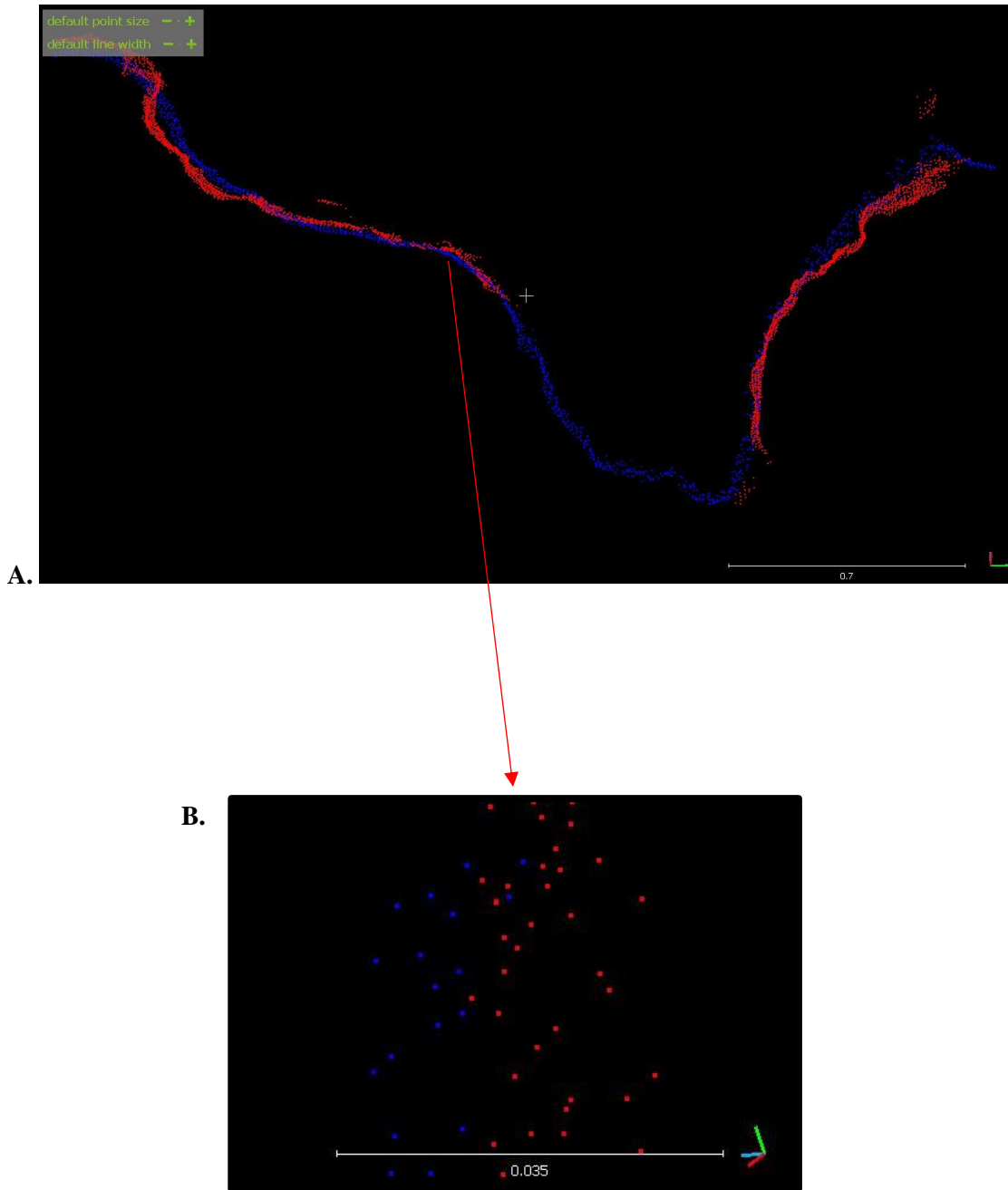
Figure A6. A. Figure showing cross-section of coalignment of TLS point cloud (red) with SfM point cloud (blue) for a section of eroded gully where TLS is occluded (19 December 2018). Scale bar is in meters. **B.** Zoomed in figure showing alignment of TLS cloud (red) and SfM cloud (blue). Scale bar in meters.
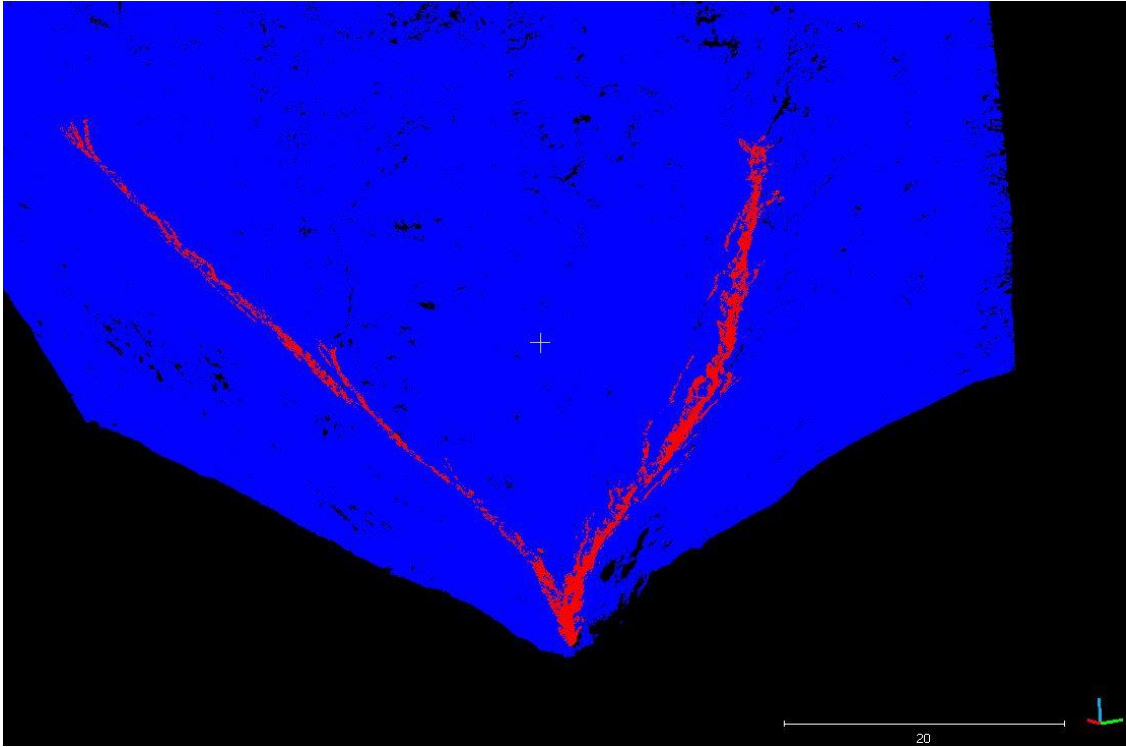
Figure A7. A. Figure showing oblique view of TLS cloud (blue) and coaligned SfM cloud (red) used to fill in occluded gully area. Scale bar is in meters.
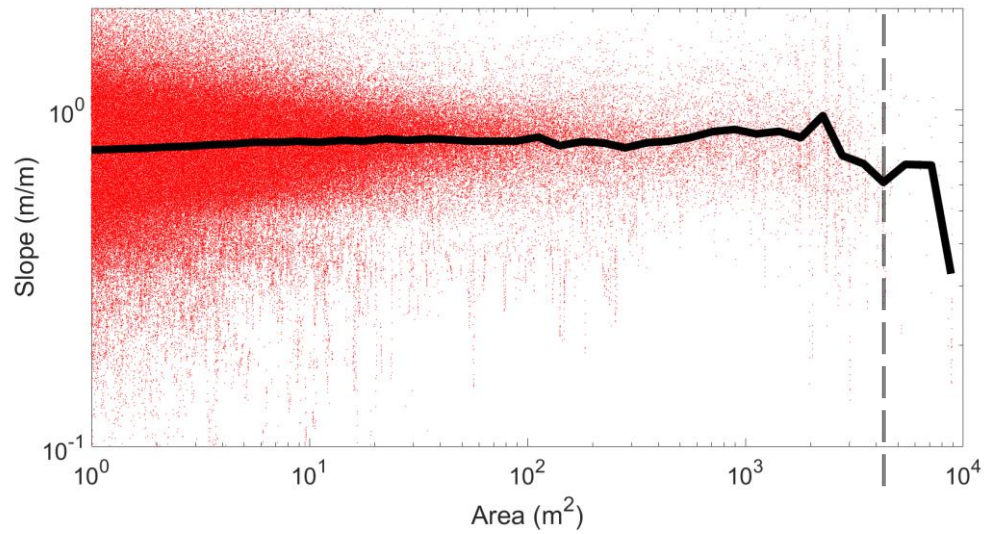
Figure A8. Slope-area plot with all pixels (red points) and logarithmically-binned averages (black line) from an SfM-derived DEM from 18 December 2018. The dashed line shows the fluvial roll-over (where logarithmic binning shows slope decay) occurs at a drainage area of ~0.2 ha.

Figure A9. Small-scale runoff plot designed after Moody and Ebel (2012a) used to measure point-scale runoff production (location in Figure 1B). Runoff from the bounded plot is routed through a PVC pipe into a re-purposed tipping bucket gage with a mesh screen to prevent highly concentrated sediment from compromising tipping bucket measurements.

Figure A10. Photograph taken on 04 January 2019 along mainstem channel of Leach Canyon showing fresh coarse angular deposits indicative of debris flow transport overlying older (pre-Holy Fire) debris flow and alluvial deposits (center left) and channel scoured to bedrock (center right).

Figure A11. Top: Orthoimagery showing ravel and rockfall loaded channel at outlet of TLS scan zone (0.95 ha watershed). Bottom: orthoimagery following the initial storms that mobilized coarse rockfall (orange arrow), ravel, and colluvial fill. Note this photo is coeval and collocated with picture in Figure 2.8C (of main text).
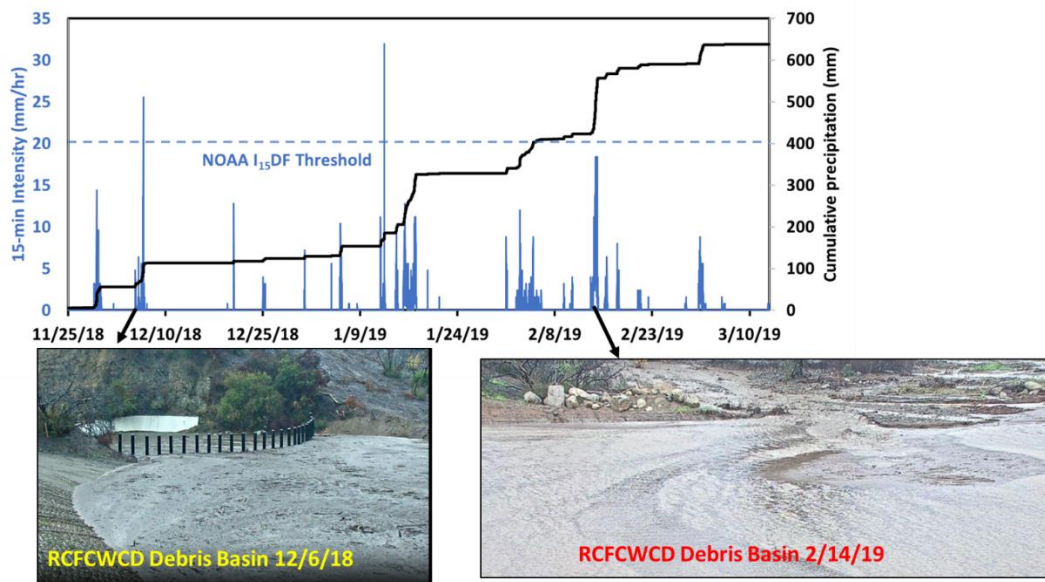
Figure A12. Figure showing debris basin time-lapse stills (with permission from Riverside County) at the mouth of Leach Canyon during peak outflow for two storms which had evidence of debris flows generated in the uplands. These flows were muddy and water-dominated. (NOAA/NWS debris flow warning threshold shown).

Supplemental Tables

Table A1. Empirical error estimates using the root mean square error of sixteen conservative surfaces that were not used in alignment. These ranges were used to define the ranges of uncertainty in our fuzzy inference model in the Geomorphic Change Detection software.

	DoD1	DoD2	DoD3
Mean RMSE(x) (mm)	3.2	2.4	2.5
Mean RMSE(y) (mm)	3.1	1.2	2.4
Mean RMSE(z) (mm)	2.1	1.8	1.8
Mean RMSE(xyz) (mm)	5.1	3.5	4.0
Range RMSE(xyz) (mm)	1.8 - 10.6	1.2 - 6.6	1.40 - 7.0
Mean Systematic Error(xyz) (mm)	0.6	0.2	0.3

Table S2. Empirical root mean square error estimates using the root mean square error of comparisons between SfM clouds to TLS clouds in the same survey sequence following iterative closest point registration of SfM to TLS in the zero-order catchment. Note that because we had sufficient coverage of colluvial hollows prior to gully formation, we did not use SfM in the zero-order catchment.

	December 2019	January 2019	March/April 2019
RMSE_X (mm)	16.8	14.8	10.0
RMSE_Y (mm)	18.4	15.6	10.0
RMSE_Z (mm)	17.9	16.3	13.1
RMSE_XYZ (mm)	**30.7**	**27.0**	**19.3**
Mean Systematic Error_XYZ (mm)	-1.3	1.8	0.9

Table A3. Empirical root mean square error estimates for SfM outside of the TLS scan zone using the root mean square error of comparisons between SfM clouds on boundaries of the channel where surface change due to erosion/deposition was minor and likely well below limits of detection of SfM.

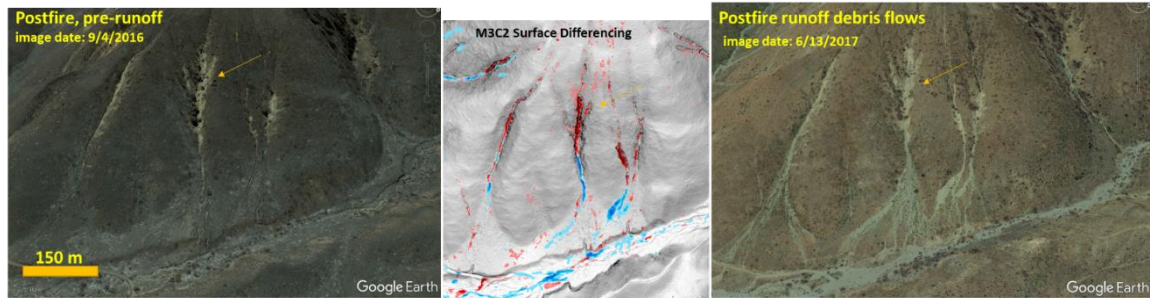|	DoD1 (Oct-Dec)	DoD2 (Dec-Jan)	DoD3 (Jan-Mar)
RMSE_X (mm)	22.1	16.3	16.9
RMSE_Y (mm)	22.2	16.0	16.7
RMSE_Z (mm)	24.8	20.4	20.9
RMSE_XYZ (mm)	**40.0**	**30.7**	**31.7**
Mean Systematic Error_XYZ (mm)	2.5	0.6	0.4

Appendix B. Supplemental for Chapter 3

Figure B1. A. Google Earth before and after google earth imagery in Blue Cut burn scar (burned Aug 2016) showing probable postfire debris flows with corresponding surface difference maps shown (in middle). Red pixels correspond to erosion and blue pixels correspond to deposition. Image acquisition dates indicated and orange arrow shows severely-eroding (>2m) headwater channel.
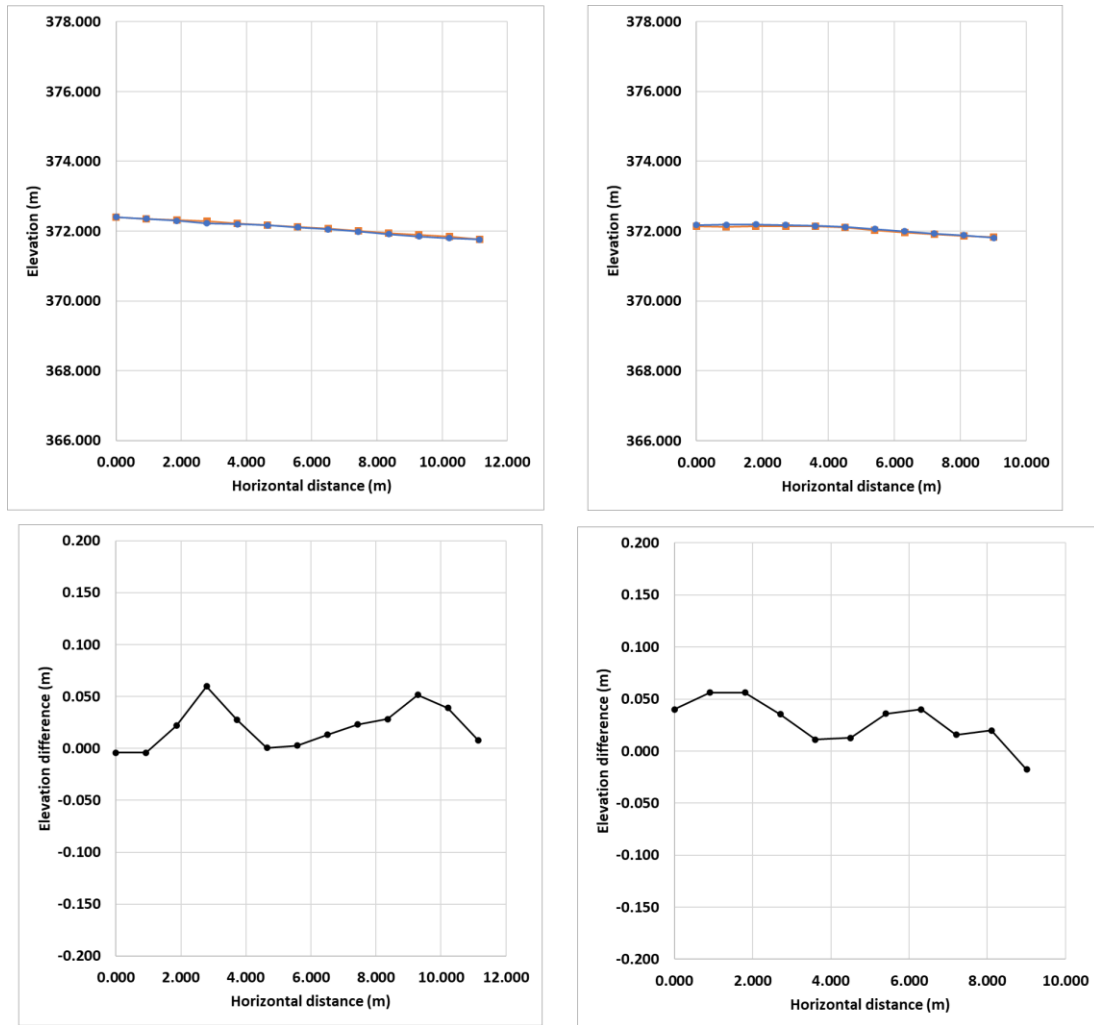
Figure B2. Repeat airborne lidar alignment checks for San Gabriel Complex (Fish and Reservoir Fires) showing vertical accuracy of primarily stable surfaces.
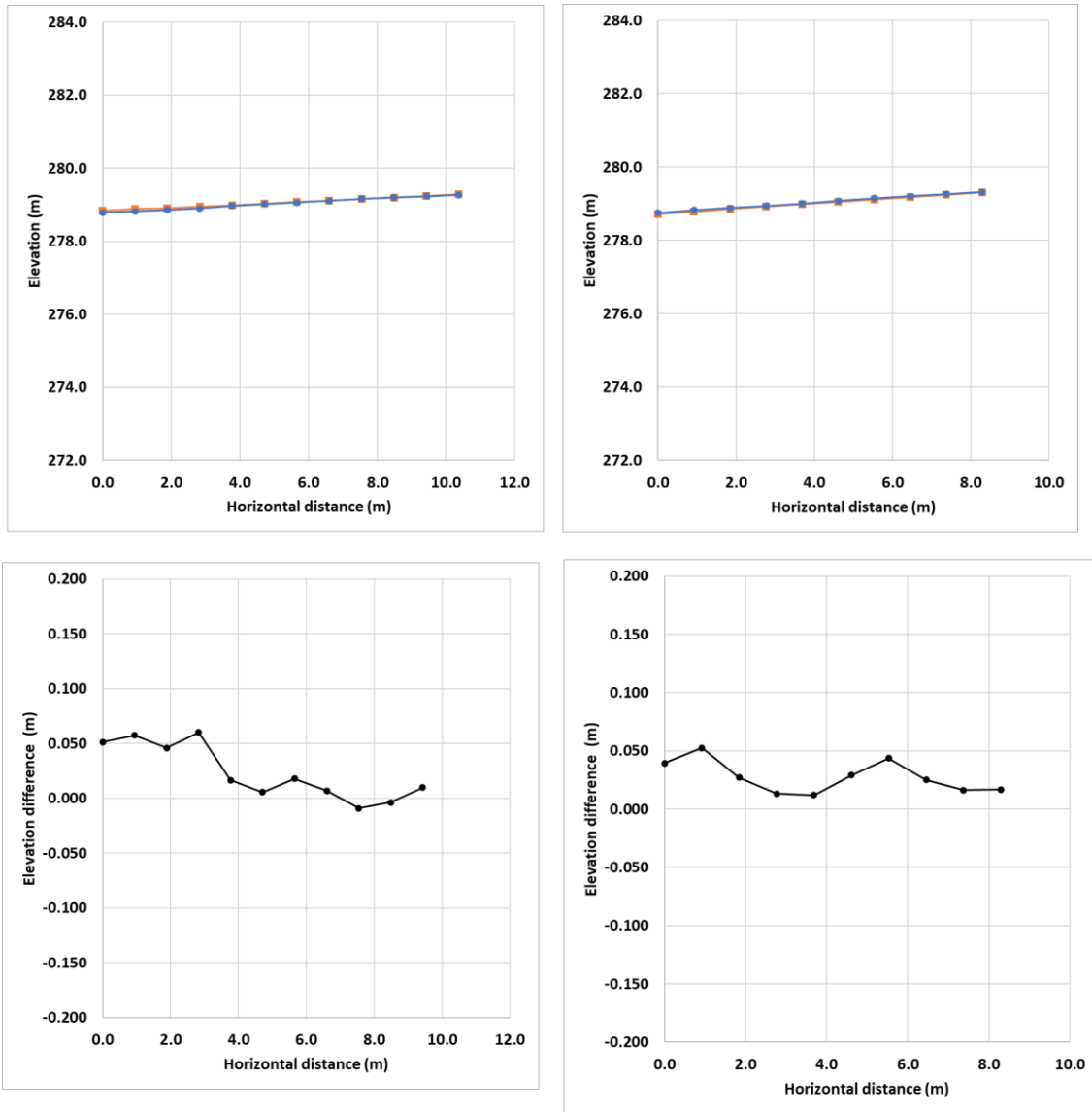
Figure B3. Repeat airborne lidar alignment checks for Woolsey Fire showing vertical accuracy of primarily stable surfaces.
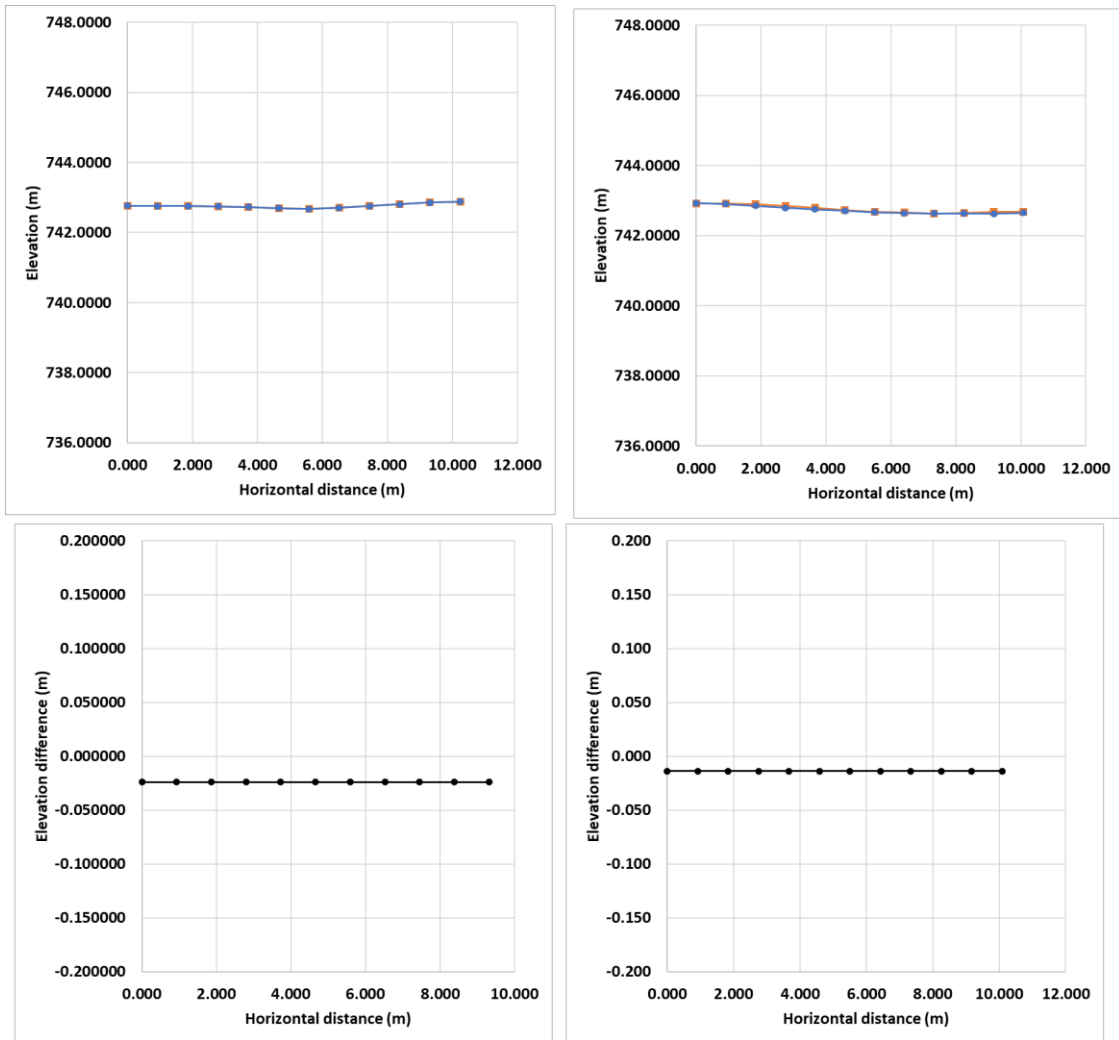
Figure B4. Repeat airborne lidar alignment checks for Blue Cut Fire showing vertical accuracy of primarily stable surfaces.
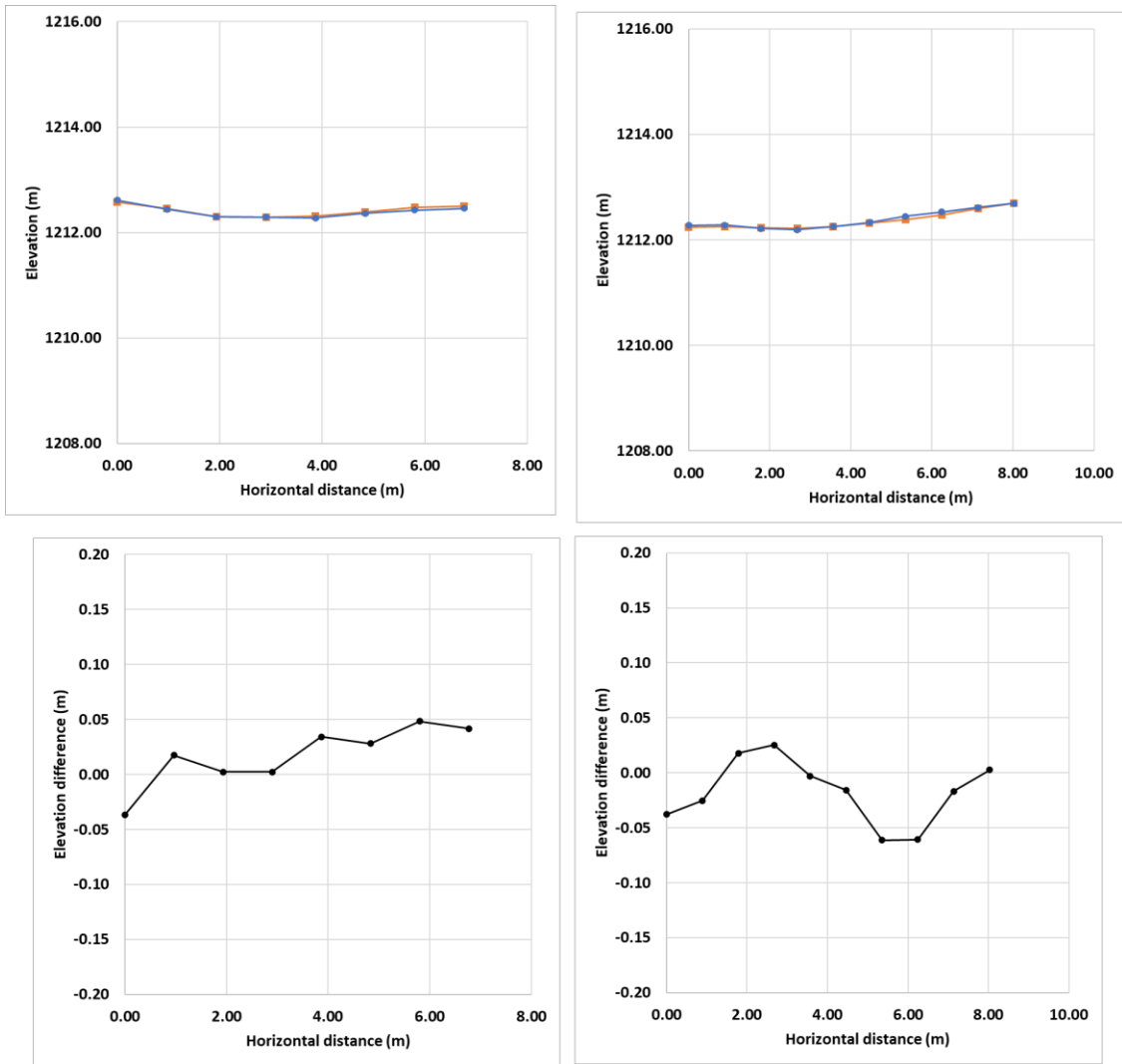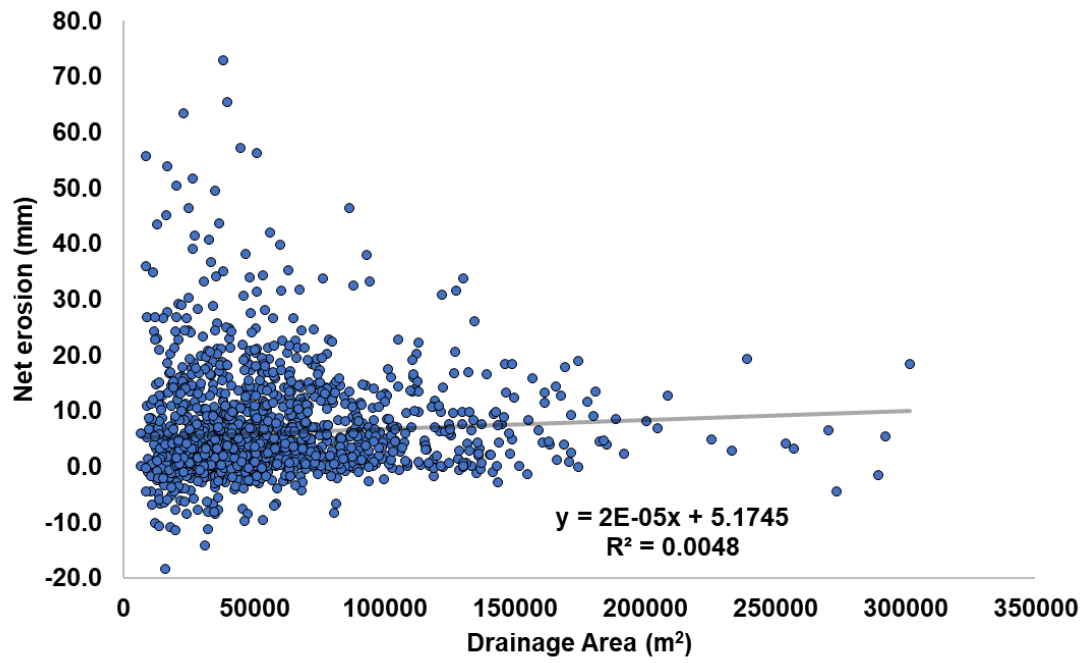
Figure B5. Repeat airborne lidar alignment checks for Holy Fire showing vertical accuracy of primarily stable surfaces.

Figure B6. Plot showing area-normalized net erosion plotted against drainage area for all five fires. Note the significant but very weak trend between drainage area and erosion and the decreasing variability with increasing drainage are.
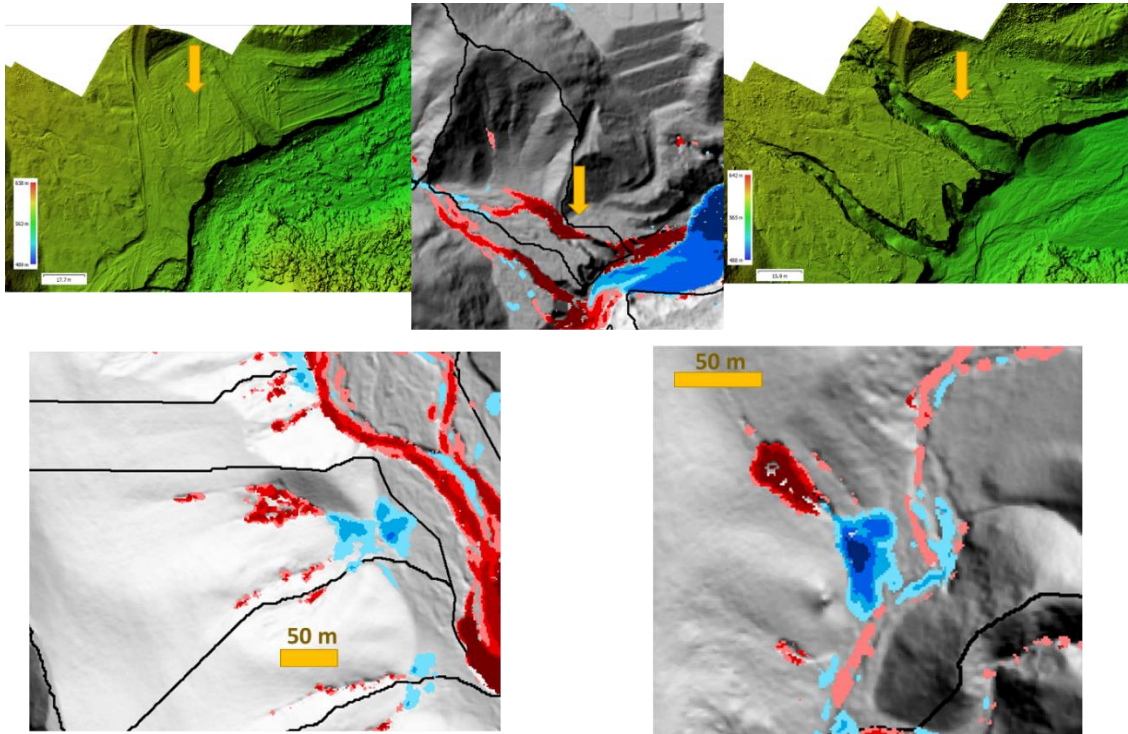
Fig B7. Top: Example of a small watershed selected as an outlier that was subject to intense incision and landsliding (>7m surface decrease in very red patch of M3C2 map in middle, indicated by yellow arrow) during a long-duration storm on Feb 14 2019 (ALS Epoch 4). This incision and landsliding into thick alluvium was likely exacerbated by an exposed pit wall face exposed center right in UAV-derived shadd relief maps that was the subject of gravel mining operations (since abandoned). **Bottom:** Other examples of M3C2 map of non-anthropogenically aggravated shallow landslides in other catchments as well (red = erosion, blue = deposition).
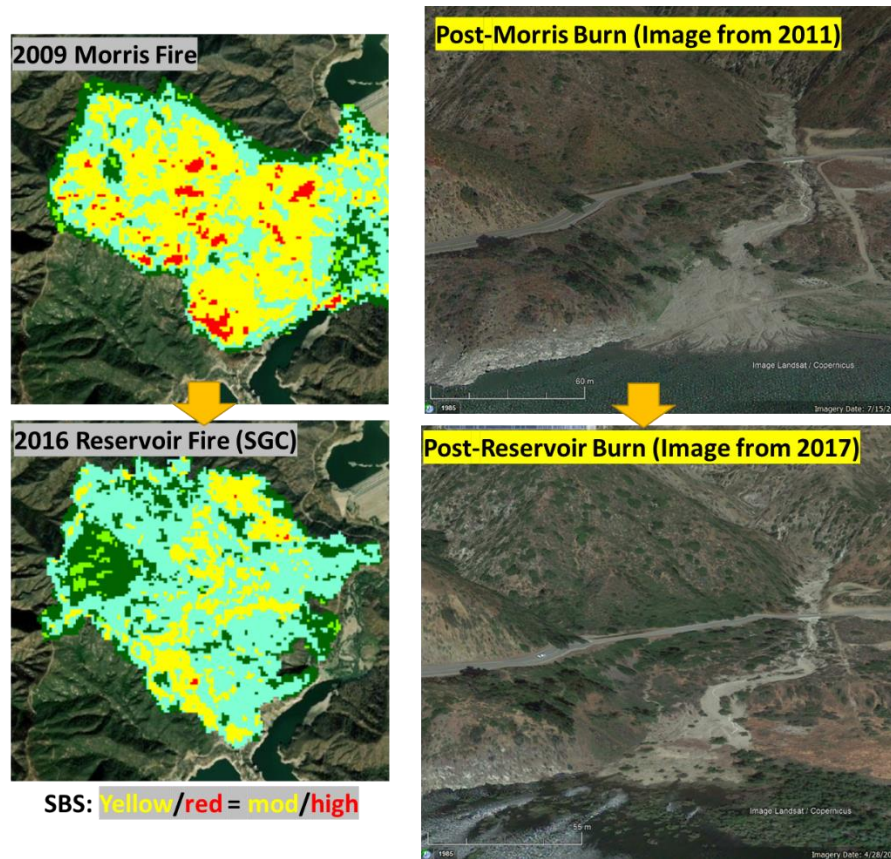
Fig B8. Example of steep terrain experiencing rapid re-burning (<10yrs) with evidence of potential fuel limitations and possible sediment supply limitations. **Left:** Soil burn severity (SBS) from MTBS showing repeat burns in the San Gabriel Mountains near Azusa, CA. **Right:** Google Earth imagery showing a prograding postfire delta in Morris Reservoir following two seasons worth of postfire erosion from the 2009 Morris burn scar (the first season was classified as wet) and a repeat image of the same location following the 2016 Reservoir Fire showing a sediment slug (though visually less voluminous than the Morris Fire associated erosion).